

**Synthetic, Spectroscopic and Structural Studies on
Carbametallaboranes containing
Aromatic and Fused Aromatic Ring Systems**

Zoë G. Lewis

Thesis Presented for the Degree of
Doctor of Philosophy
University of Edinburgh

1991



Declaration

Except where specific reference is made to other sources, the work presented in this thesis is the original work of the author. It has not been submitted, in whole or in part, for any other degree. Certain of the results have been accepted for publication.

For my parents

Acknowledgements

First and foremost, I would like to thank my supervisor, Dr. Alan Welch, without whose advice, encouragement and boundless enthusiasm this work would not have been achieved.

Thanks are also due to Dr. David Reed for his help in recording and interpreting n.m.r. spectra.

I am also grateful to John Millar and Heather Grant, who obtained numerous other n.m.r. spectra, and to Elaine M^cDougall, who performed the elemental analyses.

I have very much appreciated the constant encouragement and advice from all those who have worked in laboratories 290-293 over the years. In particular I would like to thank Kenny Shaw and Stuart Macgregor for their help and support, especially in the final weeks of writing this thesis.

Finally, thanks are due to the University of Edinburgh for the use of their facilities, and to the Department of Education for Northern Ireland for financial support.

Abstract

Chapter 1 consists of a brief overview of carbaborane chemistry related to this work, including concepts of cluster bonding and slip distortions in carbametallaboranes derived from $[7,8\text{-nido-C}_2\text{B}_9\text{H}_{11}]^{2-}$. This is followed by an introduction to the transition metal chemistry of fused aromatic ligands, with specific reference to the similar bonding capabilities of these and carbaborane species. The Chapter culminates in a discussion of the structure of the first reported fused aromatic carbametallaborane, namely 3-($\eta^5\text{-C}_9\text{H}_7$)-3,1,2-*closo*- $\text{C}_2\text{B}_9\text{H}_{11}$ (**1**), including a rationalisation of the observed *cisoid* molecular conformation.

Chapter 2 is divided into two sections, *A* and *B*. *Section A* presents the syntheses and structures of three indenyl carbametallaboranes, where one or two aryl or alkyl functions have been introduced at the cage carbon atoms, *i.e.* 1-Ph-3-($\eta^5\text{-C}_9\text{H}_7$)-3,1,2-*closo*- $\text{C}_2\text{B}_9\text{H}_{10}$ (**2**),
1-(CH_2OCH_3)-3-($\eta^5\text{-C}_9\text{H}_7$)-3,1,2-*closo*- $\text{C}_2\text{B}_9\text{H}_{10}$ (**3**) and
1,2-(CH_2OCH_3)₂-3-($\eta^5\text{-C}_9\text{H}_7$)-3,1,2-*closo*- $\text{C}_2\text{B}_9\text{H}_9$ (**4**). In the mono-substituted species, **2** and **3**, the indenyl ligand adopts a conformation analogous to that in **1**, *i.e.* the indenyl ring junction carbon atoms are *cisoid* with respect to the cage carbon atoms. In **4** the presence of two ether substituents has resulted in the adoption of the "next best" staggered conformation. A series of EHMO calculations performed on idealized models of **1** - **4** predict theoretical energy minimum conformations which are in broad agreement with those observed crystallographically. *Section B* describes the synthesis and structural determination of the first reported fluorenyl carbametallaborane complex, 3-($\eta^5\text{-C}_{13}\text{H}_9$)-3,1,2-*closo*- $\text{C}_2\text{B}_9\text{H}_{11}$ (**5**). The molecular conformation has been rationalised in terms of the *trans* influence of the facial cage boron atoms, and is in full accord with that predicted by the results of EHMO calculations on an idealised model of **5**.

Chapter 3 documents the synthesis of the previously unreported species " $[(C_9H_7)RhCl_2]_2$ ", and its reactions with a series of dithallium carbaboranes. The structure of the novel indenyl rhodium carbaborane compound $3-(C_2B_9H_{11})-8-((C_9H_6)Rh(C_9H_7))-3,1,2-closo-C_2B_9H_{10}$ (6a) is discussed. Subsequently the structures of further species incorporating a $\{(C_9H_7)Rh(C_9H_6)\}$ fragment, i.e. $7-R-10-((C_9H_6)Rh(C_9H_7))-7,8-nido-C_2B_9H_{10}$ [R = H (6b), R = CH_2OCH_3 (7)], $9-((C_9H_6)Rh(C_9H_7))-7,8-nido-C_2B_9H_{11}$ (6c) and $7-Ph-9/11-((C_9H_6)Rh(C_9H_7))-7,8-nido-C_2B_9H_{10}$ (8b), together with the initially targeted *closo* MC_2B_9 carboranes, $1-R^1-2-R^2-3-(\eta^5-C_9H_7)-3,1,2-closo-C_2B_9H_9$, [R¹ = Ph, R² = H (8a), R¹ = R² = CH_2OCH_3 (9)] have been deduced from analysis of spectral data. The indenyl rhodium dichloride precursor has retrospectively been assigned to have a complex polymeric composition.

Chapter 4 contains structural information on diphenylcarbaborane and some transition metal derivatives. The parent carbaborane, $1,2-Ph_2-1,2-closo-C_2B_{10}H_{10}$ (10) crystallises with two independent molecules per asymmetric unit, and the cage carbon-carbon bond length in each is longer than that observed in *orthocarbaborane*, which has been attributed to repulsions between adjacent phenyl π -systems. Moreover, the variation in degree of twist in the aromatic functions of molecules A and B has been correlated with the inter cage carbon carbon distances. The synthesis and structural determination of $7,8-Ph_2-10-endo-Ph_3PHg-7,8-nido-C_2B_9H_9$ (11), in which the phenyl substituents are substantially more twisted than in 10, is discussed. This twist has been attributed to the relatively short cage carbon-carbon bond length (1.58 Å). Finally a structural determination of $1,2-Ph_2-3-Cp^*-3,1,2-pseudo-closo-Rh(C_2B_9H_9)$ (13), has shown substantial distortion in the twelve vertex polyhedron, with the cage carbon atoms 2.50 Å apart. This has been attributed to repulsions between adjacent *ortho* hydrogen atoms on the phenyl

substituents, which are substantially twisted to accommodate the bulky Cp* ligand.

Chapter 5 gives details of the experimental procedures leading to the results discussed in the main body of the work, and comprises three sections, *A B* and *C*. *Section A* describes synthetic methods, and includes spectral and microanalytical data, *Section B* covers crystallographic techniques and *Section C* discusses molecular orbital calculations.

Abbreviations

AO	atomic orbital
BNCT	Boron-Neutron Capture Therapy
cod	cyclooctadiene
coe	cyclooctene
COSY	correlation spectroscopy
Cp	cyclopentadienyl
Cp*	pentamethylcyclopentadienyl
EHMO	extended Hückel molecular orbital
Et	ethyl
eV	electron volts
HA	hinge angle
i.r.	infrared
LCAO	linear combination of atomic orbitals
Me	methyl
MO	molecular orbital
n.m.r	nuclear magnetic resonance
Ph	phenyl
p.p.m.	parts per million
RA	rotation angle
S.E.P.	skeletal electron pair
thf	tetrahydrofuran }

Abbreviations for Specific Complexes

- (1) 3-(η^5 -C₉H₇)-3,1,2-*closo*-CoC₂B₉H₁₁
- (2) 1-Ph-3-(η^5 -C₉H₇)-3,1,2-*closo*-CoC₂B₉H₁₀
- (3) 1-(CH₂OCH₃)-3-(η^5 -C₉H₇)-3,1,2-*closo*-CoC₂B₉H₁₀
- (4) 1,2-(CH₂OCH₃)₂-3-(η^5 -C₉H₇)-3,1,2-*closo*-CoC₂B₉H₉
- (5) 3-(η^5 -C₁₃H₉)-3,1,2-*closo*-CoC₂B₉H₁₁
- (6a) 3-(C₂B₉H₁₁)-8-((C₉H₆)Rh(C₉H₇))-3,1,2-*closo*-RhC₂B₉H₁₀
- (6b) 10-((C₉H₆)Rh(C₉H₇))-7,8-*nido*-C₂B₉H₁₁
- (6c) 9-((C₉H₆)Rh(C₉H₇))-7,8-*nido*-C₂B₉H₁₁
- (7) 7-(CH₂OCH₃)-10-((C₉H₆)Rh(C₉H₇))-7,8-*nido*-C₂B₉H₁₀
- (8a) 1-Ph-3-(η^5 -C₉H₇)-3,1,2-*closo*-RhC₂B₉H₁₀
- (8b) 7-Ph-9/11-((C₉H₆)Rh(C₉H₇))-7,8-*nido*-C₂B₉H₁₀
- (9) 1,2-(CH₂OCH₃)₂-3-(η^5 -C₉H₇)-3,1,2-*closo*-CoC₂B₉H₉
- (10) 1,2-Ph₂-1,2-*closo*-C₂B₁₀H₁₀
- (11) 7,8-Ph₂-10-*endo*-Ph₃PHg-7,8-*nido*-C₂B₉H₉
- (12) 1,2-Ph₂-3-(*p*-cymene)-3,1,2-RuC₂B₉H₉
- (13) 1,2-Ph₂-3-Cp*-3,1,2-RhC₂B₉H₉

Contents

	Page
Chapter 1: Introduction	1
Introduction	1
Carbaboranes and Carbametallaboranes	3
Introduction	3
Icosahedral <i>Closo</i> -Carbaboranes	3
Selective Cage Degradation	5
Synthesis of Carbametallaboranes	5
Bonding Description of $[C_2B_9H_{11}]^{2-}$	6
Structure and Bonding in Polyhedral Clusters	9
"Slipped" Carbametallaboranes	12
Atom Numbering	15
Transition Metal Complexes of Fused Aromatic Ligands	17
Indenyl Metal Complexes	17
Fluorenyl Metal Complexes	22
Transition Metal Complexes of Naphthalene	24
Indenyl Carbametallaboranes	25
Scope of the Work Presented	28
Chapter 2: Fused Aromatic Carbacobaltaboranes	29
Section A: Indenyl Carbacobaltaboranes	29
Introduction	29
1-Ph-3-(η^5-C₉H₇)-3,1,2-<i>closo</i>-CoC₂B₉H₁₀, (2)	30
Synthesis of 2	30
N.m.r. Studies	30
Structural Study on 2	34

1-(CH₂OCH₃)-3-(η⁵-C₉H₇)-3,1,2-closo-CoC₂B₉H₁₀, (3)	43
Synthesis	43
N.m.r. Studies	43
Structural Study on 3	43
1,2-(CH₂OCH₃)₂-3-(η⁵-C₉H₇)-3,1,2-closo-CoC₂B₉H₉, (4)	51
Synthesis	51
N.m.r. Studies	52
Structural Study on 4	52
EHMO Calculations	61
Introduction	61
Results and Discussion	61
Section B: Fluorenyl Carbametallaborane Chemistry	67
Introduction	67
(η⁵-C₁₃H₉)-3,1,2-closo-CoC₂B₉H₁₁, (5)	68
Synthesis	68
Structural Study on 5	68
Conclusions	80
Chapter 3: Indenyl Rhodium Carbaborane Complexes	81
Introduction	81
Chemistry of [CpRhX ₂] _n and [Cp [*] RhCl ₂] ₂	82
Synthesis and Characterisation of "[C ₉ H ₇)RhCl ₂] ₂ "	84
Reaction of "[C ₉ H ₇)RhCl ₂] ₂ " with Ti ₂ [7,8-C ₂ B ₉ H ₁₁]	84
Elucidation of the Structure of 6a	85
Analysis of N.m.r. Spectra	85
Structural Study on 6a	90
Characterisation of 6b	97

Analysis of N.m.r. Spectra	97
Characterisation of 6c	102
Analysis of N.m.r. Spectra	102
Reaction of " $[(C_9H_7)RhCl_2]_2$ " with $Tl_2[7-CH_2OCH_3-7,8-C_2B_9H_{10}]$	106
Characterisation of 7	106
Analysis of N.m.r. Spectra	106
Reaction between " $[(C_9H_7)RhCl_2]_2$ " and $Tl_2[7-Ph-7,8-C_2B_9H_{10}]$	110
Characterisation of 8a	110
Characterisation of 8b	111
Analysis of N.m.r. Spectra	111
Reaction of " $[(C_9H_7)RhCl_2]_2$ " with $Tl_2[7,8-(CH_2OCH_3)_2-7,8-C_2B_9H_9]$	114
Characterisation of 9	114
Analysis of N.m.r Spectra	114
Reconsideration of the Structure of " $[(C_9H_7)RhCl_2]_2$ "	116
Conclusions	120
Chapter 4: Transition Metal Derivatives of Diphenylcarbaborane	121
Introduction	121
1,2-Ph₂-1,2-closo-C₂B₁₀H₁₀, (10)	122
Synthesis and Characterisation	122
Structural Study on 10	122
7,8-Ph₂-10-endo-Ph₃PHg-7,8-nido-C₂B₉H₉, (11)	136
Introduction	136
Synthesis and Spectroscopic Analysis	136
Structural Study on 11	137
Syntheses of 1,2-Ph₂-3-(η-L)-3,1,2-closo-MC₂B₉ Species	148
1,2-Ph₂-3-(p-cymene)-3,1,2-closo-RuC₂B₉H₉, (12)	148
Synthesis	148

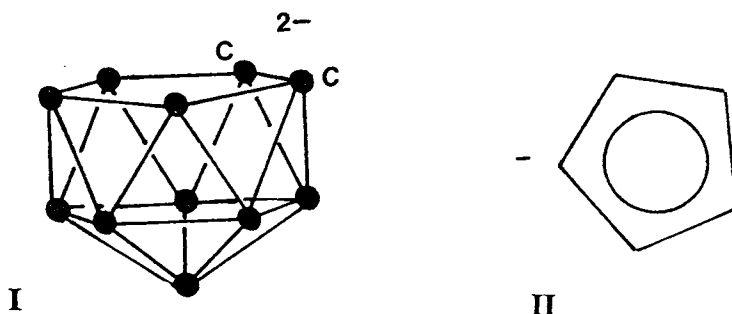
N.m.r. Studies	148
1,2-Ph₂-3,1,2-closo-RhC₂B₉H₉, (13)	152
Synthesis	152
N.m.r. Studies	152
Structural Study on 13	153
Suggestions for Further Work	169
Conclusions	171
Chapter 5: Experimental	172
Introduction	172
Section A: Synthetic Methods	173
Section B: Crystallographic Techniques	184
Section C: Extended Hückel Molecular Orbital Calculations	196
References	206
Appendices	214
Appendix 1: Additional Atom Co-ordinates	215
Appendix 2: Lectures and Courses Attended	222

Chapter 1

Introduction

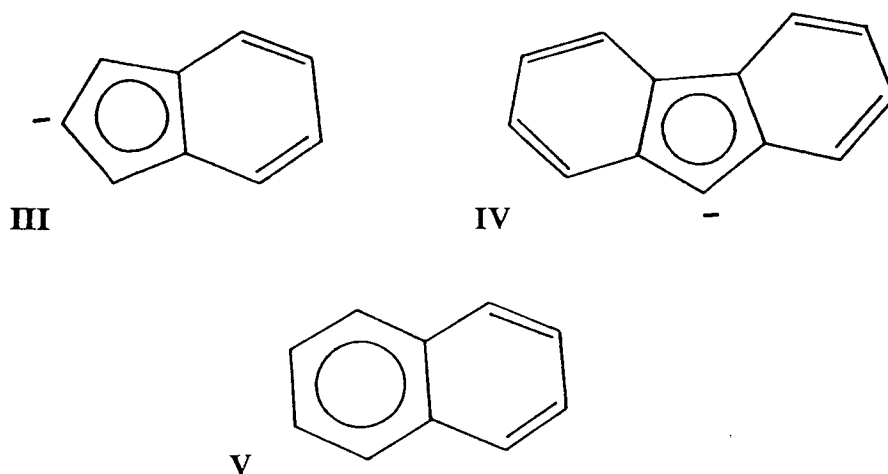
Introduction

In 1965, M. Frederick Hawthorne and co-workers reported a carbaborane analogue of ferrocene, $[\text{Fe}(\text{C}_2\text{B}_9\text{H}_{11})_2]^{2-}$, which was the first example of a carbametallaborane complex.¹ The precedent for the synthesis of this compound was the observation of similar frontier molecular orbitals (MO's) in the five-membered ring systems of $[\text{C}_2\text{B}_9\text{H}_{11}]^{2-}$, (I), (the dicarbollyl ligand), and $[\text{C}_5\text{H}_5]^-$ (Cp^-), (II), (the cyclopentadienyl ligand).^{2,3} Subsequently a vast new area of boron chemistry has evolved, involving the syntheses and characterisation of an enormous number of carbametallaboranes of varying size and atom composition.



Whilst Cp^- and $[\text{C}_2\text{B}_9\text{H}_{11}]^{2-}$ form many structurally analogous metal complexes, some dicarbollyl complexes exhibit notable distortions compared with Cp analogues, in that the metal atom is not centrally positioned above the ligand face, but is "shifted" laterally across it.^{4,5} These effects may be attributed to the lower symmetry of the bonding C_2B_3 pentagon, due to its heterogeneous nature, and are more fully discussed later.⁶⁻⁸

Slip distortions are of course not unique to carbametallaboranes, but are also observed in metal complexes of fused aromatic ligands, such as indenyl ($[\text{C}_9\text{H}_7]^-$), (III),^{9,10} fluorenyl ($[\text{C}_{13}\text{H}_9]^-$), (IV)^{11,12} and naphthalene (C_{10}H_8), (V).¹³



The indenyl and fluorenyl ligands both contain five-membered ring systems analogous to that in Cp, and can therefore also be described as formal analogues of the dicarbollyl ligand. Given the said tendency of both fused aromatic and dicarbollyl ligands to form distorted metal complexes, the incorporation of both ligands in one molecule is of potential interest.

This introductory chapter starts with a brief overview of carbaborane and carbametallaborane chemistry most pertinent to the work contained in this thesis, including the concepts of cluster bonding and slip distortions in carbametallaboranes. This is followed by an introduction to the chemistry of fused aromatic ligands, with particular emphasis on indenyl transition metal complexes, which have been studied in some detail. The two areas are, as it were, fused, with a discussion of the structure of the first known indenyl carbametallaborane,¹⁴ including rationalisation of the preferred solid-state conformation, which forms the basis of the on-going work.

Carbaboranes and Carbametallaboranes

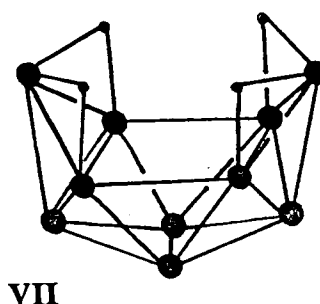
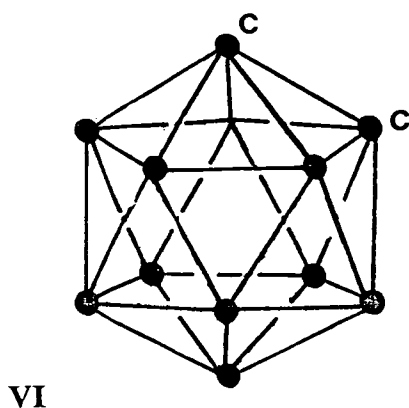
Introduction

Carbaboranes and carbametallaboranes are essentially derivatives of boron hydride precursors, and exhibit very similar cage geometries to their polyboron analogues. Much initial interest in carbaborane chemistry arose from the greater stability exhibited by many of these cluster species compared with structurally analogous air- and moisture-sensitive boron hydrides, particularly among the smaller and more open-faced polyhedra. Most known carbaboranes contain five to twelve cage atoms, usually with one or two carbon atoms per molecule, although clusters with a larger number of carbon atoms are also known.

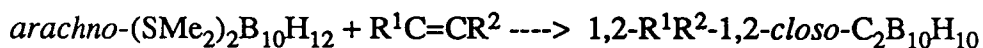
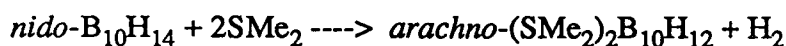
As time and space available here preclude full coverage of the wide spectrum of carbaborane chemistry, the following pages concentrate upon the chemistry of carbaboranes and carbametallaboranes derived from *ortho*-carbaborane (1,2-*closo*-C₂B₁₀H₁₂), (VI), which is of most relevance to this work.

Icosahedral *Closo*-Carbaboranes

Ortho-carbaborane, together with its isomers *meta*- and *para*-carbaborane, (1,7- and 1,12-*closo*-C₂B₁₀H₁₂ respectively) is exceptional in its ease of preparation and high stability. The 1,2 - isomer is the most readily available, and its chemistry has been particularly extensively studied.



The most convenient synthesis of *ortho*-carbaborane, and indeed a whole range of carbon-substituted derivatives, is the reaction of decaborane, $B_{10}H_{14}$, (VII), with the appropriate alkyne in the presence of a Lewis base¹⁵ (eg SMe_2 , MeCN) involving the following typical reaction scheme:



From kinetic studies it is suggested that the rate determining step involves the attack of alkyne on, *e.g.*, the monosulphide, $Me_2SB_{10}H_{12}$.¹⁶

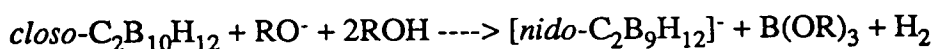
This method of synthesis has yielded numerous twelve-vertex *closo*-carbaboranes incorporating a wide variety of cage substituents R^1 and R^2 .¹⁷ The nature of the substituents is often of importance in dictating the ultimate stereochemistry of subsequent reaction products.

The structure of *ortho*-carbaborane has been determined by electron diffraction methods,¹⁸ and the cage is found to be a slightly distorted icosahedron, reflecting shorter distances between and to the two carbon atoms. In addition to this structural determination, a number of X-ray crystal structures of mono- and di-substituted

derivatives of *ortho*-carbaborane have been studied.^{19,20} Molecular parameters for these compounds are similar to those in the unsubstituted carbaborane. Typical C-C distances are in the range 1.63-1.70Å, B-C distances in the range 1.66-1.77Å and B-B distances are between 1.70 and 1.89Å.

Selective Cage Degradation

The reaction of 1,2-R₂-1,2-*closo*-C₂B₁₀H₁₀ with strong bases, such as the alkoxide ion, affords [7,8-R₂-7,8-*nido*-C₂B₉H₁₀]⁻.^{21,22} The boron atom removed is the one in closest proximity to the carbon atoms, *i.e.* B(3) or B(6). Similarly, the 1,7-*closo* species produces [7,9-R₂-7,9-*nido*-C₂B₉H₁₀]⁻. The reaction scheme is the following:

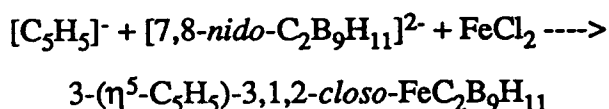
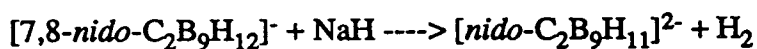


Deprotonation of the monoanionic species, using sodium hydride, or prolonged reflux with a considerable excess of alkoxide, yields [R₂C₂B₉H₉]²⁻, the so-called dicarbollyl ligand, named after the Spanish word "olla", which is a type of water jug shaped like an eleven-vertex *nido* icosahedron. Reactions of this ligand have been of major importance in the development of carbametallaborane chemistry.

Synthesis of Carbametallaboranes

The construction of polyhedral cages containing metal, boron and carbon atoms has been achieved by a variety of methods, the most common of which involve the reaction of an existing carbaborane cage framework with a metal reagent.

The use of [C₂B₉H₁₁]²⁻ was historically the first route employed for syntheses of carbametallaboranes, with Hawthorne reporting the structure of [Fe(C₂B₉H₁₁)₂]²⁻ in 1965.¹ The dicarbollyl dianion used in this, and numerous further reactions by the Hawthorne group, was formed by deprotonation of [C₂B₉H₁₂]⁻. A typical reaction is the following:

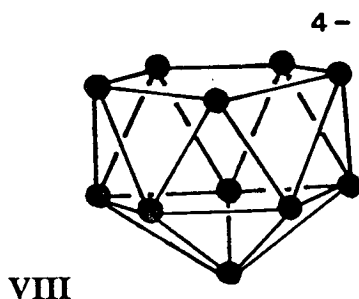


In 1972 F.G.A. Stone and co-workers reported the preparation and synthetic utility of the thallium complexes $\text{Tl}_2[\text{R}_2\text{C}_2\text{B}_9\text{H}_9]$,²³ which precipitate upon addition of thallium (I) acetate to an aqueous solution of $[7,8\text{-C}_2\text{B}_9\text{H}_{12}]^-$ or its alkyl derivatives, and more recently an improved synthesis of dithallium carbaboranes has been reported.²⁴ The nature of bonding of thallium to the cage is discussed later in this Chapter. Reaction with halogeno-derivatives of the transition metals, eg FeCl_2 , CoCl_2 and $\text{Pt}(1,5\text{-C}_8\text{H}_{12})\text{Cl}_2$ leads to the formation in high yield of corresponding 3,1,2- MC_2B_9 derivatives.

Bonding Description of $[\text{C}_2\text{B}_9\text{H}_{11}]^{2-}$

The attempts to synthesise dicarbollyl analogues of metallocenes were based on the observation that cyclopentadienyl and dicarbollyl anions both possess 6π -electrons which occupy similar frontier orbitals associated with their open pentagonal faces.

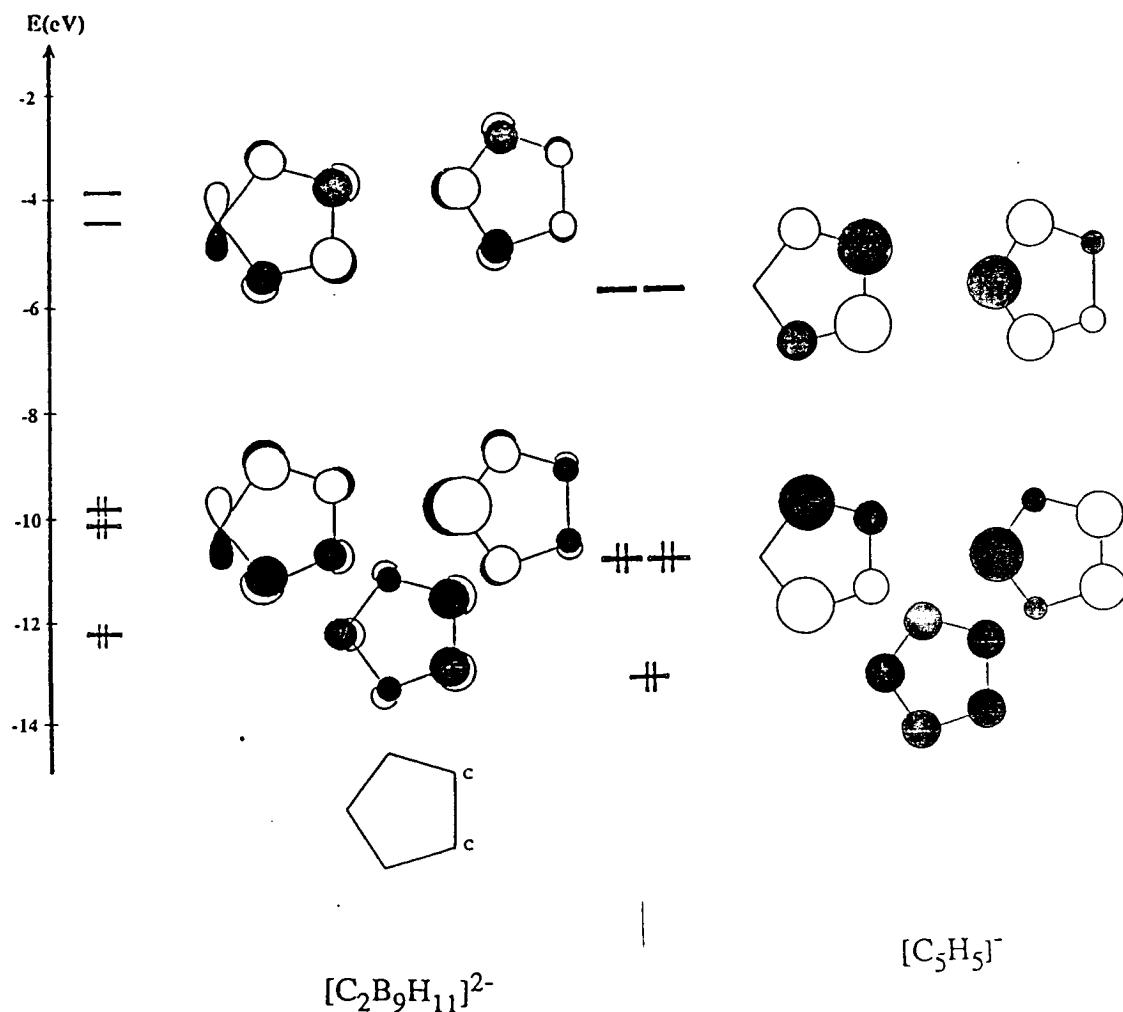
The MO scheme for $[\text{C}_2\text{B}_9\text{H}_{11}]^{2-}$ has been derived from the bonding description of the isostructural borane, $[\text{B}_{11}\text{H}_{11}]^{4-}$ (VIII).³



Extended Hückel molecular orbital (EHMO) calculations on this species have confirmed that it has 24 bonding MO's, in agreement with simple electron counting rules. There are five MO's available for metal complexation, which are localized predominantly on the open B_5 face and are directed towards the vacant apex position of this face. These comprise three bonding orbitals (a_1 , which is strongly bonding, and two degenerate, e_1 , which are more weakly bonding), and two antibonding orbitals (e_2). Exact orbital degeneracy will be removed in the case of $[C_2B_9H_{11}]^{2-}$, but the essential pattern of orbital composition and relative energy will not substantially change. This orbital scheme is represented in Figure 1.1,²⁵ along with a similar orbital scheme for $[C_5H_5]^-$,²⁶ which shows the resemblance in the frontier MO's of the two ligands.

The structure of the ferrocene analogue, $[(C_2B_9H_{11})_2Fe]^{2-}$ can be described in terms of valence bond theory, in a similar way to that of Cp_2Fe .^{27,28} Each $[C_2B_9H_{11}]^{2-}$ ligand can be assumed to donate three pairs of electrons to Fe^{II} , which accommodates the six pairs in d^2sp^3 hybrid orbitals, while its d^6 electrons pair up in the remaining, non-bonding, 3d orbitals, thus satisfying the 18-electron rule.

Figure 1.1 π -MO's of $[\text{C}_5\text{H}_5]^-$ and $[\text{C}_2\text{B}_9\text{H}_{11}]^{2-}$



However, the structure of carbametallaboranes may also be rationalized in terms of cluster bonding, where the metal fragment is incorporated as a vertex in the polyhedron. *Closo*- MC_2B_9 icosahedra are essentially isostructural with the "parent" *closo*- C_2B_{10} carbaborane,¹⁸ as well as $\text{B}_{12}\text{H}_{12}^{2-}$.²⁹ Indeed there are clear structural relationships in isoelectronic borane and heteroborane polyhedra of all sizes. The nature of bonding in these boron cage structures, for many years a chemical puzzle, is now reasonably well understood, and the subject is addressed in the following section.

Structure and Bonding in Polyhedral Clusters

Earlier this century the term "electron deficient" was applied to boron cage compounds, as there are fewer electrons than would normally be required for a "classical structure", where ordinary electron-pair bonds exist between each pair of bonded atoms. Obviously some kind of multi-centre bonding is involved, with extensive delocalisation of electrons within the polyhedron. In fact, the notion of "electron deficient" boranes is a very misleading one, as most species have closed-shell electronic structures, and indeed many, particularly carbaboranes and carbametallaboranes, compare favourably with hydrocarbons, in terms of thermal and chemical stability.

There are three ways in which bonding in boron hydride cages may be understood:

- 1) Localized valence-bond structures incorporating two- and three-centre electron-pair bonds,³⁰
- 2) Quantitative molecular orbital treatments of individual cluster systems, and
- 3) Consideration of the total number of skeletal electrons involved in the polyhedral framework.^{31,32}

Localized valence-bond arguments were developed largely by William Lipscomb and co-workers.³⁰ Although useful for describing smaller and more open-cage boron hydrides, the method becomes complicated for large, closed polyhedral systems. Detailed molecular orbital calculations have been carried out on a number of boranes and carbaboranes, but inclusion of metal atoms in the polyhedral cluster increases the complexity of the calculations.

The last approach has been found to be the most widely applicable, particularly following the advent of a general set of rules devised by Kenneth Wade in 1971,³¹ which recognize the relationship between the cage geometry and the number of electrons involved in the skeletal framework.

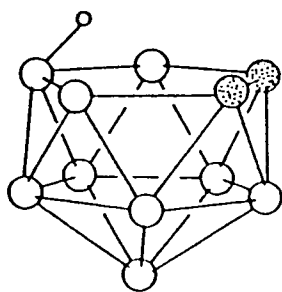
which recognize the relationship between the cage geometry and the number of electrons involved in the skeletal framework.

Briefly, there are four main classes of polyhedral cage, namely *closo*, *nido*, *arachno*, *hypho*, names derived from Greek or Latin words describing the extent of "opening out" of the cage. *Closo* cages are closed polyhedra consisting entirely of triangulated faces. Removal of one vertex from a closed cage structure yields a *nido* cage, which has the same basic shape as the parent compound, but with one open face. Removal of one more vertex from this face results in the corresponding *arachno* structure, and loss of a third vertex from the open face of the *arachno* cage gives a *hypho* derivative, which has the same cage geometry as its parent *closo* borane, but with three vertices missing. The point to note is that if removal of a vertex does not change the polyskeletal electron count, the overall cage geometry remains the same.

The general rules predicting cage geometry from the number of electron-pairs involved in skeletal bonding are summarized below:

Number of Cage Atoms	Number of Skeletal Electron Pairs	Assigned Cage Geometry
n	n + 1	<i>closo</i>
n	n + 2	<i>nido</i>
n	n + 3	<i>arachno</i>
n	n + 4	<i>hypho</i>

For example, the rules can be seen to rationalize the structure of [*nido*-C₂B₉H₁₂]⁻, (IX), which has been determined crystallographically.³³



IX

This species contains BH and CH units, as well as an *endo*-hydrogen atom associated with one of the boron atoms on the open face. For main group elements in general the number of electrons (e) available for skeletal bonding is $v+x-2$, where v is the number of valence shell electrons of the neutral atom, and x the number of electrons supplied by the *exo*-polyhedral atom(s). Each boron and carbon atom form a localized bond with its associated *exo*-polyhedral hydrogen atom ($x=1$). This leaves each of the BH units (where $v=3$) three orbitals and two electrons, and the CH units (where $v=4$) three orbitals and three electrons, to bind together and generate molecular orbitals extending within and over the polyhedral surface.

The total polyhedral electron count, for an eleven-vertex cage, is therefore calculated as follows:

Skeletal Electron Source	Number of Electrons
2 X {CH}	6
8 X {BH}	16
1 X {BH ₂ }	3
-ve charge	1
	=> 26
	=> 2n + 4
	=> n + 2 S.E.P's

$n+2$ S.E.P's (skeletal electron pairs) corresponds to a *nido* cage geometry.

Although transition metals have a total of nine valence orbitals, they, like boron and carbon atoms, contribute only three orbitals to cluster bonding, leaving six remaining atomic orbitals for bonding to external ligands, and for storing "non-bonding" pairs. Since these orbitals are usually filled (to satisfy the 18-electron rule), electron donation from the transition metal fragment to the cage is given by $e=v+x-12$ (v is the number of valence electrons of the neutral metal, *i.e.* no assumptions are made concerning metal oxidation state). Thus the total electron count for $\text{CpCoC}_2\text{B}_9\text{H}_{11}$, which has a closed polyhedral structure,¹⁴ is the following:

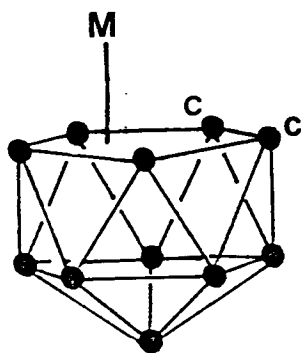
Skeletal Electron Source	Number of Electrons
1 X {CpCo}	2
2 X {CH}	6
9 X {BH}	18
	=> 26
	=> $2n + 2$
	=> $n + 1$ S.E.P.'s

$n+1$ skeletal electron pairs corresponds to a *closo* cage geometry.

N.B. The CpCo moiety is isolobal with a BH unit.

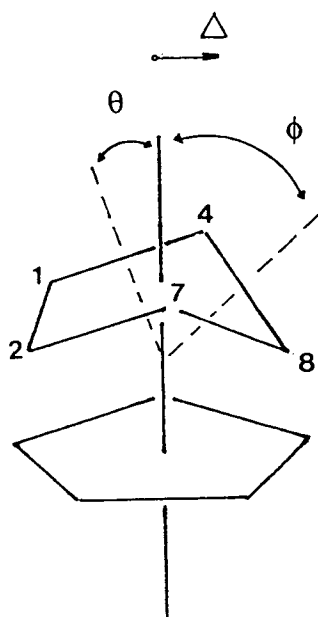
"Slipped" Carbametallaboranes

Although electron counting formalisms conveniently describe the geometries of many cluster species, there are some anomalous structures which cannot be reasoned purely in these terms. Examples of these occur among a number of carbametallaboranes of the type $1,2\text{-R}_2\text{-3-L-3,1,2-MC}_2\text{R}_2\text{B}_9\text{H}_9$, where the metal is not centrally positioned above the carbaborane face, (X).



X

The slip distortions observed can be defined in terms of displacement (Δ^P) of the metal atom from its more usual position above the centroid of the open pentagonal face of the ligand towards the unique facial boron atom.⁷ Formally this is the distance from the perpendicular of the reference plane to the metal atom, the perpendicular passing through the centroid of the lower pentagonal belt B(5,6,11,12,9). This lower belt is usually used as a reference since Wallbridge and co-workers^{34,35} recognized that in slipped carbametallaboranes there is an increase in non-planarity of the C_2B_3 face bound to the metal. This is expressed in terms of "fold" angles θ^P and ϕ^P , folding occurring along the B(4).....B(7) axis. Both "slip" and "fold" parameters are illustrated below:



$[M(C_2B_9H_{11})_2]^{n-}$ species

Slip distortions are exhibited by bis-dicarbollyl complexes in which the metal atom has eight or more d electrons, *e.g.* Ni^{II} , Pd^{II} , Cu^{II} , Au^{II} ($n=2$); Cu^{III} , Au^{III} ($n=1$).^{4,5,6} The two cages are shifted laterally across the metal atom by an average of *ca.* 0.5\AA , in contrast with more symmetric conformations found in complexes of d^3 - d^7 metals.

The simple explanation is that the metal atom slips to avoid an undesirable ($>18e^-$) configuration. More detailed explanation lies in results of MO calculations, which suggest that slippage of the metal atom away from a central position over each cage face results in the stabilization of the occupied and formally antibonding molecular orbitals.³⁶

$L_2MC_2B_9H_{11}$ species

Similar slip distortions are observed for complexes of heavier and late transition metals, *e.g.* Pt^{II} , Pd^{II} , $L=PR_3$.^{7,8} For example, in $(Et_3P)_2Pt(C_2B_9H_{11})$ $\Delta^P=0.42\text{\AA}$ and θ^P and ϕ^P are 4.7 and 4.4° respectively.⁷

Explanation of this has also been derived from analysis of the results of molecular orbital calculations, with optimum overlap of metal and ligand orbitals occurring for lateral distortion of the angular ML_2 fragment towards the unique facial boron atom.⁷

Pseudo σ -Bonded Carbametallaboranes

An extreme distortion is found in a small number of carbametallaboranes of the type $(LMC_2B_9H_{11})^{0,-1}$, where the metal atom is attached to the carbaborane moiety essentially by a σ -bond with the unique facial boron atom, B(10), with weaker interactions to the other two [B(9,11)]. This form of distortion occurs for d^{10} metal atoms, *e.g.* Hg^{II} ³⁷ and Au^I ,²⁵ where $L=PR_3$, and the metal fragments can be regarded

as one-orbital donors to the ligand (formally isolobal with a hydrogen atom), adopting an *endo* position over the open face (*cf* [$C_2B_9H_{12}$]⁻³³).

This is presumably because Au^I and Hg^{II} prefer linear co-ordination (vs. tetrahedral), as their 6px and 6py atomic orbitals are too high lying to form valence orbitals along with the s-pz hybrid. In contrast Cu has four sp^3 hybrid orbitals available for bonding, as the copper 4px and 4py orbitals lie at relatively lower energies.³⁸ Thus $[PPh_3CuC_2B_9H_{11}]^-$ has a *closo*-cage structure, with the metal η^5 -bonded to the cage.³⁹

The $[3,1,2-TlC_2B_9H_{11}]^-$ ion represents a very extreme case of this type of distortion. Tl^I has a fully saturated $d^{10}s^2$ configuration, and the Tl- cage distances are very long, suggesting a situation close to an ion-pair formation, $[Tl]^+[C_2B_9H_{11}]^{2-}$.³⁷ The weak thallium cage bonding is consistent with the facile displacement of thallium by other metals, which offers a convenient route for syntheses of new carbametallaboranes (see earlier).²³

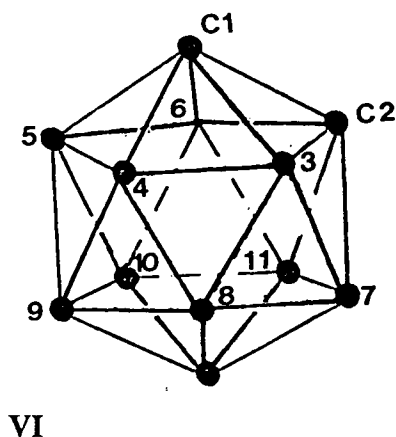
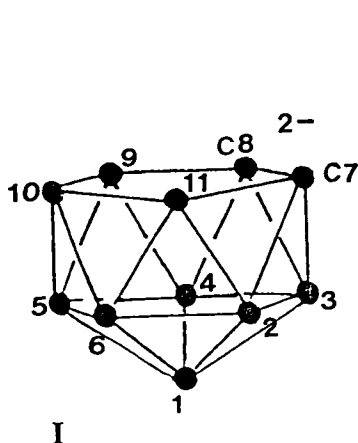
In summary, the vast majority of MC_2B_9 carbametallaboranes have *closo* structures which may be rationalized by Wade's rules. However, a number of "slipped" carbametallaboranes are also known. In these cases the formal oxidation state and electron configuration of the metal must be considered, together with the formal coordination geometry of the metal fragment.

Atom Numbering

At this stage it is perhaps appropriate to clarify the numbering schemes used to define atoms in carbaborane cages.

In the *nido* cage system, $[C_2B_9H_{11}]^{2-}$, the number sequence starts with the apex boron atom (that which is furthest from the open C_2B_3 face), with successive pentagonal rings numbered in a clock-wise direction; to go from number 6 -> 7 one

connectivity is crossed. Heteroatoms take the lowest numbers possible, and for two or more different heteroatom types rules of precedence have been established. Thus the two carbon atoms, which lie in the "top" pentagonal belt, are numbered 7 and 8 (see diagram of I below).



In *closo*- $C_2B_{10}H_{12}$, where there is no geometrically unique apex, one of the carbon atoms is assigned the number one position, and successive five-membered rings numbered in accordance with the above rules, the second carbon atom numbered 2 (see diagram of VI above).

In the case of carbametallaboranes, the cage numbering scheme depends on the position of the metal above the cage. In closed MC_2B_9 species, where the metal has essentially replaced a BH vertex, the metal is numbered third, after the two carbon atoms (*i.e.* one of the carbon atoms retains the principal apical position), *e.g.* 3-Cp-3,1,2-*closo*- $FeC_2B_9H_{11}$. However, in slipped *pseudo* σ -bonded MC_2B_9 species the metal atom is best not considered as a formal vertex, and regarded merely as a substituent, *e.g.* 10-*endo*- $HgPPh_3$ -7,8-*nido*- $C_2B_9H_{11}$.

Transition Metal Complexes of Fused Aromatic Ligands

Indenyl Metal Complexes

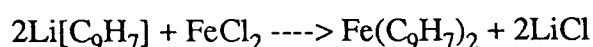
Introduction

The indenyl ligand, $[\text{C}_9\text{H}_7]^-$, essentially comprises a five- and a six-membered ring fused together *via* two so-called ring-junction carbon atoms. With transition metals it readily forms complexes which are analogous to those of the cyclopentadienyl ligand.

Initial interest in indenyl transition metal complexes stemmed from recognition of their enhanced reactivity relative to cyclopentadienyl analogues. For instance they act as more efficient catalysts in inter-molecular hydroacylation reactions,⁴⁰ cyclo-trimerisation of alkynes to benzenes,⁴¹ and cyclo-co-trimerisation of alkynes and nitriles to pyridines.⁴² In addition $(\eta\text{-C}_9\text{H}_7)\text{ML}_n$ complexes show enhanced reactivity in both $\text{S}_\text{N}1$ ⁴³ and $\text{S}_\text{N}2$ ⁴³⁻⁴⁵ ligand substitution reactions. All these processes are presumed to proceed *via* slippage ($\eta^5 \rightarrow \eta^3$) at some stage in the mechanism, which is well known to be more facile in indenyl complexes, than in analogous cyclopentadienyl complexes.

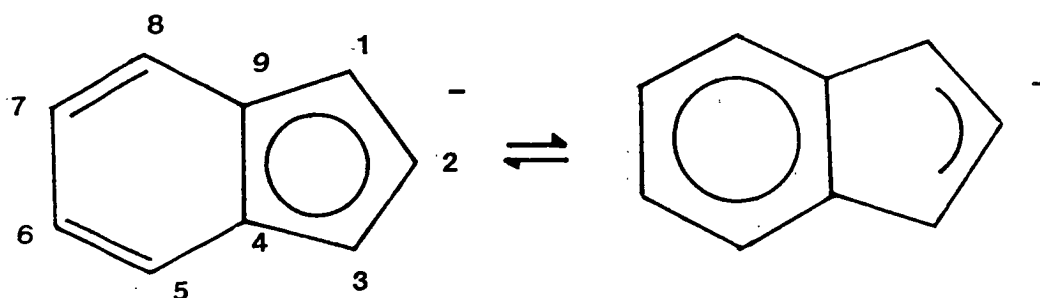
Syntheses

Syntheses of indenyl metal complexes is achieved using routes similar to those employed in synthesising Cp analogues. The CH_2 group in indene is easily deprotonated, *e.g.* with Bu^tLi , and the resulting lithium indenide may then be reacted with the appropriate metal halide, as in the following example:

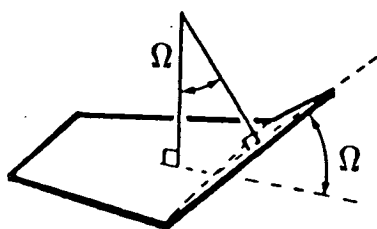


η^5 -Bonded Indenyl Complexes

In most structurally characterized metal complexes the indenyl ligand is essentially η^5 -bonded, *via* its five-membered ring. However, significant slip distortions from η^5 toward η^3 , usually toward C(2), exist in all cases, and can be explained in terms of recovery of some resonance energy as $p\pi$ atomic orbitals of the ring junction carbon atoms are more delocalized over the indenyl π -system, as illustrated in the diagram below, which also shows a common numbering scheme used throughout this work.



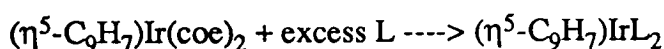
"Slip" and "fold" distortions have been calculated for a number of indenyl metal complexes. The slip can be defined in two ways; firstly as Δ^h ,⁹ which is calculated according to Mingos' definition for analogous distortions in carbametallaboranes, where the slip distortion is the distance between the normal to a reference plane and the metal, the normal passing through the centroid of the five-membered ring; or secondly, as $\Delta M-C$,¹⁰ which is the difference between the average of the metal-carbon distances C(1), C(2), C(3) and C(4), C(9). Associated with the slip is a folding of the C_5 ring, along the C(1).....C(3) axis, the fold angle, Ω , [or HA (hinge-angle)] being defined as the dihedral angle between the planes of the three-carbon and four-carbon fragment of the five-membered ring.



Δ^h values for a selection of complexes are in the range 0.125 $[(\eta^5\text{-C}_9\text{H}_7)\text{CrNO}(\text{CO})_2]$ ⁴⁶ to 0.298 Å $[(\eta^5\text{-C}_9\text{H}_7)_3\text{UCl}]$ ⁴⁷, (corresponding $\Delta\text{M-C}$ values 0.11 to 0.19 Å respectively), with fold angles typically quite small, ranging from 3.5° $[(\eta^5\text{-C}_9\text{H}_7)_2\text{Zr}(\text{CH}_3)_2]$ ⁴⁸ to 8.9° $[(\eta^5\text{-C}_9\text{H}_7)\text{Rh}(\text{cod})]$.⁴⁹

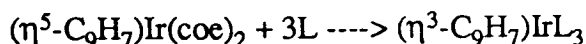
η^3 -Bonded Indenyl Complexes

A number of structures incorporating a formally η^3 -bonded indenyl ligand are known, including $(\eta^3\text{-C}_9\text{H}_7)(\eta^5\text{-C}_9\text{H}_7)\text{W}(\text{CO})_2$,⁵⁰ $(\eta^3\text{-C}_9\text{H}_7)\text{Ir}(\text{PMe}_2\text{Ph})_3$,⁵¹ and $(\eta^3\text{-C}_9\text{H}_7)(\eta^5\text{-C}_9\text{H}_7)\text{V}(\text{CO})_2$.⁵² The tungsten species is one of two products of the reaction between C_9H_8 and $\text{W}(\text{CO})_6$, the other product being $(\eta^5\text{-C}_9\text{H}_7)(\text{CO})_3\text{W}_2$. The iridium example is interesting, in that $(\eta^3\text{-C}_9\text{H}_7)$ is only obtained when small phosphine ligands are used, *i.e.*



where L = PEt_3 , (cone angle 145°)

but:



where L = PMe_3 , PPhMe_3 (cone angles 118 and 122° respectively)

The third mentioned species is the product of the reaction between $(\eta^5\text{-C}_9\text{H}_7)_2\text{V}$ and CO, demonstrating relatively facile slippage to accommodate incoming ligands.

In all cases of η^3 -bonding the metal atom is substantially slipped away from C(4) and C(9), with $\Delta M-C$ values of 0.783, 0.853 and 0.559 Å for the tungsten, iridium and vanadium species respectively. Corresponding fold angles (Ω), are also much greater than η^5 -bonded indenyl ligands, with values of 26, 28 and 21° respectively.

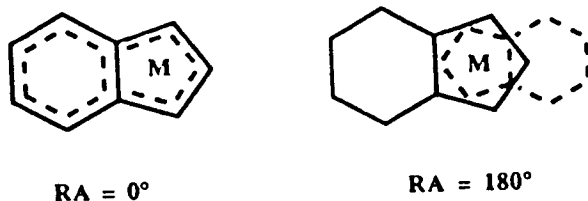
Conformation

The resonance energy gained in the distortion to an allyl-ene-type five-membered ring in indenyl complexes has the effect of stabilising various conformations of the ring relative to the other ligands on the metal. Such conformations can usually be predicted by using simple *trans* influence arguments; the preferred conformation of the indenyl relative to the ML_x fragment is such that the ligands with the greatest *trans* influence are *trans* to the six-membered ring. Thus in $[(\eta^5-C_9H_7)Ir\{P(C_6H_5)_3\}H]BF_4$ ⁹ the hydride is *trans* to the ring-junction carbon atoms of the indenyl ring, and in $(\eta^5-C_9H_7)MoCO_2(\eta^3-C_4H_7)$ ⁹ the two carbonyl ligands, which have greater *trans* influence than the allyl ligand, share the side *trans* to the ring-junction carbon atoms.

The driving force for these conformations is presumably that the weaker metal-ring-junction carbon atom bonds (which result from the $p\pi$ orbitals on these atoms being only partially released from involvement with the metal) are compensated by the stronger metal-ligand bonds to the functions diagonally opposite.

It is interesting to note the change in conformation which accompanies a progressive increase in slippage in a series of bis-indenyl metal complexes, $(C_9H_7)_2M$, ($M = Fe^{II}$, Co^{II} , Ni^{II}),¹⁰ (which are d^6 , d^7 , and d^8 species respectively), as broad parallels may be drawn between these species and bis-dicarbollyl metal analogues. An additional parameter has been used to describe the relative rotational orientation of the two indenyl ring systems.¹⁰ This is the rotation angle, RA , the angle

between planes including the metal, C(2), and the mid-point of the ring junction carbon atoms for each indenyl ligand. A rotation angle of 0° indicates a completely eclipsed geometry, whilst an angle of 180° corresponds to a fully staggered arrangement, as sketched below:



Indenyl conformation, together with slip and fold parameters for these three species are summarised in **Table 1.1**.

Table 1.1 Comparison of Slip and Fold Parameters and Rotation Angles for a Series of $(\eta^5\text{-C}_9\text{H}_7)_2\text{M}$ Complexes

Compound	$\Delta_{m-c}(\text{\AA})$	$\Omega(^\circ)$	RA($^\circ$)
$(\eta^5\text{-C}_9\text{H}_7)_2\text{Fe}$	0.05	2.6	13.0
$(\eta^5\text{-C}_9\text{H}_7)_2\text{Co}$	0.11	7.3	10.7
$(\eta^5\text{-C}_9\text{H}_7)_2\text{Ni}$	0.42	13.7	175.0

The iron complex has an 18-electron count at the metal, and consequently no major distortion is expected (or indeed observed). An "extra" electron in the cobalt analogue results in slightly greater distortion, although the ligand is still essentially η^5 -bonded. In both these complexes the indenyl six-membered rings lie *cis* to each other. However, the bis-indenyl nickel complex exhibits quite distinct distortion, with slip and fold parameters somewhere in between those expected for formally η^5 - and η^3 -bonding modes. In addition, the six-membered ring systems are now *trans* to

each other. This can be compared with the $(\text{allyl})_2\text{Ni}$ system, where a *trans* configuration is favoured.⁵³

Analogous complexes of cyclopentadienyl species $(\eta^5\text{-C}_5\text{H}_5)_2\text{M}$, (M = Fe⁵⁴, Co⁵⁵, Ni⁵⁶) all exhibit nearly perfect five-fold symmetry in the solid-state. Addition of electrons to the doubly degenerate M-ring anti-bonding level results in a gradual increase in M-C bond lengths (from 2.046Å in Cp₂Fe to 2.185Å in Cp₂Ni), but not a side-ways slip.

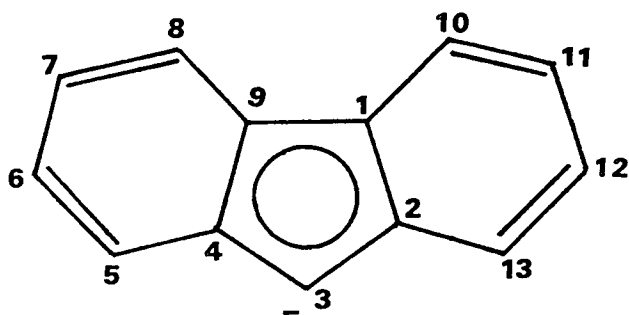
Distortions in the indenyl complexes are obviously fundamentally different, and may be attributed to the fact that the "unused" $p\pi$ orbitals and electrons can be stabilized by entering into the indenyl π system, which is not the case for Cp analogues.

The slippage, and related conformational change of ligands in bis-indenyl complexes can be compared with the Ni^{IV},⁵⁷ Ni^{III},⁵⁸ Ni^{II},⁵⁹ bis-dicarbollyl analogues, where a somewhat similar pattern is observed. In the Ni^{IV} complex the cage carbon atoms are *cisoid* to each other and the metal is essentially symmetrically bonded to both C₂B₃ ligand faces. The d⁸ Ni^{II} bis-dicarbollyl complex has a large lateral slip distortion (*ca.* 0.4Å), and the carbon atoms are *transoid* with respect to each other. The Ni^{III} bis-dicarbollyl species represents an intermediate non-slipped, *transoid* conformation. The reasons for slip distortions in bis-dicarbollyl complexes of d⁸ and d⁹ metals, which have been discussed earlier, are based on optimum overlap of metal and ligand orbitals.

Fluorenyl Metal Complexes

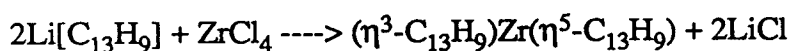
The fluorenyl ligand, [C₁₃H₉]⁻, comprises a five-membered ring and two six-membered rings fused *via* two pairs of ring-junction carbon atoms, C(1), C(2) and

C(4), C(5), given the carbon numbering scheme indicated below:



Considering the propensity of cyclopentadienyl and indenyl ions to form metal complexes, a surprisingly small number of fluorenyl analogues are known.

Those that have been reported are typically synthesised by the reaction of alkali metal fluorenyl with the appropriate metal halide, *e.g.*



Structurally characterized fluorenyl complexes include $(\eta^3\text{-C}_{13}\text{H}_9)(\eta^5\text{-C}_{13}\text{H}_9)\text{ZrCl}_2$,¹¹ $(\eta^5\text{-C}_{13}\text{H}_9)\text{Cr}(\text{CO})_2\text{NO}$ ¹² and $\text{Fe}(\eta^5\text{-C}_5\text{H}_5)(\eta^6\text{-C}_{13}\text{H}_9)$,⁶⁰ which show three possible bonding modes of the fluorenyl ligand.

Slip distortions similar to those found in indenyl metal complexes are found in η^5 and η^3 -fluorenyl systems. For instance in bis-fluorenyl zirconium dichloride Δ^h values for the formally η^5 - and η^3 -bonded ligands are 0.244 and 0.474 Å respectively. In fact, this complex was the first example of trihapto bonding in a planar π -system.

The first reported fluorenyl containing iron complex has an unprecedented "zwitterionic" structure. $\text{FeCp}(\eta^6\text{-C}_{13}\text{H}_9)$ is formed on deprotonation of $[\text{FeCp}(\eta^6\text{-C}_{13}\text{H}_{10})]^+$, where migration of metal coordination from the six- to the

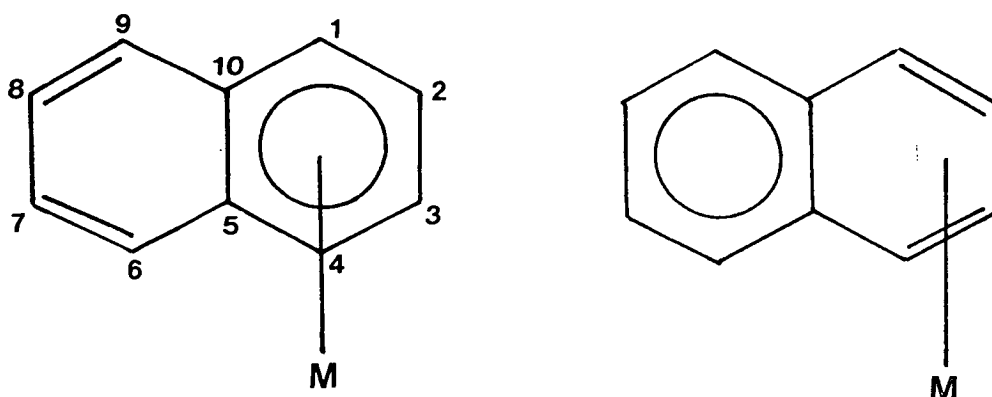
five-membered ring does not occur, as might be expected. This contrasts the facile migration in protonation-deprotonation reactions of $\text{Fe}(\eta^5\text{-C}_9\text{H}_7)_2$.⁶¹



The stability of the unusual zwitterionic fluorenyl structure may be explained in terms of retention of benzenoid character in the six-membered ring.

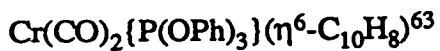
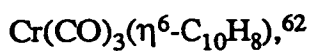
Transition Metal Complexes of Naphthalene

A number of transition metal complexes containing π -bound naphthalene ligands are known. Structural data available for naphthalene complexes illustrate the presence of slip distortions similar to those observed in indenyl complexes. In this case resonance stabilization is facilitated by $\eta^6 \rightarrow \eta^4$ ring slippage, as illustrated below:

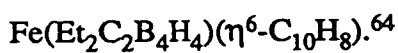


For instance in the recently reported structure of $\text{Ru}(\eta^6\text{-C}_{10}\text{H}_8)(\eta^4\text{-cod})$,¹³ the ring-junction carbon atoms C(5) and C(10) are significantly (*ca.* 0.1 Å) further from the metal than carbons C(1) to C(4), with $\Delta=0.07\text{Å}$. Also apparent is a non-planarity associated with the bonded ring, with an angle of 8.4° between the planes defined by C(1) to C(4) and C(1),C(4),C(5),C(10).

Distortions of a similar type and magnitude have also been observed for



and



Some η^4 -bonded compounds are also known, *e.g.* $\text{Ru}(\eta^6\text{-C}_6\text{Me}_6)(\eta^4\text{-C}_{10}\text{H}_8),^{65}$ and this slippage has occurred with correspondingly large deviation from planarity of the naphthalene ring, with a deformation angle of 41.5° .

Finally, an icosahedral naphthalene containing carbametallaborane, $1-(\eta^6\text{-C}_{10}\text{H}_8)\text{-}2,4\text{-Me}_2\text{-}1,2,4\text{-FeC}_2\text{B}_9\text{H}_9$,²⁴ has been reported, although no structural parameters are available for this complex. Presumably the naphthalene ligand is η^6 -bonded to iron (giving an 18-electron configuration), but the fact that the naphthalene ligand is relatively easily displaced, *e.g.* by CO, can be attributed to relatively facile $\eta^6 \rightarrow \eta^4$ slippage of the bonded six-membered ring system. Thus naphthalene carbametallaboranes might act as useful precursors in the syntheses of potentially interesting molecules. For instance the naphthalene ligand may be displaced by other, non-fused aromatic species, such as amino-acids containing aromatic side-chains (phenylalanine, tyrosine), of possible relevance in the field of Boron-Neutron Capture Therapy (BNCT).

Indenyl Carbametallaboranes

Whilst numerous cyclopentadienyl carbametallaboranes have been synthesised and characterised,⁶⁶ only one indenyl analogue had been synthesised previous to this work.¹⁴ This is the cobalt species $3-(\eta^5\text{-C}_9\text{H}_7)\text{-}3,1,2\text{-}closo\text{-CoC}_2\text{B}_9\text{H}_{11}$ (1), which formed in modest yields upon the reaction of $\text{Li}[\text{C}_9[\text{H}_7]]$, $\text{Co}(\text{acac})_3$ and $\text{Ti}_2[\text{C}_2\text{B}_9\text{H}_{11}]$

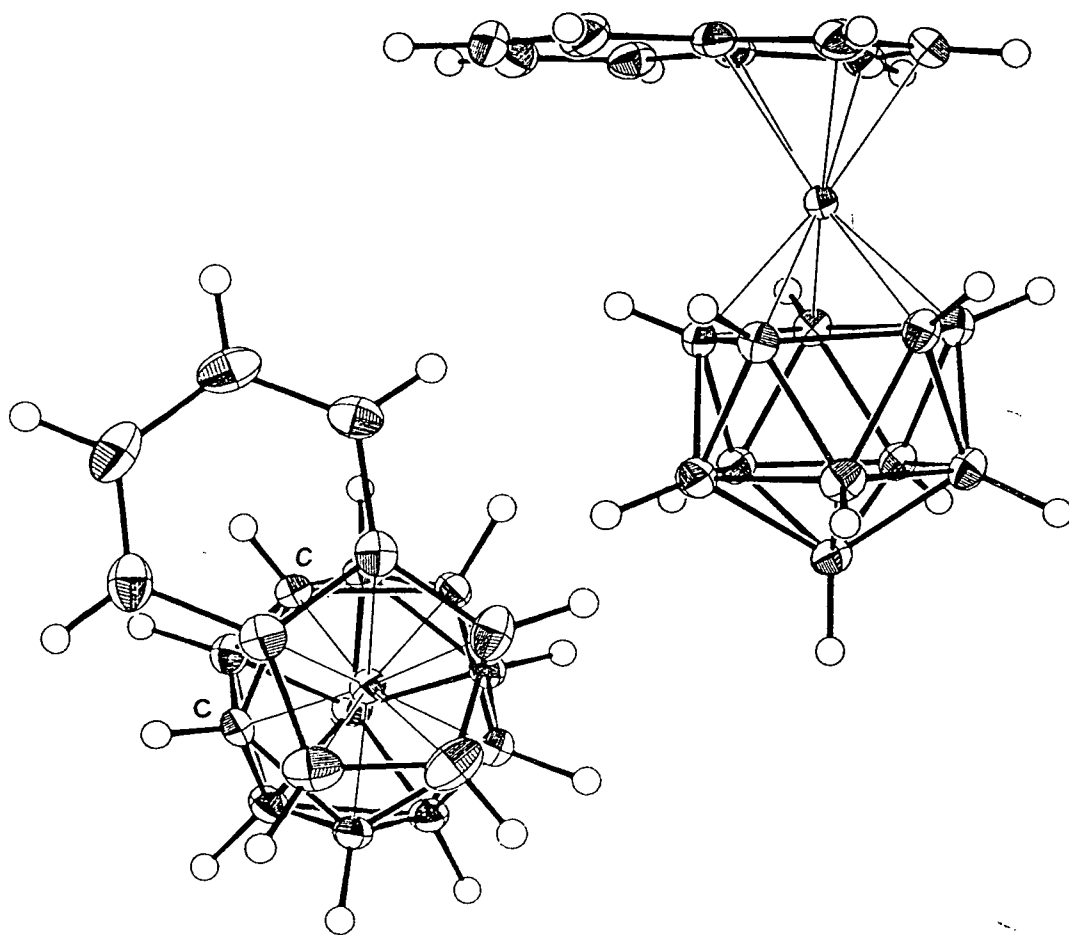
in thf. The synthesis of indenyl carbametallaboranes is of interest for two reasons:

1) To study selective slip distortions - indenyl metal fragment across carbaborane ligand vs carbaborane metal fragment across indenyl ligand, and

2) To study the conformation of metal-bonded ligands with respect to each other.

Both points are considered in the structure of **1**, which was determined crystallographically, as illustrated in Figure 1.2 below. This shows that the metal atom is essentially symmetrically located above the C_2B_3 face ($\Delta P=0.028$), forming the twelfth vertex in the *closo* polyhedron.

Figure 1.2 Perspective and Plan Views of **1**



The C_2B_3 face is slightly folded, with θ^P and ϕ^P values of 0.49 and 2.35° respectively. These modest slip and fold distortions are fully expected for a d^6 metal centre.

Although also formally η^5 -bonded, the indenyl ligand is slightly slipped across the metal atom, such that the metal-C(34,39) distance is longer than the average distance to C(31-33), with $\Delta^h = 0.089\text{\AA}$.

The conformation of the indenyl ligand with respect to polyhedral carbon atoms is *cisoid*. The hydrocarbon ligand is staggered with respect to the carbaborane face, which is easily explained by the fact that the *exo*-hydrogen atoms on the cage are elevated at an angle of *ca.* 26° above the upper pentagonal belt. An eclipsed arrangement would increase steric interaction between *exo*-hydrogen atoms and the hydrocarbon ring H atoms, which is clearly unfavourable.

The *cisoid* conformation can be explained in the same terms as those used to discuss the observed conformation in other transition metal complexes containing the indenyl ligand.⁹ That is that the presence of ligands of greatest *trans* influence opposite the ring-junction atoms can compensate for relatively weak bonding to metal of the latter, by virtue of partial delocalisation of their $p\pi$ atomic orbitals into the indenyl six-membered ring π -system. The *trans* influence of the facial boron atoms of $[C_2B_9H_{11}]^{2-}$ is greater than that of the carbon atoms, as the frontier orbitals of the *nido*-carbaborane ligand are localized on the boron atoms.²⁵ Thus the observed *cisoid* conformation is readily understood.

Scope of the Work Presented

The studies presented in this thesis primarily investigate the conformations adopted by carbametallaboranes derived from dicarbollyl ligands in which bulky alkyl or aryl substituents have been introduced at the cage carbon atoms. Initially, this work centred upon species containing fused aromatic systems, with the attempted syntheses of a number of cobalt and rhodium analogues of the previously reported indenyl carbacobaltaborane, **1**.

During the course of these studies, the more general transition metal chemistry of the *nido* cage derivative of diphenylcarbaborane, 1,2-Ph₂-1,2-*closo*-C₂B₁₀H₁₀, developed into an area of unprecedented interest, and this forms the subject of the later work.

In an industrial context, some substantial research has been directed towards a family of carboradaboranes incorporating bulky cage substituents, which are potentially effective catalysts in, for example, alkene hydrogenation and isomerisation.⁶⁷ Thus the work discussed herein may be of some significance in these, and related, studies.

Chapter 2

Fused Aromatic Carbacobaltaboranes

Section A : Indenyl Carbacobaltaboranes

Introduction

The synthesis and structural characterisation of an indenyl carbametallaborane, namely 3-(η^5 -C₉H₇)-3,1,2-*closo*-CoC₂B₉H₁₁ (1), was first reported in 1986.¹⁴ The conformation observed in the solid state structure, in which the ring junction carbon atoms of the indenyl ligand are *cisoid* with respect to the cage carbon atoms, has been shown to be electronically preferred by the results of molecular orbital calculations, as already outlined in Chapter 1.

This Chapter details the resulting molecular conformations in a series of analogous indenyl carbacobaltaboranes, where bulky alkyl or aryl functions have been introduced at the cage carbon atoms. In such cases electronic preferences may come into competition with steric effects introduced by these cage substituents. Two monosubstituted derivatives, and one disubstituted derivative, have been synthesised and spectroscopically and structurally characterised. In addition the observed orientation of the indenyl ligand with respect to the cage has in each case been compared with the theoretically calculated minimum energy conformation.

1-Ph-3-(η^5 -C₉H₇)-3,1,2-closo-CoC₂B₉H₁₀, (2)

Synthesis of 2

Compound 2 was formed during the reaction of Tl₂[7-Ph-7,8-C₂B₉H₁₀] with LiC₉H₇ and Co(acac)₃ in thf, and was isolated as an orange solid by preparative thin layer chromatography (tlc), as described in Chapter 5.

Microanalysis figures were consistent with the proposed formulation of the compound.

N.m.r. Studies

The ¹¹B-({¹H}) n.m.r. spectrum shows 8 signals, with 2 boron nuclei resonating coincidentally, consistent with the low symmetry of the monosubstituted cage. As anticipated, all boron atoms exhibit coupling to an *exo*-polyhedral hydrogen atom in the proton coupled spectrum, with ¹J_{BH} in the region of 120-150Hz.

The ¹H spectrum cannot be so readily interpreted. At 298K the spectrum contains resonances due to H(2) (2.51p.p.m.) and 7 indenyl protons, but only 3 phenyl protons. In view of this inconsistency the high frequency region of the spectrum was monitored as a function of decreasing temperature, and proton resonances were assigned by a series of selective decoupling experiments.

All proton resonances except those of H(12), H(13), H(15) and H(16) can be assigned at 298K. H(13) and H(15) were distinguished as a result of decoupling H(16) at 185K, with the signal due to H(15) collapsing from an apparent triplet to a doublet. There is one coincidence at 185K, at *ca.* 7.3 p.p.m., involving H(13) and H(14). A complete list of ¹H assignments at 298K and 185K is given in Table 2.1. (For atom labelling see Figure 2.3)

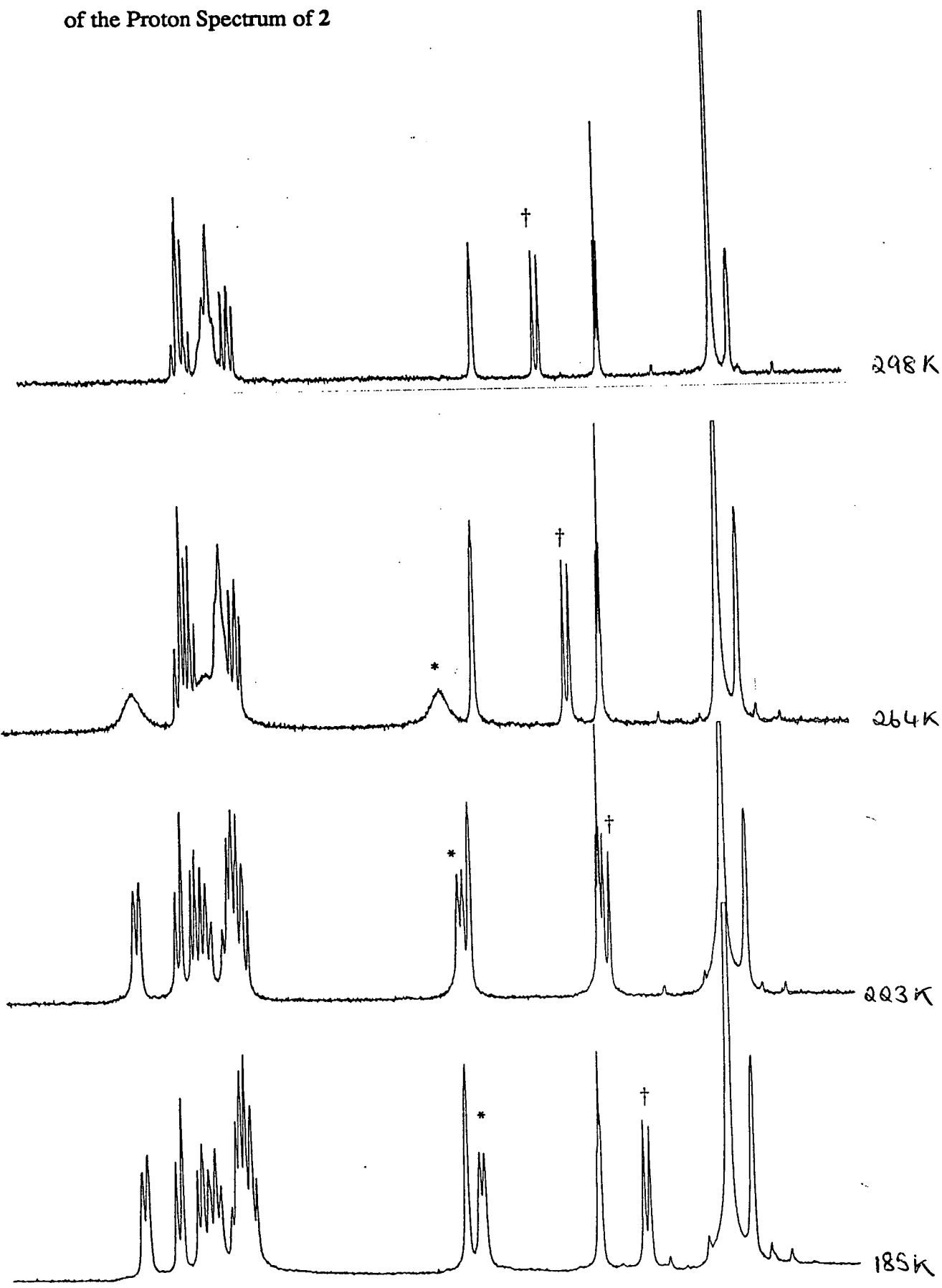
Table 2.1 Chemical Shifts (p.p.m.) and Assignments in the High Frequency Region of the ^1H Spectra of **2**, at 298K and 185K

H Atom	$\delta(298\text{K})$	$\delta(185\text{K})$
H(31)	6.30	6.40
H(32)	5.79	5.85
H(33)	5.26	5.23
H(35)	6.04	5.66
H(36)	7.28	7.26
H(37)	7.46	7.44
H(38)	7.50	7.55
H(13)	7.3 - 7.4	<i>ca.</i> 7.3
H(14)	7.3 - 7.4	<i>ca.</i> 7.3
H(15)	7.3 - 7.4	7.40
H(12)	-	6.34
H(16)	-	7.68

The decoupling experiments also bring to notice a number of fine couplings. So called zig-zag coupling occurs between H(33) and H(38), and H(31) and H(35), with $^5J_{\text{HH}}$ in the region of 1 Hz. W-coupling is also present between H(31) and H(33), with a similar coupling constant.

The high frequency region of the spectrum has been monitored as a function of decreasing temperature, and the results of these experiments are presented in **Figure 2.1**. Although H(12) and H(16) are not observed at 298K, broad signals due to them begin to appear at 264K, and by 223K each has been resolved into a doublet. In addition, the signal due to H(13) and H(15) broadens at 264K and is resolved into 2 distinct resonances at lower temperatures. It must also be noted that resonances due to H(12) and H(35), marked * and † respectively on **Figure 2.1**, move progressively to lower frequency as the temperature is lowered.

Figure 2.1 Variable Temperature N.M.R. Experiment on the High Frequency Region of the Proton Spectrum of **2**



The n.m.r. studies are consistent with restricted rotation of the phenyl substituent about the C(1)-C(11) axis on progressive cooling of the solution. Let us first consider the movement of resonances due to H(12) and H(35) to lower frequency at lower temperatures. It will be useful to refer to Figure 2.3 for their positions in the crystallographically determined structure, presumably the preferred conformation in the solid state (see later in this section). If this is indeed also the preferred conformation in solution as the temperature decreases, the rotation of the phenyl ring will become increasingly restricted by the presence of the indenyl ligand, lying *cisoid* with respect to the cage carbon atoms. Hence H(12) and H(35) will experience magnetic anisotropy of the C(34)-C(39) and C(11)-C(16) ring systems respectively, which explains the upfield progression of their resonances as the system is cooled.

Further evidence for restricted rotation of the pendent phenyl group lies in the fact that the *ortho* and *meta* hydrogen atoms of the ring undergo coalescence as the solution is cooled. If the phenyl group is rotating rapidly, both H(12) and H(16) (*ortho* hydrogen atoms) and H(13) and H(15) (*meta* hydrogen atoms) will be chemically equivalent to each other, and only one signal for each pair will be observed. However, should rotation be restricted, they will cease to be chemically equivalent, and each hydrogen will exhibit independent signals.

The *ortho* hydrogen atoms, H(12) and H(16) initially appear at 264K, as two broad signals which are resolved into two doublets at 223K. 298K is presumably close to coalescence temperature, as the two broad resonances have become one, which is now so broad that it is not observed above the base line. A single resolved resonance can presumably be expected for the two hydrogen atoms upon further warming of the system, as the phenyl substituent is able to rotate freely, these two then becoming chemically equivalent. Similarly, the single resonance for H(13) and H(15) at 298K is resolved into two distinct resonances at 223K, coalescence for the 2 *meta* hydrogen atoms occurring at *ca.* 264K.

Structural Study on 2

Introduction

An accurate, low temperature X-ray crystal diffraction experiment was carried out in order to investigate the effect of cage substitution on the molecular conformation. Diffraction quality crystals were grown by slow diffusion of n-hexane into a methylene chloride solution of the compound at -30°C. Details of crystallographic procedures and crystal data may be found in Section B of Chapter 5.

Discussion

Perspective and plan views of 2 are shown in **Figure 2.2** and **Figure 2.3** respectively, with the appropriate molecular numbering scheme. All H atoms have the same number as the B or C atom to which they are bound. **Table 2.2** gives final atomic co-ordinates for refined atoms, **Table 2.3** bond distances and selected interbond angles, and **Table 2.4** lists anisotropic thermal parameters.

It is immediately obvious from **Figure 2.3** that the indenyl six membered ring is *cisoid* with respect to the cage carbon atoms, and hence substitution of a hydrogen atom by a phenyl group at C(1) does not significantly change the conformation from that observed for 1.

Figure 2.2 Perspective View of 1-Ph-3-(η^5 -C₉H₇)-3,1,2-closo-CoC₂B₉H₁₀, (2)

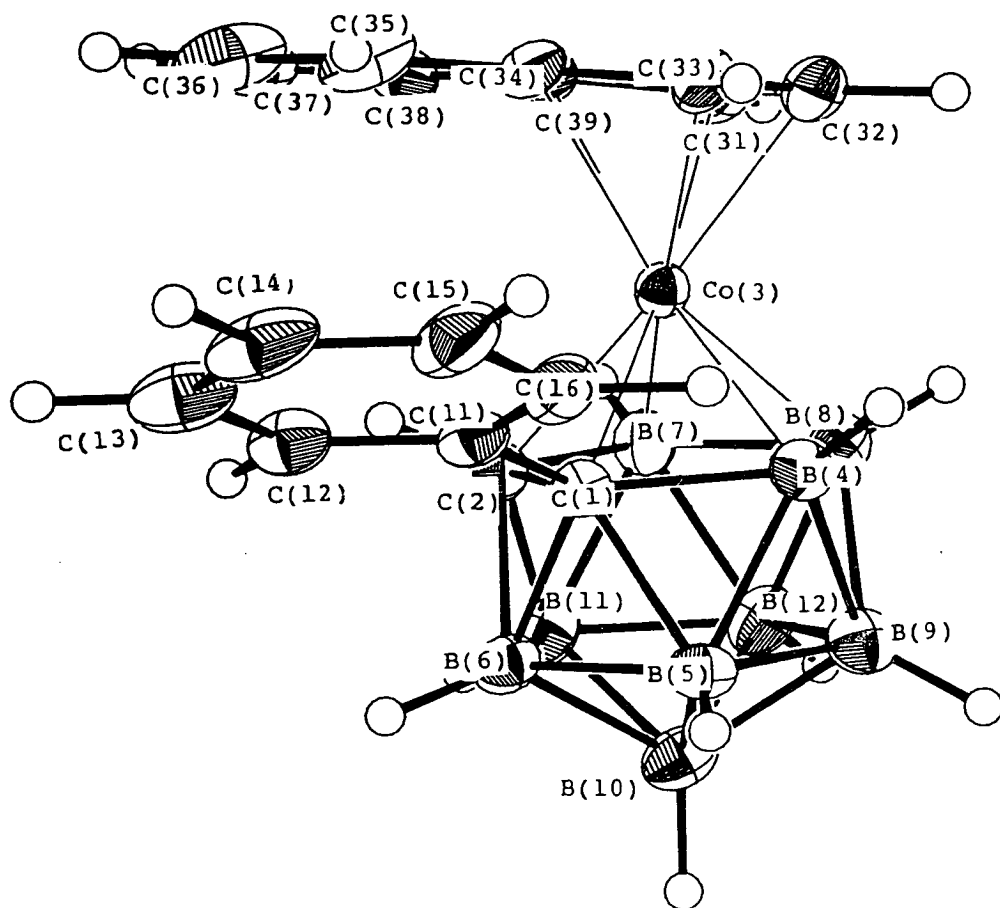


Figure 2.3 Plan View of 1-Ph-3-(η^5 -C₉H₇)-3,1,2-closo-CoC₂B₉H₁₀ (2) (B(5), B(6), B(9), B(10), B(11) and B(12) removed for clarity)

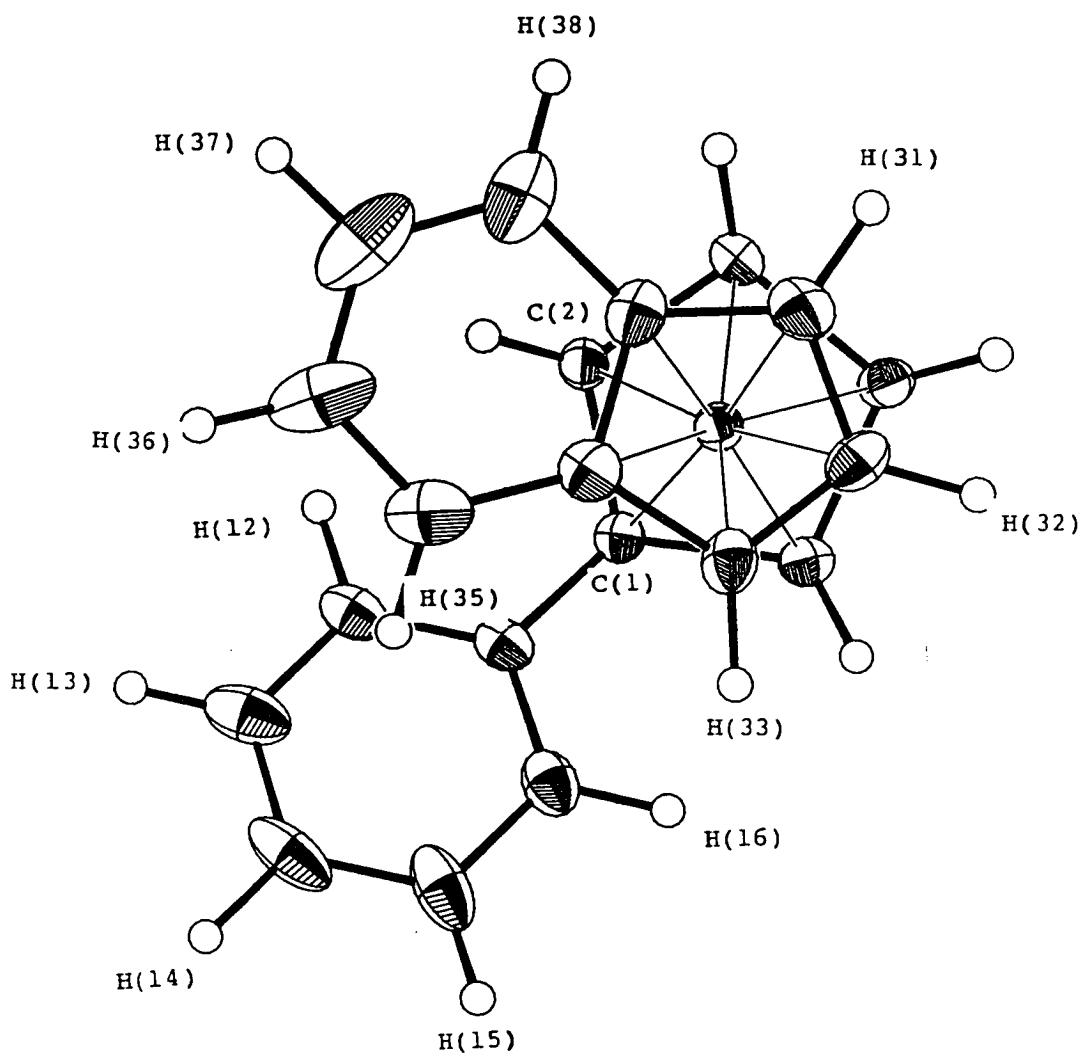


Table 2.2 Co-ordinates of Refined Atoms and Equivalent Isotropic Thermal Parameters (\AA^2) for 1-Ph-3-(η^5 -C₉H₇)-3,1,2-*closo*-CoC₂B₉H₁₀. (2)

	x	y	z	Ueq
C(1)	0.24792(20)	0.32281(24)	0.28358(20)	0.0251(19)
C(2)	0.30718(21)	0.41553(25)	0.27690(20)	0.0257(20)
Co(3)	0.30772(3)	0.29205(3)	0.21093(3)	0.0231(3)
B(4)	0.30644(25)	0.2129(3)	0.31007(24)	0.0282(23)
B(5)	0.2886(3)	0.2831(3)	0.38692(24)	0.0291(23)
B(6)	0.2879(3)	0.4125(3)	0.36373(24)	0.0309(25)
B(7)	0.40671(25)	0.3778(3)	0.29732(25)	0.0305(24)
B(8)	0.4104(3)	0.2461(3)	0.32195(25)	0.0300(24)
B(9)	0.3906(3)	0.2356(3)	0.4118(3)	0.034(3)
B(10)	0.3789(3)	0.3601(3)	0.44467(25)	0.034(3)
B(11)	0.3872(3)	0.4469(3)	0.37312(25)	0.0318(25)
B(12)	0.4530(3)	0.3386(3)	0.4047(3)	0.0323(25)
C(11)	0.15309(20)	0.3286(3)	0.23316(19)	0.0281(20)
C(12)	0.11082(22)	0.4201(3)	0.20741(21)	0.0340(23)
C(13)	0.02383(24)	0.4232(4)	0.16288(22)	0.045(3)
C(14)	-0.02276(24)	0.3345(4)	0.14259(22)	0.048(3)
C(15)	0.01873(25)	0.2423(4)	0.16754(22)	0.046(3)
C(16)	0.10686(23)	0.2386(3)	0.21340(21)	0.0351(23)
C(33)	0.23109(23)	0.2026(3)	0.10938(20)	0.0324(22)
C(32)	0.31771(24)	0.1813(3)	0.13706(22)	0.0347(23)
C(31)	0.35882(23)	0.2709(3)	0.13057(21)	0.0358(24)
C(39)	0.29575(23)	0.3477(3)	0.09311(20)	0.0335(23)
C(38)	0.3008(3)	0.4511(3)	0.07369(24)	0.051(3)
C(37)	0.2270(4)	0.5064(3)	0.0413(3)	0.065(4)
C(36)	0.1497(3)	0.4642(4)	0.02926(24)	0.058(3)
C(35)	0.1419(3)	0.3655(3)	0.04713(22)	0.0427(25)
C(34)	0.21622(22)	0.3058(3)	0.08028(19)	0.0311(21)

Table 2.3 Interatomic Distances (Å) and Selected Interbond Angles (°) for

1-Ph-3-(η^5 -C₉H₇)-3,1,2-closo-CoC₂B₉H₁₀ (2)

C(1) -Co(3)	2.047(4)	B(7) -B(11)	1.783(6)
C(1) - B(4)	1.719(5)	B(7) -B(12)	1.775(6)
C(1) - B(5)	1.719(5)	B(8) - B(9)	1.787(6)
C(1) - B(6)	1.734(5)	B(8) -B(12)	1.791(6)
C(1) -C(11)	1.506(5)	B(9) -B(10)	1.785(6)
C(2) -Co(3)	2.008(4)	B(9) -B(12)	1.791(6)
C(2) - B(6)	1.724(5)	B(10) -B(11)	1.764(6)
C(2) - B(7)	1.707(6)	B(10) -B(12)	1.776(6)
C(2) -B(11)	1.702(6)	B(11) -B(12)	1.766(6)
Co(3) - B(4)	2.054(4)	C(11) -C(12)	1.384(5)
Co(3) - B(7)	2.065(4)	C(11) -C(16)	1.393(5)
Co(3) - B(8)	2.075(4)	C(12) -C(13)	1.378(6)
Co(3) -C(33)	2.064(4)	C(13) -C(14)	1.383(6)
Co(3) -C(32)	2.023(4)	C(14) -C(15)	1.385(6)
Co(3) -C(31)	2.026(4)	C(15) -C(16)	1.397(6)
Co(3) -C(39)	2.133(4)	C(33) -C(32)	1.412(5)
Co(3) -C(34)	2.150(4)	C(33) -C(34)	1.436(5)
B(4) - B(5)	1.790(6)	C(32) -C(31)	1.420(5)
B(4) - B(8)	1.811(6)	C(31) -C(39)	1.429(5)
B(4) - B(9)	1.769(6)	C(39) -C(38)	1.419(6)
B(5) - B(6)	1.754(6)	C(39) -C(34)	1.434(5)
B(5) - B(9)	1.770(6)	C(38) -C(37)	1.375(7)
B(5) -B(10)	1.776(6)	C(37) -C(36)	1.404(7)
B(6) -B(10)	1.744(6)	C(36) -C(35)	1.361(7)
B(6) -B(11)	1.752(6)	C(35) -C(34)	1.414(6)
B(7) - B(8)	1.785(6)	C(1) - C(2)	1.651(5)
Co(3) - C(1) - B(4)	65.42(18)	B(4) - B(9) - B(5)	60.78(25)
B(4) - C(1) - B(5)	62.77(23)	B(4) - B(9) - B(8)	61.25(25)
B(5) - C(1) - B(6)	61.05(23)	B(5) - B(9) -B(10)	59.92(25)
Co(3) - C(2) - B(7)	67.00(19)	B(8) - B(9) -B(12)	60.07(25)
B(6) - C(2) -B(11)	61.50(24)	B(10) - B(9) -B(12)	59.5(3)
B(7) - C(2) -B(11)	63.08(24)	B(5) -B(10) - B(6)	59.78(25)
C(33) -Co(3) -C(32)	40.41(15)	B(5) -B(10) - B(9)	59.60(25)
C(33) -Co(3) -C(34)	39.79(14)	B(6) -B(10) -B(11)	59.92(25)
C(32) -Co(3) -C(31)	41.06(15)	B(9) -B(10) -B(12)	60.4(3)
C(31) -Co(3) -C(39)	40.11(15)	B(11) -B(10) -B(12)	59.86(25)
C(39) -Co(3) -C(34)	39.11(14)	C(2) -B(11) - B(6)	59.85(23)
C(1) -Co(3) - C(2)	48.04(14)	C(2) -B(11) - B(7)	58.58(23)
C(1) -Co(3) - B(4)	49.55(15)	B(6) -B(11) -B(10)	59.46(25)
C(2) -Co(3) - B(7)	49.52(16)	B(7) -B(11) -B(12)	60.01(25)
B(4) -Co(3) - B(8)	52.05(17)	B(10) -B(11) -B(12)	60.4(3)
B(7) -Co(3) - B(8)	51.08(17)	B(7) -B(12) - B(8)	60.07(25)
C(1) - B(4) -Co(3)	65.02(18)	B(7) -B(12) -B(11)	60.47(25)
C(1) - B(4) - B(5)	58.61(22)	B(8) -B(12) - B(9)	59.84(25)
Co(3) - B(4) - B(8)	64.58(19)	B(9) -B(12) -B(10)	60.1(3)
B(5) - B(4) - B(9)	59.62(24)	B(10) -B(12) -B(11)	59.74(25)
B(8) - B(4) - B(9)	59.86(24)	C(1) -C(11) -C(12)	122.1(3)
C(1) - B(5) - B(4)	58.61(22)	C(1) -C(11) -C(16)	118.5(3)
C(1) - B(5) - B(6)	59.92(23)	C(12) -C(11) -C(16)	119.4(3)
B(4) - B(5) - B(9)	59.59(24)	C(11) -C(12) -C(13)	120.9(4)

B(6) - B(5) -B(10)	59.21(24)	C(12) -C(13) -C(14)	120.3(4)
B(9) - B(5) -B(10)	60.48(25)	C(13) -C(14) -C(15)	119.5(4)
C(1) - B(6) - C(2)	57.04(21)	C(14) -C(15) -C(16)	120.5(4)
C(1) - B(6) - B(5)	59.03(23)	C(11) -C(16) -C(15)	119.5(4)
C(2) - B(6) -B(11)	58.65(23)	C(32) -C(33) -C(34)	107.8(3)
B(5) - B(6) -B(10)	61.01(25)	C(33) -C(32) -C(31)	108.9(3)
B(10) - B(6) -B(11)	60.61(25)	C(32) -C(31) -C(39)	107.8(3)
C(2) - B(7) -Co(3)	63.48(19)	C(31) -C(39) -C(38)	132.2(4)
C(2) - B(7) -B(11)	58.34(23)	C(31) -C(39) -C(34)	107.8(3)
Co(3) - B(7) - B(8)	64.73(20)	C(38) -C(39) -C(34)	119.9(3)
B(8) - B(7) -B(12)	60.40(25)	C(39) -C(38) -C(37)	117.2(4)
B(11) - B(7) -B(12)	59.52(25)	C(38) -C(37) -C(36)	122.1(5)
Co(3) - B(8) - B(4)	63.37(19)	C(37) -C(36) -C(35)	122.6(5)
Co(3) - B(8) - B(7)	64.19(20)	C(36) -C(35) -C(34)	117.1(4)
B(4) - B(8) - B(9)	58.89(24)	C(33) -C(34) -C(39)	107.6(3)
B(7) - B(8) -B(12)	59.52(24)	C(33) -C(34) -C(35)	131.4(3)
B(9) - B(8) -B(12)	60.09(25)	C(39) -C(34) -C(35)	121.0(3)
Co(3) - C(1) - C(2)	64.73(17)	C(2) - C(1) - B(6)	61.15(22)
Co(3) - C(2) - C(1)	67.23(17)	C(1) - C(2) - B(6)	61.81(22)

Table 2.4 Anisotropic Thermal Parameters (\AA^2) for 1-Ph-3-($\eta^5\text{-C}_9\text{H}_7$)-3,1,2-closo- $\text{CoC}_2\text{B}_9\text{H}_{10}$, (2)

	U11	U22	U33	U23	U13	U12
C(1)	0.0238(17)	0.0233(17)	0.0222(15)	-0.0003(13)	0.0104(14)	-0.0007(14)
C(2)	0.0229(18)	0.0219(16)	0.0252(17)	-0.0002(13)	0.0097(15)	-0.0015(14)
Co(3)	0.0213(3)	0.0212(2)	0.0217(2)	-0.0014(2)	0.0105(2)	-0.0006(2)
B(4)	0.0269(20)	0.0245(18)	0.0270(19)	0.0014(16)	0.0134(17)	0.0027(17)
B(5)	0.0297(21)	0.0285(20)	0.0224(18)	0.0039(15)	0.0121(17)	0.0047(17)
B(6)	0.0335(23)	0.0279(20)	0.0239(19)	-0.0025(16)	0.0131(18)	0.0037(18)
B(7)	0.0217(20)	0.0306(21)	0.0321(21)	-0.0005(17)	0.0123(18)	-0.0005(17)
B(8)	0.0282(22)	0.0254(19)	0.0288(20)	-0.0019(16)	0.0124(18)	0.0031(18)
B(9)	0.0353(23)	0.0283(22)	0.0308(21)	0.0048(16)	0.0144(19)	0.0087(18)
B(10)	0.0301(23)	0.0367(23)	0.0255(20)	-0.0020(17)	0.0092(18)	0.0071(18)
B(11)	0.0277(22)	0.0272(21)	0.0305(21)	-0.0043(17)	0.0086(18)	0.0020(18)
B(12)	0.0216(21)	0.0354(22)	0.0296(21)	-0.0033(18)	0.0051(18)	0.0034(18)
C(11)	0.0237(18)	0.0355(18)	0.0201(16)	-0.0019(14)	0.0111(15)	0.0007(15)
C(12)	0.0240(19)	0.0440(22)	0.0266(18)	0.0011(16)	0.0102(16)	0.0033(16)
C(13)	0.0313(22)	0.0670(29)	0.0275(19)	0.0047(19)	0.0114(18)	0.0147(21)
C(14)	0.0194(19)	0.0924(35)	0.0232(19)	-0.0033(21)	0.0045(16)	0.0006(22)
C(15)	0.0322(22)	0.0722(30)	0.0265(20)	-0.0131(19)	0.0122(18)	-0.0203(22)
C(16)	0.0289(19)	0.0421(22)	0.0274(18)	-0.0076(15)	0.0132(16)	-0.0080(17)
C(33)	0.0342(20)	0.0309(19)	0.0248(17)	-0.0086(15)	0.0140(16)	-0.0070(16)
C(32)	0.0417(22)	0.0259(18)	0.0288(18)	-0.0056(14)	0.0185(18)	0.0011(16)
C(31)	0.0322(20)	0.0429(23)	0.0274(18)	-0.0060(15)	0.0184(16)	-0.0032(16)
C(39)	0.0415(22)	0.0294(19)	0.0239(17)	-0.0044(14)	0.0196(17)	-0.0053(16)
C(38)	0.0743(32)	0.0363(22)	0.0323(20)	-0.0016(17)	0.0301(22)	-0.0133(23)
C(37)	0.1100(44)	0.0312(22)	0.0336(23)	0.0069(18)	0.0317(28)	0.0098(27)
C(36)	0.0741(35)	0.0538(28)	0.0289(21)	0.0031(19)	0.0171(22)	0.0302(26)
C(35)	0.0416(23)	0.0532(25)	0.0215(18)	-0.0033(17)	0.0081(17)	0.0134(20)
C(34)	0.0311(19)	0.0357(19)	0.0198(16)	-0.0054(14)	0.0111(15)	-0.0011(16)

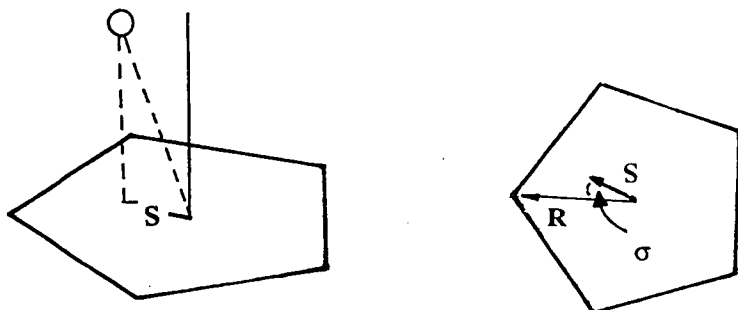
A number of geometrical calculations were carried out, all related to the lower, more planar, pentagonal belt of the icosahedral cage of **2** [B(5), B(6), B(11), B(12), B(9)]. The phenyl substituent subtends an elevation angle at C(1) of 21.6°, resulting in a distance of only 2.82Å between H(35) and the best (least-squares) plane through the C(11)-C(16) ring. Given that the sum of the van der Waals radius for a hydrogen atom (1.2Å) and the thickness of a benzene ring (1.675Å) is close to this value, it is to be expected that significant ring current effects are experienced by H(35) in low temperature n.m.r. studies. In addition the phenyl group is twisted by *ca.* 9.0° about the C(1)-C(11) bond, such that C(16) is more elevated than C(12). This phenomenon may be explained in terms of a reduction of close non-bonded contacts between H(16)···H(4) and H(12)···H(2). In the observed structure these values are 2.12(4) and 2.23(3)Å respectively, close to the sum of the van der Waals radii of 2 hydrogen atoms (2.4Å).

The best plane through the indenyl ligand makes a dihedral angle of *ca.* 7.4° with the lower B₅ belt. However, this angle comprises both a sideways "twist" of *ca.* 5.1°, where C(35) is more elevated than C(38), and an upward "tilt" of *ca.* 4.7°, with C(36) lying at a higher elevation than C(34). These values may be attributed to the presence of the phenyl substituent on C(1), equivalent "twist" and "tilt" angles in the unsubstituted compound (**1**) being significantly smaller (*ca.* 3.7 and 0.6° respectively.) Therefore, although the presence of the pendent phenyl group has not forced the indenyl ligand to adopt an entirely different conformation with respect to the C₂B₃ face, it has necessitated the adoption of a subtly different molecular structure.

The top face of the carbaborane cage is envelope folded across the B(4)···B(7) vector, such that B(4) and B(7) lie at higher elevation than B(8), C(1) and C(2), resulting in ϕ^P and θ^P values of 0.42 and 1.73° respectively. As expected there is no substantial slip of the d⁶ metal atom across this face ($\Delta^P = 0.035\text{Å}$). However, a more

substantial slip is observed w.r.t the indenyl ligand, with the cobalt atom slipped away from the ring-junction carbon atoms towards C(32) ($\Delta^h = 0.118\text{\AA}$). The slip parameter is slightly higher than that observed in **1**, reflecting the already mentioned side-ways twist and upward tilt of the indenyl ligand. The five-membered ring is slightly folded about the C(31)–C(33) vector ($\Omega = 3.53^\circ$). Definitions for the angles ϕ^P and θ^P ,³⁴ together with the slip parameters Δ^P ,⁷ Δ^h ,⁹ are given in Chapter 1.

In addition to these parameters, the direction of the slip distortion may be formally defined by σ , which is the angle between the slip vector, S (a vector connecting the projection of the metal atom onto the plane through the indenyl five-membered ring and the ring centroid), and a reference vector, R [where R is the vector from the ring centroid to the unique atom C(2)].



σ is assigned a positive value when S points towards C(31) (or is anticlockwise w.r.t. R when seen from above). In **2** the value of σ is $+15.1^\circ$, which is close to the value observed in the structure of **1** ($+16.6^\circ$).

Although the slippage of the metal away from C(34) and C(39) presumably allows for greater electron delocalisation over the indenyl six-membered ring, the latter still exhibits distinct non-aromatic character, with two carbon-carbon distances [C(35)–C(36) and C(37)–C(38)] significantly shorter than the others, giving a butadiene-like carbon atom sequence. The bond distances are essentially the same as those observed in the indenyl six-membered ring of **1**.

1-CH₂OCH₃-3-(η^5 -C₉H₇)-3,1,2-closo-6,2-C₂B₉H₁₀, (3)

Synthesis

Compound 3, the monoether derivative of 1, was formed similarly to 1 and 2, by stirring, in this case, Ti₂[7-(CH₂OCH₃)-7,8-C₂B₉H₁₀] with LiC₉H₇ and Co(acac)₃ in thf, the pure species being again isolated in fairly modest yield by preparative tlc. Full details may be found in Section A of Chapter 5.

N.m.r. Studies

The ¹¹B n.m.r. spectrum shows nine signals of equal integral, all boron atoms showing the expected coupling to *exo*-polyhedral hydrogen atoms in the proton coupled spectrum. These results are fully consistent with the proposed compound, where all boron nuclei are chemically inequivalent.

The ¹H spectrum exhibits the expected signals for the indenyl hydrogen atoms in the high frequency region, and for H(2), at δ 2.52 p.p.m. The CH₂ group of the pendent ether function gives rise to a so-called AB pattern, as its hydrogen atoms can never be magnetically equivalent, but are nearly so, and two independent doublet resonances are observed. The methyl hydrogen atoms give the expected singlet resonance at δ 3.53 p.p.m.

Structural Study on 3

Introduction

Brick red crystals suitable for diffraction were grown by slow diffusion of hexane into a dichloromethane solution at -30°C. Details of the crystallographic procedures and crystal data for the structure are detailed in Chapter 5, Section B.

Discussion

Perspective and plan views of **3** are shown in **Figure 2.4** and **Figure 2.5** respectively, together with the appropriate numbering scheme. All indenyl and cage hydrogen atoms have the same number as the B or C atom to which they are bound.

Table 2.5 lists final atomic co-ordinates for all atoms, **Table 2.6** bond distances and selected interbond angles, and **Table 2.7** anisotropic thermal parameters for all non hydrogen atoms.

Figure 2.5 gives a clear view of the conformation of the indenyl ligand with respect to the metal-bonded carbaborane face. As in **2**, the presence of one substituent, in this case an ether function, has not caused a significant change in conformation; the ring junction carbon atoms are still *cisoid* with respect to the cage carbon atoms.

A notable feature, best represented in **Figure 2.4**, is the unexpected position of the ether oxygen atom, which lies above the metal-bonded C_2B_3 face, with a significant twist at C(11). The torsion angle C(1)-C(11)-O(1)-C(12) has a value of 94.27° , compared with near 180° torsions for the ether functions in the diether derivative, **4** (see later). The former may be traced to an intramolecular interligand hydrogen bond, O(1)····H(33), the distance between the two atoms being $2.544(22)\text{\AA}$. This value is within the range of typical hydrogen bond distances, between 2.4 and 2.9\AA .²⁶ Moreover, the angles H(33)····O(1)-C(11) and H(33)····O(1)-C(12) are $112.7(5)$ and $122.7(5)^\circ$ respectively.

Figure 2.4 Perspective View of 1-CH₂OCH₃-3-(η^5 -C₉H₇)-3,1,2-closo-6-Co₂B₉H₁₀

(3)

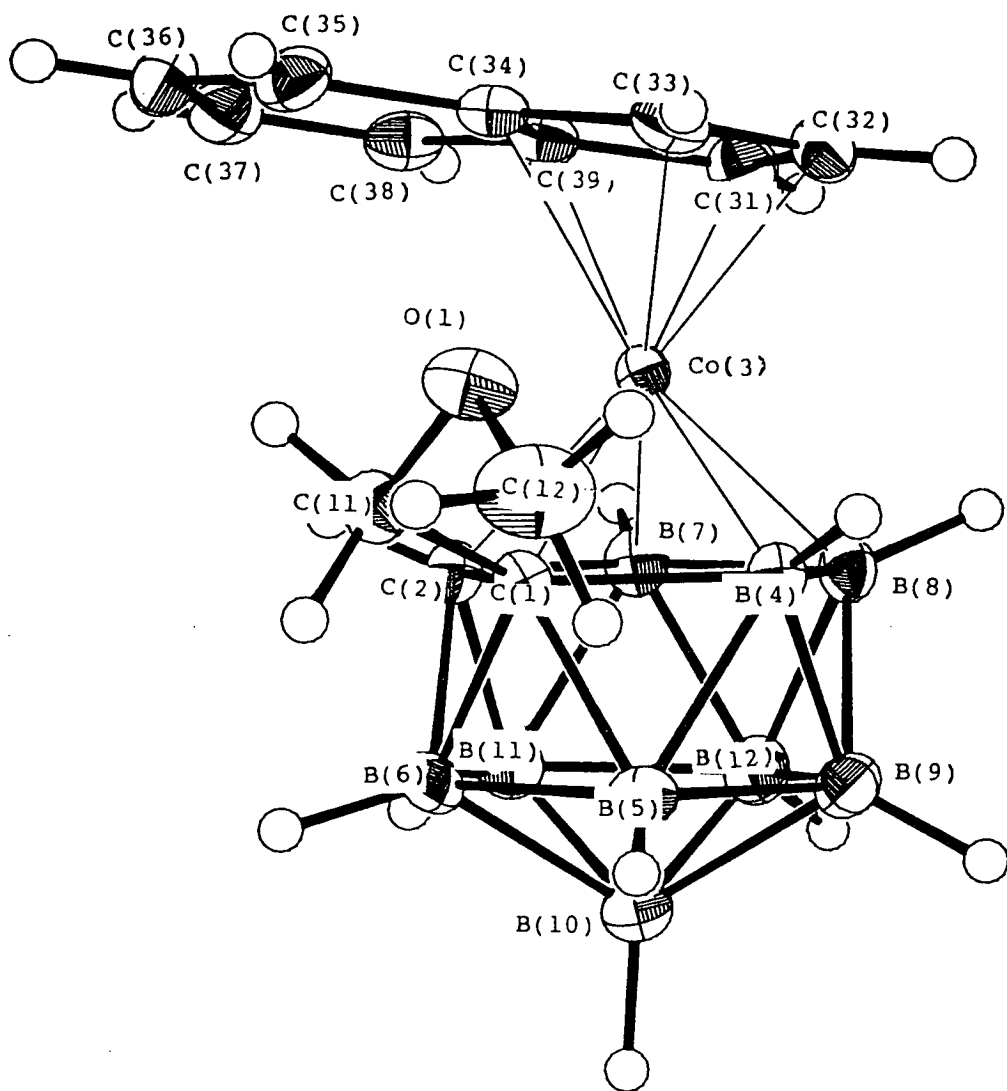


Figure 2.5 Plan View of 1-CH₂OCH₃-3-(η^5 -C₉H₇)-3,1,2-closo-6(B₉H₁₀) (3) (B(5), B(6), B(9), B(10), B(11) and B(12) removed for clarity)

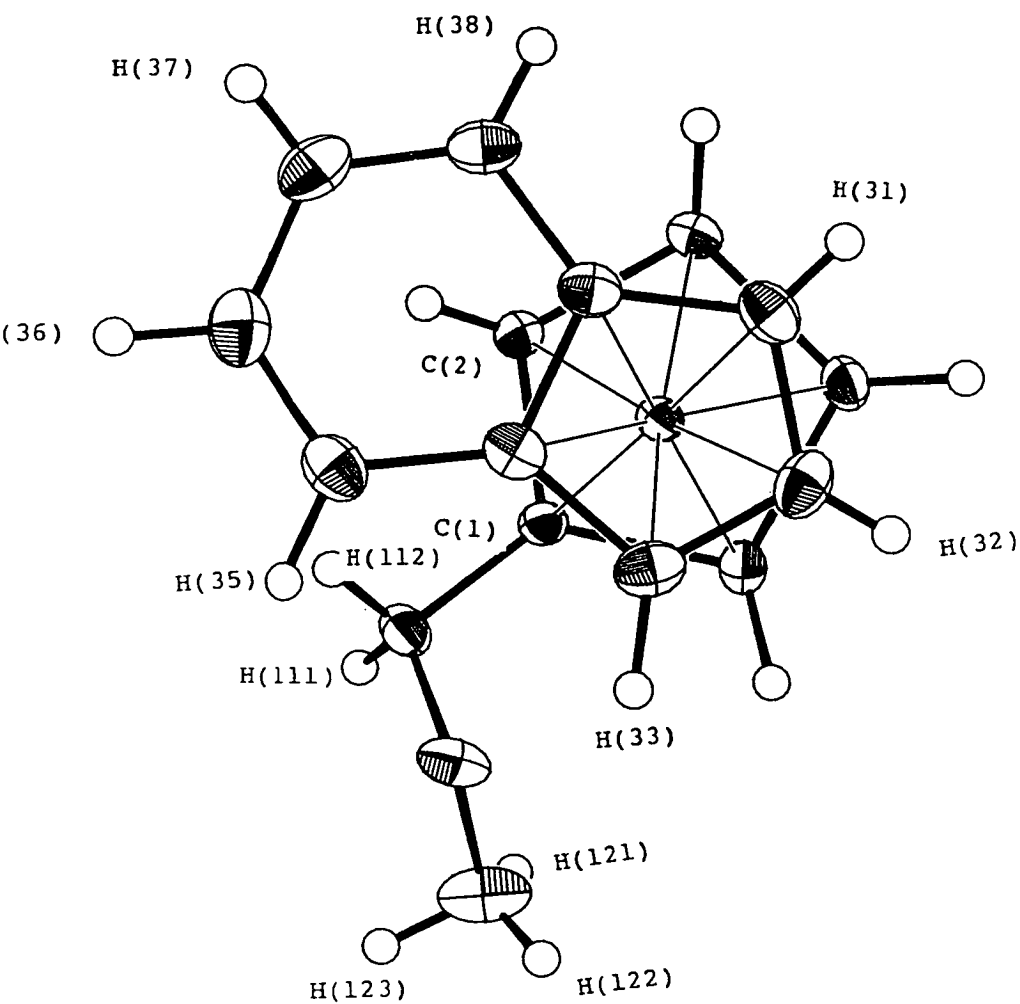


Table 2.5 Co-ordinates of Refined Atoms and Equivalent Isotropic Thermal Parameters (\AA^2) for 1- CH_2OCH_3 -3-(η^5 - C_9H_7)-3,1,2-*closo*- $\text{C}_2\text{B}_9\text{H}_{10}$, (3)

	x	y	z	Ueq
Co(3)	0.21493(2)	-0.01772(3)	0.30020(1)	0.0169(2)
C(34)	0.19109(15)	0.19219(21)	0.36155(11)	0.0222(9)
C(39)	0.24920(15)	0.08687(22)	0.42636(11)	0.0230(10)
C(37)	0.39897(17)	0.26021(25)	0.46809(13)	0.0303(11)
C(33)	0.08871(15)	0.12353(23)	0.31656(12)	0.0261(10)
C(38)	0.35623(16)	0.12415(23)	0.47939(12)	0.0265(10)
C(36)	0.34140(18)	0.36584(24)	0.40537(14)	0.0334(11)
C(32)	0.08131(19)	-0.01741(24)	0.35488(14)	0.0281(11)
C(31)	0.18101(18)	-0.04448(25)	0.42009(13)	0.0274(11)
C(35)	0.23984(17)	0.33445(22)	0.35208(13)	0.0291(11)
C(11)	0.22841(16)	0.18760(21)	0.14905(13)	0.0243(10)
O(1)	0.11566(11)	0.22962(16)	0.13481(8)	0.0287(7)
C(12)	0.05465(22)	0.2130(3)	0.04558(16)	0.0423(14)
C(1)	0.24949(16)	0.02441(19)	0.18019(13)	0.0185(9)
C(2)	0.35872(17)	-0.01265(20)	0.26232(14)	0.0200(10)
B(8)	0.20901(17)	-0.24387(23)	0.26493(14)	0.0232(11)
B(12)	0.33300(18)	-0.31684(24)	0.24012(15)	0.0269(12)
B(10)	0.34865(18)	-0.2379(3)	0.13899(15)	0.0283(12)
B(6)	0.36955(17)	-0.04269(25)	0.15494(14)	0.0231(11)
B(5)	0.23779(18)	-0.11121(25)	0.10079(14)	0.0246(11)
B(4)	0.14978(17)	-0.11117(23)	0.17707(13)	0.0222(11)
B(11)	0.42823(17)	-0.1680(3)	0.24182(15)	0.0261(11)
B(9)	0.21319(18)	-0.2802(3)	0.15267(14)	0.0263(11)
B(7)	0.34318(17)	-0.17211(24)	0.31985(14)	0.0233(11)
H(12)	0.3619(17)	-0.433(3)	0.2606(14)	0.0292(53)
H(11)	0.5205(19)	-0.172(3)	0.2650(14)	0.0355(58)
H(37)	0.4626(23)	0.289(3)	0.5006(15)	0.0467(70)
H(33)	0.0336(17)	0.1699(25)	0.2665(14)	0.0275(53)
H(4)	0.0646(18)	-0.074(3)	0.1507(14)	0.0314(55)
H(38)	0.3917(21)	0.052(3)	0.5179(16)	0.0405(63)
H(5)	0.1971(19)	-0.077(3)	0.0271(15)	0.0407(62)
H(7)	0.3837(18)	-0.184(3)	0.3868(15)	0.0342(57)
H(10)	0.3927(20)	-0.301(3)	0.0929(16)	0.0424(66)
H(9)	0.1631(21)	-0.369(3)	0.1085(17)	0.0570(76)
H(111)	0.2501(16)	0.1969(24)	0.0927(14)	0.0240(52)
H(112)	0.2707(17)	0.251(3)	0.1963(13)	0.0263(55)
H(32)	0.0269(21)	-0.070(3)	0.3362(16)	0.0441(71)
H(35)	0.1993(19)	0.406(3)	0.3057(15)	0.0467(71)
H(36)	0.3730(20)	0.463(3)	0.4020(16)	0.0365(63)
H(8)	0.1512(17)	-0.3083(25)	0.2976(14)	0.0278(54)
H(123)	0.065(3)	0.308(5)	0.017(3)	0.102 (13)
H(6)	0.4120(18)	0.0358(23)	0.1278(14)	0.0224(52)
H(2)	0.3988(17)	0.068(3)	0.2851(13)	0.0206(49)
H(31)	0.1933(19)	-0.125(3)	0.4487(15)	0.0329(61)
H(121)	0.079(3)	0.144(4)	0.0168(21)	0.077 (10)
H(122)	-0.0138(25)	0.212(3)	0.0460(17)	0.0450(71)

**Table 2.6 Interatomic Distances (Å) and Selected Angles (°) for
1-CH₂OCH₃-3-(η⁵-C₉H₇)-3,1,2-closo-CoC₂B₉H₁₀ (3)**

Co(3) -C(34)	2.1511(18)	C(1) - C(2)	1.659(3)
Co(3) -C(39)	2.1198(19)	C(1) - B(6)	1.731(3)
Co(3) -C(33)	2.0685(19)	C(1) - B(5)	1.708(3)
Co(3) -C(32)	2.0294(22)	C(1) - B(4)	1.720(3)
Co(3) -C(31)	2.0161(22)	C(2) - B(6)	1.724(3)
Co(3) - C(1)	2.0420(19)	C(2) -B(11)	1.699(3)
Co(3) - C(2)	2.0025(20)	C(2) - B(7)	1.713(3)
Co(3) - B(8)	2.0856(21)	C(2) - H(2)	0.895(22)
Co(3) - B(4)	2.0671(21)	B(8) -B(12)	1.791(3)
Co(3) - B(7)	2.0690(22)	B(8) - B(4)	1.824(3)
C(34) -C(39)	1.439(3)	B(8) - B(9)	1.785(3)
C(34) -C(33)	1.433(3)	B(8) - B(7)	1.797(3)
C(34) -C(35)	1.427(3)	B(8) - H(8)	1.127(22)
C(39) -C(38)	1.425(3)	B(12) -B(10)	1.772(3)
C(39) -C(31)	1.433(3)	B(12) -B(11)	1.771(3)
C(37) -C(38)	1.351(3)	B(12) - B(9)	1.790(3)
C(37) -C(36)	1.420(3)	B(12) - B(7)	1.772(3)
C(37) -H(37)	0.87(3)	B(12) -H(12)	1.118(22)
C(33) -C(32)	1.402(3)	B(10) - B(6)	1.768(3)
C(33) -H(33)	0.995(22)	B(10) - B(5)	1.769(3)
C(38) -H(38)	0.92(3)	B(10) -B(11)	1.780(3)
C(36) -C(35)	1.362(3)	B(10) - B(9)	1.780(3)
C(36) -H(36)	0.95(3)	B(10) -H(10)	1.145(25)
C(32) -C(31)	1.421(3)	B(6) - B(5)	1.760(3)
C(32) -H(32)	0.82(3)	B(6) -B(11)	1.770(3)
C(31) -H(31)	0.837(24)	B(6) - H(6)	1.023(21)
C(35) -H(35)	1.00(3)	B(5) - B(4)	1.788(3)
C(11) - O(1)	1.4117(24)	B(5) - B(9)	1.768(3)
C(11) - C(1)	1.536(3)	B(5) - H(5)	1.175(25)
C(11) -H(111)	0.976(21)	B(4) - B(9)	1.780(3)
C(11) -H(112)	0.973(22)	B(4) - H(4)	1.089(23)
O(1) -C(12)	1.421(3)	B(11) - B(7)	1.783(3)
C(12) -H(123)	0.98(4)	B(11) -H(11)	1.114(23)
C(12) -H(121)	0.86(3)	B(9) - H(9)	1.14(3)
C(12) -H(122)	0.85(3)	B(7) - H(7)	1.049(23)
C(34) -Co(3) -C(39)	39.37(7)	B(8) -B(12) - B(9)	59.81(12)
C(34) -Co(3) -C(33)	39.64(7)	B(8) -B(12) - B(7)	60.59(12)
C(39) -Co(3) -C(31)	40.46(8)	B(10) -B(12) -B(11)	60.30(13)
C(33) -Co(3) -C(32)	40.00(8)	B(10) -B(12) - B(9)	59.96(13)
C(32) -Co(3) -C(31)	41.12(9)	B(11) -B(12) - B(7)	60.41(12)
C(1) -Co(3) - C(2)	48.43(8)	B(12) -B(10) -B(11)	59.83(13)
C(1) -Co(3) - B(4)	49.49(8)	B(12) -B(10) - B(9)	60.51(13)
C(2) -Co(3) - B(7)	49.74(8)	B(6) -B(10) - B(5)	59.68(13)
B(8) -Co(3) - B(4)	52.10(8)	B(6) -B(10) -B(11)	59.85(13)
B(8) -Co(3) - B(7)	51.26(8)	B(5) -B(10) - B(9)	59.76(13)
C(39) -C(34) -C(33)	107.56(16)	C(1) - B(6) - C(2)	57.40(12)
C(39) -C(34) -C(35)	119.85(17)	C(1) - B(6) - B(5)	58.59(12)
C(33) -C(34) -C(35)	132.58(17)	C(2) - B(6) -B(11)	58.18(12)
C(34) -C(39) -C(38)	119.73(17)	B(10) - B(6) - B(5)	60.18(13)
C(34) -C(39) -C(31)	107.20(16)	B(10) - B(6) -B(11)	60.41(13)
C(38) -C(39) -C(31)	133.04(18)	C(1) - B(5) - B(6)	59.86(12)

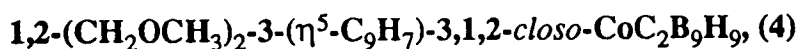
C(38) -C(37) -C(36)	122.38(20)	C(1) - B(5) - B(4)	58.90(12)
C(34) -C(33) -C(32)	108.33(17)	B(10) - B(5) - B(6)	60.14(13)
C(39) -C(38) -C(37)	118.28(18)	B(10) - B(5) - B(9)	60.44(13)
C(37) -C(36) -C(35)	121.55(20)	B(4) - B(5) - B(9)	60.09(12)
C(33) -C(32) -C(31)	108.77(19)	Co(3) - B(4) - C(1)	64.49(9)
C(39) -C(31) -C(32)	107.99(18)	Co(3) - B(4) - B(8)	64.47(9)
C(34) -C(35) -C(36)	118.20(19)	C(1) - B(4) - B(5)	58.24(12)
O(1) -C(11) - C(1)	112.90(16)	B(8) - B(4) - B(9)	59.36(12)
C(11) - O(1) -C(12)	113.86(16)	B(5) - B(4) - B(9)	59.40(12)
Co(3) - C(1) - C(2)	64.56(10)	C(2) -B(11) - B(6)	59.57(12)
Co(3) - C(1) - B(4)	66.01(9)	C(2) -B(11) - B(7)	58.90(12)
C(2) - C(1) - B(6)	61.11(12)	B(12) -B(11) -B(10)	59.87(13)
B(6) - C(1) - B(5)	61.55(12)	B(12) -B(11) - B(7)	59.80(12)
B(5) - C(1) - B(4)	62.87(12)	B(10) -B(11) - B(6)	59.74(13)
Co(3) - C(2) - C(1)	67.03(10)	B(8) - B(9) -B(12)	60.12(12)
Co(3) - C(2) - B(7)	67.15(10)	B(8) - B(9) - B(4)	61.54(12)
C(1) - C(2) - B(6)	61.49(12)	B(12) - B(9) -B(10)	59.53(13)
B(6) - C(2) -B(11)	62.26(13)	B(10) - B(9) - B(5)	59.80(13)
B(11) - C(2) - B(7)	62.98(13)	B(5) - B(9) - B(4)	60.52(12)
Co(3) - B(8) - B(4)	63.42(9)	Co(3) - B(7) - C(2)	63.11(10)
Co(3) - B(8) - B(7)	63.89(10)	Co(3) - B(7) - B(8)	64.85(10)
B(12) - B(8) - B(9)	60.07(12)	C(2) - B(7) -B(11)	58.12(12)
B(12) - B(8) - B(7)	59.18(12)	B(8) - B(7) -B(12)	60.23(12)
B(4) - B(8) - B(9)	59.10(12)	B(12) - B(7) -B(11)	59.78(12)

Table 2.7 Anisotropic Thermal Parameters (\AA^2) for
 $1\text{-CH}_2\text{OCH}_3\text{-3-(}\eta^5\text{-C}_9\text{H}_7\text{)-3,1,2-closo-C}_9\text{B}_9\text{H}_{10}$ (3)

	U11	U22	U33	U23	U13	U12
Co(3)	0.0165(2)	0.0166(2)	0.0165(2)	0.0022(1)	0.0037(1)	0.0004(1)
C(34)	0.0241(9)	0.0215(9)	0.0203(8)	-0.0008(7)	0.0082(7)	0.0046(7)
C(39)	0.0241(9)	0.0255(10)	0.0183(9)	0.0000(7)	0.0057(7)	0.0022(7)
C(37)	0.0253(10)	0.0395(12)	0.0243(9)	-0.0099(8)	0.0041(8)	-0.0037(9)
C(33)	0.0189(9)	0.0331(11)	0.0253(9)	-0.0019(8)	0.0067(7)	0.0056(8)
C(38)	0.0263(10)	0.0330(11)	0.0183(9)	-0.0022(8)	0.0024(7)	0.0047(8)
C(36)	0.0386(12)	0.0262(11)	0.0342(11)	-0.0049(9)	0.0126(9)	-0.0072(9)
C(32)	0.0238(11)	0.0341(11)	0.0259(10)	-0.0042(8)	0.0103(9)	-0.0080(8)
C(31)	0.0325(11)	0.0269(11)	0.0222(10)	0.0049(8)	0.0108(8)	0.0009(9)
C(35)	0.0360(11)	0.0202(9)	0.0296(10)	-0.0007(8)	0.0098(8)	0.0038(8)
C(11)	0.0255(9)	0.0212(10)	0.0249(10)	0.0061(7)	0.0066(8)	0.0008(8)
O(1)	0.0274(7)	0.0327(8)	0.0244(7)	0.0064(6)	0.0057(5)	0.0115(6)
C(12)	0.0346(13)	0.0561(17)	0.0321(12)	-0.0011(11)	-0.0012(10)	0.0144(12)
C(1)	0.0153(9)	0.0212(9)	0.0179(9)	0.0028(7)	0.0036(7)	0.0005(7)
C(2)	0.0173(9)	0.0193(9)	0.0217(10)	0.0006(7)	0.0027(7)	-0.0001(7)
B(8)	0.0242(10)	0.0167(10)	0.0274(11)	0.0027(8)	0.0068(8)	-0.0005(8)
B(12)	0.0264(11)	0.0184(10)	0.0342(12)	0.0031(9)	0.0072(9)	0.0039(8)
B(10)	0.0284(11)	0.0231(11)	0.0325(12)	-0.0041(9)	0.0111(9)	0.0006(9)
B(6)	0.0183(10)	0.0233(11)	0.0274(11)	-0.0010(9)	0.0099(8)	0.0005(8)
B(5)	0.0258(10)	0.0254(11)	0.0219(10)	-0.0024(8)	0.0082(8)	-0.0017(9)
B(4)	0.0218(10)	0.0199(10)	0.0236(10)	0.0004(8)	0.0058(8)	-0.0028(8)
B(11)	0.0195(10)	0.0237(11)	0.0335(11)	0.0009(9)	0.0064(9)	0.0049(8)
B(9)	0.0252(10)	0.0236(11)	0.0285(11)	-0.0037(9)	0.0057(9)	-0.0007(9)
B(7)	0.0216(10)	0.0216(10)	0.0246(11)	0.0055(8)	0.0020(8)	0.0025(8)

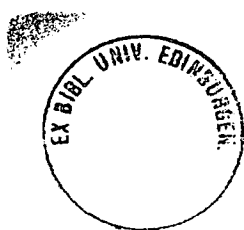
The indenyl ligand is "twisted" sideways by 6.5° in the same direction as in **2**, *i.e.* such that C(35) is more elevated than C(38). It is also "tilted" upwards [C(36) more elevated than C(34)] by an angle of 5.4° , making an overall dihedral angle of *ca.* 8.1° with the reference B_5 lower belt. As in **2**, these values may be attributed to the presence of a substituent on the cage, in this case a monoether function.

The C_2B_3 face is envelope folded, with ϕ^P and θ^P values of 0.46° and 2.36° respectively. Once again there is no substantial slip of the cobalt atom across the face of the cage. The five-membered ring of the indenyl ligand is also slightly folded, with a fold angle, Ω , of 3.71° , and Δ^h (0.114\AA) is again greater than in the unsubstituted species, **1**. The latter may be traced to the increased twist and tilt of the indenyl ligand to accommodate the cage substituent. Indeed the slightly increased twisting of the indenyl ligand in this complex compared with that in **2** (6.5° vs. 5.1°) may contribute to the relatively greater value of σ , $+25.7^\circ$. Finally, bond distances in the indenyl six-membered ring show the same pattern and are in the same range as in the previous species.



Synthesis

The disubstituted analogue of **3** was synthesised by the reaction of $Tl_2[7,8-(CH_2OCH_3)_2-7,8-C_2B_9H_9]$ with LiC_9H_7 and $Co(acac)_3$ in thf, and isolated as a brick red solid by preparative tlc. Details of the procedure may be found in Chapter 5, Section A.



N.m.r. Studies

The ^{11}B spectrum exhibits six resonances in the ratio 1:1:2:2:2:1, with all boron nuclei showing coupling to an *exo*-polyhedral hydrogen atoms in the proton coupled spectrum. This is in full accord with there being a mirror plane of symmetry through the molecule, implying either a static, symmetric structure or (more likely) rapid rotation of the indenyl ligand about the Co(3)-B(10) axis on the n.m.r time scale.

Such free rotation appears to continue, even on substantial cooling, as the spectrum remains essentially unchanged at -90°C .

The ^1H n.m.r. spectrum shows the expected signals for indenyl hydrogen atoms in the high frequency region. The methylene hydrogen atoms of the pendent ether groups give rise to an AB pattern, similar to that observed for **3**, the two inner methylene hydrogen atoms, H(211) and H(212) (see positions in **Figure 2.7**) being magnetically equivalent, and the two outer hydrogen atoms, H(221) and H(222), also being equivalent. A single resonance is observed for hydrogen atoms of both methyl groups, at δ 3.34 p.p.m.

Structural Study on **4**

Introduction

Large crystals suitable for diffraction were grown by slow diffusion of hexane into a dichloromethane solution of **4** at -30° . Full details of the crystallographic procedures and crystal data for the structure can be found in Chapter 5.

Discussion

Perspective and plan views of **4** are shown in **Figure 2.6** and **Figure 2.7** respectively, which also show the appropriate numbering scheme. All indenyl and

cage hydrogen atoms have the same number as the B or C atom to which they are bonded. Table 2.8 lists final atomic co-ordinates for all atoms, Table 2.9 bond distances and selected interbond angles, and Table 2.10 gives anisotropic thermal parameters for all non-hydrogen atoms.

Figure 2.7 gives a clear view of the molecular conformation. The indenyl ligand is rotated by *ca.* 72° from its position in 1-3, since the ring junction carbon atoms now lie above B(7). This presumably arises as a result of the steric crowding which would ensue between the upwardly directed ether functions and the indenyl six-membered ring if the the molecule were to adopt a *cisoid* conformation. It is interesting to note that in the recently reported compound $(\eta\text{-C}_9\text{H}_7)\text{Fe}(\text{Et}_2\text{C}_2\text{B}_4\text{H}_4)\text{Ni}(\eta\text{-C}_5\text{Me}_5)$, the indenyl-cage conformation appears to be *cis*⁶⁸ (unfortunately no atomic co-ordinates were published by which to check this proposition). In this case the ethyl substituents on the eight membered carbadimetallaborane are not substantially inclined toward the indenyl ligand, whilst in 4 C(11) and C(12) are at angles of 22.66 and 23.51° from C(1) and C(2) respectively. Thus the associated methylene hydrogen atoms, H(111), H(112), H(211) and H(212) are particularly elevated with respect to the cage. It is also worth noting that, in contrast to the monoether derivative, there is no substantial twist in either pendent ether group. Torsion angles C(1)-C(11)-O(11)-C(111) and C(2)-C(21)-O(21)-C(211) are 175.92 and 174.10° respectively.

The indenyl ligand is twisted by 6.7°, such that C(35) is more elevated than C(38), which may be traced to a close contact between H(211) and H(35) [2.53(3)Å]. Similarly, close proximity of H(112) and H(32), which are 2.51Å apart, may explain why the ligand is not "tilted" to the same extent as in 2 and 3, the angle of tilt being only 1.4° [where C(36) is slightly more elevated than C(34)].

1,2-(CH₂OCH₃)₂-3-(η⁵-C₉H₇)-3,1,2-closo-CoC₂B₉H₉, (4)

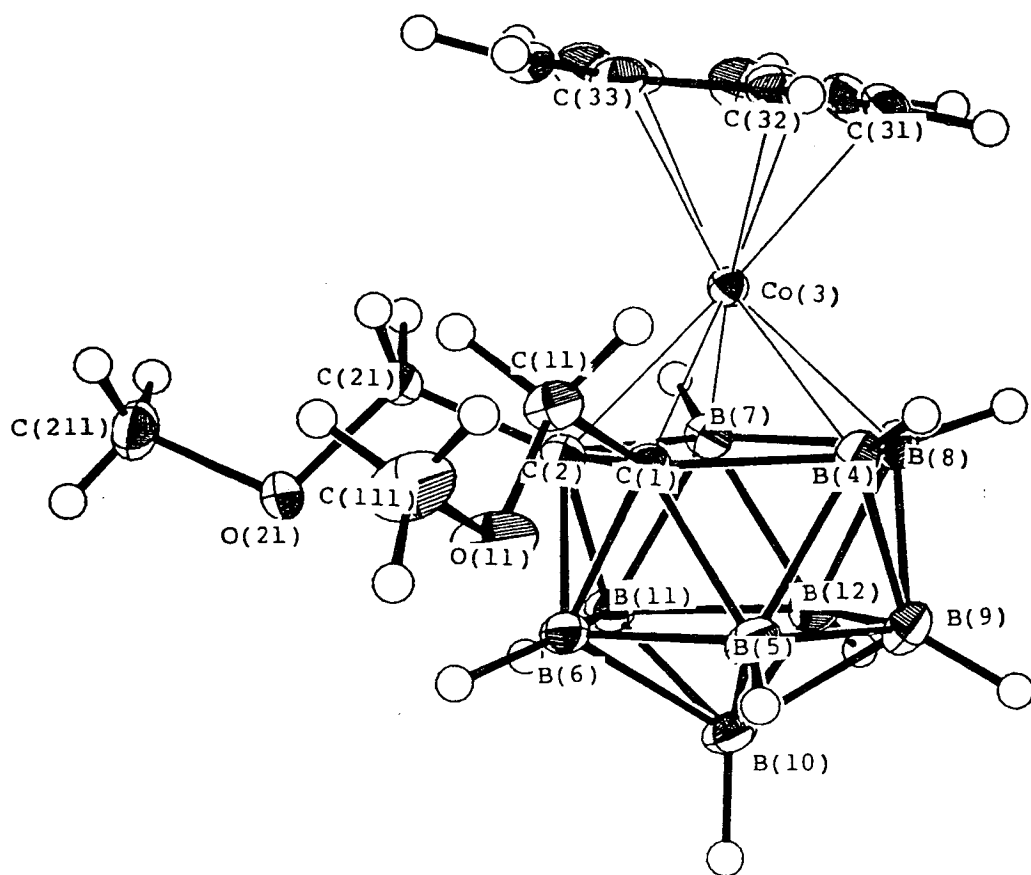


Table 2.8 Co-ordinates of Refined Atoms and Equivalent Isotropic Thermal Parameters (\AA^2) for 1,2-(CH_2OCH_3)₂-3-($\eta^5\text{-C}_9\text{H}_7$)-3,1,2-*closo*- $\text{CoC}_2\text{B}_9\text{H}_9$, (4)

	x	y	z	U _{eq}
Co(3)	1.03917(2)	0.18742(1)	0.20390(2)	0.0127(2)
C(31)	1.17834(17)	0.13323(13)	0.11320(16)	0.0212(9)
C(32)	1.09570(19)	0.17652(14)	0.03835(17)	0.0227(10)
C(33)	0.97908(17)	0.13553(12)	0.04881(15)	0.0199(9)
C(34)	0.99084(16)	0.06041(12)	0.12568(14)	0.0188(9)
C(35)	0.90647(17)	-0.00515(13)	0.16455(16)	0.0218(10)
C(36)	0.94663(19)	-0.06859(13)	0.24057(17)	0.0267(10)
C(37)	1.07049(19)	-0.07015(13)	0.28023(17)	0.0273(10)
C(38)	1.15387(18)	-0.00848(13)	0.24561(16)	0.0234(10)
C(39)	1.11507(16)	0.05936(12)	0.16642(15)	0.0198(9)
C(1)	0.95974(17)	0.31065(10)	0.22592(16)	0.0153(9)
C(2)	0.89459(15)	0.22661(11)	0.30056(14)	0.0144(8)
C(11)	0.90199(18)	0.34627(13)	0.11653(16)	0.0199(9)
O(11)	0.84941(15)	0.43246(9)	0.13319(11)	0.0330(8)
C(111)	0.80252(25)	0.46988(16)	0.03107(20)	0.0358(13)
C(21)	0.77673(17)	0.18077(12)	0.25982(17)	0.0177(10)
O(21)	0.67370(11)	0.21609(10)	0.31514(12)	0.0268(7)
C(211)	0.56552(19)	0.16704(17)	0.28552(20)	0.0273(11)
B(9)	1.13831(20)	0.33362(15)	0.39383(19)	0.0215(10)
B(4)	1.11761(20)	0.31003(13)	0.24596(19)	0.0191(11)
B(6)	0.87938(19)	0.33667(14)	0.34785(17)	0.0180(10)
B(11)	0.91015(18)	0.24561(14)	0.44174(16)	0.0179(10)
B(12)	1.07009(19)	0.24342(14)	0.47158(17)	0.0196(10)
B(7)	1.00636(19)	0.16531(15)	0.37284(17)	0.0169(10)
B(8)	1.15091(18)	0.22000(14)	0.34442(17)	0.0183(10)
B(5)	1.02049(19)	0.38972(14)	0.31622(17)	0.0199(10)
B(10)	0.99178(19)	0.34939(15)	0.45567(18)	0.0204(10)
H(211)	0.7818(19)	0.1095(16)	0.2726(18)	0.0255(53)
H(6)	0.7935(18)	0.3731(14)	0.3379(16)	0.0194(49)
H(10)	0.9753(19)	0.3979(15)	0.5233(18)	0.0256(54)
H(12)	1.1019(20)	0.2198(16)	0.5512(20)	0.0292(56)
H(8)	1.244(3)	0.1985(17)	0.346(3)	0.0505(79)
H(37)	1.0984(18)	-0.1258(15)	0.3263(18)	0.0244(53)
H(111)	0.8376(20)	0.3028(14)	0.0842(19)	0.0200(52)
H(38)	1.2379(22)	-0.0080(16)	0.2686(19)	0.0317(60)
H(7)	0.9849(17)	0.0921(13)	0.3925(16)	0.0176(48)
H(9)	1.2145(20)	0.3690(15)	0.4285(19)	0.0327(59)
H(5)	1.0207(19)	0.4601(16)	0.2931(18)	0.0261(55)
H(11)	0.8364(20)	0.2239(16)	0.5041(19)	0.0303(58)
H(33)	0.9025(22)	0.1499(16)	-0.0006(20)	0.0328(59)
H(35)	0.8237(22)	-0.0167(17)	0.1324(21)	0.0390(67)
H(32)	1.1161(19)	0.2264(16)	-0.0045(20)	0.0248(55)
H(4)	1.1681(18)	0.3418(14)	0.1782(17)	0.0143(45)
H(112)	0.9686(22)	0.3492(17)	0.0506(21)	0.0343(60)
H(36)	0.8930(24)	-0.1213(19)	0.2578(21)	0.0450(69)
H(31)	1.2548(22)	0.1506(17)	0.1284(19)	0.0299(59)
H(212)	0.7680(21)	0.1835(13)	0.1831(22)	0.0196(54)
H(1A)	0.859(3)	0.4720(20)	-0.026(3)	0.0515(81)
H(1B)	0.743(3)	0.4308(24)	0.004(3)	0.078(11)
H(2A)	0.5745(25)	0.0973(20)	0.3120(24)	0.0523(76)
H(1C)	0.7842(23)	0.5297(20)	0.0452(21)	0.0430(69)
H(2B)	0.509(3)	0.1963(18)	0.3142(25)	0.0437(78)
H(2C)	0.5481(23)	0.1727(20)	0.210(3)	0.0474(89)

Table 2.9 Interatomic Distances (Å) and Selected Interbond Angles (°) for
1,2-(CH₂OCH₃)₂-3-(η⁵-C₉H₇)-3,1,2-closo-CoC₂B₉H₉, (4)

Co(3) -C(31)	2.0319(19)	O(11) -C(111)	1.415(3)
Co(3) -C(32)	2.0596(21)	C(111)-H(1A)	0.92(3)
Co(3) -C(33)	2.0818(18)	C(111)-H(1B)	0.93(3)
Co(3) -C(34)	2.1506(17)	C(111)-H(1C)	0.92(3)
Co(3) -C(39)	2.1107(18)	C(21) -O(21)	1.4069(23)
Co(3) - C(1)	2.0313(18)	C(21) -H(211)	1.063(22)
Co(3) - C(2)	2.0412(16)	C(21) -H(212)	0.910(23)
Co(3) - B(4)	2.0589(21)	O(21) -C(211)	1.426(3)
Co(3) - B(7)	2.0534(21)	C(211)-H(2A)	1.08(3)
Co(3) - B(8)	2.1031(20)	C(211)-H(2B)	0.83(3)
C(31) -C(32)	1.409(3)	C(211)-H(2C)	0.91(3)
C(31) -C(39)	1.438(3)	B(9) - B(4)	1.790(3)
C(31) -H(31)	0.890(24)	B(9) -B(12)	1.783(3)
C(32) -C(33)	1.417(3)	B(9) - B(8)	1.779(3)
C(32) -H(32)	0.920(23)	B(9) - B(5)	1.776(3)
C(33) -C(34)	1.4359(25)	B(9) -B(10)	1.782(3)
C(33) -H(33)	1.036(24)	B(9) - H(9)	1.061(23)
C(34) -C(35)	1.415(3)	B(4) - B(8)	1.798(3)
C(34) -C(39)	1.4352(25)	B(4) - B(5)	1.792(3)
C(35) -C(36)	1.365(3)	B(4) - H(4)	1.083(20)
C(35) -H(35)	0.992(25)	B(6) -B(11)	1.770(3)
C(36) -C(37)	1.427(3)	B(6) - B(5)	1.772(3)
C(36) -H(36)	1.00(3)	B(6) -B(10)	1.768(3)
C(37) -C(38)	1.353(3)	B(6) - H(6)	1.087(20)
C(37) -H(37)	1.029(21)	B(11) -B(12)	1.779(3)
C(38) -C(39)	1.429(3)	B(11) - B(7)	1.785(3)
C(38) -H(38)	0.954(24)	B(11) -B(10)	1.778(3)
C(1) -C(11)	1.523(3)	B(11) -H(11)	1.142(23)
C(1) - B(4)	1.739(3)	B(12) - B(7)	1.774(3)
C(1) - B(6)	1.735(3)	B(12) - B(8)	1.782(3)
C(1) - B(5)	1.708(3)	B(12) -B(10)	1.790(3)
C(2) -C(21)	1.5274(25)	B(12) -H(12)	1.056(23)
C(2) - B(6)	1.724(3)	B(7) - B(8)	1.808(3)
C(2) -B(11)	1.694(3)	B(7) - H(7)	1.129(19)
C(2) - B(7)	1.736(3)	B(8) - H(8)	1.07(3)
C(11) -O(11)	1.4091(24)	B(5) -B(10)	1.779(3)
C(11) -H(111)	1.023(22)	B(5) - H(5)	1.072(22)
C(11) -H(112)	1.071(24)	B(10) -H(10)	1.088(22)
C(1) - C(2)	1.6822(24)		
C(31) -Co(3) -C(32)	40.27(8)	Co(3) - B(4) - B(8)	65.68(9)
C(31) -Co(3) -C(39)	40.56(7)	C(1) - B(4) - B(5)	57.85(11)
C(32) -Co(3) -C(33)	40.01(8)	B(9) - B(4) - B(8)	59.47(12)
C(33) -Co(3) -C(34)	39.62(7)	B(9) - B(4) - B(5)	59.45(12)
C(34) -Co(3) -C(39)	39.35(7)	C(1) - B(6) - C(2)	58.18(10)
C(1) -Co(3) - C(2)	48.79(7)	C(1) - B(6) - B(5)	58.28(11)
C(1) -Co(3) - B(4)	50.31(8)	C(2) - B(6) -B(11)	58.00(11)
C(2) -Co(3) - B(7)	50.16(7)	B(11) - B(6) -B(10)	60.33(12)
B(4) -Co(3) - B(8)	51.17(8)	B(5) - B(6) -B(10)	60.34(12)
B(7) -Co(3) - B(8)	51.55(8)	C(2) -B(11) - B(6)	59.65(11)
C(32) -C(31) -C(39)	107.97(16)	C(2) -B(11) - B(7)	59.79(11)

C(31) -C(32) -C(33)	108.87(17)	B(6) -B(11) -B(10)	59.79(12)
C(32) -C(33) -C(34)	108.02(16)	B(12) -B(11) - B(7)	59.72(11)
C(33) -C(34) -C(35)	132.59(17)	B(12) -B(11) -B(10)	60.43(12)
C(33) -C(34) -C(39)	107.31(15)	B(9) -B(12) - B(8)	59.89(12)
C(35) -C(34) -C(39)	120.09(16)	B(9) -B(12) -B(10)	59.82(12)
C(34) -C(35) -C(36)	118.34(17)	B(11) -B(12) - B(7)	60.28(11)
C(35) -C(36) -C(37)	121.56(18)	B(11) -B(12) -B(10)	59.74(11)
C(36) -C(37) -C(38)	121.97(18)	B(7) -B(12) - B(8)	61.11(12)
C(37) -C(38) -C(39)	118.10(18)	Co(3) - B(7) - C(2)	64.55(9)
C(31) -C(39) -C(34)	107.66(15)	Co(3) - B(7) - B(8)	65.65(9)
C(31) -C(39) -C(38)	132.40(17)	C(2) - B(7) -B(11)	57.53(11)
C(34) -C(39) -C(38)	119.94(16)	B(11) - B(7) -B(12)	59.99(11)
Co(3) - C(1) - B(4)	65.67(9)	B(12) - B(7) - B(8)	59.64(11)
B(4) - C(1) - B(5)	62.64(12)	Co(3) - B(8) - B(4)	63.14(9)
B(6) - C(1) - B(5)	61.94(11)	Co(3) - B(8) - B(7)	62.81(9)
Co(3) - C(2) - B(7)	65.29(9)	B(9) - B(8) - B(4)	60.03(12)
B(6) - C(2) -B(11)	62.35(11)	B(9) - B(8) -B(12)	60.09(12)
B(11) - C(2) - B(7)	62.68(11)	B(12) - B(8) - B(7)	59.25(11)
C(1) -C(11) -O(11)	111.03(15)	C(1) - B(5) - B(4)	59.51(11)
C(11) -O(11) -C(111)	112.17(16)	C(1) - B(5) - B(6)	59.78(11)
C(2) -C(21) -O(21)	111.51(15)	B(9) - B(5) - B(4)	60.21(12)
C(21) -O(21) -C(211)	111.35(15)	B(9) - B(5) -B(10)	60.15(12)
B(4) - B(9) - B(8)	60.50(12)	B(6) - B(5) -B(10)	59.72(12)
B(4) - B(9) - B(5)	60.34(12)	B(9) -B(10) -B(12)	59.89(12)
B(12) - B(9) - B(8)	60.02(12)	B(9) -B(10) - B(5)	59.83(12)
B(12) - B(9) -B(10)	60.30(12)	B(6) -B(10) -B(11)	59.88(12)
B(5) - B(9) -B(10)	60.02(12)	B(6) -B(10) - B(5)	59.94(12)
Co(3) - B(4) - C(1)	64.02(9)	B(11) -B(10) -B(12)	59.83(11)
Co(3) - C(1) - C(2)	65.91(8)	B(6) - C(1) - C(2)	60.58(11)
Co(3) - C(2) - C(1)	65.30(8)	B(6) - C(2) - C(1)	61.23(11)

Table 2.10 Anisotropic Thermal Parameters (\AA^2) for
 $1,2-(\text{CH}_2\text{OCH}_3)_2-3-(\eta^5-\text{C}_9\text{H}_7)-3,1,2\text{-closo-CoC}_2\text{B}_9\text{H}_9$, (4)

	U11	U22	U33	U23	U13	U12
Co(3)	0.0126(2)	0.0128(2)	0.0127(2)	-0.0001(1)	0.0006(1)	0.0000(1)
C(31)	0.0180(9)	0.0229(10)	0.0228(9)	-0.0038(7)	0.0079(7)	0.0004(8)
C(32)	0.0264(11)	0.0251(10)	0.0166(9)	-0.0007(8)	0.0073(8)	-0.0009(8)
C(33)	0.0244(9)	0.0211(9)	0.0143(8)	-0.0036(7)	-0.0005(7)	0.0005(7)
C(34)	0.0213(9)	0.0182(9)	0.0169(9)	-0.0061(7)	0.0016(7)	0.0035(7)
C(35)	0.0205(10)	0.0193(9)	0.0254(10)	-0.0092(8)	0.0012(7)	-0.0026(7)
C(36)	0.0323(11)	0.0151(9)	0.0328(11)	-0.0023(8)	0.0063(8)	-0.0024(8)
C(37)	0.0346(11)	0.0165(9)	0.0308(10)	0.0024(8)	0.0018(8)	0.0048(8)
C(38)	0.0208(10)	0.0226(10)	0.0269(10)	-0.0021(8)	0.0018(8)	0.0078(8)
C(39)	0.0181(9)	0.0191(9)	0.0221(9)	-0.0066(7)	0.0043(7)	0.0022(7)
C(1)	0.0172(9)	0.0128(8)	0.0158(9)	0.0003(6)	-0.0012(7)	-0.0007(6)
C(2)	0.0153(8)	0.0128(8)	0.0150(8)	-0.0004(7)	0.0006(6)	0.0013(7)
C(11)	0.0262(10)	0.0155(9)	0.0178(9)	0.0009(7)	-0.0047(7)	0.0034(7)
O(11)	0.0529(9)	0.0226(7)	0.0233(7)	-0.0023(6)	-0.0153(6)	0.0164(7)
C(111)	0.0542(15)	0.0234(11)	0.0297(12)	0.0029(9)	-0.0181(11)	0.0099(11)
C(21)	0.0146(9)	0.0227(11)	0.0156(10)	-0.0027(7)	0.0010(7)	0.0007(7)
O(21)	0.0126(6)	0.0339(8)	0.0339(8)	-0.0153(6)	0.0022(5)	-0.0015(6)
C(211)	0.0160(10)	0.0401(12)	0.0256(11)	-0.0036(10)	-0.0004(8)	-0.0052(9)
B(9)	0.0209(11)	0.0212(10)	0.0224(11)	-0.0013(8)	-0.0070(8)	-0.0029(9)
B(4)	0.0169(10)	0.0186(11)	0.0219(11)	-0.0003(8)	-0.0031(8)	-0.0028(7)
B(6)	0.0194(10)	0.0160(9)	0.0186(10)	-0.0036(8)	-0.0027(8)	0.0025(8)
B(11)	0.0195(10)	0.0192(10)	0.0151(10)	-0.0016(8)	-0.0004(7)	0.0029(8)
B(12)	0.0216(10)	0.0219(10)	0.0153(10)	0.0004(8)	-0.0041(8)	0.0026(8)
B(7)	0.0180(10)	0.0178(9)	0.0149(10)	0.0015(8)	-0.0002(8)	0.0027(8)
B(8)	0.0159(10)	0.0201(10)	0.0188(10)	0.0003(8)	-0.0038(7)	0.0017(8)
B(5)	0.0236(10)	0.0149(10)	0.0210(10)	-0.0025(8)	-0.0049(8)	-0.0010(8)
B(10)	0.0243(11)	0.0195(11)	0.0173(10)	-0.0051(8)	-0.0054(8)	0.0014(8)

The C_2B_3 face is folded into an envelope, with values of ϕ^P and θ^P 1.23 and 2.37 \AA respectively. As in 1-3 the five-membered ring of the indenyl ligand is folded about C(31).....C(33) and $\Omega = 4.15^\circ$. Notably Δ^h (0.082 \AA) is slightly lower than in the three previous examples and the value of σ (+34.9 $^\circ$) indicates that the slip vector **S** is now almost exactly between C(31) and C(32). These values reflect a subtle change in the Co-indenyl five-membered ring distances with the Co-C(39) bond length now essentially intermediate between Co-C(34) and Co-C(33).

These differences (albeit small) may be explained by the change in conformation of the indenyl ligand w.r.t. the C_2B_3 face, enforced by the presence of two ether functions on the carbaborane ligand face. The *cisoid* conformation, where the stronger bonds from the facial boron atoms to the metal are *trans* to the ring junction carbon atoms of the indenyl ligand, presumably allows for increased delocalisation of their $p\pi$ atomic orbitals, and weaker bonding to the metal, relative to C(31)-(33). In 4, C(39) is no longer *trans* to two boron atoms, which may allow slightly less delocalisation of the $p\pi$ atomic orbitals and more interaction with the metal orbitals, resulting in less slippage of the cobalt atom across the five-membered ring away from C(39). In addition the longer Co-C(33) distance may be compensated by there being two boron atoms *trans* to C(33). However, the change in molecular conformation in this species relative to 1, 2 and 3 has not had a noticeable effect on the bond distances in the indenyl six-membered ring, which are of similar pattern and values to those in the latter three complexes.

EHMO Calculations

Introduction

In order to compare observed with theoretically predicted molecular conformations, a series of extended Hückel molecular orbital (EHMO) calculations were performed on idealised models of 1-4.

The change in the sum of 1-electron energies for each of the four compounds was monitored as a function of rigid rotation of the C_9H_7 ligand about the $Co \cdots B(10)$ axis. Plots of the relative energy vs α , the dihedral angle between the perpendicular bisectors of the aromatic and carbaborane ligands, show theoretical maximum and minimum energy conformations for each model compound.

Details of model parameters and a general methodology for these, and later calculations, are contained in Chapter 5, Section C.

Results and Discussion

Figure 2.8 and Figure 2.9 represent potential energy curves for idealised models of 1 and 2, labelled I and II, whilst Figure 2.10 and Figure 2.11 show similar curves for $1-CH_3-3-(\eta^5-C_9H_7)-3,1,2-closo-CoC_2B_9H_{10}$ (III) and $1,2-(CH_3)_2-(\eta^5-C_9H_7)-3,1,2-closo-CoC_2B_9H_9$ (IV), which are models for 3 and 4. Figure 2.12 presents the relative energy plots on a common scale.

Figure 2.8 Relative Energy Plot for I, an Idealised Model of 1

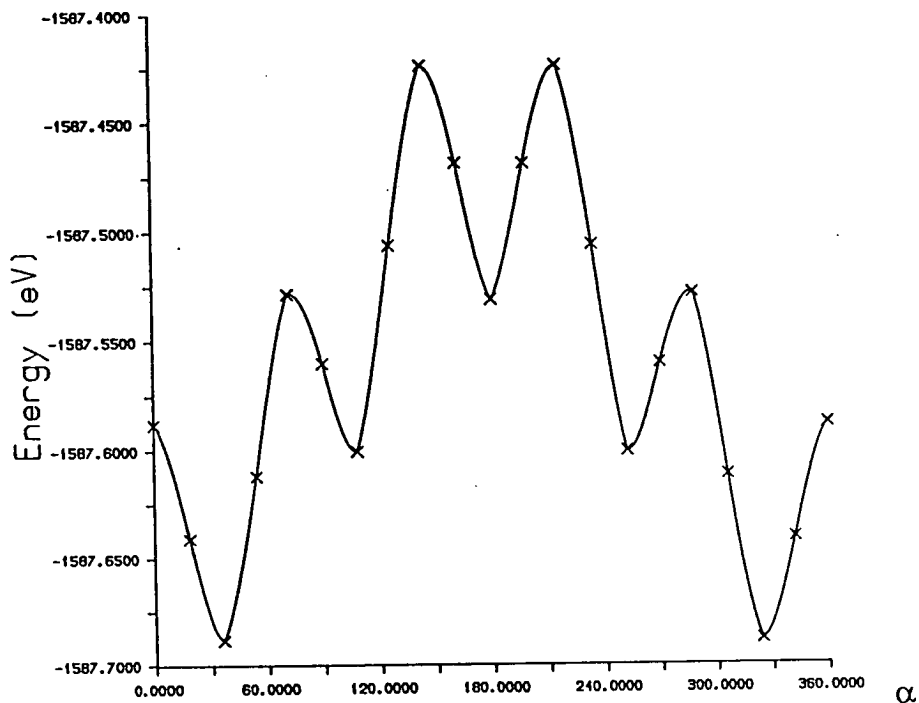
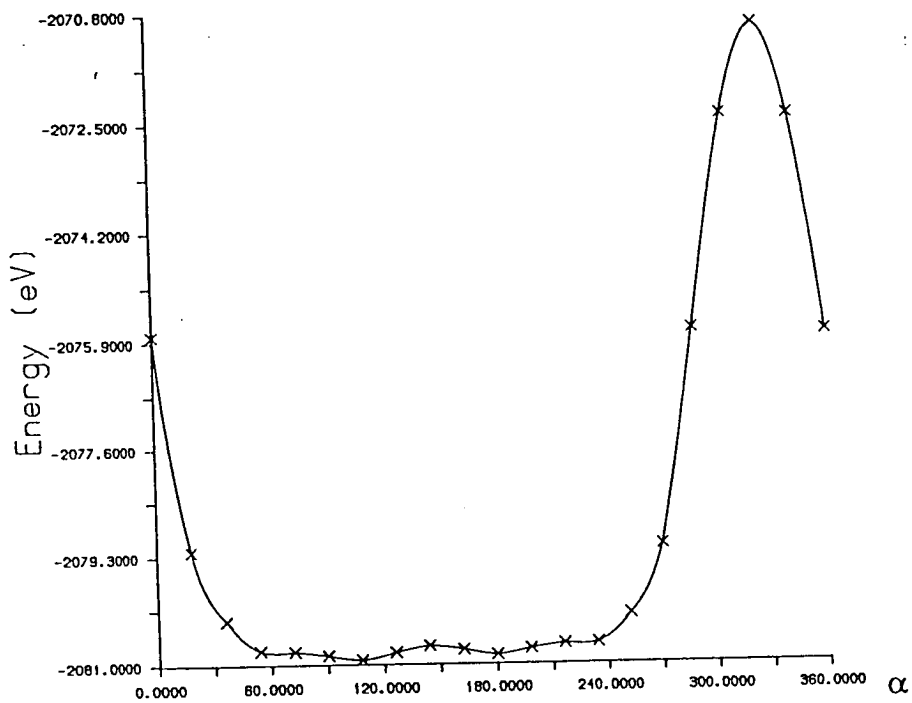


Figure 2.9 Relative Energy Plot for II, an Idealised Model of 2



For I, the theoretical minimum occurs at $\alpha=36^\circ$, which is in good agreement with the observed conformation.¹⁴ Note that local maxima and minima of the curve shown in Figure 2.8 correspond to eclipsed and staggered forms respectively. This is not unprecedented, as significant repulsions between the indenyl hydrogen atoms and those of the C_2B_3 metallabonded face will occur when they are lying directly over each other. The theoretical barrier to rotation is in the region of 0.26eV. As the indenyl ligand rotates freely about the Co...B(10) axis, even at low temperatures, it is impossible to obtain a comparative experimental value for this barrier.

The relative energy plot for the model compound II shows a local minimum energy conformation approximating to that observed in the structure of 2. Generally, local maxima and minima correspond to eclipsed and staggered conformations, but there is one exception; the maximum energy conformation occurs when $\alpha=324^\circ$, where carbon atoms are *cis*-staggered with respect to each other, with C(1) lying underneath the C(34)-C(39) bond. This is in fact not so surprising, as at this point there will be maximum steric interaction between the six-membered ring and the substituent phenyl group. Indeed, the calculated barrier to rotation for the model compound is very large, *ca.* 10eV, which is quite consistent with the observation that the low temperature n.m.r. spectrum of 2 shows restricted rotation of the indenyl ligand about the Co...B(10) axis.

Figure 2.10 Relative Energy Plot for III, an Idealised Model of 3

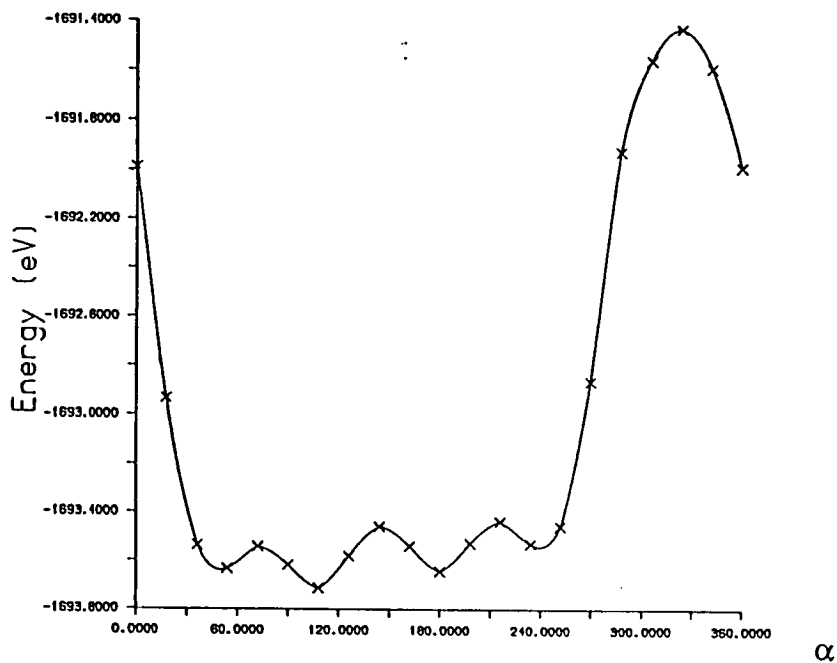


Figure 2.11 Relative Energy Plot for IV, an Idealised Model of 4

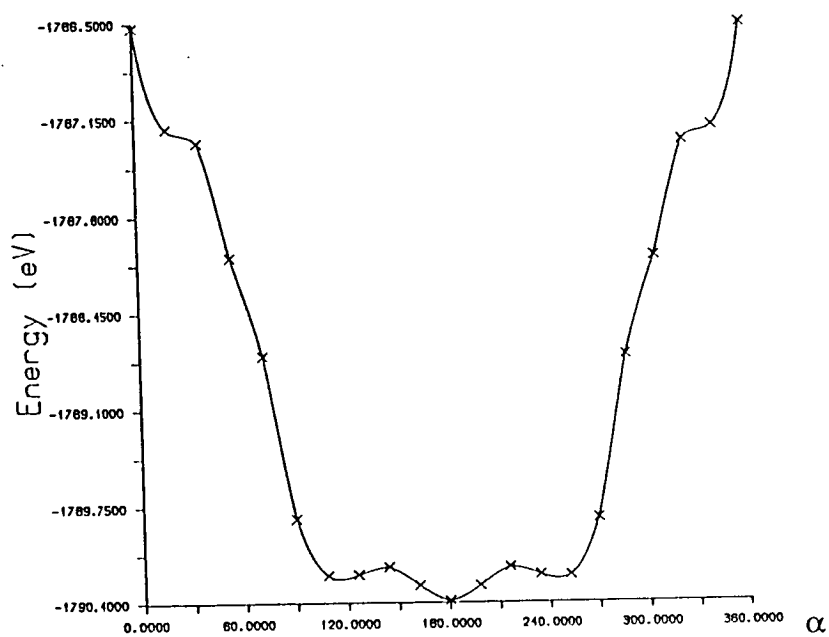
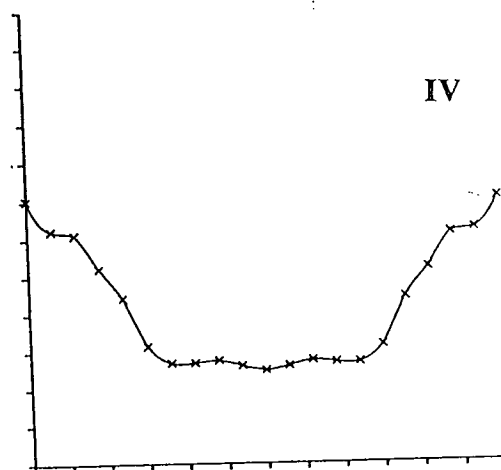
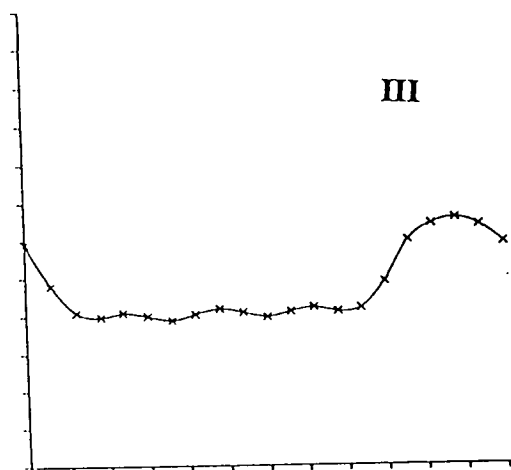
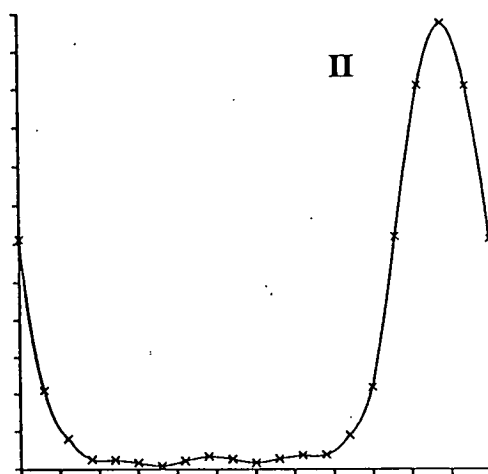
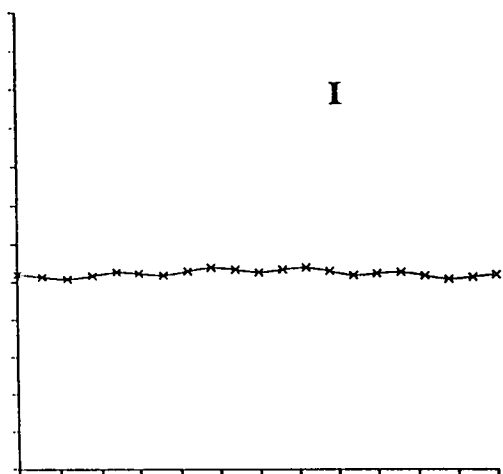


Figure 2.12 Relative Energy Plots for I - IV on a Common Scale



A similar, though naturally smaller barrier to rotation (of *ca.* 2.12eV) is calculated for model III, which represents the monoether derivative. Once again local minima correspond to staggered conformations of the ring junction carbon/cage atoms, except once more when $\alpha=324^\circ$, and the indenyl ligand is closest to the cage substituent. The conformation of the indenyl ligand in the crystal structure corresponds to a local energy minimum for the model.

The plot for IV, modelling the diether derivative, clearly shows that the *cisoid* conformation observed in 1-3 is unfavoured, with the first local minimum energy for the system occurring at $\alpha=108^\circ$, close to the conformation observed in 4. It is notable that the maximum energy for IV occurs at the *cis* eclipsed conformation ($\alpha=0,360^\circ$). At this point both ether functions come into closest contact with the indenyl six-membered ring. The calculated barrier to rotation is *ca.* 3.7eV (roughly twice that for 3).

In conclusion theoretically calculated energy minimum conformations for models of the indenyl carbacobaltaborane series are in good agreement with those observed in the crystal structures. In addition, barriers to rotation have been calculated for I to IV, with the greatest barrier predicted to occur in the monophenyl derivative. Although this barrier is almost certainly overestimated for the real molecule, 2, (since a simple rigid rotor model is used in the calculations), it is nevertheless significant that the solution fluctuonality of 2 may be arrested by cooling, whilst that of 4 has not been.

Section B : Fluorenyl Carbametallaborane Chemistry

Introduction

The fluorenyl anion, $[\text{C}_{13}\text{H}_9]^-$, is formed on the treatment of fluorene with bases of appropriate strength. Given that it is to the indenide anion as indenide is to cyclopentadienide, *i.e.* it comprises two *pseudo*-aromatic six-carbon rings fused to the C_5 unit, it has also been considered a likely candidate to form metal complexes. Following the characterisation of ferrocene^{27,28}, numerous organometallic complexes incorporating the cyclopentadienyl ligand were synthesised. It is somewhat surprising, therefore, that only a few fluorenyl analogues have been reported, of which there is a brief resume in Chapter 1.

Having successfully characterised a number of indenyl carbacobbaltaboranes, it seemed appropriate to attempt the synthesis of at least one fluorenyl analogue. Obviously the same question arises for fluorenyl carbametallaboranes as for indenyl complexes, namely which of the various possible conformations the aromatic ligand will adopt in the solid state. The work detailed in this section includes the synthesis and structural determination of the first fluorenyl carbametallaborane, $3-(\eta^5\text{-C}_{13}\text{H}_9)\text{-}3,1,2\text{-}closo\text{-CoC}_2\text{B}_9\text{H}_{11}$, together with the results of EHMO calculations on an idealised model, which predicts a molecular conformation in full accord with that observed in the crystal structure.

3-(η^5 -C₁₃H₉)-3,1,2-closo-CoC₂B₉H₁₁, 5

Synthesis

The fluorenyl carbacobaltaborane compound **5** was synthesised by an analogous route to that previously described for the related indenyl species. Lithium fluorenyl was added drop-wise to a cold suspension of Co(acac)₃ and Tl₂[7,8-C₂B₉H₁₁] in thf, and subsequent work-up of the reaction mixture afforded the target compound. Full details are contained in Chapter 5, Section A. Although obtained in too low a yield for n.m.r. spectroscopic analysis, the compound formed crystals suitable for diffraction, and the following structural study was carried out.

Structural Study on 5

Introduction

A crystal structure determination of the fluorenyl carbacobaltaborane complex was carried out in order to fully characterise the compound, and to identify the preferred conformation of the fused aromatic ligand with respect to the metalla-bonded carbaborane face. Crystals of **5** were obtained by slow diffusion of n-hexane into a methylene chloride solution of the compound at -30°. Details of the crystal data, data collection and solution and refinement of the structure may be found in Chapter 5, Section B.

Discussion

Figure 2.13 shows a perspective view of a single molecule with the appropriate numbering scheme, hydrogen atoms having the same number as the carbon or boron atom to which they are bound. **Figure 2.14** shows a plan view, with all but the five atoms of the upper C_2B_3 face of the carbaborane ligand removed for clarity.

Table 2.11 lists refined atom co-ordinates, **Table 2.12** interbond distances and selected angles, and **Table 2.13** anisotropic thermal parameters.

Both plan and perspective views show that the fluorenyl ligand is clearly η^5 -bonded to cobalt, although the metal atom is substantially slipped across the C_5 ring, towards C(33). In contrast to the indenyl analogues, where C(34) and C(39) are always substantially further from the metal than C(31)-(33), C(31) and C(39) are furthest away from the cobalt atom [2.142(10) and 2.160(10)Å respectively], C(32) and C(34) are at intermediate distances [2.098(10) and 2.118(10)Å respectively], with the shortest M-C distance being that between Co and C(33) [2.026(10)Å]. The slip distortion, Δ^h , has a value of 0.095Å, with σ [in this case the angle between the slip vector **S** and a reference vector from the ring centroid to C(33)] being +11.85° (*i.e.* **S** is positionally anti-clockwise w.r.t. **R** when viewed from above, as in **Figure 2.13**).

Slippage towards the more electron rich C(33) is observed in other formally η^5 fluorenyl metal complexes, namely $(\eta^5-C_{13}H_9)Cr(CO)_2NO$ ¹² ($\Delta^h = 0.011$ Å) and $(\eta^5-C_{13}H_9)(\eta^3-C_{13}H_9)ZrCl_2$ ¹¹ (Δ^h for the η^5 -bonded ligand = 0.244Å). Although the latter value in particular seems quite large, the ligand is still described as being formally η^5 -bonded, with Δ^h for the η^3 -fluorenyl ligand having the much greater value of 0.474Å.

Figure 2.13 Perspective View of 3-(η^5 -C₁₃H₉)-3,1,2-closo-CoC₂B₉H₁₁, (5)

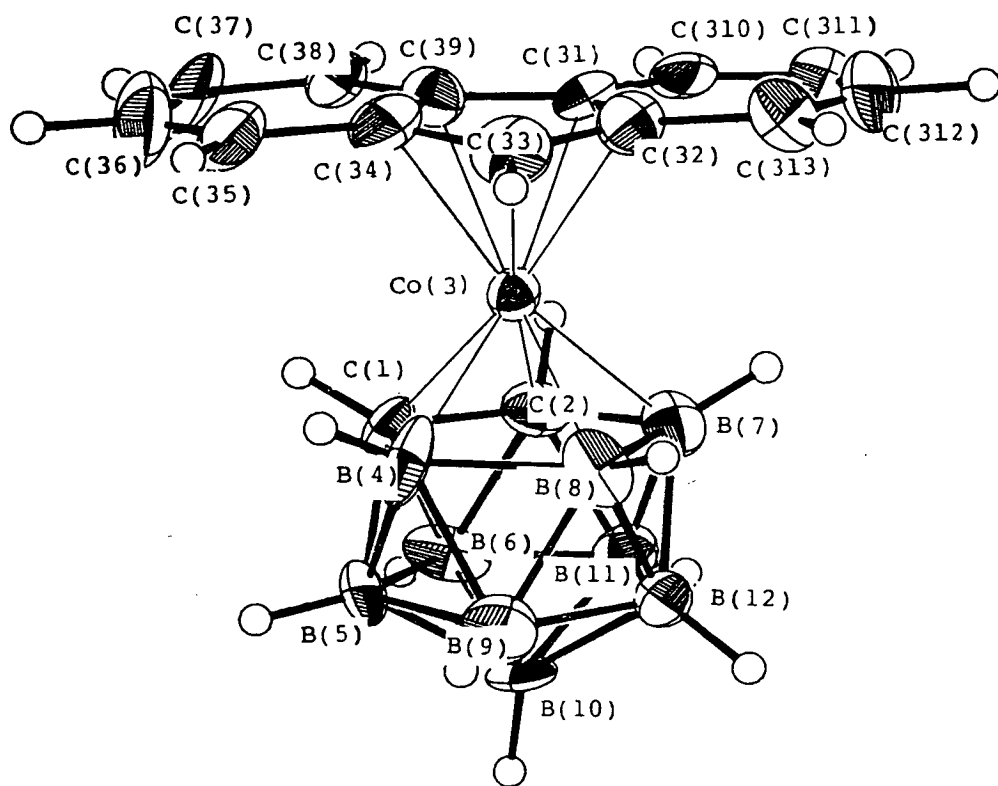


Figure 2.14 Plan View of 3-(η^5 -C₁₃H₉)-3,1,2-*closo*-CoC₂B₉H₁₁ (5) (B(5), B(6), B(9), B(10), B(11) and B(12) removed for clarity)

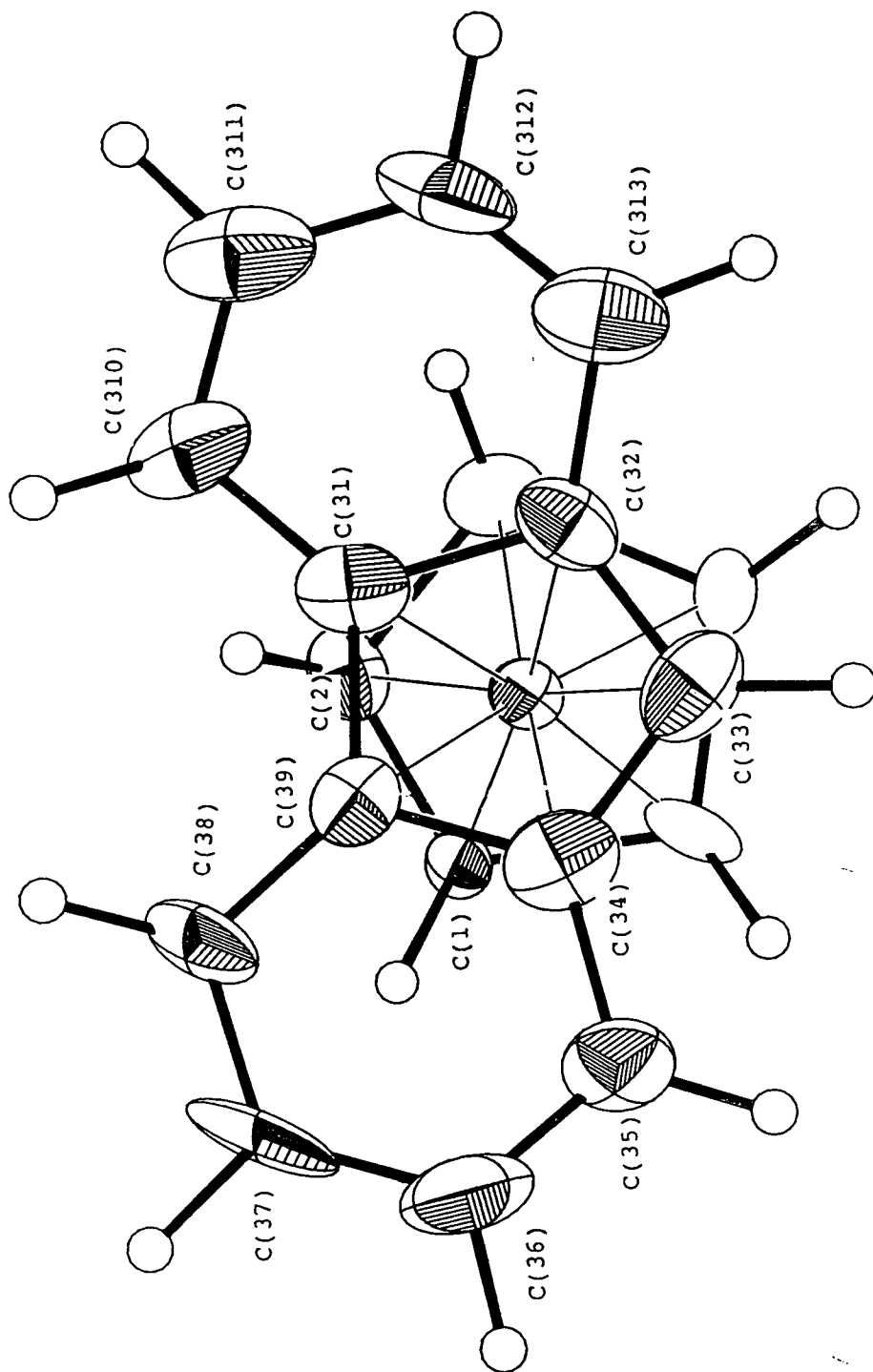


Table 2.11 Co-ordinates of Refined Atoms and Equivalent Isotropic Thermal Parameters (\AA^2) for 3-(η^5 -C₁₃H₉)-3,1,2-closo-CoC₂B₉H₁₁, (5)

	x	y	z	Ueq
Co(3)	0.32496(14)	0.07999(9)	1.10255(8)	0.0281(5)
C(1)	0.2923(9)	0.0570(6)	1.2277(6)	0.030(6)
B(4)	0.2404(14)	0.1767(11)	1.1933(10)	0.049(9)
C(2)	0.4649(12)	0.0293(7)	1.1976(6)	0.040(7)
B(8)	0.4007(14)	0.2266(9)	1.1367(7)	0.041(8)
B(7)	0.5410(13)	0.1253(10)	1.1362(7)	0.042(8)
B(11)	0.5957(14)	0.1033(10)	1.2473(9)	0.045(9)
B(12)	0.5527(14)	0.2298(9)	1.2102(8)	0.037(8)
B(6)	0.4378(16)	0.0584(9)	1.3046(7)	0.044(8)
B(5)	0.2956(14)	0.1527(10)	1.3036(7)	0.044(8)
B(10)	0.4906(14)	0.1845(10)	1.3132(7)	0.042(8)
B(9)	0.3709(15)	0.2604(10)	1.2495(10)	0.054(9)
C(32)	0.3426(12)	0.0788(8)	0.9664(5)	0.041(5)
C(31)	0.3627(10)	-0.0272(8)	0.9991(6)	0.042(7)
C(39)	0.2214(11)	-0.0536(7)	1.0438(6)	0.038(6)
C(33)	0.2047(11)	0.1180(8)	0.9947(6)	0.051(7)
C(38)	0.1737(13)	-0.1422(7)	1.0881(6)	0.047(6)
C(34)	0.1237(11)	0.0330(8)	1.0374(7)	0.048(7)
C(35)	-0.0250(11)	0.0336(8)	1.0774(7)	0.052(7)
C(36)	-0.0653(12)	-0.0519(10)	1.1200(8)	0.070(9)
C(37)	0.0299(13)	-0.1385(10)	1.1269(7)	0.071(9)
C(310)	0.5019(10)	-0.0845(10)	0.9858(6)	0.053(7)
C(313)	0.4634(13)	0.1186(9)	0.9136(6)	0.060(8)
C(312)	0.5872(13)	0.0633(10)	0.9002(7)	0.064(8)
C(311)	0.6130(13)	-0.0367(10)	0.9368(7)	0.066(8)

Table 2.12 Interatomic Distances (Å) and Selected Interbond Angles (°) for
 $3-(\eta^5-C_{13}H_9)-3,1,2-closo-CoC_2B_9H_{11}$, (5)

Co(3) - C(1)	1.967(8)	B(11) -B(12)	1.785(18)
Co(3) - B(4)	2.021(14)	B(11) - B(6)	1.741(18)
Co(3) - C(2)	2.018(10)	B(11) -B(10)	1.730(18)
Co(3) - B(8)	2.090(12)	B(12) -B(10)	1.775(17)
Co(3) - B(7)	2.049(12)	B(12) - B(9)	1.749(18)
Co(3) -C(32)	2.098(10)	B(6) - B(5)	1.750(17)
Co(3) -C(31)	2.142(10)	B(6) -B(10)	1.713(17)
Co(3) -C(39)	2.160(9)	B(5) -B(10)	1.764(17)
Co(3) -C(33)	2.026(10)	B(5) - B(9)	1.761(18)
Co(3) -C(34)	2.118(10)	B(10) - B(9)	1.743(18)
C(1) - B(4)	1.709(16)	C(32) -C(31)	1.481(14)
C(1) - C(2)	1.621(13)	C(32) -C(33)	1.382(14)
C(1) - B(6)	1.738(15)	C(32) -C(313)	1.430(15)
C(1) - B(5)	1.708(15)	C(31) -C(39)	1.456(13)
B(4) - B(8)	1.775(18)	C(31) -C(310)	1.444(14)
B(4) - B(5)	1.790(18)	C(39) -C(38)	1.405(14)
B(4) - B(9)	1.801(19)	C(39) -C(34)	1.420(14)
C(2) - B(7)	1.703(16)	C(33) -C(34)	1.471(14)
C(2) -B(11)	1.682(16)	C(38) -C(37)	1.395(15)
C(2) - B(6)	1.704(16)	C(34) -C(35)	1.440(15)
B(8) - B(7)	1.803(17)	C(35) -C(36)	1.340(16)
B(8) -B(12)	1.747(17)	C(36) -C(37)	1.408(17)
B(8) - B(9)	1.808(18)	C(310) -C(311)	1.379(16)
B(7) -B(11)	1.796(18)	C(313) -C(312)	1.318(16)
B(7) -B(12)	1.777(17)	C(312) -C(311)	1.439(16)
C(1) -Co(3) - B(4)	50.7(5)	B(11) -B(12) -B(10)	58.1(7)
C(1) -Co(3) - C(2)	48.0(4)	B(10) -B(12) - B(9)	59.3(7)
B(4) -Co(3) - B(8)	51.1(5)	C(1) - B(6) - C(2)	56.2(6)
C(2) -Co(3) - B(7)	49.5(4)	C(1) - B(6) - B(5)	58.6(6)
B(8) -Co(3) - B(7)	51.7(5)	C(2) - B(6) -B(11)	58.4(7)
C(32) -Co(3) -C(31)	40.9(4)	B(11) - B(6) -B(10)	60.1(7)
C(32) -Co(3) -C(33)	39.1(4)	B(5) - B(6) -B(10)	61.2(7)
C(31) -Co(3) -C(39)	39.6(4)	C(1) - B(5) - B(4)	58.4(6)
C(39) -Co(3) -C(34)	38.7(4)	C(1) - B(5) - B(6)	60.3(6)
C(33) -Co(3) -C(34)	41.5(4)	B(4) - B(5) - B(9)	61.0(7)
Co(3) - C(1) - B(4)	66.3(5)	B(6) - B(5) -B(10)	58.3(7)
Co(3) - C(1) - C(2)	67.6(5)	B(10) - B(5) - B(9)	59.3(7)
B(4) - C(1) - B(5)	63.2(7)	B(11) -B(10) -B(12)	61.2(7)
C(2) - C(1) - B(6)	60.9(6)	B(11) -B(10) - B(6)	60.8(7)
B(6) - C(1) - B(5)	61.1(6)	B(12) -B(10) - B(9)	59.6(7)
Co(3) - B(4) - C(1)	63.0(5)	B(6) -B(10) - B(5)	60.4(7)
Co(3) - B(4) - B(8)	66.4(6)	B(5) -B(10) - B(9)	60.3(7)
C(1) - B(4) - B(5)	58.4(6)	B(4) - B(9) - B(8)	58.9(7)
B(8) - B(4) - B(9)	60.7(7)	B(4) - B(9) - B(5)	60.3(7)
B(5) - B(4) - B(9)	58.7(7)	B(8) - B(9) -B(12)	58.8(7)
Co(3) - C(2) - C(1)	64.4(5)	B(12) - B(9) -B(10)	61.1(7)
Co(3) - C(2) - B(7)	66.2(5)	B(5) - B(9) -B(10)	60.4(7)
C(1) - C(2) - B(6)	63.0(6)	C(31) -C(32) -C(33)	110.0(8)
B(7) - C(2) -B(11)	64.1(7)	C(31) -C(32) -C(313)	116.3(9)

B(11) - C(2) - B(6)	61.9(7)
Co(3) - B(8) - B(4)	62.4(6)
Co(3) - B(8) - B(7)	63.0(5)
B(4) - B(8) - B(9)	60.3(7)
B(7) - B(8) -B(12)	60.0(7)
B(12) - B(8) - B(9)	58.9(7)
Co(3) - B(7) - C(2)	64.3(5)
Co(3) - B(7) - B(8)	65.3(5)
C(2) - B(7) -B(11)	57.4(7)
B(8) - B(7) -B(12)	58.4(7)
B(11) - B(7) -B(12)	59.9(7)
C(2) -B(11) - B(7)	58.5(7)
C(2) -B(11) - B(6)	59.7(7)
B(7) -B(11) -B(12)	59.5(7)
B(12) -B(11) -B(10)	60.6(7)
B(6) -B(11) -B(10)	59.1(7)
B(8) -B(12) - B(7)	61.5(7)
B(8) -B(12) - B(9)	62.3(7)
B(7) -B(12) -B(11)	60.6(7)

C(33) -C(32) -C(313)	133.7(9)
C(32) -C(31) -C(39)	106.2(8)
C(32) -C(31) -C(310)	122.3(9)
C(39) -C(31) -C(310)	131.4(9)
C(31) -C(39) -C(38)	132.5(9)
C(31) -C(39) -C(34)	107.0(8)
C(38) -C(39) -C(34)	120.5(9)
C(32) -C(33) -C(34)	106.5(9)
C(39) -C(38) -C(37)	116.6(9)
C(39) -C(34) -C(33)	109.8(9)
C(39) -C(34) -C(35)	121.4(9)
C(33) -C(34) -C(35)	128.5(9)
C(34) -C(35) -C(36)	116.2(10)
C(35) -C(36) -C(37)	123.3(11)
C(38) -C(37) -C(36)	122.0(11)
C(31) -C(310)-C(311)	116.1(9)
C(32) -C(313)-C(312)	119.9(10)
C(313)-C(312)-C(311)	124.3(11)
C(310)-C(311)-C(312)	120.8(10)

Table 2.13 Anisotropic Thermal Parameters (\AA^2) for 3-(η^5 -C₁₃H₉)-3,1,2-closo-CoC₂B₉H₁₁, (5)

	U11	U22	U33	U23	U13	U12
Co(3)	0.0284(5)	0.0274(6)	0.0285(5)	0.0015(8)	0.0003(8)	-0.0018(8)
C(1)	0.0218(57)	0.0186(58)	0.0510(61)	-0.0030(44)	-0.0021(46)	-0.0064(42)
B(4)	0.0292(70)	0.0534(90)	0.064 (10)	0.0308(76)	-0.0001(71)	-0.0183(71)
C(2)	0.0545(69)	0.0350(63)	0.0303(63)	0.0017(50)	-0.0052(58)	-0.0012(60)
B(8)	0.0484(77)	0.0340(75)	0.0406(76)	0.0118(60)	0.0072(64)	0.0171(66)
B(7)	0.0356(76)	0.0647(94)	0.0268(68)	0.0060(64)	-0.0048(57)	0.0038(71)
B(11)	0.0395(74)	0.052 (10)	0.0443(76)	-0.0006(72)	-0.0079(68)	-0.0042(69)
B(12)	0.0430(78)	0.0314(75)	0.0362(73)	-0.0024(62)	0.0052(65)	-0.0094(65)
B(6)	0.0740(91)	0.0320(90)	0.0273(69)	0.0035(59)	-0.0120(68)	0.0157(75)
B(5)	0.0482(94)	0.0546(82)	0.0305(71)	-0.0012(61)	0.0220(65)	-0.0170(75)
B(10)	0.0484(84)	0.0515(85)	0.0250(71)	-0.0155(64)	-0.0125(66)	-0.0153(72)
B(9)	0.0540(98)	0.0441(85)	0.0633(92)	-0.0121(82)	0.0053(80)	0.0014(74)
C(32)	0.0483(61)	0.0459(56)	0.0298(45)	0.0090(62)	-0.0048(55)	-0.0087(78)
C(31)	0.0333(64)	0.0522(70)	0.0398(60)	-0.0119(54)	-0.0089(52)	-0.0144(55)
C(39)	0.0365(60)	0.0420(72)	0.0358(58)	-0.0021(52)	-0.0011(47)	0.0053(49)
C(33)	0.0369(69)	0.0652(77)	0.0494(66)	-0.0035(58)	-0.0156(58)	0.0140(61)
C(38)	0.0570(63)	0.0360(56)	0.0483(69)	-0.0095(51)	0.0107(76)	-0.0295(63)
C(34)	0.0354(63)	0.0615(75)	0.0465(68)	-0.0087(63)	-0.0134(56)	-0.0058(61)
C(35)	0.0353(63)	0.0509(70)	0.0685(88)	-0.0116(60)	-0.0026(59)	-0.0120(58)
C(36)	0.0343(61)	0.083 (11)	0.094 (11)	-0.0064(86)	0.0223(73)	-0.0039(69)
C(37)	0.0669(89)	0.0698(90)	0.075 (10)	0.0023(76)	0.0142(76)	-0.0598(78)
C(310)	0.0421(58)	0.0569(68)	0.0587(71)	-0.0424(71)	0.0079(55)	-0.0110(71)
C(313)	0.0636(77)	0.0795(90)	0.0381(75)	-0.0016(62)	0.0089(66)	-0.0128(70)
C(312)	0.0745(79)	0.0710(88)	0.0465(62)	0.0068(89)	0.0241(75)	-0.0289(74)
C(311)	0.0586(79)	0.088 (10)	0.0513(73)	-0.0342(67)	0.0154(62)	-0.0231(72)

The C₅ ring in **5** is also folded towards Co(3) in an envelope conformation, by 6.87° across the C(32).....C(34) vector. Although all fluorenyl carbon atoms are not entirely co-planar, as a whole the ligand is tilted such that C(37) is *ca.* 0.25Å closer to the lower B₅ belt than C(313).

As expected there is no substantial slippage of the metal atom across the C₂B₃ carbaborane face, the actual value of Δ^P, the slip parameter, being zero to within experimental error. The C₂B₃ face is, however, envelope folded about the B(4)...B(7) vector, with fold angles θ^P= 2.69° and φ^P= 1.37°.

As previously stated, an important feature of the structure of **5** is the conformation of the fluorenyl ligand relative to the metal-bonded carbaborane face. For indenyl carbametallaboranes it has been shown that, in the absence of more than one bulky substituent, the indenyl ligand preferentially lies such that its six-membered ring is *cisoid* with respect to the cage carbons. In this orientation the relatively weak metal-C_{ring-*junction*} bonding can be compensated by relatively strong metal-boron bonding, the frontier molecular orbitals of the carbaborane ligand being localised on the facial boron atoms. Extending this argument to **5**, in which there are now two pairs of ring-*junction* carbon atoms in the carbocyclic ligand, of the three possible staggered conformations shown in Figure 2.15 the observed conformation is intuitively expected to be A, which involves one pair of bridge-carbon atoms, C(34) and C(39) lying *trans* to two boron atoms, with the other pair, C(31) and C(32) *trans* to one boron atom and one carbon atom. In B C(31) and C(32) are *trans* to 2 carbon atoms, and in C both sets of bridge-carbon atoms are *trans* to one carbon and one boron atom.

A series of EHMO calculations were performed on an idealized model of **5** in order to compare the crystallographically observed conformation with that predicted theoretically. As for the related indenyl carbacobaltaboranes, the change in the sum

of 1-electron energies was monitored as a function of rigid rotation of, in this case, the $[\text{C}_{13}\text{H}_9]^-$ ligand about the $\text{Co}(3)\cdots\text{B}(10)$ vector.

Figure 2.16 presents the results of the calculations in the form of an energy curve. The theoretical minimum energy conformation of the system occurs at $\alpha = 144^\circ$, which corresponds to the conformation observed in the crystal structure [$\alpha = 0$ corresponds to a *cis-staggered* conformation, in which C(94) and C(99) lie directly above the cage atom B(1)]. As for the corresponding model of the indenyl carbacobaltaborane, **1**, local maxima correspond to eclipsed forms, and local minima to the staggered conformations A, B and C, as depicted in Figure 2.15. The calculated barrier to rotation is 0.27eV.

In addition, it is worth noting the cobalt ring-junction carbon distances in relation to calculated atom-atom overlap populations. As C(34) and C(39) are both *trans* to two boron atoms, and metal-boron bonding is expected to be somewhat stronger than metal-cage carbon bonding, correspondingly weaker interactions between Co(3) and C(34,39) can be expected than between Co(3) and C(31,32), which are both *trans* to one carbon and one boron atom. Although measured errors in the observed distances are too large to render the differences statistically significant, it is nevertheless worth noting that Co(3)-C(39) is indeed 0.018(13)Å longer than Co(3)-C(31), and Co(3)-C(34) is 0.020(14)Å longer than Co(3)-C(32). Moreover, the relative distances are in accord with calculated atom-atom overlap populations, shown in Figure 2.15, diagram A.

Figure 2.15 The Possible Staggered Conformations of 5

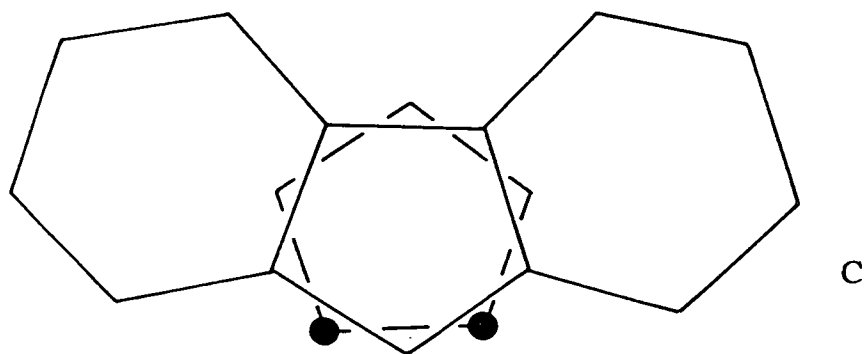
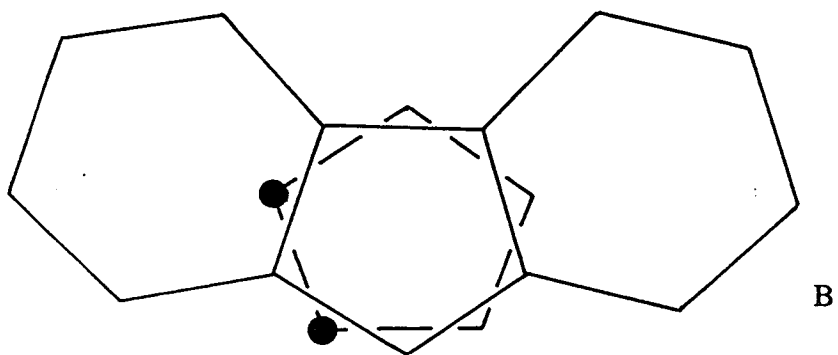
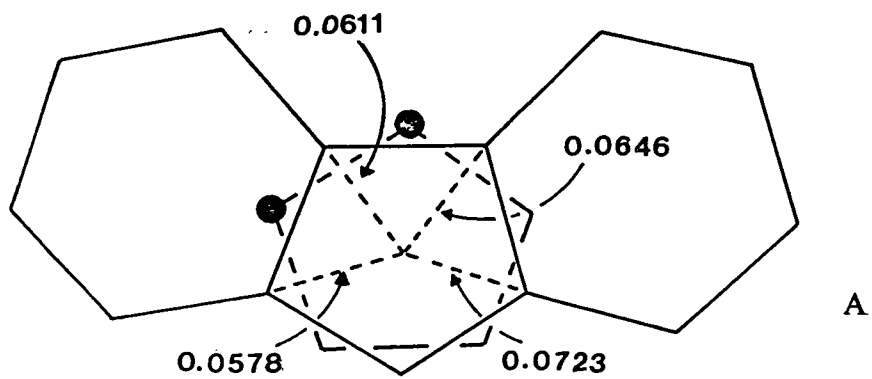
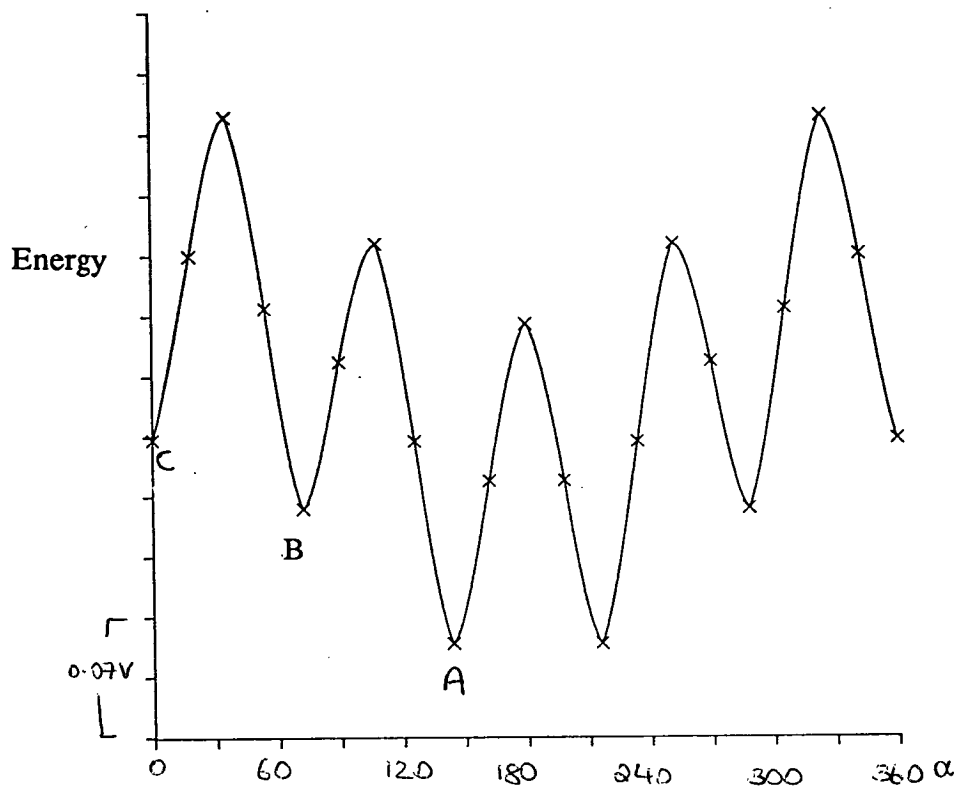


Figure 2.16 Relative Energy Plot for an Idealised Model of **5**



Finally, the observed conformation of **5** can be compared with that of another fluorenyl complex, $(\eta^5\text{-C}_{13}\text{H}_9)\text{Cr}(\text{CO})_2\text{NO}$ ¹², where more than one orientation of the carbocyclic ligand is possible. In the latter compound the metal is bonded on one side by the fluorenyl group, and on the other by one nitrosyl and two carbonyl ligands. The crystallographically determined conformation is one in which the more electron withdrawing nitrosyl group is *trans* to the relatively electron rich carbon, C(1) [equivalent to C(33) in **5**]. The weaker junction carbon-metal bonds are *trans* to those between the neutral carbonyl ligands and chromium.

This is fully comparable to the situation occurring in the fluorenyl carbacobaltaborane, where the more electronegative cage carbon atoms are *trans* to relatively electron rich C(33), and the facial boron atoms, more strongly bound to the metal, are *trans* to the ring junction carbons of the aromatic ligand.

Conclusions

Three indenyl carbacobaltaborane complexes, incorporating carbaborane ligands in which bulky alkyl or aryl functions have been introduced at the cage carbon atoms, have been synthesised and spectroscopically and structurally characterised. In the case of the two monosubstituted derivatives, **2** and **3**, the observed conformation of the indenyl six-membered ring w.r.t. the cage carbon atoms is *cisoid*, which is also the conformation observed in the previously reported unsubstituted species, **1**. However, the presence of two ether functions in **4** has resulted in the adoption of the "next best" staggered conformation. A series of EHMO calculations performed on idealised models of the four complexes **1-4** have predicted theoretical minimum energy conformations which are close to those observed in the crystal structure determinations.

In addition, an analogous fluorenyl carbacobaltaborane has been synthesised and structurally characterised. The conformation of the fused aromatic ligand w.r.t. the cage carbon atoms has been readily explained in terms of relative bond strengths between the cobalt atom and the metalla-bonded ligand atoms, such that relatively strong Co-B(4,7,8) bonds are *trans* to the weaker fluorenyl-Co bonds. This observed conformation is in full accord with that predicted from a series of EHMO calculations performed on an idealised model of the compound.

Chapter 3

Indenyl Rhodium Carbaborane Complexes

Introduction

The indenyl carbacobaltaboranes described in the previous Chapter generally form in quite modest yields, as do metallaboranes and carbametallaboranes incorporating $\{\text{CpCo}\}^{69}$ and $\{\text{Cp}^*\text{Co}\}^{70}$ moieties ($\text{Cp}^* = (\text{CH}_3)_5\text{C}_5$). This may well be attributed to the somewhat arbitrary route employed in the synthesis of these compounds, involving the reaction of CoCl_2 or $\text{Co}(\text{acac})_3$ with the appropriate cyclopentadienide and carbaborane anions.

In contrast, some metallaboranes and carbametallaboranes incorporating a $\{\text{CpRh}\}/\{\text{Cp}^*\text{Rh}\}$ moiety have been reported in relatively good yields, from reactions involving the metal halide complexes $[\text{CpRhX}_2]_n^{71}$ (where $\text{X} = \text{I}$ and n is greater than 2) and $[\text{Cp}^*\text{RhCl}_2]_2^{72,73}$. In such reactions the cyclopentadienyl metal dichloride precursor introduces an already intact ligand-metal fragment to the borane or carbaborane anion, thus reducing the likelihood of numerous side-reactions, and resulting in higher yields of target products compared with cobalt analogues. Potentially higher yield syntheses of a number of analogous indenyl metalla- and carbametallaboranes were thus envisaged, starting with the hitherto unknown indenyl analogue of $[\text{Cp}^*\text{RhCl}_2]_2$ and the non-methylated amorphous species $[\text{CpRhCl}_2]_n$.

This Chapter details the reactions of the previously unreported species " $[(\text{C}_9\text{H}_7)\text{RhCl}_2]_2$ " with a number of carbaborane anions of the type $[\text{R}_1\text{R}_2\text{C}_2\text{B}_9\text{H}_9]^{2-}$, resulting in the formation of a variety of carbarhodaboranes of novel structure. It begins with a brief introduction to the syntheses and reaction chemistry of $[\text{CpRhX}_2]_n$ and $[\text{Cp}^*\text{RhCl}_2]_2$, forming the precedent for the attempted synthesis of an indenyl

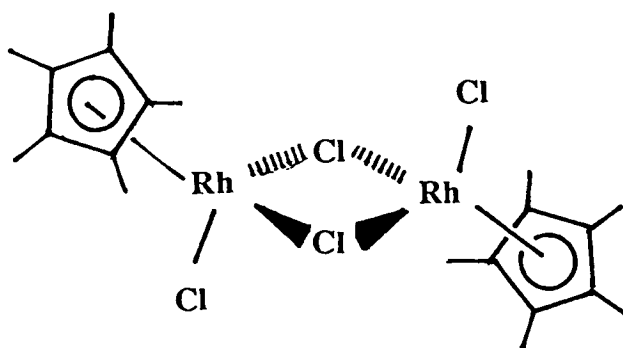
analogue. The syntheses and characterisation of a number of indenyl rhodium carbaborane complexes are then discussed, followed by a general consideration of the nature of the reactions involved.

Chemistry of $[\text{CpRhX}_2]_n$ and $[\text{Cp}^*\text{RhCl}_2]_2$

The synthesis of $[\text{CpRhBr}_2]_n$ from the reaction of $(\text{C}_5\text{H}_5)\text{Rh}(\text{C}_5\text{H}_4\text{Ph})$ with bromine, was reported in 1963.⁷⁴ Five years later, a synthetic route to the chloride was reported, which involves a multi-step reaction starting with $\text{RhCl}_2(\eta^3\text{-C}_3\text{H}_5)_2$ and TiCp .⁷⁵ A more convenient synthesis of the latter was detailed by Maitlis and co-workers, from the reaction of $\text{RhCl}_3 \cdot 3\text{H}_2\text{O}$ with freshly cracked cyclopentadiene in refluxing methanol.⁷⁶ This was published together with the synthesis and characterisation of $[\text{Cp}^*\text{RhCl}_2]_2$, the first known complex containing a $\{\text{Cp}^*\text{Rh}\}$ moiety. The latter was, in fact, prepared serendipitously, during the reaction of $\text{RhCl}_3 \cdot 3\text{H}_2\text{O}$ with hexamethyl (Dewar) benzene, (hexamethylbicyco[2.2.0]hexa-2,5-diene).

The structure of the pentamethylated derivative, which is soluble in organic solvents, has been determined crystallographically,⁷⁷ and is represented in **Figure 3.1**. The Rh_2Cl_2 bridge is planar, and the long Rh-Rh distance of 3.719 Å indicates the absence of a Rh-Rh bond. The structure of the unsubstituted Cp analogue is less well defined. The fact that it is insoluble in all organic solvents is suggestive of polymeric character. The infrared spectrum indicates that the metal is bonded to both terminal and bridging chloride ions, with polymer formation possibly occurring *via* chloride bridges.

Figure 3.1 Structure of $[\text{Cp}^*\text{RhCl}_2]_2$



The chemistry of $[\text{Cp}^*\text{MCl}_2]_2$ ($\text{M} = \text{Rh}, \text{Ir}$) has been well documented, as these compounds and their derivatives have been found to catalyse the hydrogenation of alkenes and arenes.⁷⁸ The dimeric complexes undergo a variety of reactions; in addition to metathetical replacement by other halides and pseudo-halides, the chloride bridge is split on reaction with donor ligands (*e.g.* phosphines)⁷⁶ to yield monomeric species. Such reactions have extended into the field of boron chemistry, with the *arachno* borane anion, $[\text{B}_9\text{H}_{14}]^-$, and the *nido* carbaborane anion $[\text{C}_2\text{B}_9\text{H}_{12}]^-$ (in the presence of base), readily yielding the *nido* species $\text{Cp}^*\text{RhB}_9\text{H}_{13}$ ⁷² and the *closo* species $\text{Cp}^*\text{RhC}_2\text{B}_9\text{H}_{11}$ ⁷³ in 96% and 34% yields respectively, upon reaction with $[\text{Cp}^*\text{RhCl}_2]_2$ at room temperature.

The chemistry of $[\text{CpRhCl}_2]_2$ has not been as intensively investigated as its dimeric Cp^* analogue. However, it also undergoes halide bridge splitting reactions with donor ligands to give monomeric compounds. In addition, the iodo analogue, $[\text{CpRhI}_2]_n$, was reacted with $\text{Ti}_2[\text{C}_2\text{B}_9\text{H}_{11}]$, affording $\text{CpRhC}_2\text{B}_9\text{H}_{11}$ in 30% yield.⁷¹

Given the fact that many indenyl analogues of Cp and Cp^* metal complexes are

known, it was reasonable to assume that the synthesis of an indenyl rhodium dichloride dimer/polymer, a potentially useful synthetic precursor, would be relatively facile.

Synthesis and Characterisation of " $[(C_9H_7)RhCl_2]_2$ "

The synthesis of indenyl rhodium dichloride was attempted using an analogous route to that which afforded the polymeric species, $[CpRhCl_2]_n$.⁷⁶ Thus, $RhCl_3 \cdot 3H_2O$ and freshly distilled indene were reacted together in refluxing methanol for fifteen hours, during which time a light brown solid precipitated. Microanalysis figures were consistent for the formulation $(C_9H_7)RhCl_2$. The low solubility of the product in organic solvents such as methylene chloride, chloroform and acetonitrile was indicative of some polymeric character. The infrared spectrum of the solid contained absorptions at 330, 240, and 230cm^{-1} , corresponding to both terminal and bridging Rh-Cl stretches respectively.

The n.m.r. spectrum of that part of the product soluble in methylene chloride suggests a complex structure, which will be discussed in more detail following a summary of a number of reactions of indenyl rhodium dichloride with dithallium carbaboranes. For these reactions the formulation " $[(C_9H_7)RhCl_2]_2$ " was adopted to formally describe the new complex, and a ratio of one mole of carbaborane to one mole of rhodium was used.

Reaction of " $[(C_9H_7)RhCl_2]_2$ " with $Tl_2[7,8-C_2B_9H_{11}]$

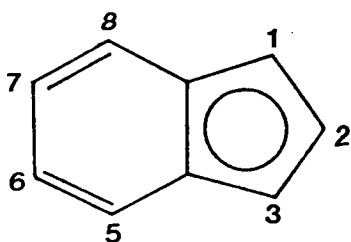
The reaction of " $[(C_9H_7)RhCl_2]_2$ " with $Tl_2[7,8-C_2B_9H_{11}]$ in methylene chloride afforded three major products, 6a, 6b and 6c, in relatively small yields (all <10%), which were isolated by preparative tlc. Full experimental details may be found in Chapter 5, Section A.

Elucidation of the Structure of 6a

This species, chromatographically the most mobile band, was isolated as a yellow microcrystalline solid. Microanalysis figures for the solid were consistent with the expected *closo*-carboradaborane, $(C_9H_7)RhC_2B_9H_{11}$. However, subsequent spectral and X-ray structural analysis showed this initial supposition to be incorrect.

Analysis of N.m.r. Spectra

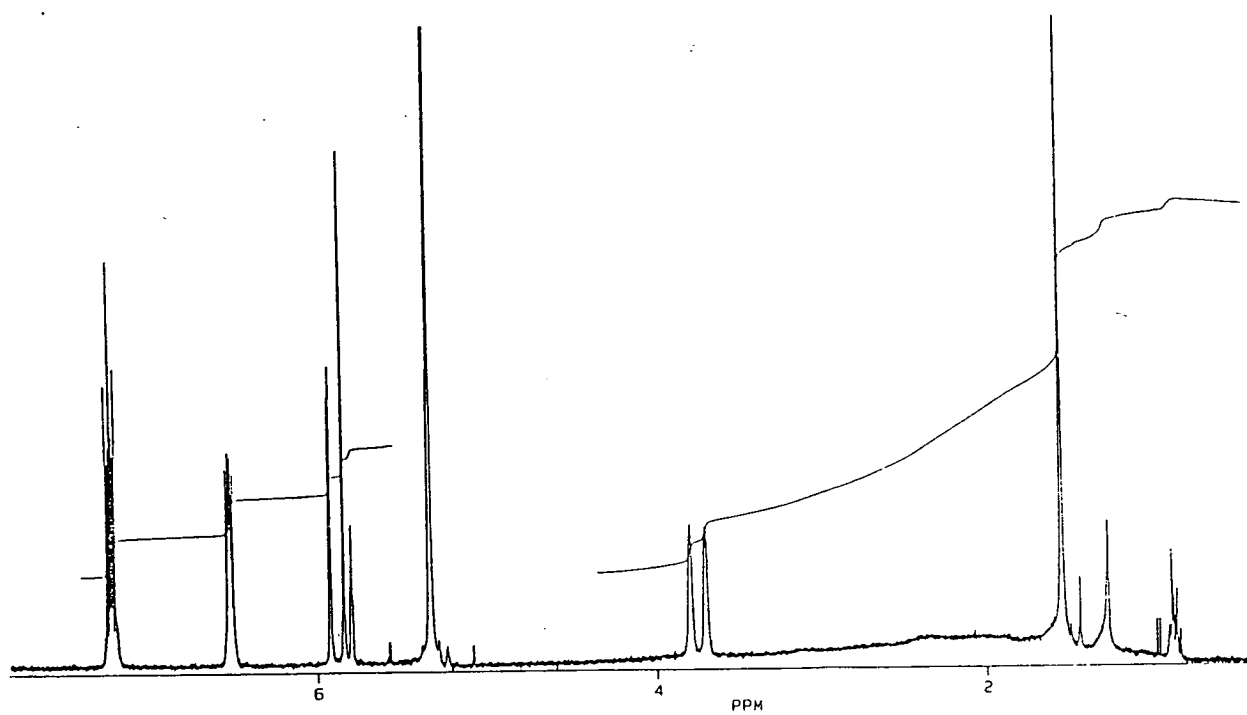
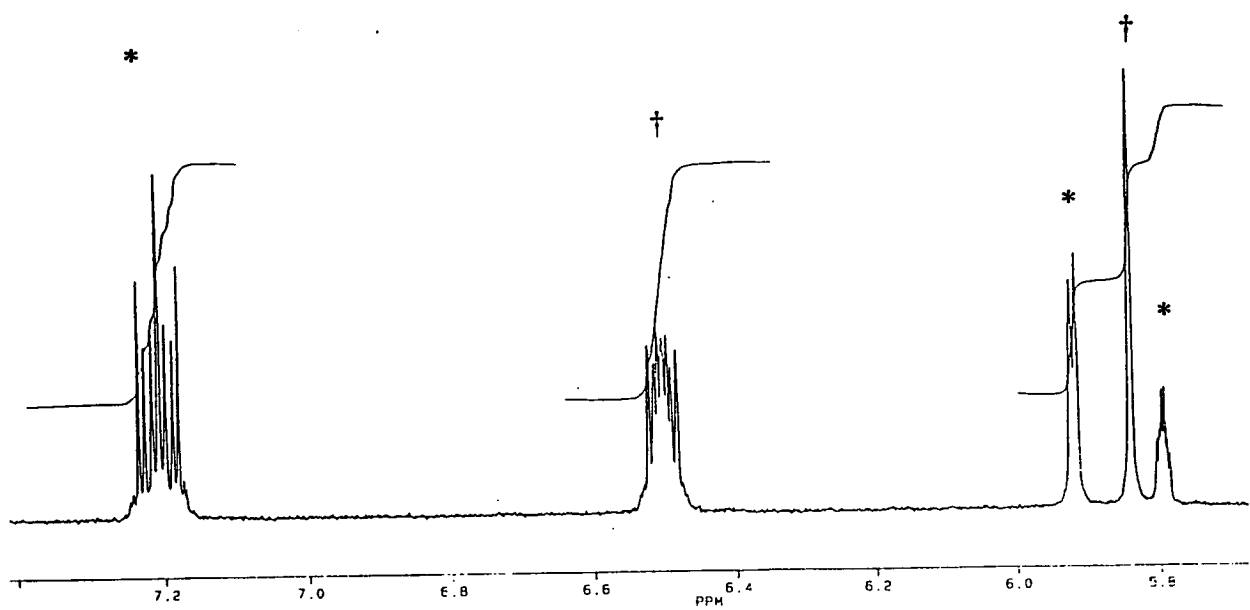
The proton spectrum, shown in Figure 3.2, exhibits some unexpected features. Considering first the aromatic region, which has been expanded for detailed analysis, it appears that more than one indenyl moiety is present in the compound. The expected resonance pattern for a metal-bonded $[C_9H_7]^-$ ligand is observed, with a multiplet, corresponding to H(5-8) (see numbering scheme below), a doublet, H(1,3) and a triplet, H(2), (all of which are marked with a * on Figure 3.2).



In addition a lower field multiplet is observed, corresponding to four protons, together with a singlet of integral 2H. These resonances, (marked by a † on Figure 3.2), may be attributed to an η^5 -bonded $\{C_9H_6\}$ moiety, where substitution of the hydrogen atom H(2) has occurred, resulting in the downfield shift of resonances due to H(5-8) and the signal corresponding to H(1) and H(3) being a singlet.

In the lower frequency region of the spectrum, there are two resonances, at δ 3.80 and 3.71 p.p.m. (both of integral 2H), corresponding to the carbon-bound *exo*-polyhedral hydrogen atoms; this suggests two C_2B_9 cages, of different nature.

Figure 3.2 ^1H N.M.R. Spectrum of 6a



The $^{11}\text{B}\text{-}\{^1\text{H}\}$ spectrum of **6a** corroborates this evidence, as it exhibits twelve resonances in the ratio 1:1:1:1:2:2:2:2:2:1:1, which integrate for a total of eighteen boron atoms. Two carbaborane cages are thus present in the complex, both having apparent mirror symmetry. The proton-coupled spectrum shows that one boron atom (that which has the highest frequency resonance, 9.19p.p.m.) does not have an associated *exo*-polyhedral hydrogen atom. Thus substitution has presumably occurred on one of the cages, and, given the evidence from the proton spectrum, it is reasonable to assume that the "missing" *exo*-H atom has been replaced by the $\{\text{C}_9\text{H}_6\}$ indenyl moiety, with the formation of a B-C bond. From comparison of this spectrum with that of the the previously assigned related carboradaborane, $\text{Cp}^*\text{RhC}_2\text{B}_9\text{H}_{11}$,⁷³ the substituted boron atom is the unique facial boron atom, B(8), which renders the cage a plane of symmetry. A $^{11}\text{B}\text{-}^{11}\text{B}$ COSY experiment was carried out, and the spectrum is presented in **Figure 3.3**. **Table 3.1** lists the associated resonance assignments for both the substituted and unsubstituted cages in **6a**, together with those made for $\text{Cp}^*\text{RhC}_2\text{B}_9\text{H}_{11}$.

On the strength of this n.m.r. data, two possible structures, **A** and **B**, illustrated in **Figure 3.4**, may be postulated. Structure **A** comprises two neutral indenyl-rhodium-carbaborane moieties fused *via* a B-C bond, whereas structure **B** is best described as a zwitterionic species, and involves the linking of positively charged bis-indenyl rhodium and negatively charged bis-dicarbollyl rhodium fragments. These two structures are not distinguishable from the n.m.r. data alone.

Figure 3.3 ^{11}B - ^{11}B COSY N.M.R. Spectrum of **6a**

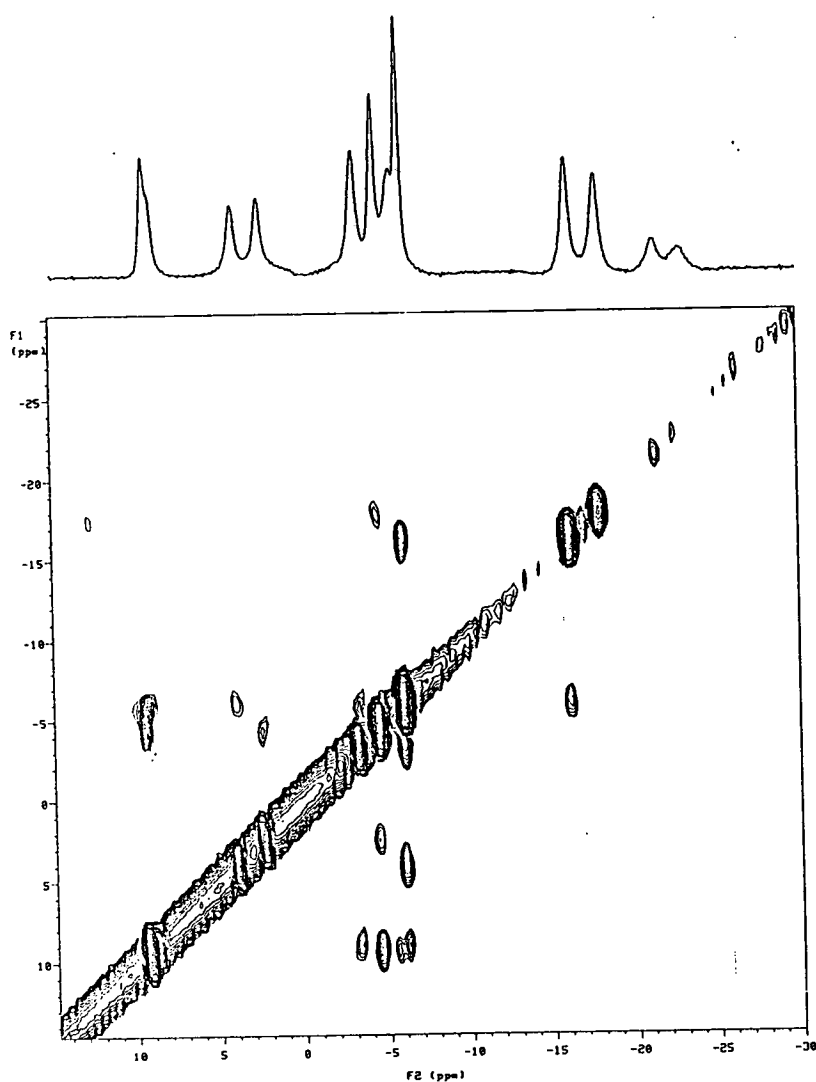
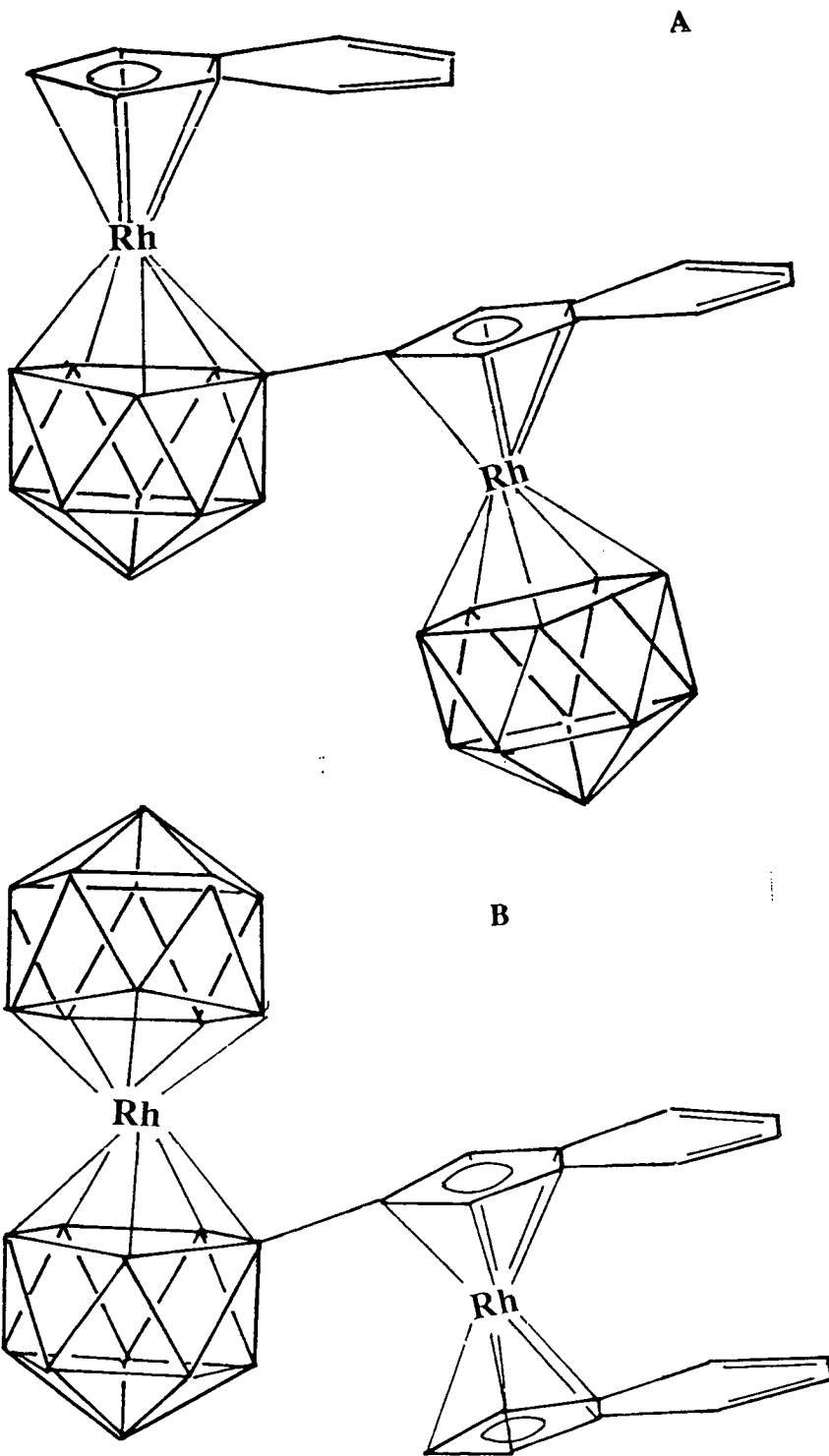


Table 3.1 ^{11}B Resonance Assignments for **6a** and $\text{Cp}^*\text{RhC}_2\text{B}_9\text{H}_{11}$

B Atom	$\text{Cp}^*\text{RhC}_2\text{B}_9\text{H}_{11}$	6a (Subst. Cage)	6a (Unsubst. Cage)
	δ	δ	δ
8	+8.6	+9.2	+9.0
10	-1.8	+2.3	+3.9
4,7	-3.5	-5.5	-3.5
9,12	-8.3	-4.5	-6.1
5,11	-18.6	-17.9	-16.1
6	-23.4	-21.2	-22.8

Figure 3.4 Two possible structures of 6a



Structural Study on 6a

In order to unequivocally establish the nature of 6a, a crystal structure determination was carried out on a very small crystal of the compound, grown by slow diffusion of hexane into a thf solution of 6a at -30°C.

Discussion

A perspective view of a single molecule of 6a is presented in Figure 3.5, with appropriate atomic numbering. The compound is clearly shown to be the zwitterionic structure, B, formally 3-(C₂B₉H₁₁)-8-((C₉H₆)Rh(C₉H₇))-3,1,2-*closo*-RhC₂B₉H₁₀. In the substituted cage, the carbon atoms were assigned by a combination of their lower thermal parameters (when refined as boron atoms), and the fact that the n.m.r spectrum suggests both cages have a plane of symmetry. In the unsubstituted cage only C(1P) could be distinguished from lower thermal parameters, with B(2P) and B(4P) [both adjacent to C(1P)] assigned part occupancies of 5.5e [(B+C)/2]. The data collected was not sufficiently accurate to enable location of the cage hydrogen atoms. Table 3.2 gives final atomic co-ordinates for refined atoms, and anisotropic thermal parameters for the two rhodium atoms, and Table 3.3 lists selected bond distances and interbond angles.

A number of observations can be made, even though the accuracy of the crystallographic determination is limited. Regarding the bis-indenyl rhodium fragment, the {C₉H₇} and {C₉H₆} moieties are both clearly η⁵-bonded to Rh(2). The large errors in Rh(2)-C distances render the calculation of slip distortions somewhat meaningless. However, the average rhodium-C(14,19) [2.18(6)Å] and C(24,29) [2.23(6)Å] distances are greater than the average distances from Rh(2) to C(11-13) [2.13(7)Å] and C(21-23) [2.12(5)Å], which is a common feature in indenyl metal complexes, and has been discussed previously in some detail in Chapters 1 and 2.

The two indenyl ligands are essentially in a *cis*-eclipsed conformation, with the rotation angle of 8° between them (the rotation angle, RA, is defined in Chapter 1). This is comparable with the previously discussed bis-indenyl species, Fe(C₉H₇)₂, incorporating a d⁶ metal, and the d⁷ Co^{II} analogue. The perpendicular distance between the planes through the two indenyl moieties is 3.5Å, the latter being virtually parallel to each other (the angle of elevation of C(11)-(19) to C(21)-(29) is 3.1°). The pivotal indenyl carbon atom, C(12), subtends an elevation angle of 12.2° at B(8), which is slightly lower than that generally observed for cage substituents. However, the plane through the C(11)-(19) indenyl ring system makes an angle of 18.2° with the reference plane in the substituted carbaborane cage [*i.e.* the lower pentagonal belt comprising B(5),B(6),B(11),B(12),B(9)].

Both carbaborane ligands are symmetrically disposed over Rh(3), with a perpendicular distance of 3.6Å between the two C₂B₃ planes (*i.e.* almost the same as in the bis-indenyl moiety). The carbon atoms are *cisoid* with respect to each other, with the term *cisoid* implying a staggered conformation. The fact that the carbaborane ligands are staggered with respect to each other, whilst the indenyl ligands are essentially eclipsed, may be explained by the elevated position of the *exo*-polyhedral atoms relative to the ligand face, whereas all atoms in the indenyl ligand lie approximately in the same plane. Notably, the non-slipped *cisoid* conformation in this carboradaborane is in full accord with that observed in other d⁶ metal bis-dicarbollyl species, and has been shown to be the most electronically favourable by the results of molecular orbital calculations.

3-(C₂B₉H₁₁)-8-((C₉H₆)Rh(C₉H₇))-3,1,2-*closo*-RhC₂B₉H₁₀, (6a)

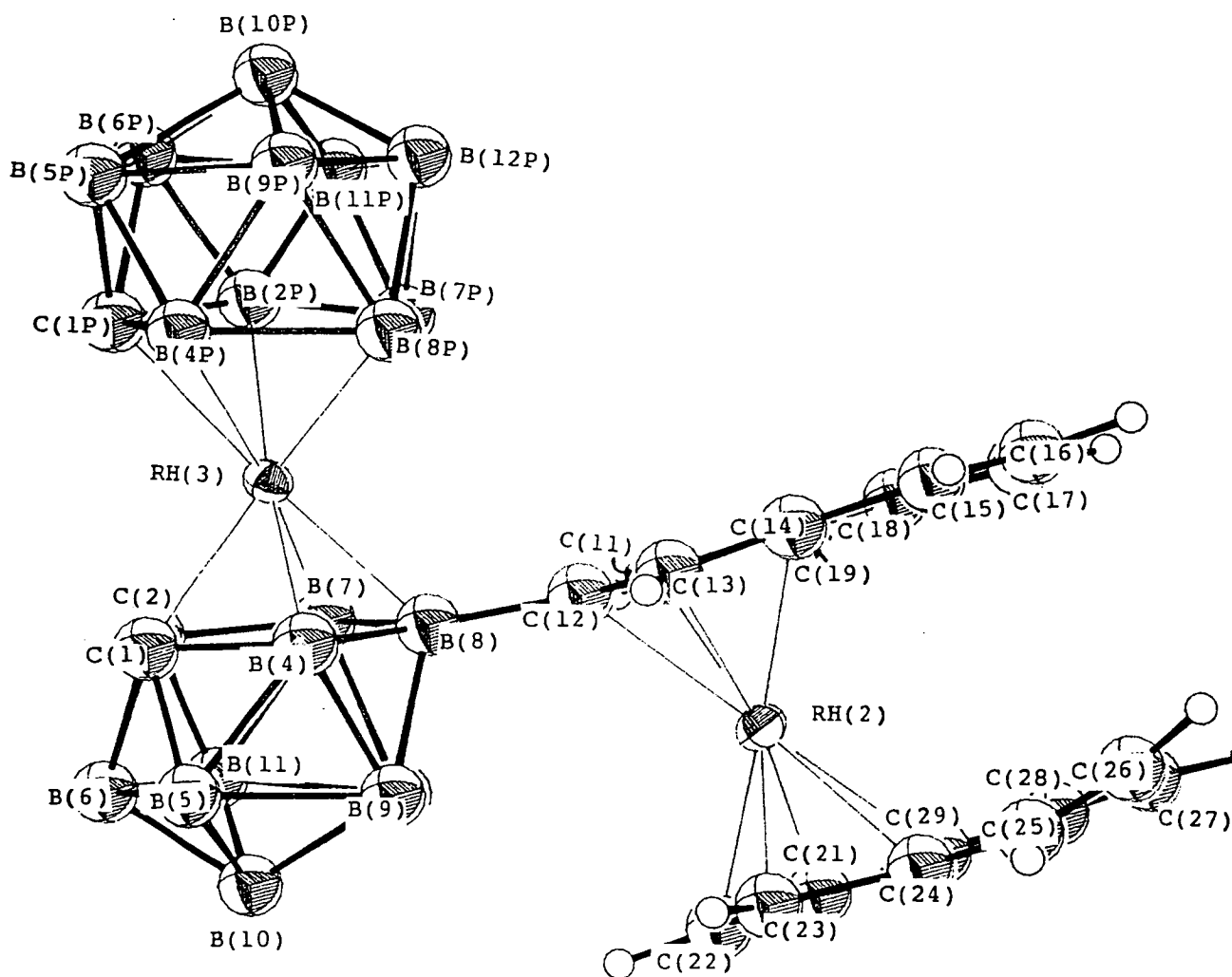


Table 3.2 Co-ordinates of Refined Atoms and Equivalent Isotropic Thermal Parameters (\AA^2) for 3-($\text{C}_2\text{B}_9\text{H}_{11}$)-8- $\{(\text{C}_9\text{H}_6)\text{Rh}(\text{C}_9\text{H}_7)\}$ -3,1,2-*closo*- $\text{RhC}_2\text{B}_9\text{H}_{10}$, (6a)

	x	y	z	Ueq
Rh(3)	0.5469(4)	0.15023(21)	0.55028(15)	0.023(3)
Rh(2)	0.8428(4)	-0.00823(21)	0.63556(16)	0.029(4)
C(12)	0.743(6)	0.057(3)	0.5909(18)	0.044(5)
C(13)	0.838(6)	0.084(3)	0.6036(19)	0.044(5)
C(11)	0.773(5)	0.000(3)	0.5687(17)	0.044(5)
C(19)	0.889(5)	-0.015(3)	0.5607(20)	0.044(5)
C(18)	0.951(5)	-0.057(3)	0.5419(20)	0.044(5)
C(14)	0.925(5)	0.050(3)	0.5859(20)	0.044(5)
C(15)	1.048(5)	0.058(3)	0.5864(19)	0.044(5)
C(16)	1.109(5)	0.008(3)	0.5669(18)	0.044(5)
C(17)	1.067(5)	-0.046(3)	0.5463(20)	0.044(5)
C(23)	0.839(5)	0.007(3)	0.7094(17)	0.044(5)
C(22)	0.766(5)	-0.047(3)	0.6938(17)	0.044(5)
C(21)	0.820(4)	-0.102(3)	0.6709(19)	0.044(5)
C(24)	0.948(6)	-0.026(3)	0.6983(19)	0.044(5)
C(29)	0.935(5)	-0.087(3)	0.6726(19)	0.044(5)
C(25)	1.053(5)	-0.007(3)	0.7026(19)	0.044(5)
C(26)	1.129(5)	-0.033(3)	0.6804(19)	0.044(5)
C(27)	1.113(5)	-0.095(3)	0.6630(18)	0.044(5)
C(28)	1.018(5)	-0.125(3)	0.6561(18)	0.044(5)
C(1)	0.448(4)	0.1711(25)	0.6095(18)	0.041(5)
C(2)	0.403(4)	0.108(3)	0.5800(19)	0.041(5)
B(5)	0.468(5)	0.156(3)	0.6650(23)	0.041(5)
B(9)	0.593(5)	0.091(3)	0.6610(23)	0.041(5)
B(4)	0.573(5)	0.156(3)	0.6182(23)	0.041(5)
B(7)	0.504(5)	0.040(3)	0.5653(23)	0.041(5)
B(6)	0.357(5)	0.111(3)	0.6375(25)	0.041(5)
B(11)	0.395(5)	0.036(3)	0.6137(25)	0.041(5)
B(8)	0.631(6)	0.088(3)	0.5985(25)	0.041(5)
B(12)	0.542(5)	0.018(3)	0.6324(24)	0.041(5)
B(10)	0.438(6)	0.064(3)	0.6696(24)	0.041(5)
C(1P)	0.469(4)	0.2149(24)	0.4969(18)	0.041(5)
B(2P)	0.534(5)	0.141(3)	0.4706(20)	0.041(5)
B(4P)	0.564(5)	0.258(3)	0.5296(21)	0.041(5)
B(11P)	0.628(5)	0.156(3)	0.4348(23)	0.041(5)
B(6P)	0.507(5)	0.215(3)	0.4358(22)	0.041(5)
B(5P)	0.521(5)	0.285(3)	0.4725(22)	0.041(5)
B(9P)	0.679(5)	0.276(3)	0.4888(24)	0.041(5)
B(7P)	0.664(5)	0.133(3)	0.4942(23)	0.041(5)
B(8P)	0.699(5)	0.203(3)	0.5295(23)	0.041(5)
B(10P)	0.639(5)	0.240(3)	0.4324(23)	0.041(5)
B(12P)	0.735(6)	0.200(3)	0.4631(22)	0.041(5)

	U11	U22	U33	U23	U13	U12
Rh(3)	0.0241(33)	0.0212(32)	0.0232(35)	0.0015(31)	0.0045(33)	-0.0015(32)
Rh(2)	0.0268(33)	0.0302(35)	0.0292(38)	0.0073(31)	-0.0025(34)	0.0000(32)

Table 3.3 Interatomic Distances (Å) and Selected Interbond Angles (°) for
 3-(C₂B₉H₁₁)-8-((C₉H₆)Rh(C₉H₇))-3,1,2-closo-RhC₂B₉H₁₀, (6a)

Rh(3) - C(1)	2.15(5)	C(1) - C(2)	1.61(8)
Rh(3) - C(2)	2.14(5)	C(1) - B(5)	1.65(8)
Rh(3) - B(4)	2.00(7)	C(1) - B(4)	1.59(8)
Rh(3) - B(7)	2.27(7)	C(1) - B(6)	1.82(8)
Rh(3) - B(8)	2.13(7)	C(2) - B(6)	1.76(9)
Rh(3) -C(1P)	2.22(5)	C(2) -B(11)	1.73(9)
Rh(3) -B(2P)	2.33(6)	B(5) - B(4)	1.88(9)
Rh(3) -B(4P)	2.22(6)	B(5) - B(6)	1.82(9)
Rh(3) -B(7P)	2.20(7)	B(5) -B(10)	1.87(9)
Rh(3) -B(8P)	2.23(6)	B(9) - B(4)	1.80(9)
Rh(2) -C(12)	2.20(6)	B(9) - B(8)	1.88(10)
Rh(2) -C(13)	2.05(6)	B(9) -B(12)	1.77(9)
Rh(2) -C(11)	2.13(6)	B(9) -B(10)	1.99(9)
Rh(2) -C(19)	2.25(6)	B(4) - B(8)	1.62(10)
Rh(2) -C(14)	2.10(6)	B(7) -B(11)	1.95(9)
Rh(2) -C(23)	2.17(5)	B(6) -B(11)	1.69(9)
Rh(2) -C(22)	2.08(6)	B(6) -B(10)	1.65(9)
Rh(2) -C(21)	2.14(5)	B(11) -B(12)	1.93(9)
Rh(2) -C(24)	2.26(6)	B(11) -B(10)	1.79(9)
Rh(2) -C(29)	2.20(6)	B(12) -B(10)	1.90(9)
C(12) -C(13)	1.34(9)	C(1P) -B(4P)	1.73(8)
C(12) -C(11)	1.35(8)	C(1P) -B(5P)	1.68(8)
C(12) - B(8)	1.52(9)	B(2P) -B(11P)	1.59(9)
C(13) -C(14)	1.37(8)	B(2P) -B(6P)	1.81(9)
C(11) -C(19)	1.48(8)	B(2P) -B(7P)	1.75(9)
C(19) -C(18)	1.25(8)	B(4P) -B(5P)	1.82(9)
C(19) -C(14)	1.54(8)	B(4P) -B(9P)	1.88(9)
C(18) -C(17)	1.46(8)	B(4P) -B(8P)	1.99(9)
C(14) -C(15)	1.52(8)	B(11P) -B(6P)	1.89(9)
C(15) -C(16)	1.36(8)	B(11P) -B(7P)	1.84(9)
C(16) -C(17)	1.33(8)	B(11P) -B(10P)	1.67(9)
C(23) -C(22)	1.45(8)	B(11P) -B(12P)	1.78(9)
C(23) -C(24)	1.52(8)	B(6P) -B(5P)	1.75(9)
C(22) -C(21)	1.44(8)	B(6P) -B(10P)	1.70(9)
C(21) -C(29)	1.46(8)	B(9P) -B(8P)	1.88(9)
C(24) -C(29)	1.42(8)	B(9P) -B(10P)	1.85(9)
C(24) -C(25)	1.35(8)	B(9P) -B(12P)	1.81(9)
C(29) -C(28)	1.35(8)	B(7P) -B(8P)	1.77(9)
C(25) -C(26)	1.25(8)	B(7P) -B(12P)	1.82(9)
C(26) -C(27)	1.33(8)	B(8P) -B(12P)	1.98(9)
C(27) -C(28)	1.33(8)	B(10P) -B(12P)	1.69(9)
C(1) -Rh(3) - C(2)	43.9(20)	C(1) - C(2) - B(6)	65.3(35)
C(1) -Rh(3) - B(4)	44.9(23)	B(6) - C(2) -B(11)	57.8(35)
C(2) -Rh(3) - B(7)	50.3(22)	C(1) - B(5) - B(4)	53.1(33)
B(4) -Rh(3) - B(8)	46.1(27)	C(1) - B(5) - B(6)	63.1(36)
B(7) -Rh(3) - B(8)	55.7(25)	B(6) - B(5) -B(10)	53.2(35)
C(1P) -Rh(3) -B(2P)	47.4(20)	B(4) - B(9) - B(8)	52.4(35)
C(1P) -Rh(3) -B(4P)	45.8(20)	B(8) - B(9) -B(12)	66.6(38)
B(2P) -Rh(3) -B(7P)	45.3(23)	B(12) - B(9) -B(10)	60.2(35)
B(4P) -Rh(3) -B(8P)	53.1(23)	Rh(3) - B(4) - C(1)	72.5(31)

B(7P) -Rh(3) -B(8P)	47.0(24)	Rh(3) - B(4) - B(8)	71.1(35)
C(1) -Rh(3) -C(1P)	101.7(19)	C(1) - B(4) - B(5)	56.1(34)
C(1) -Rh(3) -B(4P)	95.0(21)	B(5) - B(4) - B(9)	66.3(37)
C(2) -Rh(3) -C(1P)	98.3(19)	B(9) - B(4) - B(8)	66.3(40)
C(2) -Rh(3) -B(2P)	108.3(21)	C(1) - B(6) - C(2)	53.2(31)
B(4) -Rh(3) -B(4P)	101.4(24)	C(1) - B(6) - B(5)	54.1(33)
B(4) -Rh(3) -B(8P)	96.1(25)	C(2) - B(6) -B(11)	60.2(36)
B(7) -Rh(3) -B(2P)	95.7(22)	B(5) - B(6) -B(10)	65.2(39)
B(7) -Rh(3) -B(7P)	98.7(24)	B(11) - B(6) -B(10)	65.0(41)
B(8) -Rh(3) -B(7P)	94.6(25)	C(2) -B(11) - B(7)	61.1(34)
B(8) -Rh(3) -B(8P)	92.4(25)	C(2) -B(11) - B(6)	62.0(37)
C(12) -Rh(2) -C(13)	36.6(23)	B(7) -B(11) -B(12)	63.9(34)
C(12) -Rh(2) -C(11)	36.4(22)	B(6) -B(11) -B(10)	56.5(38)
C(13) -Rh(2) -C(14)	38.5(23)	B(12) -B(11) -B(10)	61.2(36)
C(11) -Rh(2) -C(19)	39.3(21)	Rh(3) - B(8) - B(4)	62.8(33)
C(19) -Rh(2) -C(14)	41.3(22)	B(9) - B(8) - B(4)	61.2(39)
C(23) -Rh(2) -C(22)	39.9(21)	B(9) -B(12) -B(10)	65.7(37)
C(23) -Rh(2) -C(24)	40.2(21)	B(11) -B(12) -B(10)	55.9(34)
C(22) -Rh(2) -C(21)	40.0(21)	B(5) -B(10) - B(9)	62.6(35)
C(21) -Rh(2) -C(29)	39.3(21)	B(5) -B(10) - B(6)	61.7(38)
C(24) -Rh(2) -C(29)	37.2(22)	B(9) -B(10) -B(12)	54.0(33)
C(13) -Rh(2) -C(23)	109.0(22)	B(6) -B(10) -B(11)	58.6(38)
C(12) -Rh(2) -C(23)	119.4(22)	B(11) -B(10) -B(12)	62.9(36)
C(12) -Rh(2) -C(22)	115.9(22)	Rh(3) -C(1P) -B(4P)	66.9(26)
C(13) -Rh(2) -C(24)	121.1(23)	B(4P) -C(1P) -B(5P)	64.6(35)
C(11) -Rh(2) -C(22)	125.7(22)	Rh(3) -B(2P) -B(7P)	63.6(28)
C(11) -Rh(2) -C(21)	116.5(21)	B(11P) -B(2P) -B(6P)	67.4(39)
C(19) -Rh(2) -C(21)	116.5(21)	B(11P) -B(2P) -B(7P)	66.5(39)
C(19) -Rh(2) -C(29)	107.5(21)	Rh(3) -B(4P) -C(1P)	67.3(26)
C(14) -Rh(2) -C(24)	111.0(22)	Rh(3) -B(4P) -B(8P)	63.6(26)
C(14) -Rh(2) -C(29)	118.0(22)	C(1P) -B(4P) -B(5P)	56.4(32)
C(13) -C(12) -C(11)	103.2(54)	B(5P) -B(4P) -B(9P)	65.8(35)
C(13) -C(12) - B(8)	126.2(57)	B(9P) -B(4P) -B(8P)	58.0(32)
C(11) -C(12) - B(8)	130.6(57)	B(2P) -B(11P) -B(6P)	61.9(37)
C(12) -C(13) -C(14)	112.5(55)	B(2P) -B(11P) -B(7P)	61.0(38)
C(12) -C(11) -C(19)	120.2(52)	B(6P) -B(11P) -B(10P)	56.7(36)
C(11) -C(19) -C(18)	142.0(58)	B(7P) -B(11P) -B(12P)	60.3(36)
C(11) -C(19) -C(14)	92.5(45)	B(10P) -B(11P) -B(12P)	58.5(38)
C(18) -C(19) -C(14)	125.5(55)	B(2P) -B(6P) -B(11P)	50.7(33)
C(19) -C(18) -C(17)	117.6(54)	B(11P) -B(6P) -B(10P)	55.0(35)
C(13) -C(14) -C(19)	111.2(51)	B(5P) -B(6P) -B(10P)	73.2(40)
C(13) -C(14) -C(15)	136.4(55)	C(1P) -B(5P) -B(4P)	59.0(33)
C(19) -C(14) -C(15)	112.3(48)	C(1P) -B(5P) -B(6P)	64.7(36)
C(14) -C(15) -C(16)	118.0(52)	B(4P) -B(9P) -B(8P)	63.7(34)
C(15) -C(16) -C(17)	123.6(54)	B(8P) -B(9P) -B(12P)	64.8(36)
C(18) -C(17) -C(16)	122.8(52)	B(10P) -B(9P) -B(12P)	54.8(35)
C(22) -C(23) -C(24)	100.1(45)	Rh(3) -B(7P) -B(2P)	71.0(30)
C(23) -C(22) -C(21)	114.5(48)	Rh(3) -B(7P) -B(8P)	67.1(30)
C(22) -C(21) -C(29)	105.6(47)	B(2P) -B(7P) -B(11P)	52.5(34)
C(23) -C(24) -C(29)	111.5(50)	B(11P) -B(7P) -B(12P)	58.2(35)
C(23) -C(24) -C(25)	135.5(55)	B(8P) -B(7P) -B(12P)	67.0(37)
C(29) -C(24) -C(25)	112.5(54)	Rh(3) -B(8P) -B(4P)	63.3(25)
C(21) -C(29) -C(24)	107.7(50)	Rh(3) -B(8P) -B(7P)	65.9(30)
C(21) -C(29) -C(28)	127.0(53)	B(4P) -B(8P) -B(9P)	58.3(32)
C(24) -C(29) -C(28)	125.1(55)	B(9P) -B(8P) -B(12P)	56.0(33)
C(24) -C(25) -C(26)	123.9(58)	B(7P) -B(8P) -B(12P)	57.7(34)
C(25) -C(26) -C(27)	117.6(57)	B(11P) -B(10P) -B(6P)	68.4(40)

C(26) -C(27) -C(28)	126.4(55)	B(11P)-B(10P)-B(12P)	63.9(40)
C(29) -C(28) -C(27)	111.1(52)	B(9P) -B(10P)-B(12P)	61.5(37)
Rh(3) - C(1) - C(2)	67.7(27)	B(11P)-B(12P)-B(7P)	61.4(37)
Rh(3) - C(1) - B(4)	62.6(29)	B(11P)-B(12P)-B(10P)	57.5(37)
C(2) - C(1) - B(6)	61.5(34)	B(9P) -B(12P)-B(8P)	59.2(34)
B(5) - C(1) - B(4)	70.7(39)	B(9P) -B(12P)-B(10P)	63.6(38)
B(5) - C(1) - B(6)	62.8(36)	B(7P) -B(12P)-B(8P)	55.3(33)
Rh(3) - C(2) - C(1)	68.4(27)		

In conclusion, although the quality of the data was such that a more detailed discussion of the structure of **6a** is not undertaken here, the definitive nature of a most unusual and interesting species has been established. The same molecule incorporates both a bis-dicarbollyl and a bis-indenyl metal fragment, fused together by a B-C bond, with the carbaborane and organic ligands each exhibiting very similar complexation of a metal atom. Thus **6a** may be viewed as a novel example of the already well established analogy between dicarbollyl and cyclopentadienyl ligands. Moreover, the establishment of the nature of the compound has been of great significance in structural assignments of related complexes to be discussed in this Chapter.

Characterisation of **6b**

Compound **6b**, the middle tlc band of the three which were isolated from this reaction, was afforded as an apricot solid, and recrystallisation, from diffusion of hexane into a methylene chloride solution of the product, yielded a microcrystalline material. Microanalysis figures for the latter were consistent with a molecular composition involving two indenyl ligands and one C_2B_9 cage per rhodium atom.

Analysis of N.m.r. Spectra

Figure 3.6 shows the 1H spectrum of compound **6b**. The aromatic region of the proton spectrum, which has been expanded, contains resonances consistent with the presence of a $\{(C_9H_6)Rh(C_9H_7)\}$ moiety, similar to that observed in **6a**. The resonances corresponding to $\{C_9H_7\}^*$ and $\{C_9H_6\}^\dagger$ moieties are marked on the spectrum (note that the triplet due to $H(2)^*$ of the former nearly overlaps with the singlet due to $H(1)^\dagger$ and $H(3)^\dagger$ of the latter moiety). It seems plausible that substitution may again have taken place on a cage by a $\{(C_9H_6)Rh(C_9H_7)\}$ fragment.

The ^{11}B -(^1H) spectrum (Figure 3.7) exhibits six signals, of relative integral 2:2:1:2:1:1, in the range δ -9 \rightarrow -40 p.p.m., corresponding to a C_2B_9 cage with a mirror plane. Upon inspection of the proton coupled spectrum, one boron atom indeed does not have an associated *exo*-polyhedral H atom (which has presumably been substituted by the bis-indenylrhodium fragment), as the signal at δ -26.40 p.p.m. remains a singlet, whilst the remaining eight boron resonances exhibit doublet coupling, with J_{BH} in the range 125-150Hz. However, the resonance at δ -26.40 p.p.m. does show distinct broadening, which has been attributed to a smaller unresolved coupling to an *endo*-hydrogen atom.

In fact, the ^{11}B resonances observed for **6b** occur at similar frequencies to those in the previously characterised species, *nido*- $\text{C}_2\text{B}_9\text{H}_{12}^{33}$, for which individual boron resonances have been assigned from an ^{11}B - ^{11}B COSY experiment. ^{11}B chemical shifts for both compounds are listed in Table 3.4. Given the presence of an *endo*-hydrogen atom on the open face of the cage, and the overall shift of the boron resonances to lower frequencies, relative to those observed in **6a**, one can assume that a rhodium atom is not η^5 bonded to the open C_2B_3 pentagon. From chemical shift assignments for individual boron atoms, the substituted boron atom, which resonates at δ -26.40p.p.m., is the unique facial atom B(10) (note that substitution has occurred at the same position in the cage as in **6a**, the change in number merely reflecting the transition from a *closo* to a *nido* polyhedron).

The presence of the *endo*-H atom is confirmed by the presence of a characteristic broad quartet at δ -1.54 in the ^1H n.m.r. spectrum. Significant enhancement of this signal is observed upon irradiation at the frequency corresponding to the B(10) resonance, and a much weaker enhancement is observed on irradiation at the frequency of the B(9,11) resonance at δ -9.60p.p.m., to which $\text{H}(10_{\text{endo}})$ is weakly bound. A single resonance is observed for both cage CH hydrogen atoms at δ 2.10.

Figure 3.6 ^1H N.M.R. Spectrum of 6b

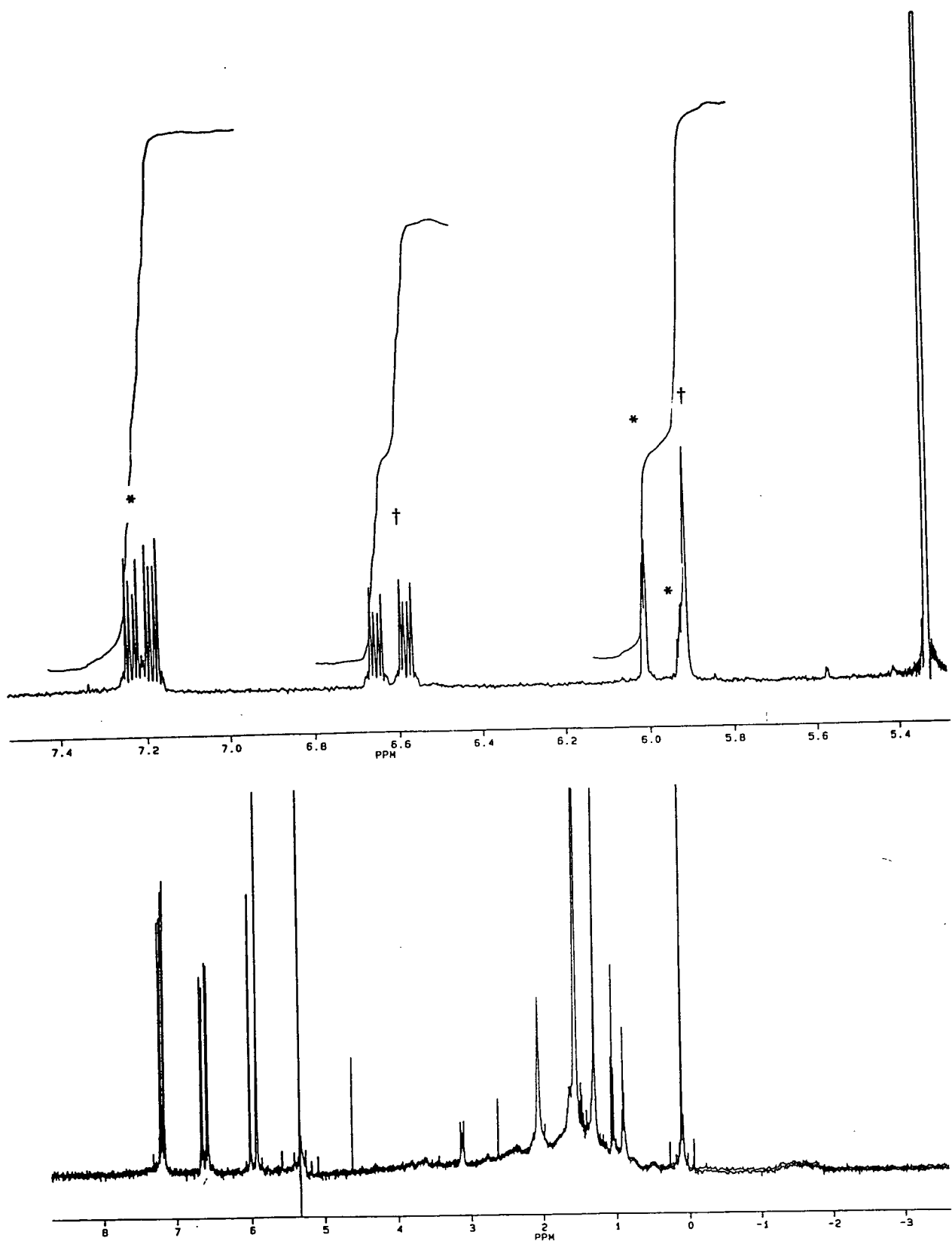


Figure 3.7 ^{11}B and ^{11}B -(^1H) N.M.R. Spectra of **6b**

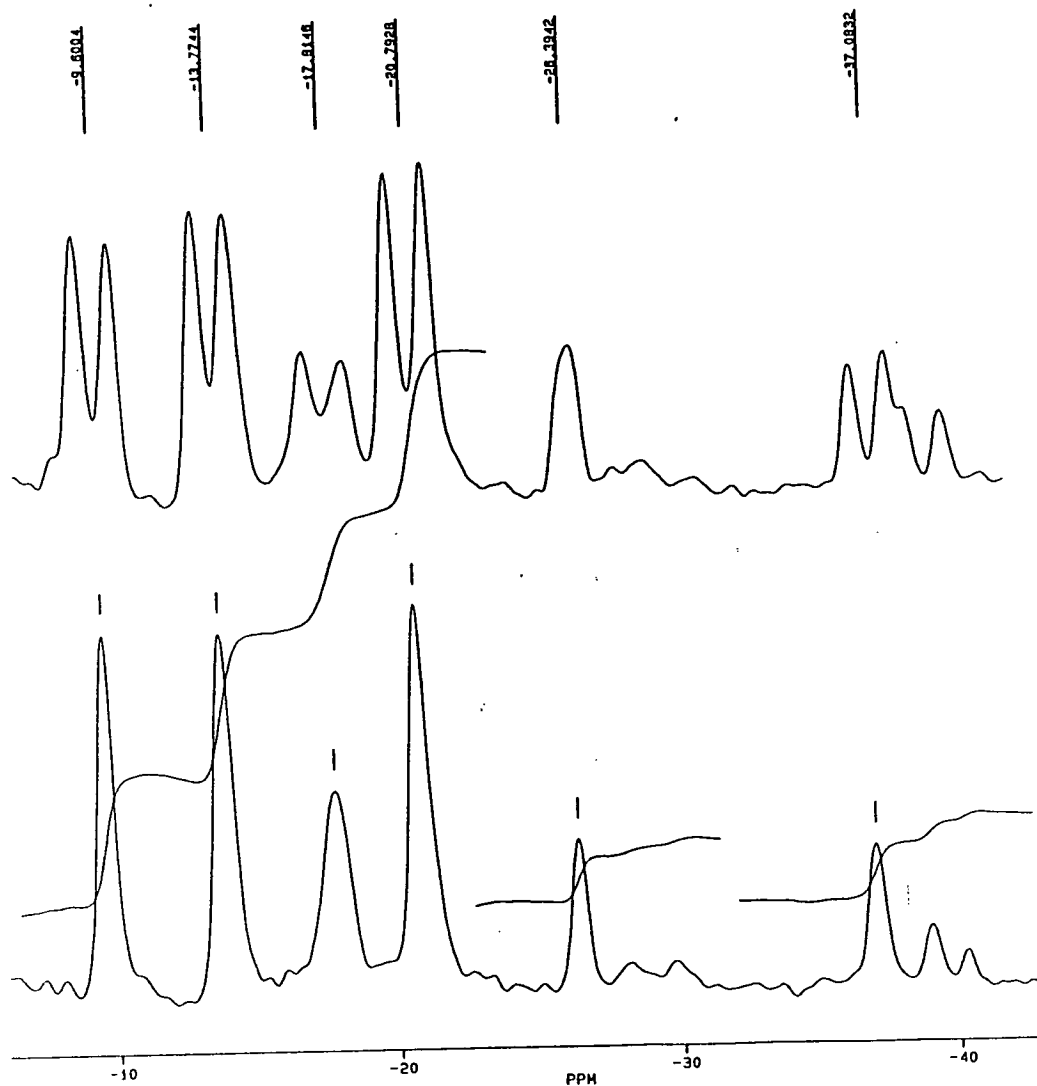
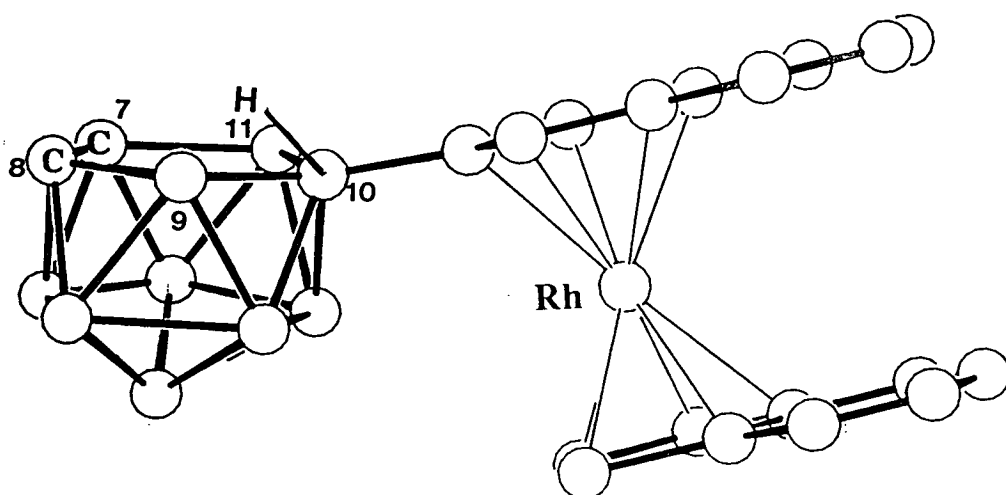


Table 3.4 Assigned ^{11}B resonances for $[\text{C}_2\text{B}_9\text{H}_{12}]^-$ and **6b**

Position	$[\text{C}_2\text{B}_9\text{H}_{12}]^-$ δ	6b δ
9,11	-10.38	-9.60
5,6	-16.46	-13.77
3	-16.46	-17.81
2,4	-21.29	-20.79
10	-32.54	-26.39
1	-37.17	-37.08

The n.m.r. data are therefore consistent with the structure illustrated in Figure 3.8, formally $10\text{-}((\text{C}_9\text{H}_6)\text{Rh}(\text{C}_9\text{H}_7))\text{-}7,8\text{-nido-C}_2\text{B}_9\text{H}_{11}$ in which the $\{\text{RhC}_2\text{B}_9\text{H}_{11}\}$ fragment in compound 6a has effectively been removed from the open face of the carbaborane ligand, with an *endo*-hydrogen atom σ -bonded to B(10). The microanalysis figures for the recrystallised solid are consistent with this formulation, but incorporating half a molecule of CH_2Cl_2 solvent per molecule of 6b.

Figure 3.8 Proposed Structure of 6b



Characterisation of 6c

Compound **6c**, the slowest moving of the three bands, was isolated as an orange solid, and recrystallised similarly to **6b**, also forming as a microcrystalline material. Microanalysis figures for this solid were virtually identical with those of **6b**, suggesting a very similar formulation.

Analysis of N.m.r. Spectra

As in the proton spectrum of **6b**, resonances due to both η^5 -bonded $\{C_9H_7\}$ and $\{C_9H_6\}$ moieties are observed (see Figure 3.9). However, in this case two singlets (δ 6.07, 5.97 p.p.m.) and two doublets (δ 6.01, 6.00 p.p.m) are observed, indicating that protons H(1,3)* and H(1,3)† are no longer in equivalent magnetic environments. In addition, two broader singlets are observed at δ 2.45 and 2.10 p.p.m., corresponding to non-equivalent cage CH atoms.

The $^{11}B\{-^1H\}$ spectrum (shown together with the ^{11}B spectrum in Figure 3.10) exhibits nine signals of equal integral, corresponding to nine unique boron nuclei. The resonances are in a similar frequency range (δ -5 \rightarrow -35 p.p.m.) to those in the spectrum of **6b**, suggesting that the cage contains an open C_2B_3 face which is not bonded to a metal atom. The proton coupled spectrum shows that the boron atom which resonates at δ -4.14 p.p.m. does not have an associated *exo*-polyhedral hydrogen atom. This resonance corresponds to B(9) [or B(11)], on the open pentagonal belt of the C_2B_9 cage. The signal at δ -29.45 [B(10)] appears as a doublet of doublets in the proton coupled spectrum, as, in addition to coupling to an *exo*-H atom, it exhibits a smaller coupling to an *endo*-H atom.

Figure 3.9 ^1H N.M.R. Spectrum of 6c

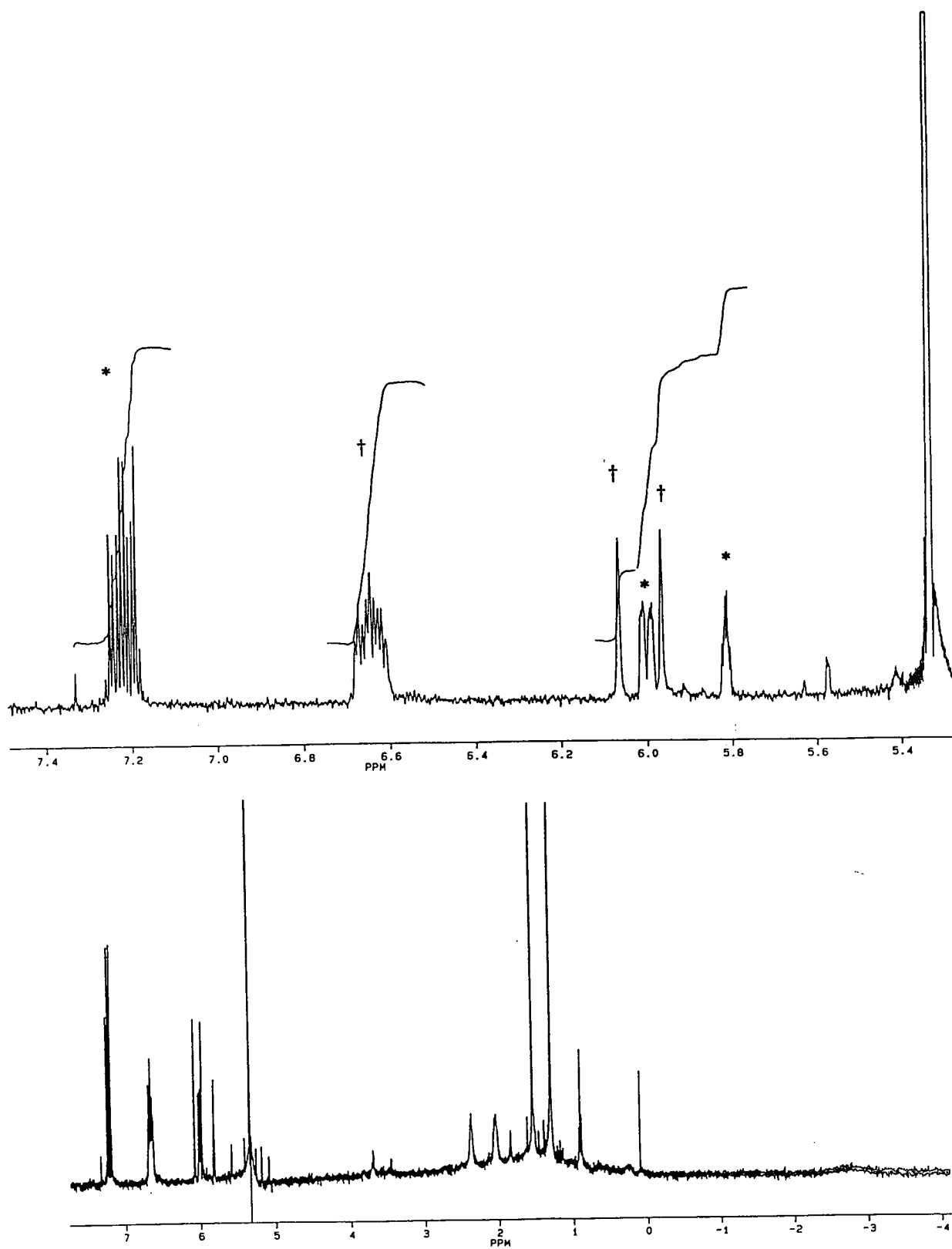
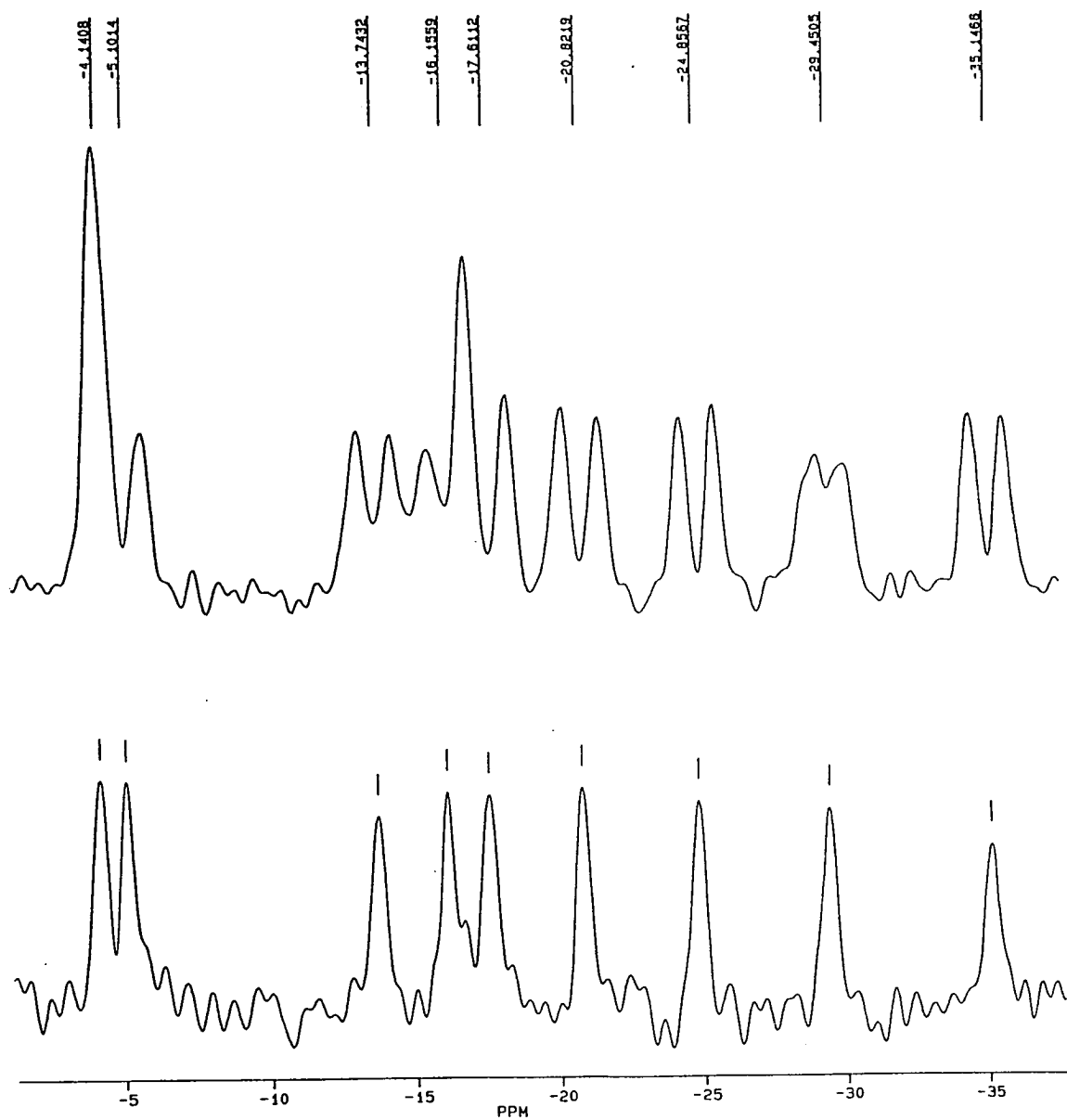


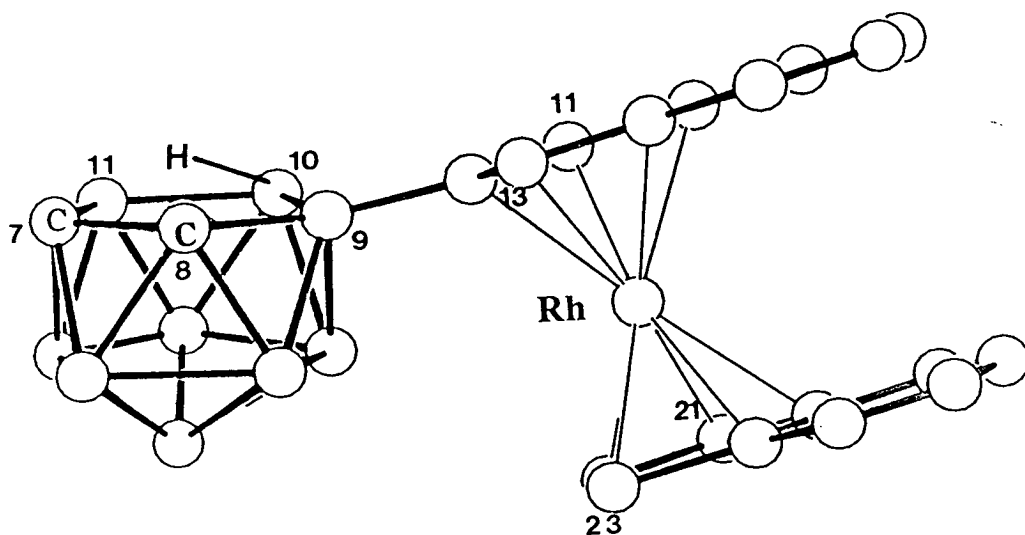
Figure 3.10 ^{11}B and $^{11}\text{B}\{-^1\text{H}\}$ N.M.R. Spectra of 6c



The presence of the *endo*-hydrogen atom is confirmed by the characteristic low frequency signal (δ -2.60 p.p.m.) in the proton spectrum, which is enhanced significantly upon irradiation at the frequency corresponding to the ^{11}B resonance at δ -29.45 (the expected weak association of the *endo*-H with B(9) and B(11) is not observed in the ^1H -(^{11}B selective) spectrum, presumably due to a poor signal to noise ratio).

The proposed structure of **6c** is illustrated in Figure 3.11, with the now familiar $\{(\text{C}_9\text{H}_6)\text{Rh}(\text{C}_9\text{H}_7)\}$ fragment σ -bonded to the $[\text{C}_2\text{B}_9\text{H}_{11}]$ cage, in this case at B(9). This structure is consistent with the asymmetry suggested in the ^{11}B n.m.r. spectrum, as the cage no longer has a mirror plane. It also explains why the indenyl hydrogen atoms, H(21,23) and H(11,13) (as labelled in Figure 3.11) are not equivalent, as they are no longer in identical environments. Similarly, the two cage CH atoms are now in different magnetic environments, and have different chemical shift values.

Figure 3.11 Proposed Structure of **6c**



Reaction of " $[(C_9H_7)RhCl_2]_2$ " with $Tl_2[7-CH_2OCH_3-7,8-C_2B_9H_{10}]$

The indenyl rhodium dichloride "dimer" was stirred together with $Tl_2[7-CH_2OCH_3-7,8-C_2B_9H_{10}]$ in methylene chloride, to yield, in small amounts, one chromatographically isolable product, **7**, as detailed in Section A of Chapter 5.

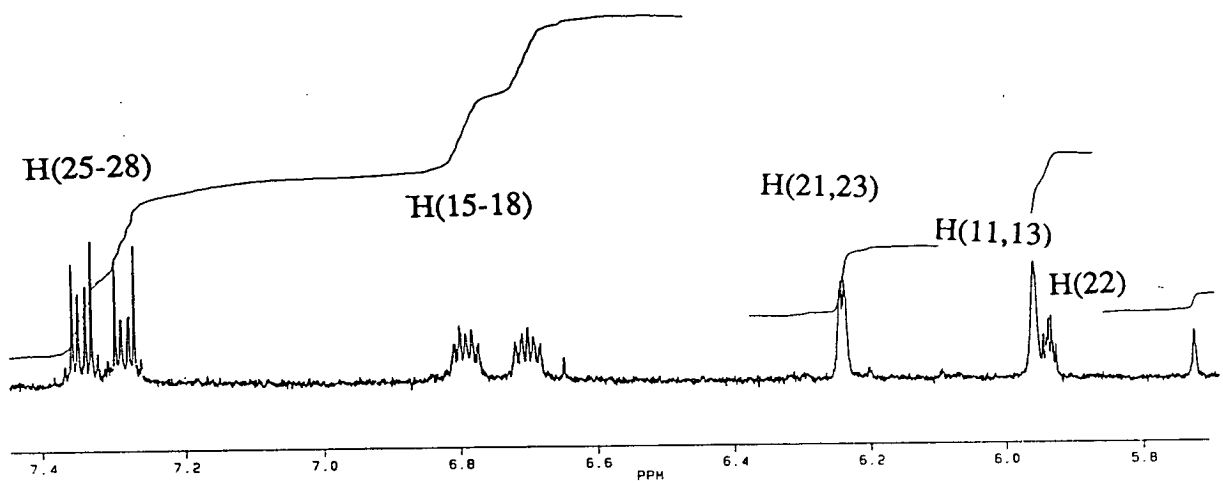
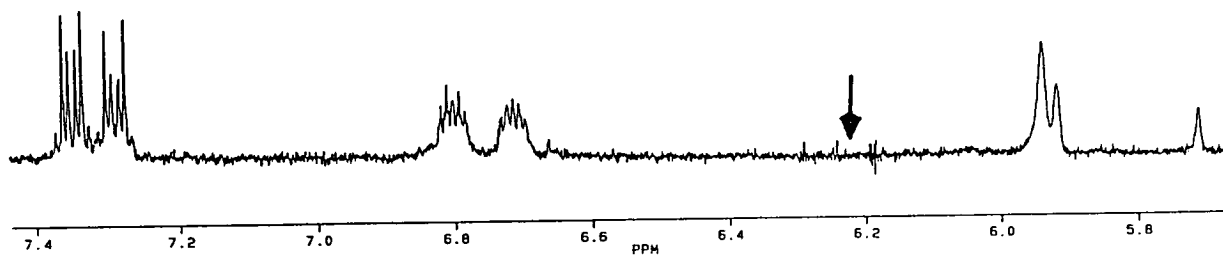
Characterisation of **7**

Compound **7** was isolated as an orange solid, which formed microcrystals after slow diffusion of hexane into a methylene chloride solution of the product. Microanalysis of the latter suggested a formulation analogous to those of **6b** and **6c**.

Analysis of N.m.r. Spectra

The aromatic region of the proton spectrum (obtained as a CD_2Cl_2 solution) suggests the presence, once again, of a $\{(C_9H_6)Rh(C_9H_7)\}$ fragment, with multiplets at δ 7.23, 7.18 [H(25-28) of the C_9H_7 moiety] and 6.66, 6.58 p.p.m. [H(15-18) in the $\{C_9H_6\}$ moiety], two doublets at δ 6.01 and 6.00 p.p.m [H(21,23)], and a singlet at δ 5.92 p.p.m. [H(11,13)]. However, the expected signal corresponding to H(22) of the $\{C_9H_7\}$ moiety is not observed. The spectrum was thus re-run in $(CD_3)_2CO$, (see **Figure 3.12** for an expansion of the aromatic region) which contained all the resonances consistent with the bis-indenyl rhodium fragment.

Figure 3.12 Expansion of the Aromatic Region of the ^1H N.M.R. Spectrum of **7** (in $(\text{CD}_3)_2\text{CO}$)

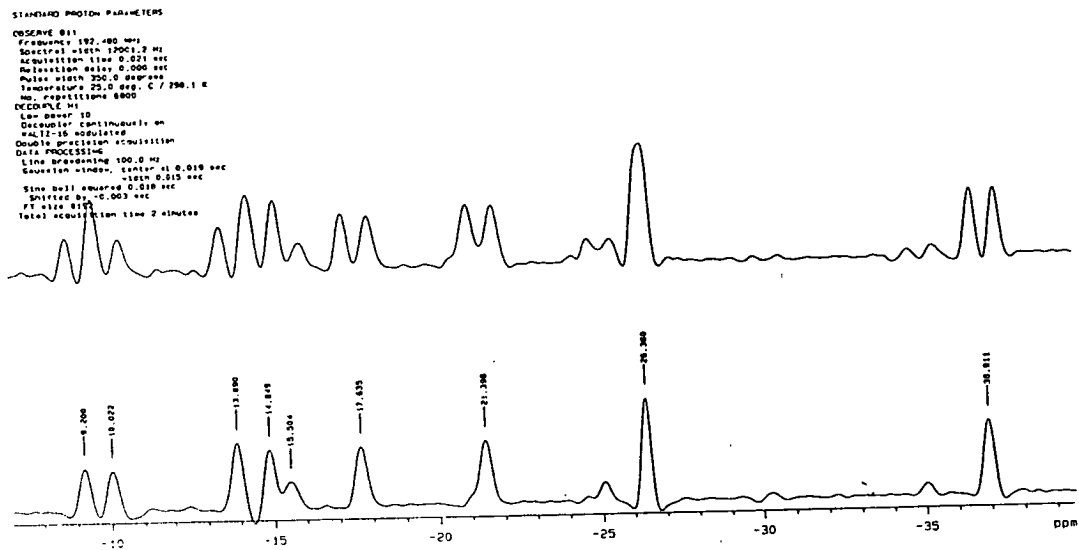


A doublet of doublets was observed at δ 5.93 p.p.m., which collapsed to a singlet upon irradiation at the frequency corresponding to the resonance due to H(21,23) at δ 6.24 p.p.m., and so the former signal may be attributed to H(22) of the (C₉H₇) ligand.

The ¹¹B-¹H spectrum (shown together with the ¹¹B spectrum in **Figure 3.13**) exhibits resonances corresponding to nine unique boron atoms, one of which, on inspection of the proton coupled spectrum, can be seen to have no associated *exo*-hydrogen atom. This boron atom, assigned B(10) from its chemical shift value (δ -26.36 p.p.m.), does however show a smaller coupling to an *endo*-hydrogen atom (J_{BH} ca. 30Hz). A characteristic low frequency signal is observed in the proton spectrum, at δ -1.40 p.p.m., significant enhancement of which is observed upon irradiation at the frequency corresponding to the B(10) resonance. A much weaker enhancement occurs on irradiation at frequencies corresponding to resonances at δ -5.92 and -10.02 p.p.m., due to weaker interaction between the *endo*-H atom and B(9) and B(11).

The n.m.r. evidence strongly suggests a structure of similar nature to **6b**, formally 7-CH₂OCH₃-10-((C₉H₆)Rh(C₉H₇))-7,8-*nido*-C₂B₉H₁₀, illustrated in **Figure 3.14**, where substitution of a hydrogen atom by a bis-indenyl rhodium cationic fragment has occurred on the *nido*-C₂B₉ species [7-(CH₂OCH₃)-7,8-*nido*-C₂B₉H₁₁]⁺ at the facial boron atom, B(10).

Figure 3.13 ^{11}B and $^{11}\text{B}-\{^1\text{H}\}$ N.M.R. Spectra of 7



small amber crystals formed. A unit cell and spacegroup determination of a typical crystal showed it to be the originally targeted *closo*-carbaborane species, 1-Ph-3-(C₉H₇)-3,1,2-*closo*-RhC₂B₉H₁₀, by analogy with the previously characterised cobalt species, **2**. This fact, coupled with its weak diffraction, did not justify data collection. Full details of the crystal data obtained are given in Chapter 5, Section 2.

Characterisation of **8b**

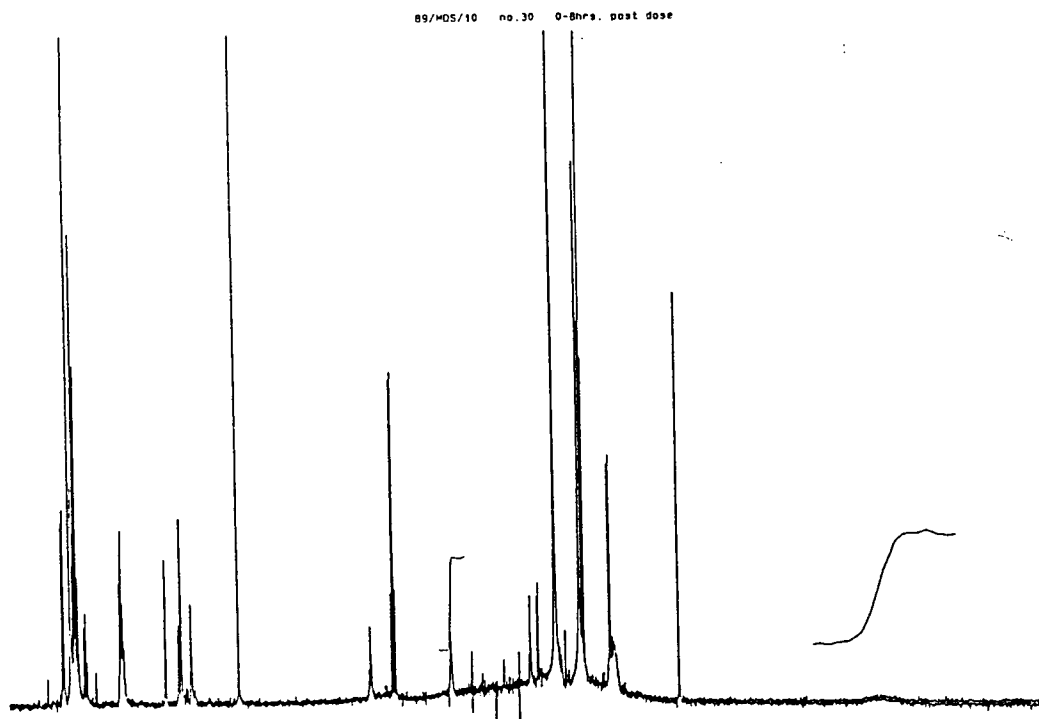
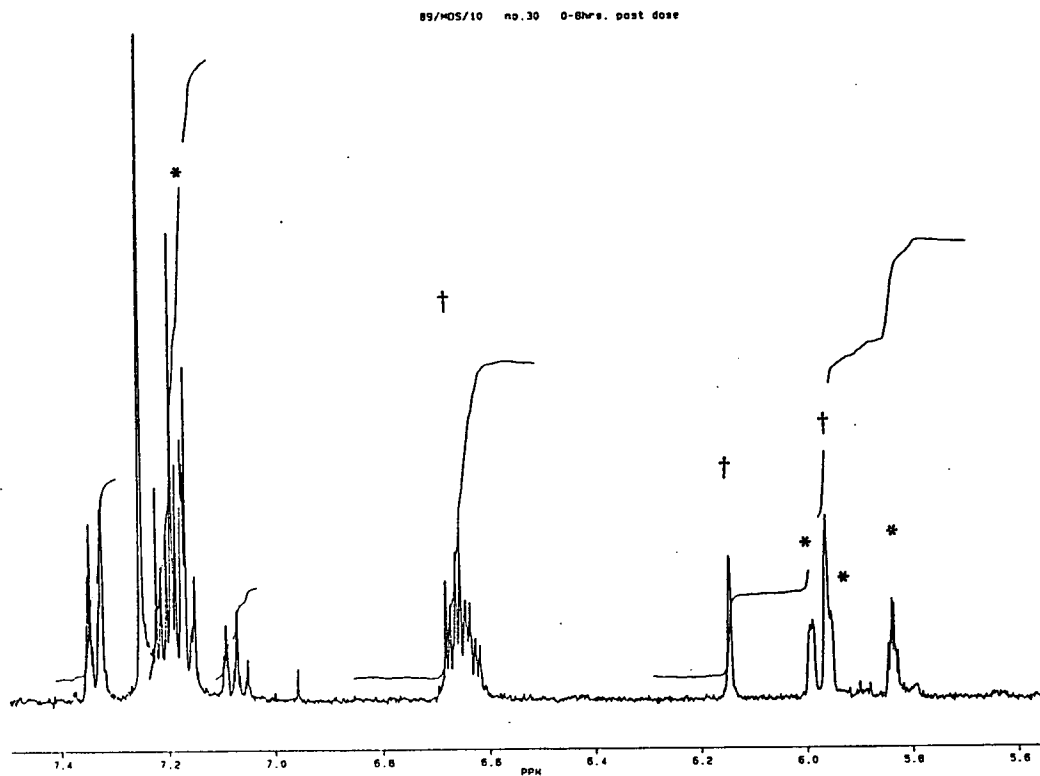
Compound **8b** was isolated as an orange solid, which formed microcrystals after slow diffusion of hexane into a methylene chloride solution of the product.

Analysis of N.m.r. Spectra

The ¹H spectrum of **8b** is shown in Figure 3.15, and immediately suggests the presence of {(C₉H₆)Rh(C₉H₇)} cationic moiety, with resonances corresponding to {C₉H₇}* and {C₉H₆}[†], marked as before. The spectrum bears strong resemblance to the proton spectrum of **6c**, in that H(11),H(13) and H(21),H(23) are not magnetically equivalent. Two singlets are observed at δ 6.15 and 5.96 p.p.m. (corresponding to the former), and two doublets at δ 5.99 and 5.95 p.p.m. (corresponding to the latter indenyl hydrogen atoms).

The ¹¹B-¹H spectrum (not illustrated) exhibits eight resonances, with two nearly coincident signals. As expected, one resonance does not show coupling to an *exo*-polyhedral hydrogen atom, that at δ -4.29 p.p.m. (*i.e.* the highest frequency resonance), assigned to B(9) or B(11).

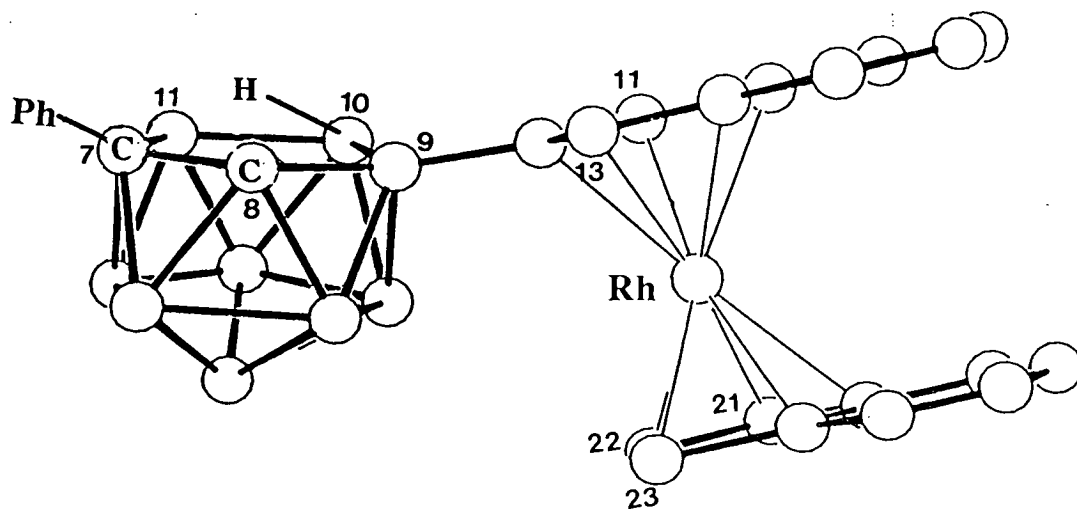
Figure 3.15 ^1H N.M.R. Spectrum of 8b



The resonance at δ -28.39 p.p.m., corresponding to B(10), appears as a doublet of doublets in the proton coupled spectrum, the extra doublet coupling (J_{BH} ca. 30 Hz) associated with an *endo*-hydrogen atom. The latter is observed in the proton spectrum, with a low frequency broad quartet at δ -2.30 p.p.m., which is of equal integral to the single cage CH atom at δ 2.79 p.p.m.

The postulated structure for **8b**, formally 7-Ph-9/11- $\{(\text{C}_9\text{H}_6)\text{Rh}(\text{C}_9\text{H}_7)\}$ -7,8-*nido*- $\text{C}_2\text{B}_9\text{H}_{10}$, is illustrated in Figure 3.16, and shows substitution by the $\{(\text{C}_9\text{H}_6)\text{Rh}(\text{C}_9\text{H}_7)\}$ moiety at either B(11), which is adjacent to the phenyl-substituted carbon, or B(9). With the information available B(9) and B(11) cannot be distinguished, and so there is some doubt about the exact structural assignment.

Figure 3.16 Proposed Structure of **8b**



with substitution at B(9)

Reaction of "[$(C_9H_7)RhCl_2$] $_2$ " with $Tl_2[7,8-(CH_2OCH_3)_2-7,8-C_2B_9H_9]$

"[$(C_9H_7)RhCl_2$] $_2$ " and $Tl_2[7,8-(CH_2OCH_3)_2-7,8-C_2B_9H_9]$ were stirred together in methylene chloride for fifteen hours, with subsequent work-up involving preparative tlc affording only one isolable product, **9**, in very low yield. This was obtained as a yellow solid, which formed dark yellow microcrystals on slow diffusion of hexane into a methylene chloride solution. The full experimental procedures are detailed in Chapter 5, Section A.

Characterisation of **9**

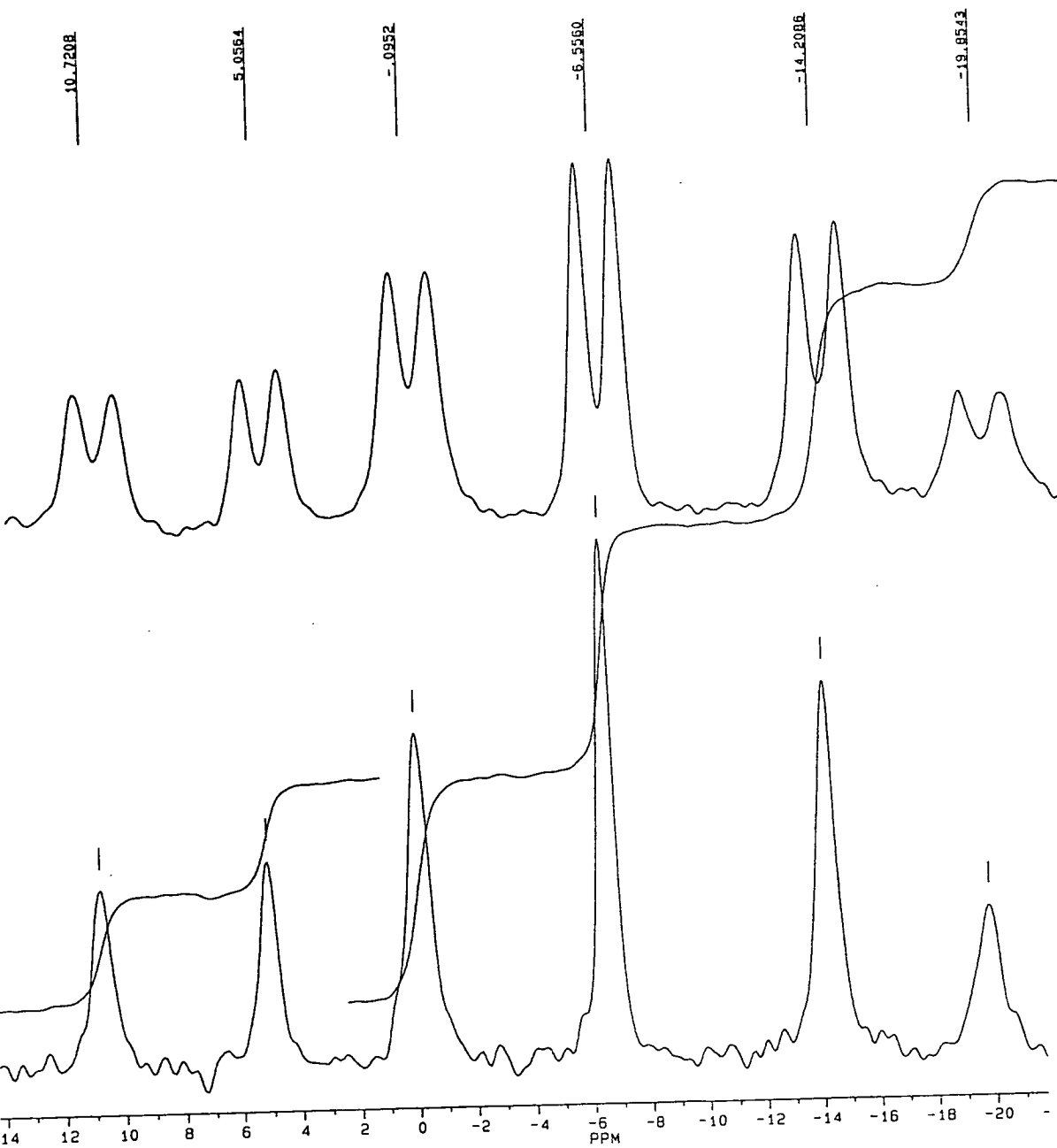
Analysis of N.m.r. Spectra

The ^{11}B -(1H) spectrum (seen together with the proton coupled spectrum in Figure 3.17) shows six signals of relative intensity 1:1:2:2:2:1, with frequencies in the range δ 10 \rightarrow -20 p.p.m, suggestive of a *closo*- MC_2B_9 cage. In contrast to the previous spectra, all nine boron atoms have an associated *exo*-polyhedral hydrogen atom, as seen in the ^{11}B spectrum.

Accordingly, the proton spectrum exhibits just one η^5 -bonded [C_9H_7] $^-$ ligand, with signals in the ratio 4:2:1 corresponding to H(35-38), H(31,33) and H(32).

The structure is thus presumably the rhodium analogue of the indenyl cobalt species, **4**, *i.e.* 1,2- $(CH_2OCH_3)_2$ -3- $(\eta^5-C_9H_7)$ -3,1,2-*closo*- $RhC_2B_9H_9$.

Figure 3.17 ^{11}B and $^{11}\text{B}\{-^1\text{H}\}$ N.M.R. Spectra of 9



Reconsideration of the Structure of " $[(C_9H_7)RhCl_2]_2$ "

Given the variety of products which form as a result of reacting " $[(C_9H_7)RhCl_2]_2$ " with dithallium carbaboranes, the structure of indenyl rhodium dichloride is clearly of a more complex nature than that of its cyclopentadienyl analogues, $[CpRhCl_2]_n$ and $[Cp^*RhCl_2]_2$. Although the target compounds, 1,2- R_1R_2 -3-(η^5 - C_9H_7)-3,1,2-*closo*- $RhC_2B_9H_9$ have been isolated (where $R_1 = H$, $R_2 = Ph$, and $R_1 = R_2 = CH_2OCH_3$), these species form in very low yields. Instead, the major products (and even these form in yields less than 10%) are a series of novel zwitterionic complexes, where a $\{(C_9H_6)Rh(C_9H_7)\}$ moiety is σ -bonded to a C_2B_9 cage, *via* a C-B bond.

In the light of its reaction chemistry, the structure of " $[(C_9H_7)RhCl_2]_2$ " deserves reconsideration. Although microanalysis consistently confirms an overall stoichiometry of $(C_9H_7)RhCl_2$ (the synthesis has been carried out on a number of separate occasions), and the infrared spectrum of " $[(C_9H_7)RhCl_2]_2$ " suggests that rhodium is bonded both to terminal and bridging chloride ions, it is apparently not as "simple" a polymeric species as its $[CpRhX_2]_2$ analogues, wherein polymer formation has been suggested to occur *via* halide bridges.

The latter amorphous species readily afford monomeric compounds on treatment with donor ligands. For example $[CpRhX_2]_n$ ($X = Cl$) reacts with $C_6H_{11}NC$,⁷⁹ (CyNC), affording $CyNCRhCpCl_2$, in almost quantitative yield. Similarly, $[CpRhX_2]_n$ ($X = I$), reacts with $Tl_2[C_2B_9H_{11}]$ to give a 30% yield of 3-Cp-1,2-*closo*- $RhC_2B_9H_{11}$.⁷¹ The complex reaction products of reactions of " $[(C_9H_7)RhCl_2]_2$ " with the latter have already been discussed. In addition the reaction between " $[(C_9H_7)RhCl_2]_2$ " and CyNC was attempted, also affording a complex number of products, which in this case could not be separated to enable their characterisation. Thus polymer formation in the indenyl species presumably does not

occur by chloride bridging alone.

The fact that a $\{C_9H_6\}$ moiety is σ -bonded to a cage boron atom in **6a**, **6b**, **6c**, **7** and **8b** may imply that $\{C_9H_6\}$ moieties are also present in the dichloride starting material. This may be envisaged in terms of linking between indenyl ligands, *via* C(2)-C(2) bonds, giving fulvalene-like structures within polymeric chains, as illustrated in Figure 3.18 (the known Rh(II) fulvalene species, $Rh_2(\eta^{10}-C_{10}H_8)L_4$ ⁸⁰ (L = PPh₃) is shown in Figure 3.19). Indeed, a proton n.m.r. spectrum obtained from a CH₂Cl₂ soluble portion of " $[(C_9H_7)RhCl_2]_2$ " exhibits signals which may be attributable to both $\{C_9H_7\}$ and $\{C_9H_6\}$ moieties, with multiplets at δ 7.33, 7.15, a doublet at 6.10, and a multiplet at *ca.* 6.02 p.p.m., corresponding to the former, and a multiplet (δ 6.52) and singlet (6.17 p.p.m.) corresponding to the latter (substituted) indenyl moiety. However, it must be stressed that the spectrum contains a number of other (unassignable) signals, and this in any case only represents the methylene chloride soluble portion of the indenyl rhodium dichloride species.

With the available information, it is difficult to arrive at any definite conclusions as to the nature of reaction mechanisms involving a polymer of this type. If " $[(C_9H_7)RhCl_2]_2$ " does indeed contain fulvalene-like polymeric chains, it is hard to perceive a likely driving force for the formation of B-C bonds, and why the rhodium atom should eventually find itself sandwiched between two indenyl moieties, or, in the case of **6a**, between two carbaborane cages. However, all these complexes appear to be highly stable species, and it may be that the formation of structures of this type is thermodynamically (or kinetically) very favourable.

Figure 3.18 Possible Structures for " $[(C_9H_7)RhCl_2]_2$ "

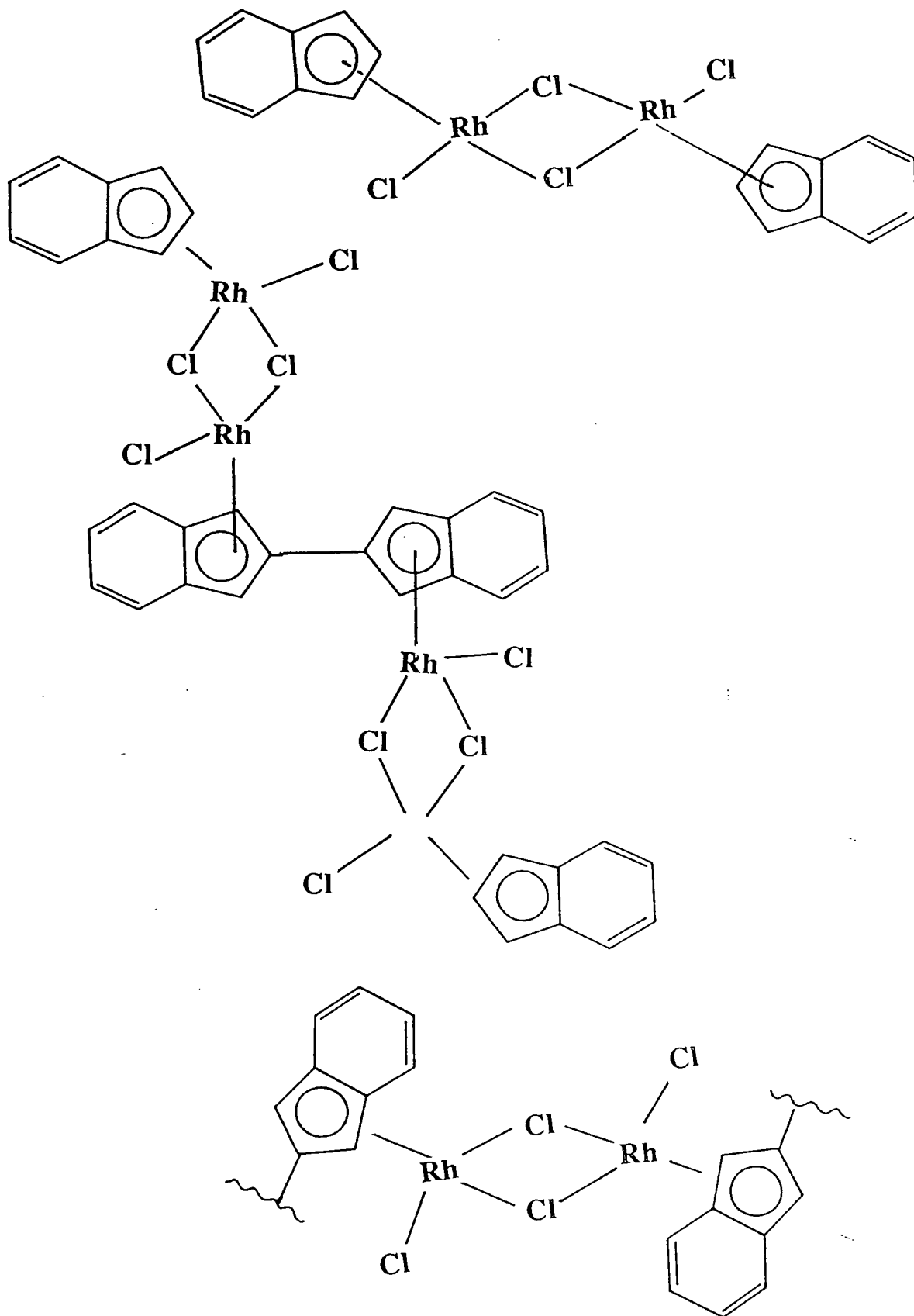
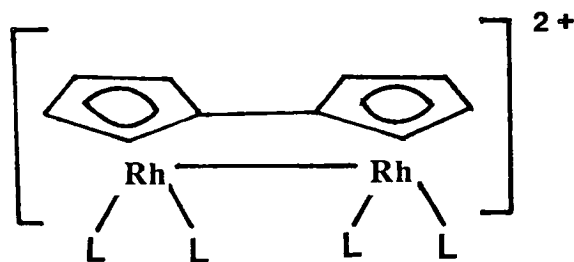


Figure 3.1 Structure of $\text{Rh}_2(\eta^{10}\text{-C}_{10}\text{H}_8)\text{L}_4$ ($\text{L} = \text{PPh}_3$)



If polymer formation occurs *via* "inter-indenyl" bonds, one way of obtaining a less polymeric indenyl rhodium dichloride precursor might be to start with methylated indene (*e.g.* 1,2,3-trimethylindene, or permethylated indene, $\text{C}_9(\text{CH}_3)_7\text{H}$). Preliminary experiments, involving 1,2,3-trimethylindene, synthesised according to a literature preparation,⁸¹ have not, however, afforded a single, easily isolable product. This initial experiment was carried out on quite a small scale, and is worth repeating with increased quantities of starting materials. Further reactions involving alternative methylated indenenes would also be of interest.

One other possible reason for the formation of the novel zwitterionic species is that " $[(\text{C}_9\text{H}_7)\text{RhCl}_2]_2$ " contains already intact $(\text{C}_9\text{H}_7)\text{Rh}(\text{C}_9\text{H}_7)^+$ ions (Cl^- counterion), together with some residual RhCl_3 (which would also be consistent with microanalysis figures). The bis-indenyl rhodium fragments may then attack the anionic cage, resulting in the formation of a B-C bond. This theory may be tested quite easily, by a trial reaction of a dithallium carbaborane species with, for example, the chloride salt of $(\text{C}_9\text{H}_7)_2\text{Rh}^+$.

Conclusions

The reaction of freshly distilled indene with $\text{RhCl}_3 \cdot 3\text{H}_2\text{O}$ affords a product of the empirical formula $\text{C}_9\text{H}_7\text{RhCl}_2$. Subsequent reactions of this species with a series of dithallium carbaborane salts have resulted in the formation of a number of novel indenyl rhodium carbaborane species incorporating a $\{(\text{C}_9\text{H}_7)\text{Rh}(\text{C}_9\text{H}_6)\}$ fragment, as well as small amounts of the originally targeted 3,1,2- MC_2B_9 indenyl carborodaboranes. The initially assigned structure, " $[(\text{C}_9\text{H}_7)\text{RhCl}_2]_2$ ", is thus questionable, and, retrospectively, a more complex polymeric composition is postulated.

Chapter 4

Transition Metal Derivatives of Diphenylcarbaborane

Introduction

Prior to the work contained in this Chapter, no transition metal derivatives of diphenylcarbaborane, 1,2-Ph₂-1,2-*closo*-C₂B₁₀H₁₀, had been reported, although the parent carbaborane has been known for over twenty years. The absence of metal derivatives is to some extent surprising, particularly considering the recently reported application of cage-substituted carboranes in homogeneous catalysis,⁶⁷ discussed in more detail towards the end of this Chapter.

For the purposes of this work, the synthesis of a metal derivative of diphenylcarbaborane was first considered in the course of the studies detailed in Chapter 2, in which the conformation of a series of indenyl carbacobaltaboranes is related to the degree of substitution at the cage carbon atoms. However, following a similar reaction procedure to that which afforded 1 - 4, using the previously unreported dithallium carbaborane, Tl₂[7,8-Ph₂-7,8-C₂B₉H₉], the diphenyl-substituted analogue of these species could not be isolated. This was attributed to potentially unfavourable interaction between the phenyl cage substituents and the six-membered ring of the indenyl ligand.

The questions arising from this were (i) to what extent might the presence of two phenyl substituents on the open pentagonal face of [7,8-Ph₂-7,8-*nido*-C₂B₉H₉]²⁻ prevent the formation of other transition metal derivatives of diphenylcarbaborane, and (ii) what possible conformations might the two cage substituents adopt on the incorporation of metal vertices. The syntheses of a series of transition metal derivatives was thus envisaged, involving a variety of metal ligand fragments, starting

with those least likely to have significant interaction with the aryl cage substituents.

However, before considering conformations within metal derivatives of diphenylcarbaborane, a structural determination of the parent *closo*-carbaborane itself was undertaken, in order to establish the orientation of the phenyl rings, and the effect of their substitution on the overall cage geometry.

1,2-Ph₂-1,2-*closo*-C₂B₁₀H₁₀, (10)

Synthesis and Characterisation

Diphenylcarbaborane formed during the reaction between decaborane and diphenylacetylene in the presence of dimethyl sulphide, and was isolated as a white crystalline solid, as described in Chapter 5, Section A. Microanalysis figures were consistent with the expected formulation of **10**.

The ¹¹B n.m.r. spectrum exhibits three resonances in the range 0 - 10 p.p.m. with integrals in the ratio 2:4:4, consistent with the anticipated C_{2v} symmetry of the disubstituted icosahedral cage, assuming two signals (each 2B) are coincident.

Structural Study on 10

Introduction

Diffraction quality crystals of **10** were grown by the slow cooling of a methanol solution of the compound. Details of the crystallographic procedures and crystal data for the structure may be found in Chapter 5, Section B.

Discussion

The compound crystallises with two independent molecules, A and B, per asymmetric unit. The structures of 10A and 10B are shown in Figure 4.1 and Figure 4.2 respectively with the appropriate atomic numbering scheme. All hydrogen atoms are given the same number as the carbon or boron atom to which they are bonded. Table 4.1 lists fractional co-ordinates for the refined atoms of both molecules, Table 4.2 bond distances and selected interbond angles, with respective values for each molecule adjacent for ease of comparison, and Table 4.3 contains anisotropic thermal parameters for all non-hydrogen atoms.

Essentially the structures of the two molecules are very similar, with C-B and B-B distances within each cage having comparable values. However, the cage carbon-carbon distance in A [1.733(4)Å] is significantly longer than that observed in B [1.720(4)Å], and in addition, the phenyl ring substituents in the latter structure appear to be twisted relative to the ring systems in the former.

Considering first the C-C bond distances in both molecules, these are significantly longer than that observed in *ortho*-carbaborane, 1,2-C₂B₁₀H₁₂ [1.65(5)], and indeed a number of other carbon-substituted 1,2-*closo*-C₂B₁₀ species (e.g. 1,2-Br₂-1,2-*closo*-C₂B₁₀H₁₀ [1.63(3)]¹⁹ and 1-Me-2-SiMe₃-1,2-*closo*-C₂B₂H₁₀ [1.669(4)]).⁸²

Figure 4.1 Structure of Molecule 10A

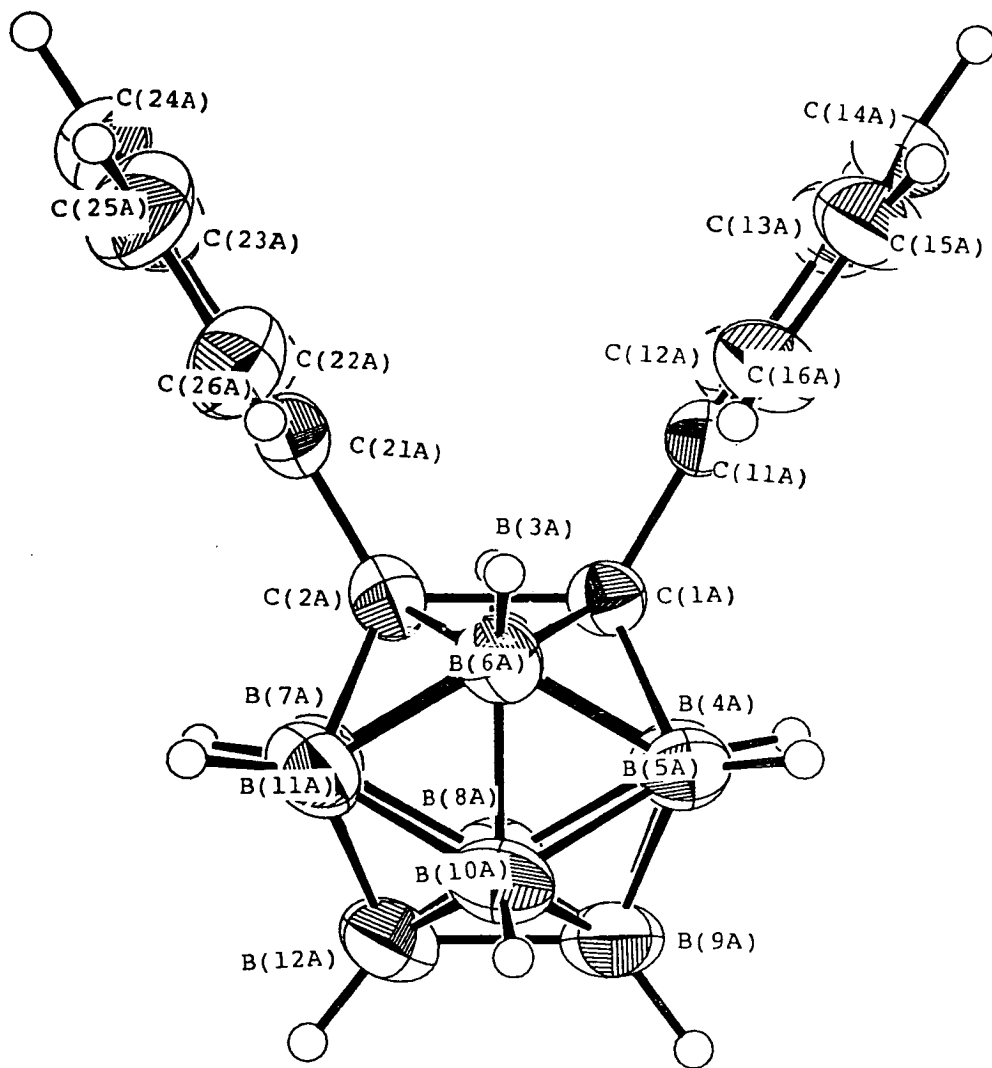


Figure 4.2 Structure of Molecule 10B

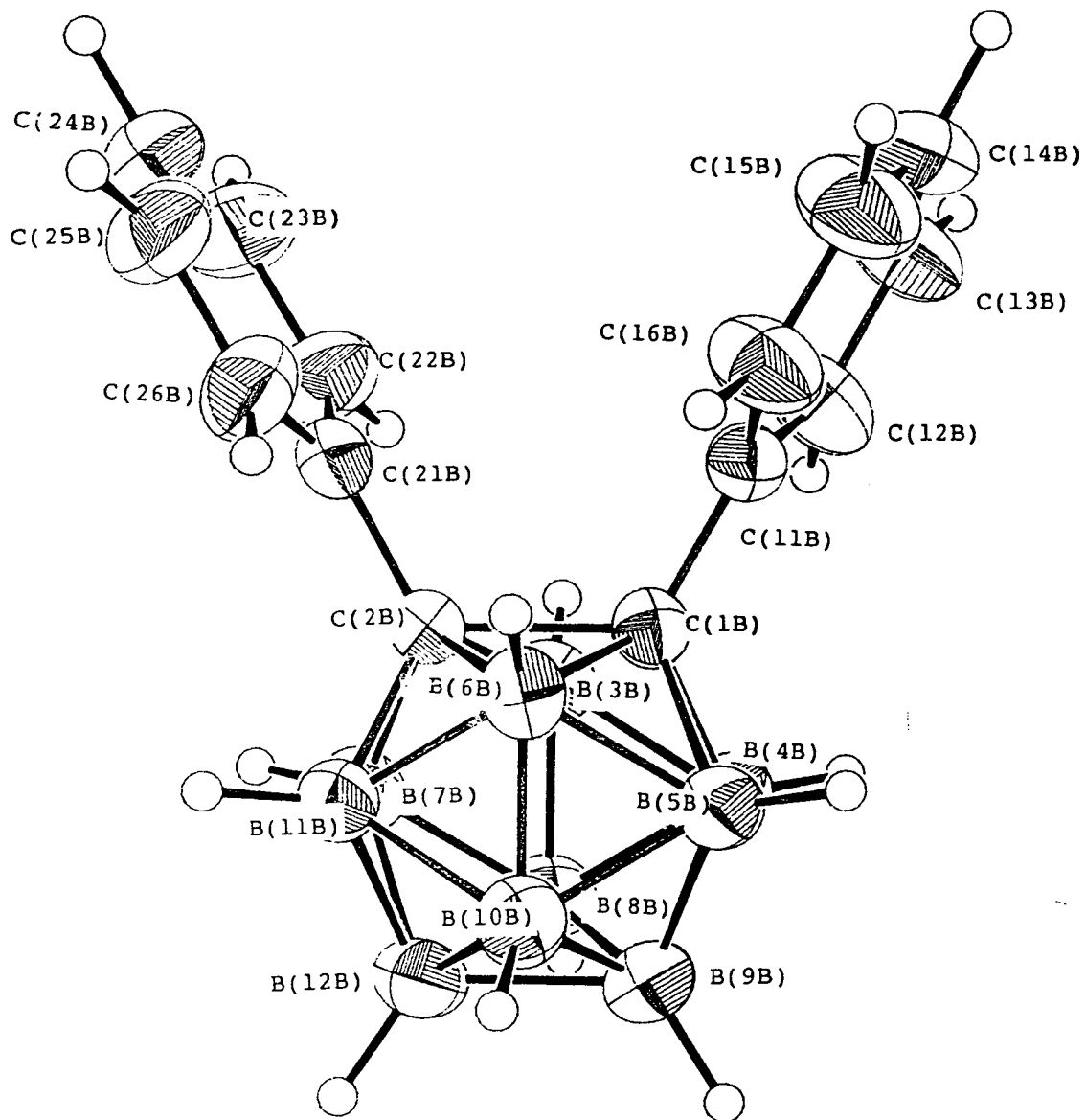


Table 4.1 Co-ordinates of Refined Atoms and Equivalent Isotropic Thermal Parameters (\AA^2) for 1,2-Ph₂-1,2-closo-C₂B₁₀H₁₀ (10)

	x	y	z	Ueq
C(1A)	0.8065(3)	0.06102(12)	0.20389(22)	0.0421(18)
C(2A)	0.7619(3)	0.00084(13)	0.24464(24)	0.0491(20)
B(11A)	0.5938(4)	0.00083(19)	0.2161(3)	0.065(3)
B(3A)	0.8413(4)	0.05004(16)	0.3334(3)	0.0500(24)
B(6A)	0.6602(4)	0.02967(16)	0.1295(3)	0.0488(23)
B(5A)	0.6684(4)	0.10036(17)	0.1480(3)	0.0527(25)
B(4A)	0.7829(4)	0.11293(16)	0.2752(3)	0.0526(25)
B(7A)	0.7066(4)	0.01318(19)	0.3428(3)	0.065(3)
B(12A)	0.5637(5)	0.05374(19)	0.2885(4)	0.073(3)
B(10A)	0.5355(4)	0.06305(19)	0.1566(3)	0.060(3)
B(8A)	0.7174(4)	0.08358(18)	0.3622(4)	0.063(3)
B(9A)	0.6092(4)	0.11480(19)	0.2471(4)	0.064(3)
C(11A)	0.9189(3)	0.06227(12)	0.16574(24)	0.0441(19)
C(12A)	1.0480(3)	0.07209(15)	0.2339(3)	0.0615(24)
C(13A)	1.1497(4)	0.07697(17)	0.1964(4)	0.077(3)
C(14A)	1.1240(4)	0.07352(17)	0.0928(4)	0.085(3)
C(15A)	0.9969(4)	0.06508(18)	0.0257(3)	0.081(3)
C(16A)	0.8948(4)	0.05894(16)	0.0614(3)	0.066(3)
C(21A)	0.8366(3)	-0.04976(13)	0.2411(3)	0.0551(22)
C(22A)	0.9466(4)	-0.06587(16)	0.3256(3)	0.069(3)
C(23A)	1.0107(4)	-0.11389(18)	0.3235(4)	0.087(4)
C(24A)	0.9669(5)	-0.14529(19)	0.2394(4)	0.099(4)
C(25A)	0.8582(6)	-0.13094(18)	0.1553(4)	0.103(4)
C(26A)	0.7900(5)	-0.08261(15)	0.1556(3)	0.077(3)
C(1B)	0.4357(3)	0.22853(12)	0.52520(22)	0.0421(18)
C(2B)	0.4043(3)	0.16842(12)	0.57262(23)	0.0416(18)
B(11B)	0.2504(3)	0.14582(16)	0.4975(3)	0.0472(23)
B(3B)	0.4000(4)	0.22685(15)	0.6367(3)	0.0476(23)
B(6B)	0.3508(4)	0.17871(15)	0.4409(3)	0.0476(23)
B(5B)	0.3005(4)	0.24680(16)	0.4183(3)	0.0505(24)
B(4B)	0.3317(4)	0.27665(16)	0.5408(3)	0.0537(25)
B(7B)	0.2812(4)	0.17586(17)	0.6200(3)	0.0517(24)
B(12B)	0.1366(4)	0.19371(18)	0.5103(3)	0.059(3)
B(10B)	0.1824(4)	0.19514(17)	0.4007(3)	0.057(3)
B(8B)	0.2309(4)	0.24375(17)	0.5987(3)	0.059(3)
B(9B)	0.1684(4)	0.25554(18)	0.4632(3)	0.061(3)
C(11B)	0.5753(3)	0.24146(12)	0.53702(23)	0.0458(19)
C(12B)	0.6519(4)	0.27499(17)	0.6147(3)	0.073(3)
C(13B)	0.7808(4)	0.28702(18)	0.6252(3)	0.081(3)
C(14B)	0.8344(4)	0.26654(18)	0.5600(4)	0.080(3)
C(15B)	0.7587(4)	0.23404(19)	0.4803(4)	0.096(4)
C(16B)	0.6299(4)	0.22111(15)	0.4693(3)	0.075(3)
C(21B)	0.5187(3)	0.13035(13)	0.62247(24)	0.0488(20)
C(22B)	0.5996(4)	0.13668(17)	0.7253(3)	0.071(3)
C(23B)	0.7008(4)	0.10070(22)	0.7716(4)	0.091(4)
C(24B)	0.7234(4)	0.05858(20)	0.7163(5)	0.096(4)
C(25B)	0.6430(5)	0.05245(17)	0.6152(4)	0.092(4)
C(26B)	0.5398(4)	0.08770(15)	0.5672(3)	0.071(3)

Table 4.2 Interatomic Distances (Å) and Selected Interbond Angles (°) for
1,2-Ph₂-1,2-closo-C₂B₁₀H₁₀ (10)

C(1A) -C(2A)	1.733(4)	C(1B) -C(2B)	1.720(4)
C(1A) -B(3A)	1.721(5)	C(1B) -B(3B)	1.735(5)
C(1A) -B(6A)	1.723(5)	C(1B) -B(6B)	1.719(5)
C(1A) -B(5A)	1.713(5)	C(1B) -B(5B)	1.715(5)
C(1A) -B(4A)	1.706(5)	C(1B) -B(4B)	1.712(5)
C(1A) -C(11A)	1.500(4)	C(1B) -C(11B)	1.494(4)
C(2A) -B(11A)	1.713(6)	C(2B) -B(11B)	1.700(5)
C(2A) -B(3A)	1.725(5)	C(2B) -B(3B)	1.716(5)
C(2A) -B(6A)	1.727(5)	C(2B) -B(6B)	1.724(5)
C(2A) -B(7A)	1.712(6)	C(2B) -B(7B)	1.705(5)
C(2A) -C(21A)	1.508(5)	C(2B) -C(21B)	1.508(4)
B(11A) -B(6A)	1.771(6)	B(11B) -B(6B)	1.764(5)
B(11A) -B(7A)	1.759(7)	B(11B) -B(7B)	1.777(6)
B(11A) -B(12A)	1.761(7)	B(11B) -B(12B)	1.772(6)
B(11A) -B(10A)	1.759(6)	B(11B) -B(10B)	1.768(6)
B(11A) -H(11A)	1.10(4)	B(11B) -H(11B)	1.07(4)
B(3A) -B(4A)	1.768(6)	B(3B) -B(4B)	1.769(6)
B(3A) -B(7A)	1.770(6)	B(3B) -B(7B)	1.760(6)
B(3A) -B(8A)	1.750(6)	B(3B) -B(8B)	1.757(6)
B(3A) -H(3A)	1.09(4)	B(3B) -H(3B)	1.02(4)
B(6A) -B(5A)	1.776(6)	B(6B) -B(5B)	1.772(6)
B(6A) -B(10A)	1.742(6)	B(6B) -B(10B)	1.746(6)
B(6A) -H(6A)	1.10(4)	B(6B) -H(6B)	1.03(4)
B(5A) -B(4A)	1.771(6)	B(5B) -B(4B)	1.773(6)
B(5A) -B(10A)	1.754(6)	B(5B) -B(10B)	1.766(6)
B(5A) -B(9A)	1.762(6)	B(5B) -B(9B)	1.776(6)
B(5A) -H(5A)	1.03(4)	B(5B) -H(5B)	1.12(4)
B(4A) -B(8A)	1.774(6)	B(4B) -B(8B)	1.781(6)
B(4A) -B(9A)	1.774(6)	B(4B) -B(9B)	1.774(6)
B(4A) -H(4A)	1.11(4)	B(4B) -H(4B)	1.04(4)
B(7A) -B(12A)	1.764(7)	B(7B) -B(12B)	1.789(6)
B(7A) -B(8A)	1.770(7)	B(7B) -B(8B)	1.766(6)
B(7A) -H(7A)	1.15(4)	B(7B) -H(7B)	1.07(4)
B(12A) -B(10A)	1.762(7)	B(12B) -B(10B)	1.773(6)
B(12A) -B(8A)	1.761(7)	B(12B) -B(8B)	1.781(6)
B(12A) -B(9A)	1.760(7)	B(12B) -B(9B)	1.757(6)
B(10A) -B(9A)	1.771(6)	B(10B) -B(9B)	1.772(6)
B(10A) -H(10A)	1.06(4)	B(10B) -H(10B)	1.16(4)
B(8A) -B(9A)	1.774(7)	B(8B) -B(9B)	1.774(6)
B(8A) -H(8A)	1.09(4)	B(8B) -H(8B)	1.10(4)
B(9A) -H(9A)	1.10(4)	B(9B) -H(9B)	1.11(4)
C(11A) -C(12A)	1.388(5)	C(11B) -C(12B)	1.373(5)
C(11A) -C(16A)	1.380(5)	C(11B) -C(16B)	1.382(5)
C(12A) -C(13A)	1.390(6)	C(12B) -C(13B)	1.381(6)
C(13A) -C(14A)	1.365(6)	C(13B) -C(14B)	1.347(6)
C(14A) -C(15A)	1.361(7)	C(14B) -C(15B)	1.371(7)
C(15A) -C(16A)	1.379(6)	C(15B) -C(16B)	1.384(6)
C(21A) -C(22A)	1.386(5)	C(21B) -C(22B)	1.381(5)
C(21A) -C(26A)	1.376(6)	C(21B) -C(26B)	1.379(5)
C(22A) -C(23A)	1.388(6)	C(22B) -C(23B)	1.375(6)
C(23A) -C(24A)	1.338(8)	C(23B) -C(24B)	1.376(7)
C(24A) -C(25A)	1.363(8)	C(24B) -C(25B)	1.360(8)
C(25A) -C(26A)	1.412(7)	C(25B) -C(26B)	1.382(7)

B(3A) -C(1A) -C(2A) 59.91(20)
 B(3A) -C(1A) -B(4A) 62.12(22)
 B(6A) -C(1A) -C(2A) 59.96(20)
 B(6A) -C(1A) -B(5A) 62.23(22)
 B(5A) -C(1A) -B(4A) 62.40(22)
 C(2A) -C(1A) -C(11A) 119.75(25)
 B(3A) -C(1A) -C(11A) 119.0(3)
 B(6A) -C(1A) -C(11A) 118.9(3)
 B(5A) -C(1A) -C(11A) 120.9(3)
 B(4A) -C(1A) -C(11A) 120.5(3)
 B(11A)-C(2A) -B(6A) 61.95(23)
 B(11A)-C(2A) -B(7A) 61.79(25)
 B(3A) -C(2A) -C(1A) 59.69(20)
 B(3A) -C(2A) -B(7A) 61.99(24)
 B(6A) -C(2A) -C(1A) 59.74(20)
 C(1A) -C(2A) -C(21A) 119.5(3)
 B(11A)-C(2A) -C(21A) 122.0(3)
 B(3A) -C(2A) -C(21A) 119.1(3)
 B(6A) -C(2A) -C(21A) 118.7(3)
 B(7A) -C(2A) -C(21A) 121.9(3)
 C(2A) -B(11A)-B(6A) 59.42(23)
 C(2A) -B(11A)-B(7A) 59.07(24)
 B(6A) -B(11A)-B(10A) 59.16(25)
 B(7A) -B(11A)-B(12A) 60.2(3)
 B(12A)-B(11A)-B(10A) 60.1(3)
 C(1A) -B(3A) -C(2A) 60.40(20)
 C(1A) -B(3A) -B(4A) 58.52(21)
 C(2A) -B(3A) -B(7A) 58.66(23)
 B(4A) -B(3A) -B(8A) 60.56(24)
 B(7A) -B(3A) -B(8A) 60.4(3)
 C(1A) -B(6A) -C(2A) 60.30(20)
 C(1A) -B(6A) -B(5A) 58.60(21)
 C(2A) -B(6A) -B(11A) 58.64(23)
 B(11A)-B(6A) -B(10A) 60.09(25)
 B(5A) -B(6A) -B(10A) 59.80(24)
 C(1A) -B(5A) -B(6A) 59.17(21)
 C(1A) -B(5A) -B(4A) 58.59(22)
 B(6A) -B(5A) -B(10A) 59.15(24)
 B(4A) -B(5A) -B(9A) 60.28(25)
 B(10A)-B(5A) -B(9A) 60.5(3)
 C(1A) -B(4A) -B(3A) 59.36(21)
 C(1A) -B(4A) -B(5A) 59.00(22)
 B(3A) -B(4A) -B(8A) 59.22(24)
 B(5A) -B(4A) -B(9A) 59.61(24)
 B(8A) -B(4A) -B(9A) 60.0(3)
 C(2A) -B(7A) -B(11A) 59.14(24)
 C(2A) -B(7A) -B(3A) 59.36(23)
 B(11A)-B(7A) -B(12A) 60.0(3)
 B(3A) -B(7A) -B(8A) 59.3(3)
 B(12A)-B(7A) -B(8A) 59.8(3)
 B(11A)-B(12A)-B(7A) 59.8(3)
 B(11A)-B(12A)-B(10A) 59.9(3)
 B(7A) -B(12A)-B(8A) 60.3(3)
 B(10A)-B(12A)-B(9A) 60.4(3)
 B(8A) -B(12A)-B(9A) 60.5(3)
 B(11A)-B(10A)-B(6A) 60.8(3)
 B(11A)-B(10A)-B(12A) 60.0(3)

B(3B) -C(1B) -C(2B) 59.56(19)
 B(3B) -C(1B) -B(4B) 61.75(22)
 B(6B) -C(1B) -C(2B) 60.66(19)
 B(6B) -C(1B) -B(5B) 62.12(21)
 B(5B) -C(1B) -B(4B) 62.31(22)
 C(2B) -C(1B) -C(11B) 118.82(25)
 B(3B) -C(1B) -C(11B) 117.5(3)
 B(6B) -C(1B) -C(11B) 119.5(3)
 B(5B) -C(1B) -C(11B) 122.7(3)
 B(4B) -C(1B) -C(11B) 121.5(3)
 B(11B)-C(2B) -B(6B) 62.01(21)
 B(11B)-C(2B) -B(7B) 62.94(22)
 B(3B) -C(2B) -C(1B) 60.66(19)
 B(3B) -C(2B) -B(7B) 61.93(22)
 B(6B) -C(2B) -C(1B) 59.90(19)
 C(1B) -C(2B) -C(21B) 118.49(25)
 B(11B)-C(2B) -C(21B) 121.6(3)
 B(3B) -C(2B) -C(21B) 118.1(3)
 B(6B) -C(2B) -C(21B) 118.4(3)
 B(7B) -C(2B) -C(21B) 121.2(3)
 C(2B) -B(11B)-B(6B) 59.68(21)
 C(2B) -B(11B)-B(7B) 58.66(21)
 B(6B) -B(11B)-B(10B) 59.25(23)
 B(7B) -B(11B)-B(12B) 60.53(23)
 B(12B)-B(11B)-B(10B) 60.12(24)
 C(1B) -B(3B) -C(2B) 59.78(19)
 C(1B) -B(3B) -B(4B) 58.49(21)
 C(2B) -B(3B) -B(7B) 58.71(21)
 B(4B) -B(3B) -B(8B) 60.65(23)
 B(7B) -B(3B) -B(8B) 60.29(23)
 C(1B) -B(6B) -C(2B) 59.92(19)
 C(1B) -B(6B) -B(5B) 58.82(21)
 C(2B) -B(6B) -B(11B) 58.31(20)
 B(11B)-B(6B) -B(10B) 60.50(23)
 B(5B) -B(6B) -B(10B) 60.25(23)
 C(1B) -B(5B) -B(6B) 59.06(21)
 C(1B) -B(5B) -B(4B) 58.77(21)
 B(6B) -B(5B) -B(10B) 59.15(23)
 B(4B) -B(5B) -B(9B) 59.99(24)
 B(10B)-B(5B) -B(9B) 60.04(24)
 C(1B) -B(4B) -B(3B) 59.76(21)
 C(1B) -B(4B) -B(5B) 58.92(21)
 B(3B) -B(4B) -B(8B) 59.34(23)
 B(5B) -B(4B) -B(9B) 60.10(24)
 B(8B) -B(4B) -B(9B) 59.89(24)
 C(2B) -B(7B) -B(11B) 58.39(21)
 C(2B) -B(7B) -B(3B) 59.35(21)
 B(11B)-B(7B) -B(12B) 59.58(23)
 B(3B) -B(7B) -B(8B) 59.78(23)
 B(12B)-B(7B) -B(8B) 60.12(24)
 B(11B)-B(12B)-B(7B) 59.89(23)
 B(11B)-B(12B)-B(10B) 59.84(23)
 B(7B) -B(12B)-B(8B) 59.31(24)
 B(10B)-B(12B)-B(9B) 60.27(25)
 B(8B) -B(12B)-B(9B) 60.21(25)
 B(11B)-B(10B)-B(6B) 60.25(23)
 B(11B)-B(10B)-B(12B) 60.03(24)

B(6A) -B(10A)-B(5A) 61.05(24)
 B(5A) -B(10A)-B(9A) 60.0(3)
 B(12A)-B(10A)-B(9A) 59.8(3)
 B(3A) -B(8A) -B(4A) 60.22(24)
 B(3A) -B(8A) -B(7A) 60.4(3)
 B(4A) -B(8A) -B(9A) 60.0(3)
 B(7A) -B(8A) -B(12A) 59.9(3)
 B(12A)-B(8A) -B(9A) 59.7(3)
 B(5A) -B(9A) -B(4A) 60.10(25)
 B(5A) -B(9A) -B(10A) 59.5(3)
 B(4A) -B(9A) -B(8A) 60.0(3)
 B(12A)-B(9A) -B(10A) 59.9(3)
 B(12A)-B(9A) -B(8A) 59.8(3)
 C(1A) -C(11A)-C(12A) 120.4(3)
 C(1A) -C(11A)-C(16A) 120.8(3)
 C(12A)-C(11A)-C(16A) 118.6(3)
 C(11A)-C(12A)-C(13A) 119.7(4)
 C(12A)-C(13A)-C(14A) 120.9(4)
 C(13A)-C(14A)-C(15A) 119.4(4)
 C(14A)-C(15A)-C(16A) 120.8(4)
 C(11A)-C(16A)-C(15A) 120.6(4)
 C(2A) -C(21A)-C(22A) 121.0(3)
 C(2A) -C(21A)-C(26A) 119.8(3)
 C(22A)-C(21A)-C(26A) 119.0(4)
 C(21A)-C(22A)-C(23A) 120.6(4)
 C(22A)-C(23A)-C(24A) 120.3(5)
 C(23A)-C(24A)-C(25A) 120.6(5)
 C(24A)-C(25A)-C(26A) 120.4(5)
 C(21A)-C(26A)-C(25A) 119.0(4)

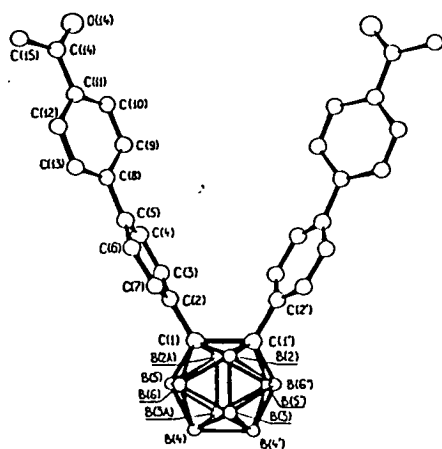
B(6B) -B(10B)-B(5B) 60.61(23)-
 B(5B) -B(10B)-B(9B) 60.28(24)
 B(12B)-B(10B)-B(9B) 59.39(25)
 B(3B) -B(8B) -B(4B) 60.01(23)
 B(3B) -B(8B) -B(7B) 59.94(23)
 B(4B) -B(8B) -B(9B) 59.88(24)
 B(7B) -B(8B) -B(12B) 60.57(24)
 B(12B)-B(8B) -B(9B) 59.21(25)
 B(5B) -B(9B) -B(4B) 59.92(24)
 B(5B) -B(9B) -B(10B) 59.68(24)
 B(4B) -B(9B) -B(8B) 60.23(24)
 B(12B)-B(9B) -B(10B) 60.33(25)
 B(12B)-B(9B) -B(8B) 60.57(25)
 C(1B) -C(11B)-C(12B) 120.5(3)
 C(1B) -C(11B)-C(16B) 121.2(3)
 C(12B)-C(11B)-C(16B) 118.3(3)
 C(11B)-C(12B)-C(13B) 120.4(4)
 C(12B)-C(13B)-C(14B) 121.2(4)
 C(13B)-C(14B)-C(15B) 119.4(4)
 C(14B)-C(15B)-C(16B) 120.1(4)
 C(11B)-C(16B)-C(15B) 120.6(4)
 C(2B) -C(21B)-C(22B) 120.0(3)
 C(2B) -C(21B)-C(26B) 120.3(3)
 C(22B)-C(21B)-C(26B) 119.6(3)
 C(21B)-C(22B)-C(23B) 119.9(4)
 C(22B)-C(23B)-C(24B) 120.7(5)
 C(23B)-C(24B)-C(25B) 119.1(5)
 C(24B)-C(25B)-C(26B) 121.3(5)
 C(21B)-C(26B)-C(25B) 119.4(4)

Table 4.3 Anisotropic Thermal Parameters (\AA^2) for 1,2-Ph₂-1,2-closo-C₂B₁₀H₁₀ (10)

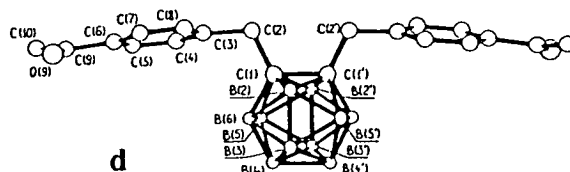
	U11	U22	U33	U23	U13	U12
C(1A)	0.0358(15)	0.0414(17)	0.0421(17)	-0.0027(13)	0.0128(13)	-0.0019(13)
C(2A)	0.0487(18)	0.0462(19)	0.0462(18)	-0.0008(15)	0.0208(15)	-0.0081(14)
B(11A)	0.0538(24)	0.0656(29)	0.0698(28)	-0.0060(23)	0.0301(22)	-0.0156(21)
B(3A)	0.0503(21)	0.0517(23)	0.0400(20)	-0.0033(17)	0.0150(17)	-0.0006(18)
B(6A)	0.0368(19)	0.0544(23)	0.0459(21)	0.0001(18)	0.0097(16)	-0.0054(16)
B(5A)	0.0415(19)	0.0520(23)	0.0551(24)	0.0052(19)	0.0140(18)	0.0068(18)
B(4A)	0.0457(21)	0.0493(23)	0.0545(24)	-0.0094(18)	0.0181(18)	0.0004(18)
B(7A)	0.0702(27)	0.0629(28)	0.0556(25)	-0.0002(21)	0.0354(22)	-0.0045(22)
B(12A)	0.0633(27)	0.0709(31)	0.0802(32)	-0.0048(24)	0.0451(25)	-0.0027(23)
B(10A)	0.0341(19)	0.0733(30)	0.0619(27)	-0.0045(22)	0.0121(19)	0.0002(19)
B(8A)	0.0619(26)	0.0623(28)	0.0567(25)	-0.0090(21)	0.0268(22)	-0.0014(21)
B(9A)	0.0487(22)	0.0620(27)	0.0743(30)	-0.0050(22)	0.0270(21)	0.0089(20)
C(11A)	0.0390(16)	0.0360(16)	0.0505(19)	0.0042(14)	0.0177(14)	0.0004(13)
C(12A)	0.0412(19)	0.0664(24)	0.0673(23)	-0.0036(18)	0.0181(17)	-0.0068(17)
C(13A)	0.0466(21)	0.0766(29)	0.0973(33)	0.0043(24)	0.0272(22)	-0.0052(19)
C(14A)	0.0691(27)	0.0747(28)	0.1095(36)	0.0116(25)	0.0598(27)	0.0081(22)
C(15A)	0.0704(26)	0.0934(33)	0.0760(28)	0.0054(23)	0.0443(23)	0.0051(23)
C(16A)	0.0550(21)	0.0834(28)	0.0545(22)	0.0046(19)	0.0264(18)	0.0010(19)
C(21A)	0.0611(20)	0.0431(19)	0.0568(20)	0.0021(16)	0.0337(18)	-0.0058(16)
C(22A)	0.0582(22)	0.0579(24)	0.0803(27)	0.0054(20)	0.0248(20)	0.0053(19)
C(23A)	0.0736(27)	0.0709(31)	0.1080(37)	0.0164(27)	0.0452(27)	0.0056(23)
C(24A)	0.1130(38)	0.0602(28)	0.1170(42)	0.0231(29)	0.0731(35)	0.0208(27)
C(25A)	0.1565(49)	0.0580(27)	0.0858(33)	-0.0077(24)	0.0685(35)	0.0042(30)
C(26A)	0.1073(33)	0.0526(24)	0.0594(24)	0.0000(18)	0.0341(23)	0.0031(22)
C(1B)	0.0426(16)	0.0377(16)	0.0409(16)	-0.0018(13)	0.0194(13)	-0.0011(13)
C(2B)	0.0357(15)	0.0388(17)	0.0439(17)	0.0017(13)	0.0146(13)	-0.0012(13)
B(11B)	0.0414(19)	0.0435(21)	0.0460(21)	0.0034(16)	0.0083(17)	-0.0048(16)
B(3B)	0.0448(21)	0.0523(22)	0.0397(20)	-0.0074(17)	0.0179(16)	-0.0041(17)
B(6B)	0.0511(21)	0.0454(21)	0.0386(19)	-0.0019(16)	0.0157(17)	-0.0058(17)
B(5B)	0.0445(20)	0.0506(23)	0.0481(21)	0.0062(17)	0.0157(17)	0.0014(17)
B(4B)	0.0529(22)	0.0417(22)	0.0591(24)	0.0000(18)	0.0248(19)	0.0049(18)
B(7B)	0.0469(20)	0.0573(24)	0.0462(21)	0.0033(18)	0.0237(17)	-0.0042(18)
B(12B)	0.0410(21)	0.0673(28)	0.0609(25)	0.0094(21)	0.0180(18)	0.0004(19)
B(10B)	0.0522(23)	0.0545(25)	0.0533(24)	0.0072(19)	0.0117(19)	-0.0033(19)
B(8B)	0.0514(22)	0.0568(25)	0.0620(25)	-0.0018(20)	0.0294(20)	0.0040(19)
B(9B)	0.0482(22)	0.0564(26)	0.0665(26)	0.0146(21)	0.0186(20)	0.0098(19)
C(11B)	0.0420(16)	0.0402(17)	0.0492(18)	0.0006(14)	0.0198(14)	0.0006(14)
C(12B)	0.0608(23)	0.0843(29)	0.0649(24)	-0.0170(21)	0.0266(19)	-0.0251(21)
C(13B)	0.0512(22)	0.0937(33)	0.0861(30)	-0.0145(25)	0.0249(21)	-0.0237(21)
C(14B)	0.0437(20)	0.0738(28)	0.1119(35)	0.0026(25)	0.0317(23)	-0.0033(19)
C(15B)	0.0735(28)	0.0810(30)	0.1304(40)	-0.0240(29)	0.0672(29)	-0.0056(24)
C(16B)	0.0595(23)	0.0613(25)	0.0981(30)	-0.0266(22)	0.0447(22)	-0.0098(19)
C(21B)	0.0423(17)	0.0441(18)	0.0529(19)	0.0072(15)	0.0192(15)	-0.0043(14)
C(22B)	0.0609(22)	0.0734(26)	0.0607(24)	0.0078(20)	0.0072(19)	0.0118(20)
C(23B)	0.0612(26)	0.1027(38)	0.0847(32)	0.0267(28)	0.0006(23)	0.0170(26)
C(24B)	0.0616(26)	0.0756(33)	0.1365(46)	0.0465(32)	0.0380(30)	0.0213(23)
C(25B)	0.0863(31)	0.0598(27)	0.1205(41)	0.0173(26)	0.0578(30)	0.0231(24)
C(26B)	0.0781(26)	0.0504(22)	0.0748(26)	0.0056(19)	0.0335(21)	0.0113(19)

However, the long C-C distances observed in diphenylcarbaborane are comparable with those observed in a series of aryl substituted carbaborane species, R_1R_2 -1,2-*closo*- $C_2B_{10}H_{10}$, where $R_1 = R_2 = C_6H_4-O-C_6H_4-COCH_3$, (a), $C_6H_4-O-C_6H_5$, (b) and $C_6H_4-C_6H_4-COCH_3$, (c), which have cage C-C distances of 1.735(3), 1.736(4) and 1.747(4)Å respectively.⁸³ The structures of these compounds are of interest as they model some carbaborane-bearing units of polyarylene materials. Notably, when the phenyl group of the last of these three species is replaced by a methylene group, *i.e.* where $R_1 = R_2 = CH_2-C_6H_4-COCH_3$, (d), the C-C distance is significantly lower [1.68(1)Å].

It is interesting to compare the structures of the latter two compounds, c and d, shown below. In c, as indeed in a and b, the phenyl groups directly bonded to the cage adopt a similar conformation relative to each other as that observed in the structures of 10A and 10B. In molecule d, however, the six-membered rings are separated from the cage carbon atoms by CH_2 groups, rendering the pendent functions greater flexibility. As a result the aromatic rings are orientated in opposite directions to each other, with planes through their C_6 rings almost parallel with the cage C-C bond.



c



d

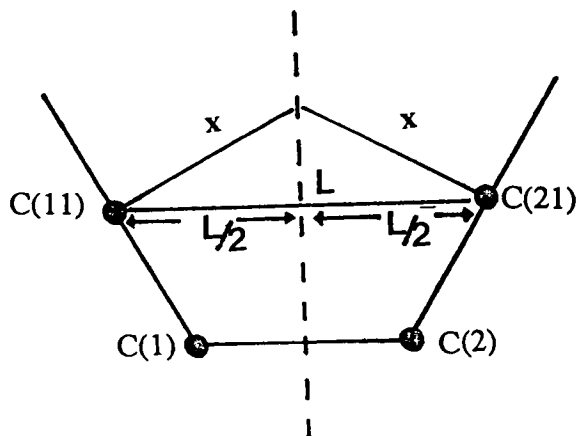
Thus it would appear that when aromatic substituents are closely situated in space, an elongation of the cage C-C distance occurs, whereas when they can lie remote from each other, as in **d**, the C-C distance is significantly shorter, and close to the bond length observed in *ortho*-carbaborane. Presumably the long C-C distances observed (in **10A**, **10B**, **a**, **b** and **c**) reflect repulsions between the π systems of the aromatic rings.

In considering the conformation of the phenyl rings substituents in these carbaborane species, the twisting of the six-membered ring systems may be defined in terms of an angle θ , the average deviation away from a 90° torsion about the C(1)-C(11) and C(2)-C(12) bonds. Essentially the torsion angle is the angle between planes defined by C(1),C(2),C(21) and C(2),C(21),C(22)/C(26) [or C(2),C(1),C(11) and C(1),C(11),C(12)/C(16)].

In **A** neither of the phenyl rings is substantially twisted, with the planes through C(11A-16A) and C(21A-26A) lying only 3 and 1° , respectively, away from what may be termed the "normal" position ($\theta = 0^\circ$). However, in **B** the twist in both phenyl rings is substantially greater, with C(11B)-C(16B) and C(21B)-C(26B) twisted synchronously, by 9 and 7° respectively (the measured distances between C(12B) and C(22B) and C(16B) and C(26B) having similar values). Recalling that the cage C-C distance in **B** is significantly shorter than that in **A**, there appears to be a correlation between the length of the cage C-C bond, and the degree of twisting exhibited by the phenyl substituents. In an attempt to rationalise this, the following factors are considered.

A combination of the cage C-C bond length, and the C-C-C_{phenyl} bond angles result in variable distances between the pivotal phenyl carbon atoms, C(11) and C(21). This distance represents the closest contact of the phenyl substituents, and thus is the source of the greatest crowding in the molecule. In **A**, where the

$C(2)-C(1)-C(11)$ and $C(1)-C(2)-C(21)$ angles are $119.50(26)$ and $119.75(25)^\circ$, the $C(11)\cdots C(21)$ distance is $3.220(5)\text{\AA}$, whereas in **B**, where $C(2B)-C(1B)-C(11B)$ and $C(1B)-C(2B)-C(21B)$ are $118.82(25)$ and $118.49(25)^\circ$ respectively, $C(11B)\cdots C(21B)$ is $3.160(4)$. A rough estimate of the degree of crowding of the π -systems of the two phenyl rings may be made by calculating x , the average length of the normal to the $C_{\text{cage}}-C_{\text{phenyl}}$ vector, as sketched below:

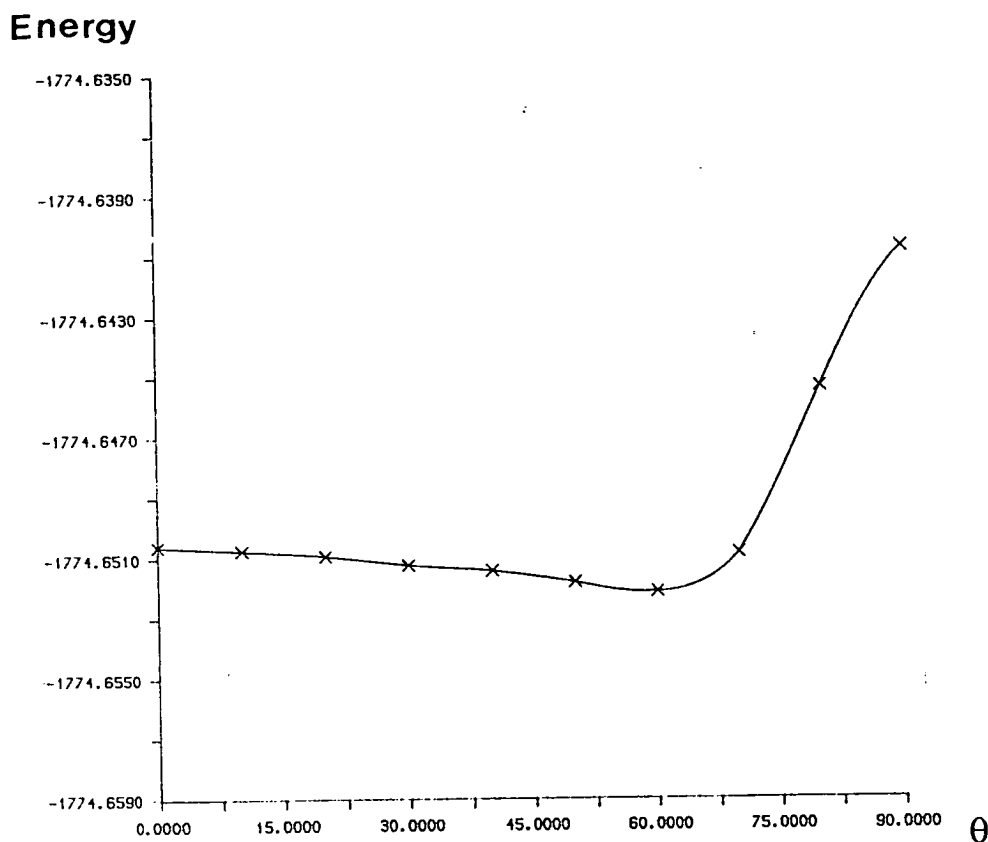


Given that half the thickness of the phenyl π -system is approximately 1.675\AA , if the distance x is close to this value, significant crowding of the two phenyl rings may be expected. The value of x in **B** (1.80\AA) is shorter than that calculated for **A** (1.85\AA), suggesting potentially greater steric strain in the former. However, the synchronous twisting of the ring systems will reduce the potentially unfavourable overlap of the p-orbitals on each pivotal carbon atom, which may explain why the cage C-C distance, and the resulting value of x , are smaller in **B**.

A series of EHMO calculations was performed on an idealised model of diphenylcarbaborane, in which the two phenyl substituents were synchronously rotated about $C(1)-C(11)$ and $C(2)-C(21)$ (labelled C9, C91 and C12, C121 in the

model). The sum of one-electron energies (*i.e.* the relative energy of the system) was monitored as a function of the increasing degree of twist (θ) away from a 90° torsion about C(1)-C(11) and C(2)-C(21). The results are plotted in Figure 4.3.

Figure 4.3 Energy Plot for the Idealised Model of 10



Although the change in energy is small (well within crystal packing forces), there is none the less a gradual decrease in the overall energy of the system as the phenyl groups twist in the same direction, until the adjacent *ortho* hydrogen atoms on either ring begin to come into close contact, at $\theta = ca. 60^\circ$.

Thus far it has been assumed that the increased C-C bond length in diaryl-substituted carbaboranes is a result of the steric repulsions between closely situated aromatic systems. It may also be the case, however, that the phenyl

substituents exert an electronic influence on the carbon-carbon bond. As the above EHMO calculations give a value for the reduced orbital overlap population between atoms (which is a crude measure of the bond strength), the degree of orbital overlap between the cage atoms in the model of diphenylcarbaborane can be compared with values obtained for similar models of 1,2-*closo*-C₂B₁₀H₁₂ and 1-Ph-1,2-*closo*-C₂B₁₀H₁₁ (when all phenyl substituents are similarly orientated, with $\theta = 0^\circ$). The respective values of 0.6321, 0.4665 and 0.4525, imply that, everything else being equal, substitution by phenyl substituents at the cage carbon atoms should in fact strengthen the C-C bond, particularly in the case of diphenylcarbaborane.

This suggests that the cage C-C bond distance (1.750Å) used in the idealised model of the icosahedral cage may, to some extent, be "masking" the steric interaction between the phenyl rings. Thus, in the calculation of orbital overlap, the degree of steric interaction has not been such that the electronic preference for a shorter bond has been countered. Similarly, the energy curve shown in **Figure 4.3** may also be somewhat unrealistic, as the long C-C bond length used in the calculations may result in the steric interactions being underestimated. In the real molecules, **10A** and **10B**, where the cage C-C distances are significantly shorter, a greater variation in the relative energy of the system might be expected as the phenyl rings twist about the C(1)-C(11) and C(2)-C(21) bonds.

It is worth noting that the reduced overlap population between cage carbon atoms in diphenylcarbaborane slightly decreases (from 0.6321 to 0.6296) at $\theta = 90^\circ$, *i.e.* when a greater degree of steric interaction occurs in the model.

In conclusion, the introduction of two phenyl functions at the cage carbon atoms has resulted in a significantly longer cage C-C bond length in both molecules of **10** relative to *ortho*-carbaborane, and this may be attributed to the unfavourable mutual interaction between the π -systems of the six-membered rings. Moreover, the greater

degree of twisting observed in the phenyl substituents in **B**, compared to **A**, is clearly correlated with the shorter distance between the cage carbon atoms in the former.

7,8-Ph₂-10-endo-Ph₃PHg-7,8-nido-C₂B₉H₉, (11)

Introduction

The d¹⁰ carbametallaborane species, 10-endo-Ph₃PHg-7,8-C₂B₉H₁₁, was the first reported example of a *pseudo* σ-bonded carbametallaborane.³⁷ The mercury atom is co-ordinated almost linearly by triphenylphosphine and the unique boron atom [B(10)] of the open C₂B₃ face, with additional, though relatively weak, bonding suggested by the other Hg-B(facial) distances. Given the substantial slippage of the metal atom away from the carbon atoms in this species, the attempted synthesis of a diphenyl-substituted analogue was considered an appropriate start to a series of transition metal derivatives of diphenylcarbaborane. Compared with other possible moieties, a σ-bonded linear metal ligand fragment is less likely to interact significantly with the aromatic cage substituents.

Synthesis and Spectroscopic Analysis

The reaction of [Ph₃PHgCl₂]₂ and Tl₂[7,8-Ph₂-7,8-C₂B₉H₉] in methylene chloride gave a cream coloured solid, a methylene chloride solution of which afforded pale yellow crystals which were subsequently identified as being the target compound, **11**.

An ¹¹B n.m.r. spectrum of a solution of these crystals exhibits doublet (¹J_{BH} 120-150Hz) signals in the frequency range -11 - -29 p.p.m. of relative integral 5:2:1:1, consistent with the substituted C₂B₉ cage having a plane of symmetry (assuming three coincident resonances occur at δ -11.2 p.p.m.)

Structural Study on 11

Introduction

A crystal structure determination on **11** was carried out in order to confirm the geometry of the cage and establish the orientation of the phenyl cage substituents relative to the C_2B_3 carbaborane face and to the exopolyhedral metal ligand group. Diffraction quality crystals of the compound were obtained by the slow evaporation of a methylene chloride solution. Full details of the crystallographic procedures and crystal data may be found in Chapter 5, Section B.

Discussion

Figure 4.4 represents a perspective view of a single molecule of **11**, which clearly shows the orientation of the phenyl cage substituents, whilst an alternative view is shown in **Figure 4.5**. Atomic co-ordinates for refined atoms are given in **Table 4.4**, bond distances and selected interbond angles in **Table 4.5**, and anisotropic thermal parameters for all non-hydrogen atoms are listed in **Table 4.6**.

The structure of **11** is generally analogous to that of the previously determined analogue with a $C_2B_9H_{11}$ cage. The mercury atom is essentially *endo* σ -bonded to B(10), with a B(10)-Hg bond length of 2.178(8)Å. The metal atom may also be regarded as being weakly bonded to the other two facial boron atoms, with Hg-B(9) and Hg-B(11) distances of 2.617(7) and 2.535(8)Å respectively. Compared with the unsubstituted species, the metal fragment is slipped slightly further away from the cage carbon atoms, with a shorter Hg-B(10), and longer Hg-B(9), Hg-B(11) distances, respective distances in the former species being 2.20(2), 2.50(2) and 2.53(2)Å.

Figure 4.4 Perspective View of 7,8-Ph₂-10-endo-Ph₃PHg-7,8-nido-C₂B₉H₉ (11)

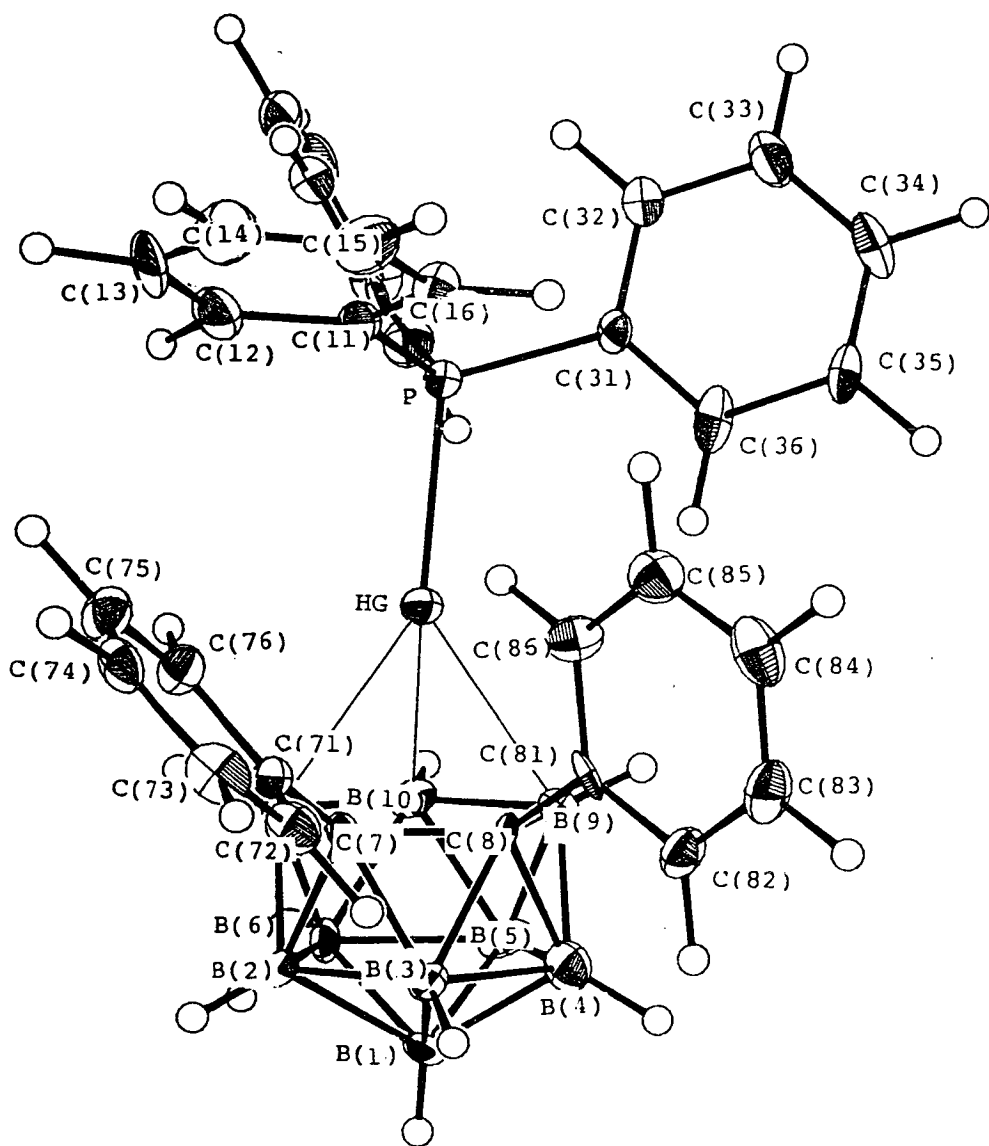


Figure 4.5 Alternative view of 7,8-Ph₂-10-endo-Ph₃PHg-7,8-nido-C₂B₉H₉ (11)

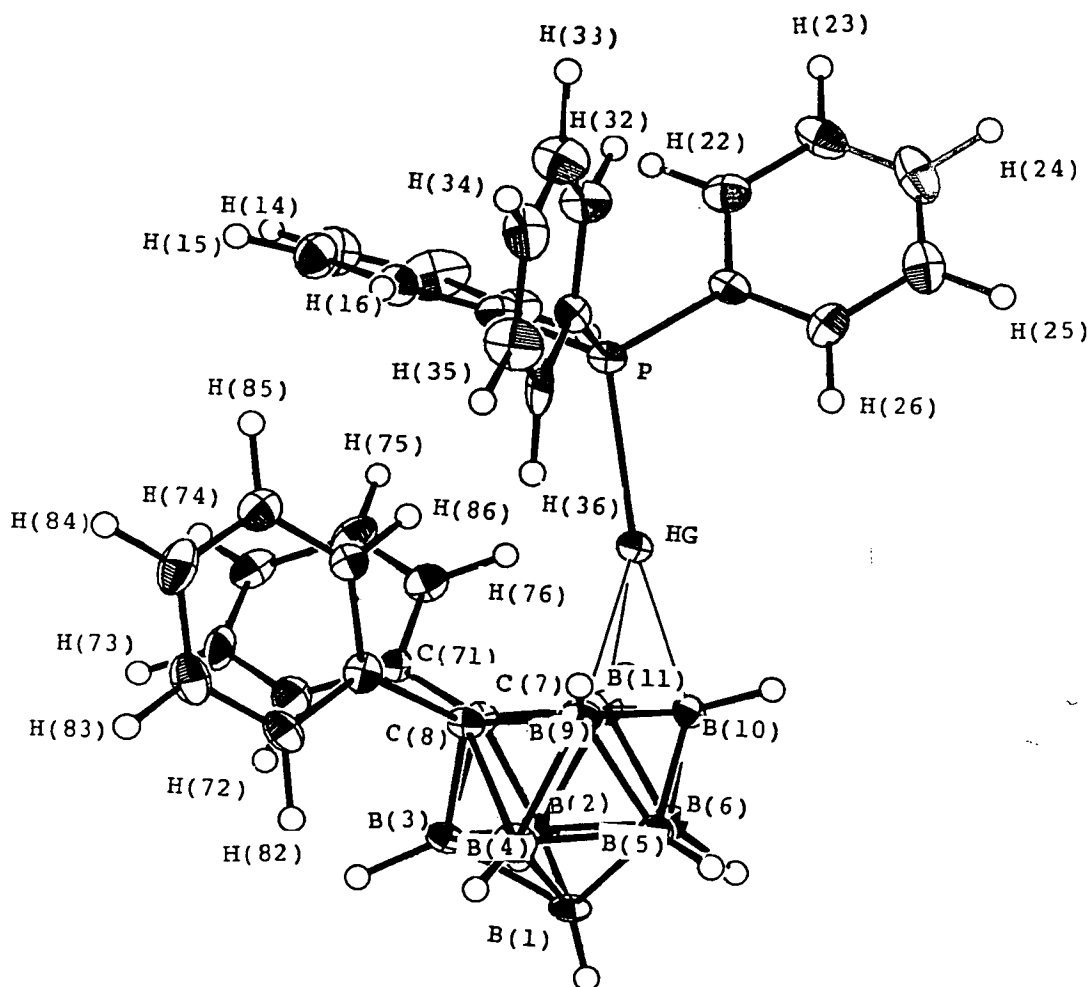


Table 4.4 Co-ordinates of Refined Atoms and Equivalent Isotropic Thermal Parameters (\AA^2) for 7,8-Ph₂-10-endo-Ph₃PHg-7,8-nido-C₂B₉H₉ (11)

	x	y	z	Ueq
Hg	0.23330(2)	0.50000(0)	0.33860(2)	0.0188(1)
P	0.36870(15)	0.57300(13)	0.19669(15)	0.0189(8)
C(11)	0.5157(5)	0.5124(10)	0.1941(5)	0.024(4)
C(12)	0.6000(6)	0.5311(6)	0.2838(6)	0.035(5)
C(13)	0.7136(7)	0.4857(11)	0.2795(7)	0.049(6)
C(14)	0.7401(7)	0.4153(7)	0.1908(7)	0.041(5)
C(15)	0.6571(7)	0.3965(6)	0.1064(7)	0.035(4)
C(16)	0.5453(6)	0.4449(5)	0.1053(6)	0.026(4)
C(21)	0.3896(6)	0.7059(5)	0.2221(5)	0.018(3)
C(22)	0.5009(7)	0.7548(6)	0.2033(6)	0.029(4)
C(23)	0.5077(7)	0.8597(6)	0.2119(7)	0.034(4)
C(24)	0.4031(8)	0.9127(6)	0.2372(7)	0.039(5)
C(25)	0.2932(7)	0.8668(6)	0.2575(7)	0.037(5)
C(26)	0.2863(6)	0.7612(6)	0.2503(6)	0.031(4)
C(31)	0.3073(5)	0.5621(5)	0.0514(5)	0.018(3)
C(32)	0.3568(6)	0.6247(6)	-0.0342(6)	0.030(4)
C(33)	0.3132(7)	0.6205(6)	-0.1459(6)	0.037(5)
C(34)	0.2182(7)	0.5568(6)	-0.1730(6)	0.033(4)
C(35)	0.1697(7)	0.4955(11)	-0.0890(6)	0.036(4)
C(36)	0.2122(6)	0.4980(10)	0.0258(6)	0.029(3)
B(10)	0.0920(7)	0.4604(6)	0.4633(8)	0.019(4)
B(6)	0.0771(7)	0.3888(6)	0.5922(7)	0.019(4)
B(2)	0.1719(7)	0.2826(6)	0.5940(7)	0.019(4)
B(3)	0.1320(7)	0.2041(6)	0.4795(7)	0.019(4)
B(4)	0.0064(10)	0.2584(7)	0.4047(7)	0.019(5)
B(5)	-0.0290(7)	0.3729(6)	0.4700(8)	0.022(4)
B(11)	0.2251(7)	0.3983(5)	0.5329(7)	0.017(4)
B(9)	0.0614(7)	0.3721(6)	0.3435(7)	0.021(4)
B(1)	0.0143(9)	0.2680(7)	0.5569(9)	0.019(5)
C(7)	0.2474(5)	0.2927(5)	0.4649(6)	0.016(3)
C(8)	0.1554(5)	0.2784(5)	0.3596(5)	0.016(3)
C(71)	0.3757(6)	0.2512(5)	0.4547(6)	0.018(4)
C(72)	0.4014(7)	0.1504(6)	0.4353(6)	0.028(4)
C(73)	0.5211(6)	0.1159(6)	0.4291(6)	0.030(4)
C(74)	0.6185(6)	0.1826(6)	0.4434(6)	0.027(4)
C(75)	0.5939(6)	0.2830(6)	0.4589(7)	0.031(4)
C(76)	0.4740(6)	0.3182(6)	0.4645(6)	0.027(4)
C(81)	0.2008(6)	0.2245(5)	0.2523(5)	0.019(3)
C(82)	0.1483(6)	0.1353(5)	0.2125(6)	0.026(4)
C(83)	0.1874(7)	0.0929(6)	0.1088(6)	0.031(4)
C(84)	0.2780(7)	0.1375(6)	0.0428(6)	0.035(4)
C(85)	0.3314(7)	0.2259(6)	0.0847(6)	0.030(4)
C(86)	0.2940(6)	0.2682(5)	0.1872(6)	0.027(4)
Cl(1)	0.01917(20)	0.11089(16)	-0.16521(19)	0.0429(12)
Cl(2)	-0.05671(24)	0.27340(21)	-0.01263(22)	0.0610(15)
C	0.0430(8)	0.2378(6)	-0.1248(7)	0.039(5)

Table 4.5 Interatomic Distances (Å) and Selected Angles (°) for
7,8-Ph₂-10-endo-Ph₃PHg-7,8-nido-C₂B₉H₉ (11)

Hg - P	2.4127(17)	B(2) - B(3)	1.737(11)
Hg -B(10)	2.178(8)	B(2) -B(11)	1.788(11)
Hg -B(11)	2.616(7)	B(2) - B(1)	1.789(12)
Hg - B(9)	2.535(8)	B(2) - C(7)	1.709(10)
P -C(11)	1.800(9)	B(3) - B(4)	1.775(12)
P -C(21)	1.802(6)	B(3) - B(1)	1.783(12)
P -C(31)	1.809(6)	B(3) - C(7)	1.735(10)
C(11) -C(12)	1.408(11)	B(3) - C(8)	1.718(10)
C(11) -C(16)	1.398(11)	B(4) - B(5)	1.741(12)
C(12) -C(13)	1.383(13)	B(4) - B(9)	1.773(12)
C(13) -C(14)	1.416(14)	B(4) - B(1)	1.761(14)
C(14) -C(15)	1.354(12)	B(4) - C(8)	1.734(12)
C(15) -C(16)	1.383(10)	B(5) - B(9)	1.764(11)
C(21) -C(22)	1.398(10)	B(5) - B(1)	1.779(13)
C(21) -C(26)	1.388(10)	B(11) - C(7)	1.625(10)
C(22) -C(23)	1.397(11)	B(9) - C(8)	1.625(10)
C(23) -C(24)	1.377(11)	C(7) - C(8)	1.589(9)
C(24) -C(25)	1.370(11)	C(7) -C(71)	1.514(9)
C(25) -C(26)	1.406(11)	C(8) -C(81)	1.513(9)
C(31) -C(32)	1.400(9)	C(71) -C(72)	1.385(10)
C(31) -C(36)	1.377(11)	C(71) -C(76)	1.401(10)
C(32) -C(33)	1.374(11)	C(72) -C(73)	1.390(10)
C(33) -C(34)	1.377(11)	C(73) -C(74)	1.396(10)
C(34) -C(35)	1.372(13)	C(74) -C(75)	1.372(11)
C(35) -C(36)	1.403(14)	C(75) -C(76)	1.396(11)
B(10) - B(6)	1.772(11)	C(81) -C(82)	1.394(10)
B(10) - B(5)	1.765(12)	C(81) -C(86)	1.394(10)
B(10) -B(11)	1.855(11)	C(82) -C(83)	1.389(10)
B(10) - B(9)	1.842(12)	C(83) -C(84)	1.384(11)
B(6) - B(2)	1.751(11)	C(84) -C(85)	1.397(11)
B(6) - B(5)	1.837(11)	C(85) -C(86)	1.371(10)
B(6) -B(11)	1.765(11)	C1(1) - C	1.767(9)
B(6) - B(1)	1.792(12)	C1(2) - C	1.758(9)
P - Hg -B(10)	169.23(22)	C(7) - B(3) - C(8)	54.8(4)
P - Hg -B(11)	144.04(17)	B(3) - B(4) - B(1)	60.6(5)
P - Hg - B(9)	137.83(19)	B(3) - B(4) - C(8)	58.6(4)
Hg - P -C(11)	112.5(3)	B(5) - B(4) - B(9)	60.3(5)
Hg - P -C(21)	111.15(22)	B(5) - B(4) - B(1)	61.1(5)
Hg - P -C(31)	111.55(21)	B(9) - B(4) - C(8)	55.2(4)
C(11) - P -C(21)	109.0(4)	B(10) - B(5) - B(6)	58.9(4)
C(11) - P -C(31)	106.2(4)	B(10) - B(5) - B(9)	62.9(5)
C(21) - P -C(31)	106.0(3)	B(6) - B(5) - B(1)	59.4(5)
P -C(11) -C(12)	119.7(6)	B(4) - B(5) - B(9)	60.8(5)
P -C(11) -C(16)	120.4(6)	B(4) - B(5) - B(1)	60.0(5)
C(12) -C(11) -C(16)	119.8(8)	B(10) -B(11) - B(6)	58.5(4)
C(11) -C(12) -C(13)	119.2(8)	B(6) -B(11) - B(2)	59.1(4)
C(12) -C(13) -C(14)	119.9(9)	B(2) -B(11) - C(7)	59.9(4)
C(13) -C(14) -C(15)	120.2(8)	B(10) - B(9) - B(5)	58.6(4)
C(14) -C(15) -C(16)	121.0(7)	B(4) - B(9) - B(5)	59.0(5)
C(11) -C(16) -C(15)	119.8(7)	B(4) - B(9) - C(8)	61.2(5)
P -C(21) -C(22)	122.7(5)	B(6) - B(1) - B(2)	58.6(5)

P	-C(21)	-C(26)	116.9(5)	B(6) - B(1) - B(5)	61.9(5)
C(22)	-C(21)	-C(26)	120.1(6)	B(2) - B(1) - B(3)	58.2(5)
C(21)	-C(22)	-C(23)	119.9(7)	B(3) - B(1) - B(4)	60.1(5)
C(22)	-C(23)	-C(24)	118.7(7)	B(4) - B(1) - B(5)	58.9(5)
C(23)	-C(24)	-C(25)	122.7(8)	B(2) - C(7) - B(3)	60.6(4)
C(24)	-C(25)	-C(26)	118.7(7)	B(2) - C(7) -B(11)	64.8(4)
C(21)	-C(26)	-C(25)	119.8(7)	B(3) - C(7) - C(8)	62.1(4)
P	-C(31)	-C(32)	117.4(5)	B(11) - C(7) -C(71)	119.5(5)
P	-C(31)	-C(36)	121.9(6)	C(8) - C(7) -C(71)	119.0(5)
C(32)	-C(31)	-C(36)	120.6(7)	B(3) - C(8) - B(4)	61.9(5)
C(31)	-C(32)	-C(33)	120.1(7)	B(3) - C(8) - C(7)	63.1(4)
C(32)	-C(33)	-C(34)	120.0(7)	B(3) - C(8) -C(81)	115.8(5)
C(33)	-C(34)	-C(35)	119.8(8)	B(4) - C(8) - B(9)	63.6(5)
C(34)	-C(35)	-C(36)	121.6(9)	B(4) - C(8) -C(81)	118.9(6)
C(31)	-C(36)	-C(35)	117.8(8)	B(9) - C(8) -C(81)	118.6(5)
Hg	-B(10)	-B(11)	80.4(4)	C(7) - C(8) -C(81)	118.2(5)
Hg	-B(10)	- B(9)	77.7(4)	C(7) -C(71) -C(72)	123.6(6)
B(6)	-B(10)	- B(5)	62.6(5)	C(7) -C(71) -C(76)	118.4(6)
B(6)	-B(10)	-B(11)	58.2(4)	C(72) -C(71) -C(76)	118.0(6)
B(5)	-B(10)	- B(9)	58.5(4)	C(71) -C(72) -C(73)	121.2(7)
B(10)	- B(6)	- B(5)	58.5(4)	C(72) -C(73) -C(74)	120.4(7)
B(10)	- B(6)	-B(11)	63.3(4)	C(73) -C(74) -C(75)	118.8(7)
B(2)	- B(6)	-B(11)	61.1(4)	C(74) -C(75) -C(76)	121.1(7)
B(2)	- B(6)	- B(1)	60.6(5)	C(71) -C(76) -C(75)	120.5(7)
B(5)	- B(6)	- B(1)	58.7(5)	C(8) -C(81) -C(82)	122.3(6)
B(6)	- B(2)	-B(11)	59.8(4)	C(8) -C(81) -C(86)	119.0(6)
B(6)	- B(2)	- B(1)	60.8(5)	C(82) -C(81) -C(86)	118.5(6)
B(3)	- B(2)	- B(1)	60.7(5)	C(81) -C(82) -C(83)	120.0(6)
B(3)	- B(2)	- C(7)	60.4(4)	C(82) -C(83) -C(84)	121.5(7)
B(11)	- B(2)	- C(7)	55.3(4)	C(83) -C(84) -C(85)	118.0(7)
B(2)	- B(3)	- B(1)	61.1(5)	C(84) -C(85) -C(86)	121.1(7)
B(2)	- B(3)	- C(7)	59.0(4)	C(81) -C(86) -C(85)	120.9(7)
B(4)	- B(3)	- B(1)	59.3(5)	C1(1) - C -C1(2)	111.0(5)
B(4)	- B(3)	- C(8)	59.5(4)		

Table 4.6 Anisotropic Thermal Parameters (\AA^2) for 7,8-Ph₂-10-endo-Ph₃PHg-7,8-nido-C₂B₉H₉ (11)

	U11	U22	U33	U23	U13	U12
Hg	0.0188(1)	0.0184(1)	0.0194(1)	0.0022(2)	0.0004(1)	-0.0015(2)
P	0.0180(8)	0.0216(8)	0.0170(9)	0.0020(7)	-0.0020(7)	-0.0033(7)
C(11)	0.0173(25)	0.0307(50)	0.0234(31)	0.0109(48)	-0.0039(22)	-0.0008(46)
C(12)	0.0294(36)	0.0484(63)	0.0268(38)	0.0131(34)	-0.0048(29)	0.0026(32)
C(13)	0.0365(41)	0.085(11)	0.0252(40)	0.0179(58)	-0.0185(30)	-0.0031(53)
C(14)	0.0289(43)	0.0458(50)	0.0471(54)	0.0103(43)	-0.0061(38)	0.0070(37)
C(15)	0.0247(38)	0.0358(42)	0.0457(51)	-0.0017(38)	0.0036(36)	0.0036(33)
C(16)	0.0255(37)	0.0273(39)	0.0259(41)	-0.0027(32)	-0.0029(31)	-0.0017(31)
C(21)	0.0274(34)	0.0207(32)	0.0072(33)	0.0009(26)	-0.0076(27)	-0.0055(28)
C(22)	0.0320(38)	0.0358(41)	0.0205(38)	0.0004(33)	-0.0012(32)	-0.0054(33)
C(23)	0.0477(48)	0.0274(38)	0.0269(43)	0.0001(33)	-0.0104(36)	-0.0166(37)
C(24)	0.0608(56)	0.0251(41)	0.0311(48)	-0.0030(35)	-0.0180(41)	0.0022(39)
C(25)	0.0421(47)	0.0310(41)	0.0382(49)	-0.0050(37)	-0.0045(38)	0.0053(37)
C(26)	0.0237(37)	0.0362(41)	0.0321(43)	-0.0023(35)	0.0048(32)	0.0043(33)
C(31)	0.0145(29)	0.0199(35)	0.0203(35)	0.0022(28)	-0.0065(25)	0.0029(27)
C(32)	0.0299(37)	0.0374(42)	0.0219(41)	0.0009(33)	-0.0053(31)	-0.0068(34)
C(33)	0.0512(49)	0.0419(46)	0.0184(42)	0.0003(35)	-0.0068(36)	-0.0092(41)
C(34)	0.0493(48)	0.0323(40)	0.0170(39)	-0.0004(34)	-0.0123(34)	0.0108(37)
C(35)	0.0387(35)	0.0429(50)	0.0274(37)	-0.0084(61)	-0.0139(29)	-0.0143(64)
C(36)	0.0309(30)	0.0253(35)	0.0301(37)	-0.0231(57)	-0.0082(27)	0.0061(61)
B(10)	0.0118(37)	0.0160(30)	0.0296(48)	0.0039(33)	0.0005(35)	0.0026(29)
B(6)	0.0194(37)	0.0259(39)	0.0122(41)	-0.0056(32)	-0.0037(31)	-0.0021(32)
B(2)	0.0169(37)	0.0228(39)	0.0168(42)	-0.0004(33)	-0.0019(31)	-0.0081(31)
B(3)	0.0154(36)	0.0187(37)	0.0224(45)	0.0037(33)	-0.0043(32)	-0.0038(31)
B(4)	0.0299(56)	0.0239(51)	0.0039(56)	0.0074(38)	-0.0072(42)	-0.0013(41)
B(5)	0.0100(35)	0.0185(39)	0.0382(53)	0.0034(36)	0.0027(34)	0.0005(30)
B(11)	0.0175(36)	0.0191(36)	0.0146(40)	0.0025(31)	-0.0052(31)	0.0015(30)
B(9)	0.0230(38)	0.0225(40)	0.0190(43)	0.0042(34)	-0.0006(33)	-0.0034(33)
B(1)	0.0183(45)	0.0218(47)	0.0160(53)	0.0103(38)	-0.0012(39)	-0.0018(35)
C(7)	0.0151(31)	0.0188(32)	0.0140(35)	0.0038(28)	-0.0039(26)	0.0026(26)
C(8)	0.0159(31)	0.0199(33)	0.0126(35)	-0.0021(27)	-0.0053(26)	-0.0080(26)
C(71)	0.0162(32)	0.0195(33)	0.0188(39)	0.0016(29)	-0.0014(28)	0.0003(27)
C(72)	0.0289(38)	0.0267(38)	0.0276(42)	0.0050(33)	-0.0006(32)	0.0059(32)
C(73)	0.0308(39)	0.0269(38)	0.0308(42)	0.0009(33)	0.0043(33)	0.0159(33)
C(74)	0.0181(34)	0.0433(44)	0.0204(40)	0.0070(34)	-0.0030(29)	0.0086(33)
C(75)	0.0181(36)	0.0465(47)	0.0274(47)	-0.0052(39)	0.0006(33)	-0.0015(34)
C(76)	0.0207(36)	0.0346(41)	0.0259(43)	-0.0008(33)	-0.0023(30)	-0.0031(32)
C(81)	0.0255(35)	0.0249(35)	0.0074(33)	0.0047(27)	-0.0072(27)	0.0061(29)
C(82)	0.0269(36)	0.0193(34)	0.0307(43)	-0.0025(32)	-0.0061(32)	-0.0056(30)
C(83)	0.0355(41)	0.0248(38)	0.0336(45)	-0.0100(34)	-0.0086(34)	-0.0025(33)
C(84)	0.0424(44)	0.0418(46)	0.0201(40)	-0.0093(35)	-0.0004(34)	0.0124(39)
C(85)	0.0265(38)	0.0332(42)	0.0294(43)	0.0004(34)	0.0026(33)	0.0023(33)
C(86)	0.0248(38)	0.0234(36)	0.0329(44)	-0.0001(32)	0.0079(32)	-0.0007(30)
C1(1)	0.0476(12)	0.0371(11)	0.0439(13)	0.0044(10)	-0.0040(10)	-0.0030(10)
C1(2)	0.0650(15)	0.0712(17)	0.0469(14)	-0.0082(13)	0.0142(12)	0.0075(14)
C	0.0497(51)	0.0360(45)	0.0323(48)	0.0006(38)	0.0034(39)	-0.0049(40)

Presumably the relatively larger angles Hg-B(10)-B(11) and Hg-B(10)-B(9) [80.4(4) vs 75.9(10)° and 77.7 vs 75.5(6)°] in **11** are related to the slight increase in slippage of the latter species. Mercury-carbon(facial) separations of 3.117(6) [C(7)-Hg] and 3.072 [C(8)-Hg] correspond to essentially non-bonding interactions. Consistent with the σ -bonded description, the hydrogen atom H(10) is displaced downward from its normal radial position, at an angle of 9.15°, whilst H(9) and H(11) subtend angles of 22.10 and 20.52° respectively (elevation angles defined in Chapter 1).

The distance between the cage carbon atoms is at first sight surprisingly short, when compared with that observed in both independent molecules of **10**, given the anticipated steric repulsions between closely situated aromatic ring systems. However, this distance, coupled with the distortion in C-B and B-B distances within the C₂B₃ pentagonal face, relative to those observed in *closo*-MC₂B₉ carbametallaboranes, are generally comparable with the unsubstituted analogue, and indeed [10-*endo*-H-7,8-*nido*-C₂B₉H₁₁]⁻³³, and the recently reported anionic gold (I) species, [10-*endo*-Ph₃PAu-7,8-*nido*-C₂B₉H₁₁]⁻²⁵. Table 4.7 shows comparative distances of the C₂B₃ facial C-C, B-C and B-B distances in 1,2-*closo*-C₂B₁₀H₁₂, 10-*endo*-Ph₃PHg-7,8-*nido*-C₂B₉H₁₁ and their diphenyl-substituted analogues, **10** (with average values for molecules A and B), and **11**. In the *closo* species, the C₂B₃ face is that capped by BH and thus the table shows the change in bond distances on replacing a BH vertex, essentially centrally located above the C₂B₃ pentagon, with a σ -bonded Ph₃PHg fragment, *i.e.*:

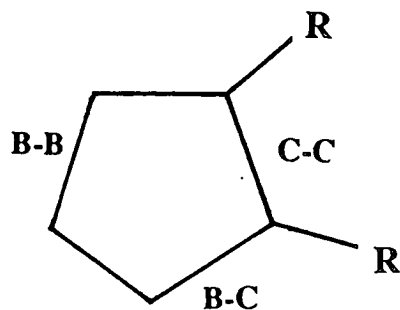
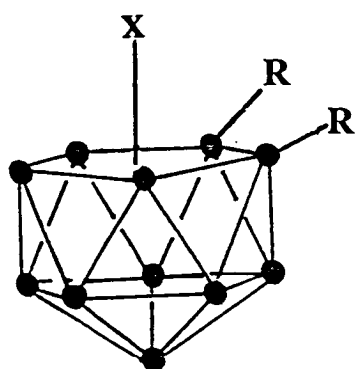


Table 4.7

X	R	C-C(Å)	B-C(Å)	B-B(Å)
BH	H	1.66	1.72	1.79
BH	Ph	1.73	1.72	1.77
Ph ₃ PHg	H	1.54	1.61	1.86
Ph ₃ PHg	Ph	1.58	1.63	1.85

The origin of the structural change in the slipped carbametallaboranes relative to "true" *closo* species has been previously considered, on the basis of the results of a charge-iterated EHMO calculation on [7,8-*nido*-C₂B₉H₁₁]²⁻.²⁵ A sketch diagram of the frontier orbitals so generated is found in Figure 4.6. When a BH vertex occupying a central position above the C₂B₃ face is replaced by a metal ligand fragment, which is slipped towards the unique facial boron atom, B(10) (using the *nido* numbering convention), the resulting distortions can be explained as follows:

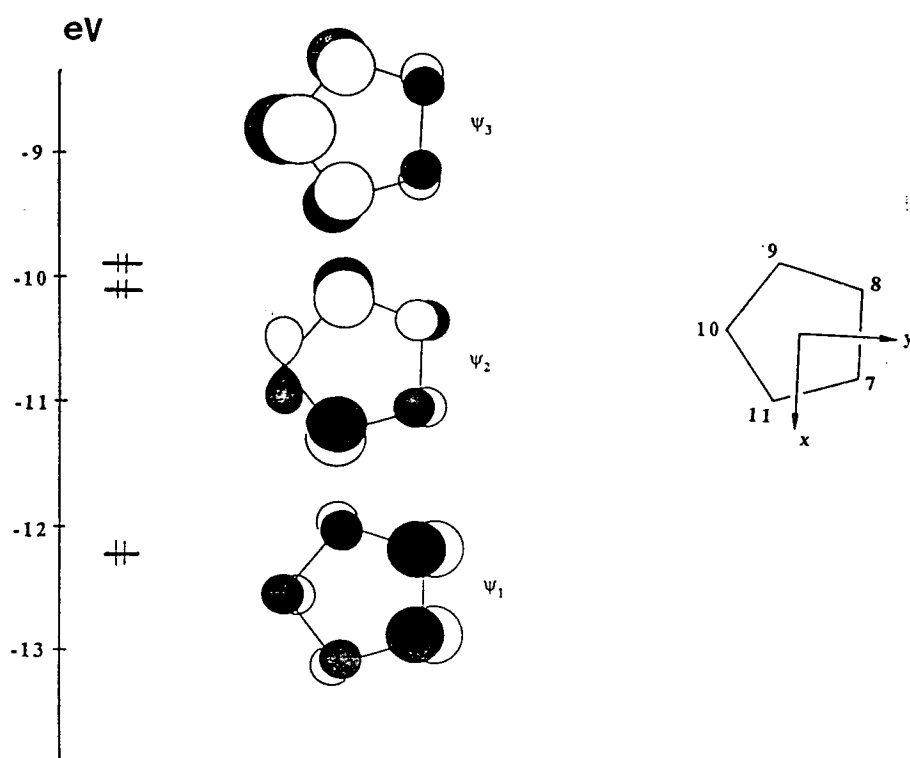
- 1) The B-B distances lengthen due to the increased depopulation of ψ_3 outweighing the decreased population of ψ_1 , as ψ_3 is heavily localised on B(9), B(10)

and B(11),

2) the B-C bonds shorten, as changes in population of all three orbitals act in concert, and

3) the C-C bond shortens, as the decreased population of ψ_1 (localised on the carbon atoms) overrides the the effects of changes in populations of ψ_2 and ψ_3 (which are both localised on the boron atoms).

Figure 4.6 The Occupied π -Frontier Molecular Orbitals of $[7,8\text{-nido-C}_2\text{B}_9\text{H}_{11}]^{2-}$



The cage C-C distance in **11** is, however, significantly longer than that observed in the unsubstituted carbamercuraborane, and this may be attributed to the steric repulsions of the phenyl cage substituents, which are obviously brought into very close proximity. The distance between C(71) and C(81) is 3.038Å and the C(7)-C(8)-C(81) and C(8)-C(7)-C(71) angles have values of 118.17 and 119.02°, giving a value of x of just 1.73Å (see earlier for a pictorial definition of x). This distance is almost equivalent to the half thickness of a phenyl ring, implying potentially significant interaction between the two π -systems. The synchronous twisting of the aryl functions, which have torsions of 30° [C(71)-C(76)] and 28° [C(81)-C(86)] away from the normal position, presumably reduces the overlap of these p-orbitals, and thus relieves the steric strain in the molecule.

The closest contact between the cage-substituted phenyl groups and the triphenylphosphine ligand is that between H(85) and H(16) (2.40Å), with no other significant interactions. This suggests that the twisting of the cage aryl functions has more to do with the steric repulsion within the carbaborane moiety itself, than the presence of the metal ligand fragment above the C_2B_3 face.

In conclusion, the structural study of **11** has shown that the "substitution" of a BH vertex in the *closo* carbaborane, **10**, by a σ -bonded mercury triphenylphosphine group has resulted in a distortion in the C_2B_3 pentagon. The substantial shortening of the C-C bond in **11** has resulted in the increased twist of the two aryl functions, which reduces the unfavourable interaction between adjacent π -systems.

Syntheses of 1,2-Ph₂-3-(η -L)-3,1,2-*closo*-MC₂B₉ species

The first reported example of a transition metal derivative of diphenylcarbaborane described in the previous section incorporates a σ -bonded linear metal ligand fragment. Subsequently, some attention has been focused on the synthesis of complexes incorporating a conical metal ligand fragment, where the metal would occupy a central position above the open C₂B₃ carbaborane face, thus forming a closed icosahedral carbametallaborane. As 3-(*p*-cymene)-3,1,2-*closo*-RuC₂B₉H₁₁⁸⁴ (*p*-cymene = (CH₃)₂CHC₆H₄CH₃) and 3-Cp^{*}-3,1,2-*closo*-RhC₂B₉H₁₁⁷³ are reported to form in high yields, the syntheses of the diphenyl-substituted analogues of these, 1,2-Ph₂-3-(*p*-cymene)-3,1,2-*closo*-RuC₂B₉H₉ and 1,2-Ph₂-3-Cp^{*}-3,1,2-*closo*-RhC₂B₉H₉, were undertaken.

1,2-Ph₂-3-(*p*-cymene)-3,1,2-*closo*-RuC₂B₉H₉, (12)

Synthesis

[(*p*-cymene)RuCl₂]₂ and Ti₂[7,8-Ph₂-7,8-C₂B₉H₉] were stirred together in methylene chloride for fifteen hours, and following work-up involving preparative tlc the target compound, 12, was isolated as an orange solid.

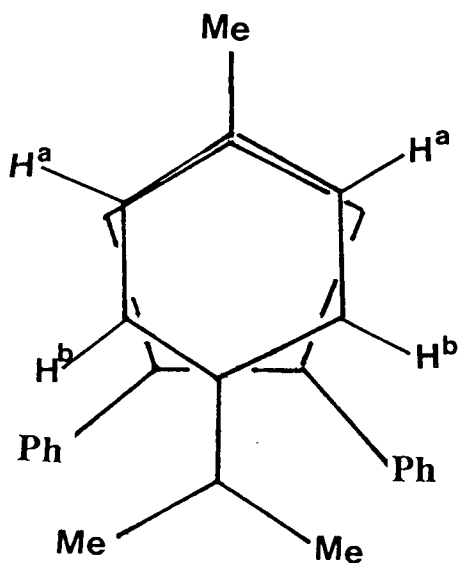
N.m.r. Studies

The ¹¹B-({¹H}) n.m.r. spectrum (shown together with the proton coupled spectrum in Figure 4.7) exhibits six resonances in the ratio 1:2:1:2:2:1, suggesting the molecule has a plane of symmetry. All boron nuclei show coupling to an *exo*-hydrogen atom (J_{BH} ca. 150Hz). Notably the signals are shifted to higher frequency relative to those in the previously assigned spectrum of the related species, 3-(*p*-cymene)-3,1,2-*closo*-RuC₂B₉H₁₁ (δ -20.1 - +30.3 compared with -24.0 - +4.2 p.p.m respectively), a point which will be discussed in more detail later in this

Chapter.

The ^1H spectrum of **12** is shown in Figure 4.8 and exhibits well resolved signals for the *ortho*, *meta* and *para* hydrogen atoms of the phenyl cage substituents, together with characteristic resonances for an η^6 -bonded p-cymene ligand, which are marked on the spectrum. The aromatic p-cymene protons, H^{a} and H^{b} (see diagram below), are magnetically inequivalent and give rise to the AB pattern observed at δ 5.38 and 5.13 p.p.m

However, the fact that both H^{a} protons and both H^{b} protons are themselves equivalent, coupled with the observed molecular symmetry in the ^{11}B spectrum, suggests either that the p-cymene ligand is rapidly rotating about the $\text{Ru}(3)\cdots\text{B}(10)$ axis, or that the molecule has an essentially static, symmetric structure, as depicted below:



Given the likely steric interaction between the carbaborane phenyl substituents and the *exo*-polyhedral aromatic ligand, the latter static representation is perhaps more plausible.

Figure 4.8 ^1H N.M.R. Spectrum of 12

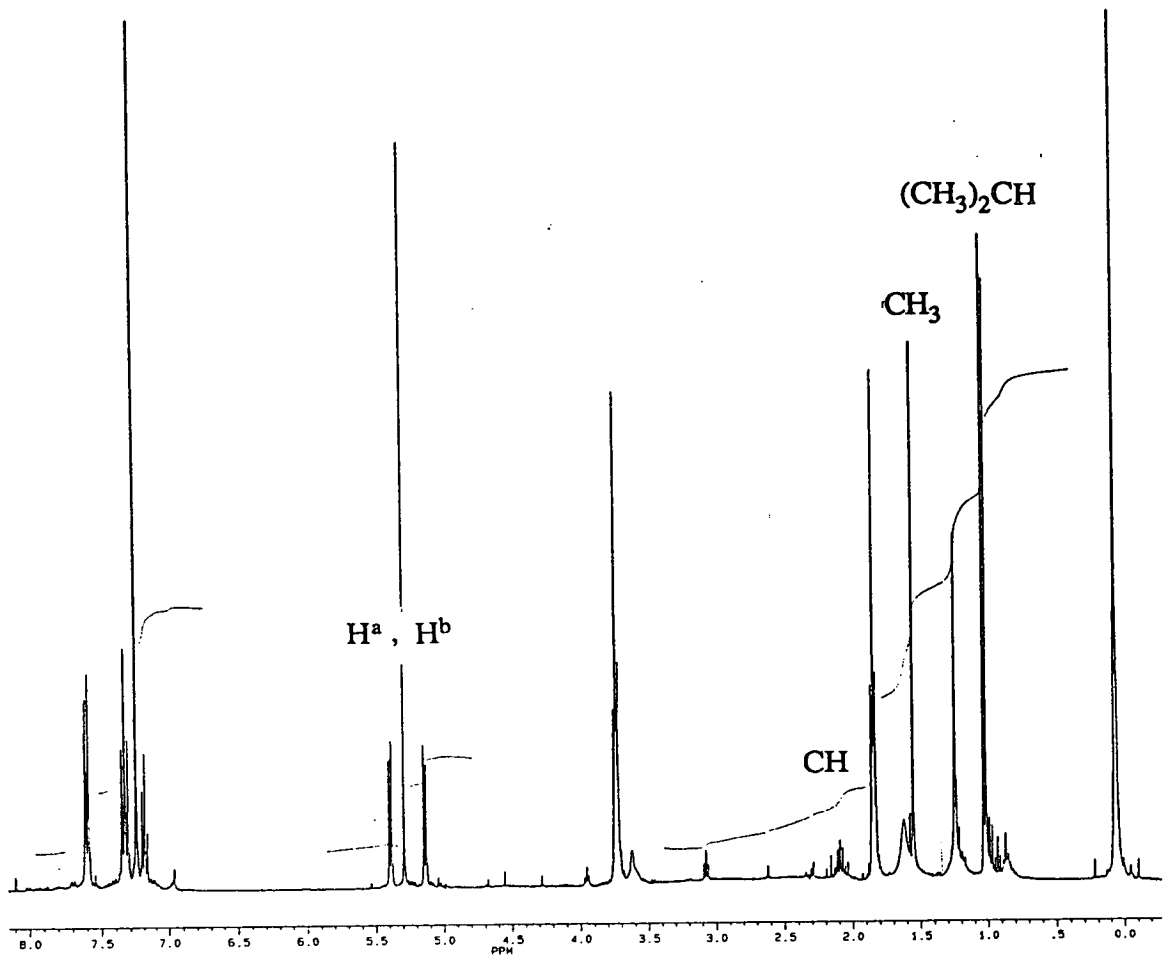
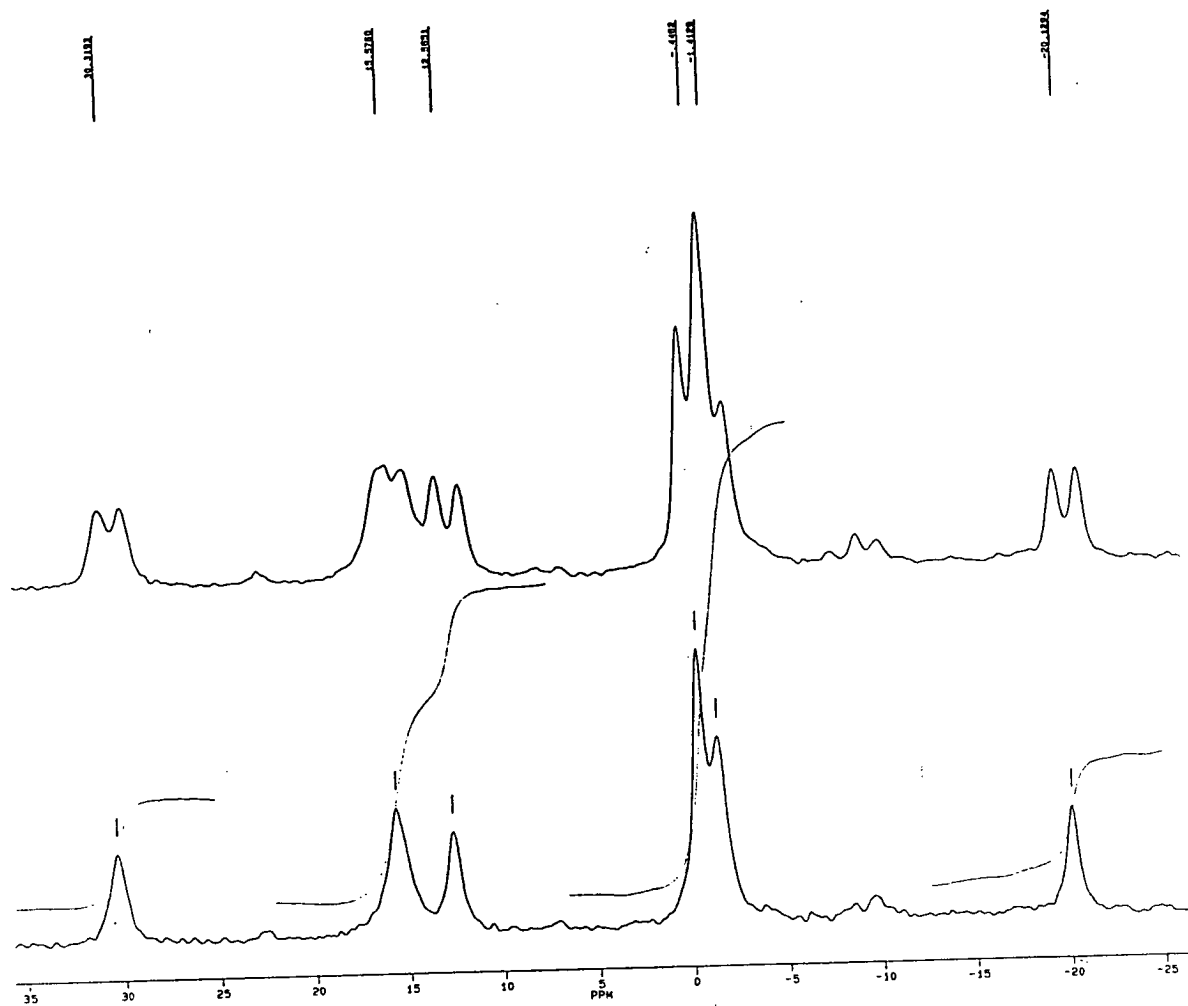


Figure 4.7 ^{11}B and $^{11}\text{B}\text{-}\{^1\text{H}\}$ N.M.R. Spectra of 12



1,2-Ph₂-3-Cp*-3,1,2-closo-RhC₂B₉H₉, (13)

Synthesis

The target complex, **13**, was prepared using a similar procedure to that which afforded the related ruthenium species, **12**, specifically the reaction of [Cp*RhCl₂]₂ with Tl₂[7,8-Ph₂-7,8-C₂B₉H₉] in methylene chloride. The compound was isolated as a red solid by preparative tlc. Microanalysis figures were fully consistent with the expected formulation.

N.m.r. Studies

The ¹H spectrum contains resonances in the aromatic region consistent with the two phenyl cage substituents, as well as a single resonance at δ 1.29 p.p.m., corresponding to the methyl protons of the Cp* ligand.

The ¹¹B-¹H} n.m.r. spectrum exhibits six resonances in the ratio 1:1:2:2:2:1, with all boron nuclei showing coupling to an *exo*-hydrogen atom in the proton coupled spectrum. As in the spectrum of **12** the chemical shift values are at consistently higher frequency than those observed in the spectrum of 3-Cp*-3,1,2-closo-C₂B₉H₁₁, as indicated in **Table 4.8**, which also gives the chemical shift values for compound **10** compared with its unsubstituted analogue.⁸⁵ Whilst substitution of the phenyl groups at the cage carbon atoms results in a slight movement to higher frequency of the resonances of **10**, the presence of the substituents in **13** (and indeed **12**) appears to have a more significant effect on the pattern of boron resonances.

Table 4.8

$C_2B_{10}H_{12}$	10	$Cp^*RhC_2B_9H_{11}$	13
-2.3(2B)	-1.7(2B)	+8.4(1B)	+33.1(1B)
-9.1(2B)	-8.5(4B)	-1.8(1B)	+12.9(1B)
-13.6(4B)	-9.72(4B)	-3.5(2B)	+10.3(2B)
-14.7(2B)		-8.3(2B)	+4.0(2B)
		-18.6(2B)	-1.1(2B)
		-23.4(1B)	-18.0(1B)

Structural Study on 13

Introduction

In order to determine the orientation of the phenyl rings relative to each other and the cage, in the presence of the Cp^*Rh fragment, and the overall cage geometry, a structural determination of **13** was considered to be of potential interest. Diffraction quality crystals were grown by slow diffusion of hexane into a methylene chloride solution at $-30^\circ C$. Details of crystal data collection and structure refinement are contained in Chapter 5, Section B.

Discussion

Compound **13** crystallises with two independent, though essentially similar, molecules per asymmetric unit, **13A** and **13B**. Perspective views of these are shown in **Figure 4.9** and **Figure 4.10** respectively, with both molecules labelled similarly with cage and phenyl hydrogen atoms given the same number as the carbon or boron atom to which they are bound. **Figure 4.11** and **Figure 4.12** illustrate plan views of molecule **A** and **B** respectively, with all but the five metalla-bonded cage atoms removed for clarity, showing the appropriate numbering scheme for the Cp* ligands. Methyl hydrogen atoms are assigned the number of the carbon atom to which the methyl group is bound, together with the letter A,B and C (molecule **A**) or X,Y,Z (molecule **B**). **Table 4.9** gives co-ordinates for refined atoms, **Table 4.10** selected bond distances and interbond angles (equivalent values for either molecule adjacent), and **Table 4.11** lists anisotropic thermal parameters for appropriate atoms.

1,2-Ph₂-3-Cp*-3,1,2-*closo*-RhC₂B₉H₉ clearly has a quite distorted geometry compared with that of previously determined *closo* MC₂B₉ carbametallaboranes, with essentially non-bonding interactions between C(1A) and C(2A) [2.51(3)Å] and between C(1B) and C(2B) [2.50(3)Å]. As a result of this deformation, B(6), in both molecules, is, as it were, pulled out of the plane of atoms B(5), B(9), B(11) and B(12), such that the angle between this plane and that defined by B(5), B(6) and B(11) is 15.5° and 22.6° in molecules **A** and **B** respectively. This gives rise to relatively short cage C-B distances, compared with those in the unsubstituted analogue, *e.g.* in molecule **A** C(1A)-B(5A) = 1.50(3), C(2A)-B(11A) = 1.52(2)Å and in molecule **B** C(1B)-B(5B) = 1.61(3), C(2B)-B(11B) = 1.64(3)Å. Moreover generally longer B-B distances to B(6) are observed, with B(6A)-B(10A) = 1.82(3)Å and B(6B)-B(10B) = 1.93(3)Å.

Figure 4.9 Perspective View of Molecule 13A

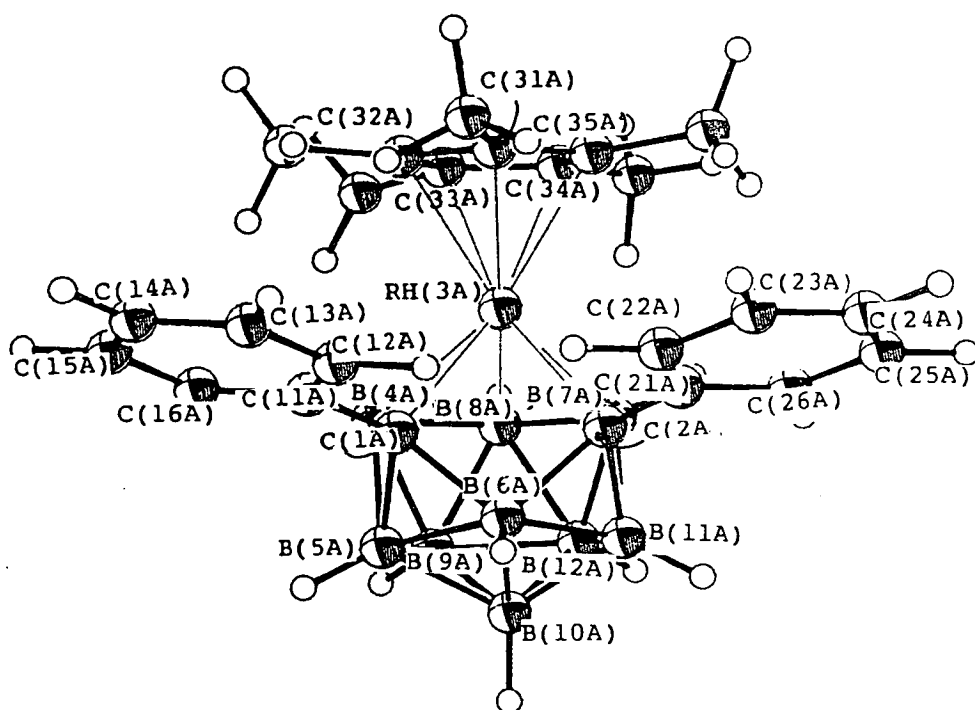


Figure 4.10 Perspective View of Molecule 13B

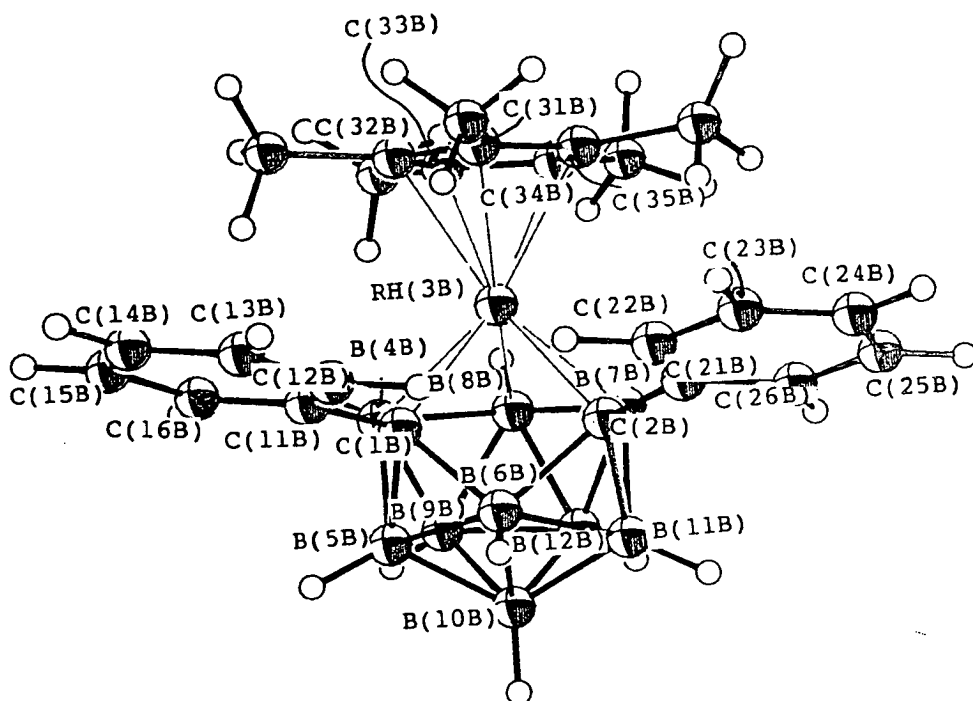


Figure 4.11 Plan View of 13A (B(5), B(6), B(9), B(10), B(11) and B(12) removed for clarity)

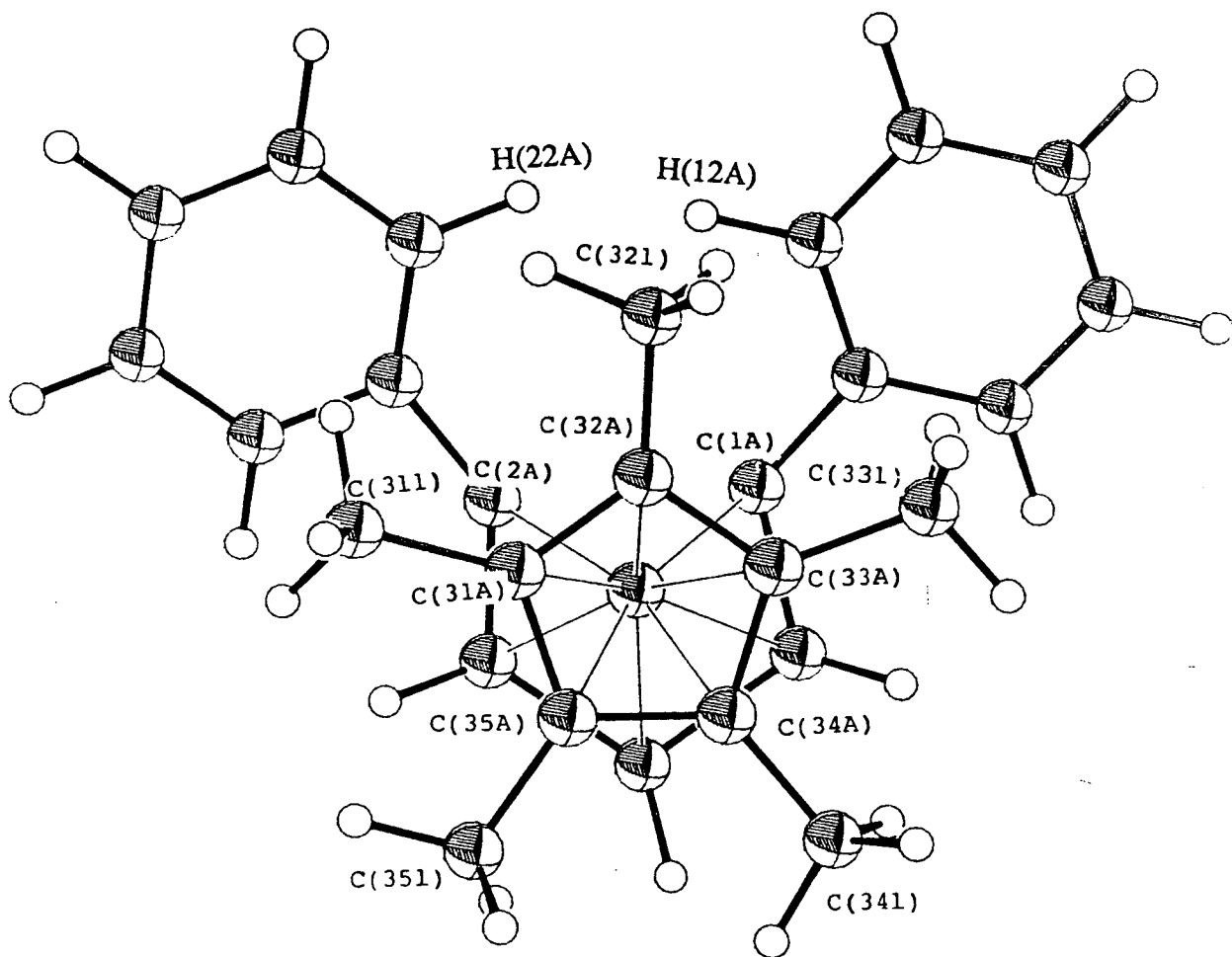


Figure 4.12 Plan View of 13B (B(5), B(6), B(9), B(10), B(11) and B(12) removed for clarity)

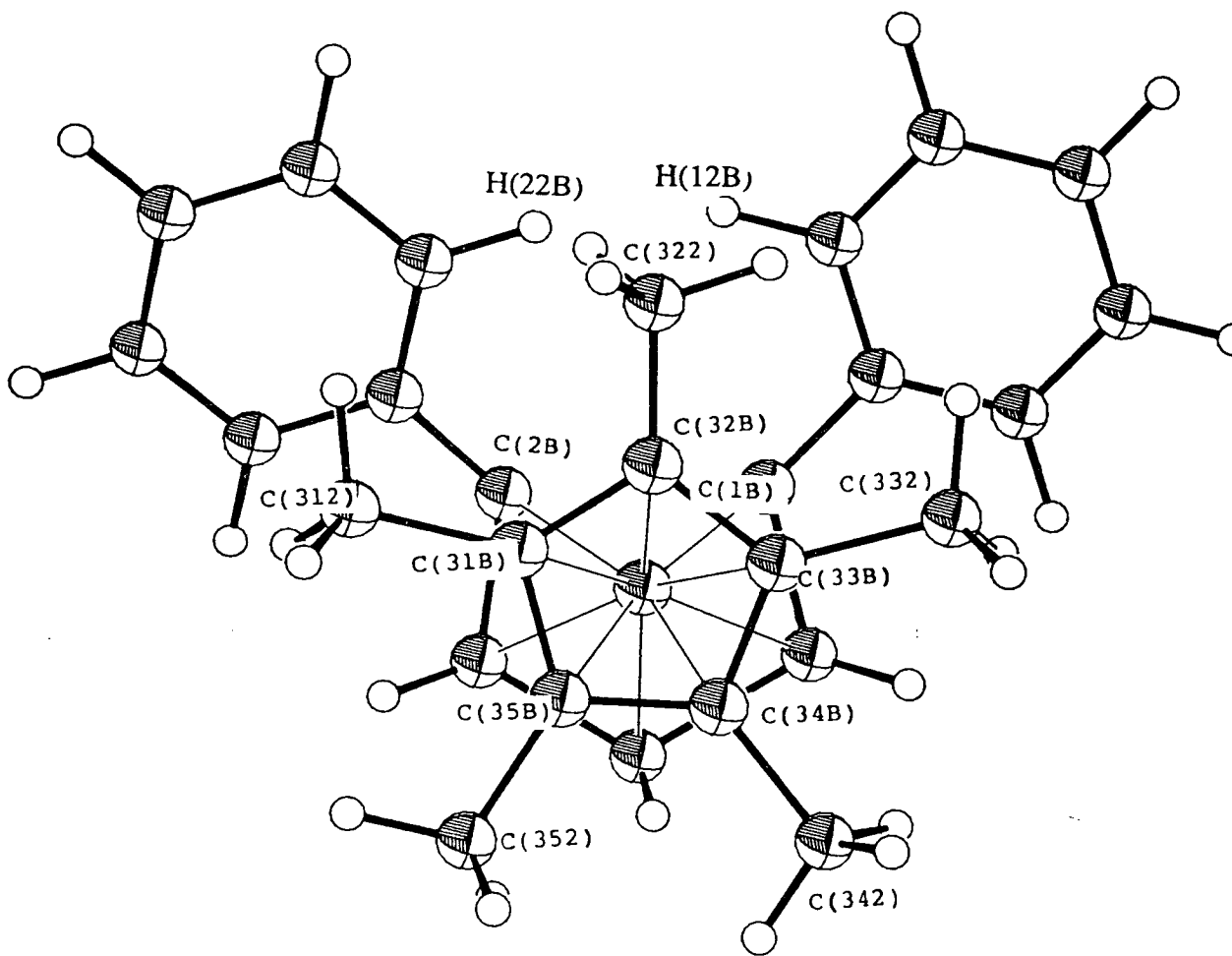


Table 4.9 Co-ordinates of Refined Atoms and Equivalent Isotropic Thermal Parameters (\AA^2) for 1,2-Ph₂-3-Cp*-3,1,2-pseudo-closo-RhC₂B₉H₉ (13)

	x	y	z	Ueq
Rh(3A)	0.03697(9)	0.21118(8)	0.48764(9)	0.0200(10)
Rh(3X)	0.0436(11)	0.2938(11)	0.4781(11)	0.0500(0)
C(1A)	0.0192(11)	0.1380(11)	0.3847(11)	0.037(7)
C(2A)	-0.0310(12)	0.2682(11)	0.3684(12)	0.035(4)
B(4A)	-0.0239(15)	0.1051(11)	0.4421(15)	0.048(7)
B(7A)	-0.0822(17)	0.2573(12)	0.4185(13)	0.047(7)
B(8A)	-0.0949(15)	0.1708(12)	0.4554(15)	0.041(7)
B(6A)	-0.0464(14)	0.1917(12)	0.3049(14)	0.034(4)
B(11A)	-0.1240(15)	0.2547(12)	0.3055(13)	0.036(7)
B(5A)	-0.0679(15)	0.1034(10)	0.3247(13)	0.033(7)
B(12A)	-0.1771(14)	0.2043(13)	0.3578(14)	0.042(7)
B(10A)	-0.1557(13)	0.1638(15)	0.2765(14)	0.043(7)
B(9A)	-0.1423(14)	0.1112(12)	0.3662(15)	0.042(7)
C(12A)	0.1539(6)	0.1443(5)	0.3681(6)	0.054(7)
C(13A)	0.2269(6)	0.1109(5)	0.3718(6)	0.045(7)
C(14A)	0.2448(6)	0.0377(5)	0.3959(6)	0.055(7)
C(15A)	0.1897(6)	-0.0021(5)	0.4163(6)	0.102(7)
C(16A)	0.1167(6)	0.0312(5)	0.4125(6)	0.066(7)
C(11A)	0.0989(6)	0.1044(5)	0.3884(6)	0.042(7)
C(22A)	0.0871(5)	0.3402(4)	0.3409(4)	0.068(7)
C(23A)	0.1149(5)	0.4097(4)	0.3324(4)	0.104(7)
C(24A)	0.0706(5)	0.4717(4)	0.3360(4)	0.076(7)
C(25A)	-0.0015(5)	0.4643(4)	0.3481(4)	0.113(7)
C(26A)	-0.0294(5)	0.3948(4)	0.3566(4)	0.096(7)
C(21A)	0.0150(5)	0.3328(4)	0.3530(4)	0.050(4)
C(31A)	0.1174(5)	0.2966(4)	0.5792(4)	0.043(7)
C(32A)	0.1709(5)	0.2455(4)	0.5666(4)	0.038(7)
C(33A)	0.1606(5)	0.1763(4)	0.5966(4)	0.043(4)
C(34A)	0.1008(5)	0.1846(4)	0.6277(4)	0.086(7)
C(35A)	0.0741(5)	0.2590(4)	0.6170(4)	0.029(6)
C(311)	0.1159(12)	0.3786(7)	0.5688(11)	0.057(5)
C(321)	0.2419(10)	0.2605(10)	0.5444(11)	0.052(5)
C(331)	0.2146(11)	0.1104(8)	0.6017(11)	0.051(4)
C(341)	0.0702(12)	0.1214(9)	0.6611(11)	0.059(5)
C(351)	0.0097(10)	0.2908(10)	0.6400(11)	0.054(4)
Rh(3B)	0.44171(9)	0.29735(8)	0.98194(8)	0.0203(9)
Rh(3Y)	0.4586(22)	0.2168(20)	0.9998(21)	0.0500(0)
C(1B)	0.3547(10)	0.3598(10)	0.8742(10)	0.026(6)
C(2B)	0.3966(10)	0.2294(9)	0.8721(11)	0.025(6)
B(4B)	0.4510(15)	0.4020(11)	0.9224(14)	0.040(7)
B(7B)	0.5023(12)	0.2387(12)	0.9172(13)	0.028(7)
B(8B)	0.5373(13)	0.3296(16)	0.9456(14)	0.050(7)
B(6B)	0.3425(14)	0.2981(13)	0.7990(13)	0.038(7)
B(11B)	0.4296(13)	0.2396(12)	0.8006(13)	0.031(7)
B(5B)	0.3798(14)	0.3919(14)	0.8054(13)	0.041(7)
B(12B)	0.5271(12)	0.2980(12)	0.8471(11)	0.027(7)
B(10B)	0.4252(14)	0.3302(12)	0.7662(11)	0.029(7)
B(9B)	0.4977(14)	0.3875(13)	0.8531(15)	0.047(7)
C(12B)	0.2011(6)	0.3549(5)	0.8514(6)	0.030(7)
C(13B)	0.1302(6)	0.3875(5)	0.8526(6)	0.035(7)

C(14B)	0.1326(6)	0.4616(5)	0.8725(6)	0.053(7)
C(15B)	0.2061(6)	0.5030(5)	0.8912(6)	0.065(7)
C(16B)	0.2771(6)	0.4704(5)	0.8900(6)	0.038(4)
C(11B)	0.2746(6)	0.3963(5)	0.8701(6)	0.043(7)
C(22B)	0.2755(4)	0.1542(4)	0.8688(4)	0.034(7)
C(23B)	0.2396(4)	0.0854(4)	0.8652(4)	0.061(7)
C(24B)	0.2847(4)	0.0223(4)	0.8659(4)	0.084(7)
C(25B)	0.3656(4)	0.0282(4)	0.8702(4)	0.081(7)
C(26B)	0.4015(4)	0.0970(4)	0.8738(4)	0.087(7)
C(21B)	0.3564(4)	0.1600(4)	0.8731(4)	0.038(7)
C(31B)	0.4467(4)	0.2168(4)	1.0811(4)	0.048(7)
C(32B)	0.3813(4)	0.2685(4)	1.0683(4)	0.035(7)
C(33B)	0.4198(4)	0.3390(4)	1.0880(4)	0.057(7)
C(34B)	0.5089(4)	0.3310(4)	1.1130(4)	0.053(7)
C(35B)	0.5255(4)	0.2554(4)	1.1087(4)	0.058(7)
C(312)	0.4467(12)	0.1334(7)	1.0800(11)	0.054(5)
C(322)	0.2901(8)	0.2467(10)	1.0456(11)	0.045(4)
C(332)	0.3733(12)	0.4109(8)	1.0865(12)	0.069(5)
C(342)	0.5703(11)	0.3961(9)	1.1460(11)	0.057(5)
C(352)	0.6181(8)	0.2293(10)	1.1420(11)	0.052(5)

Table 4.10 Selected Interatomic Distances (Å) and Interbond Angles (°) for
1,2-Ph₂-3-Cp^{*}-3,1,2-pseudo-closo-RhC₂B₉H₉ (13)

Rh(3A)-C(1A)	2.185(20)	Rh(3B)-C(1B)	2.143(18)
Rh(3A)-C(2A)	2.167(21)	Rh(3B)-C(2B)	2.144(18)
Rh(3A)-B(4A)	2.18(3)	Rh(3B)-B(4B)	2.236(25)
Rh(3A)-B(7A)	2.05(3)	Rh(3B)-B(7B)	2.201(22)
Rh(3A)-B(8A)	2.236(25)	Rh(3B)-B(8B)	2.16(3)
Rh(3A)-C(31A)	2.224(8)	Rh(3B)-C(31B)	2.286(7)
Rh(3A)-C(32A)	2.189(8)	Rh(3B)-C(32B)	2.327(7)
Rh(3A)-C(33A)	2.223(8)	Rh(3B)-C(33B)	2.257(7)
Rh(3A)-C(34A)	2.277(8)	Rh(3B)-C(34B)	2.169(7)
Rh(3A)-C(35A)	2.277(8)	Rh(3B)-C(35B)	2.187(7)
C(1A)-B(4A)	1.66(3)	C(1B)-B(4B)	1.68(3)
C(1A)-B(6A)	1.67(3)	C(1B)-B(6B)	1.70(3)
C(1A)-B(5A)	1.53(3)	C(1B)-B(5B)	1.61(3)
C(1A)-C(11A)	1.504(23)	C(1B)-C(11B)	1.531(21)
C(2A)-B(7A)	1.56(3)	C(2B)-B(7B)	1.65(3)
C(2A)-B(6A)	1.74(3)	C(2B)-B(6B)	1.74(3)
C(2A)-B(11A)	1.50(3)	C(2B)-B(11B)	1.66(3)
C(2A)-C(21A)	1.529(22)	C(2B)-C(21B)	1.457(19)
B(4A)-B(8A)	1.83(4)	B(4B)-B(8B)	1.91(4)
B(4A)-B(5A)	1.88(3)	B(4B)-B(5B)	1.88(3)
B(4A)-B(9A)	1.88(4)	B(4B)-B(9B)	1.81(4)
B(7A)-B(8A)	1.77(4)	B(7B)-B(8B)	1.76(3)
B(7A)-B(11A)	1.81(4)	B(7B)-B(11B)	1.87(3)
B(7A)-B(12A)	1.79(4)	B(7B)-B(12B)	1.87(3)
B(8A)-B(12A)	1.77(4)	B(8B)-B(12B)	1.79(3)
B(8A)-B(9A)	1.79(4)	B(8B)-B(9B)	1.81(4)
B(6A)-B(11A)	1.79(3)	B(6B)-B(11B)	1.86(3)
B(6A)-B(5A)	1.73(3)	B(6B)-B(5B)	1.82(3)
B(6A)-B(10A)	1.81(3)	B(6B)-B(10B)	1.91(3)
B(11A)-B(12A)	1.86(3)	B(11B)-B(12B)	1.85(3)
B(11A)-B(10A)	1.75(3)	B(11B)-B(10B)	1.76(3)
B(5A)-B(10A)	1.76(3)	B(5B)-B(10B)	1.72(3)
B(5A)-B(9A)	1.80(3)	B(5B)-B(9B)	1.83(4)
B(12A)-B(10A)	1.84(4)	B(12B)-B(10B)	1.79(3)
B(12A)-B(9A)	1.79(3)	B(12B)-B(9B)	1.73(3)
B(10A)-B(9A)	1.80(4)	B(10B)-B(9B)	1.81(3)
C(31A)-C(311)	1.508(21)	C(31B)-C(312)	1.523(20)
C(32A)-C(321)	1.510(21)	C(32B)-C(322)	1.511(19)
C(33A)-C(331)	1.509(20)	C(33B)-C(332)	1.541(21)
C(34A)-C(341)	1.515(21)	C(34B)-C(342)	1.526(20)
C(35A)-C(351)	1.498(21)	C(35B)-C(352)	1.523(19)
C(1A)-Rh(3A)-C(2A)	70.3(8)	C(1B)-Rh(3B)-C(2B)	71.3(7)
C(1A)-Rh(3A)-B(4A)	44.7(8)	C(1B)-Rh(3B)-B(4B)	45.1(8)
C(2A)-Rh(3A)-B(7A)	43.5(9)	C(2B)-Rh(3B)-B(7B)	44.6(8)
B(4A)-Rh(3A)-B(8A)	49.0(9)	B(4B)-Rh(3B)-B(8B)	51.4(9)
B(7A)-Rh(3A)-B(8A)	48.6(10)	B(7B)-Rh(3B)-B(8B)	47.6(9)
C(31A)-Rh(3A)-C(32A)	37.5(3)	C(31B)-Rh(3B)-C(32B)	35.8(3)
C(31A)-Rh(3A)-C(35A)	36.8(3)	C(31B)-Rh(3B)-C(35B)	36.9(3)
C(32A)-Rh(3A)-C(33A)	37.5(3)	C(32B)-Rh(3B)-C(33B)	36.1(3)
C(33A)-Rh(3A)-C(34A)	36.8(3)	C(33B)-Rh(3B)-C(34B)	37.4(3)
C(34A)-Rh(3A)-C(35A)	36.3(3)	C(34B)-Rh(3B)-C(35B)	38.0(3)
Rh(3A)-C(1A)-B(4A)	67.4(11)	Rh(3B)-C(1B)-B(4B)	70.4(11)
B(4A)-C(1A)-B(5A)	71.9(15)	B(4B)-C(1B)-B(5B)	69.7(14)

B(6A) -C(1A) -B(5A) 65.3(14)
 Rh(3A)-C(2A) -B(7A) 64.1(12)
 B(7A) -C(2A) -B(11A) 72.2(16)
 B(6A) -C(2A) -B(11A) 66.4(15)
 Rh(3A)-B(4A) -C(1A) 67.9(11)
 Rh(3A)-B(4A) -B(8A) 67.1(11)
 C(1A) -B(4A) -B(5A) 50.8(12)
 B(8A) -B(4A) -B(9A) 57.6(13)
 B(5A) -B(4A) -B(9A) 57.2(13)
 Rh(3A)-B(7A) -C(2A) 72.4(13)
 Rh(3A)-B(7A) -B(8A) 71.3(12)
 C(2A) -B(7A) -B(11A) 52.4(13)
 B(8A) -B(7A) -B(12A) 59.8(14)
 B(11A)-B(7A) -B(12A) 62.3(14)
 Rh(3A)-B(8A) -B(4A) 63.9(11)
 Rh(3A)-B(8A) -B(7A) 60.1(11)
 B(4A) -B(8A) -B(9A) 62.5(14)
 B(7A) -B(8A) -B(12A) 60.6(14)
 B(12A)-B(8A) -B(9A) 60.4(14)
 C(1A) -B(6A) -C(2A) 94.4(15)
 C(1A) -B(6A) -B(5A) 53.5(12)
 C(2A) -B(6A) -B(11A) 50.3(12)
 B(11A)-B(6A) -B(10A) 58.1(13)
 B(5A) -B(6A) -B(10A) 59.4(13)
 C(2A) -B(11A)-B(7A) 55.4(14)
 C(2A) -B(11A)-B(6A) 63.2(14)
 B(7A) -B(11A)-B(12A) 58.3(13)
 B(6A) -B(11A)-B(10A) 61.6(14)
 B(12A)-B(11A)-B(10A) 61.0(14)
 C(1A) -B(5A) -B(4A) 57.2(13)
 C(1A) -B(5A) -B(6A) 61.1(14)
 B(4A) -B(5A) -B(9A) 61.3(13)
 B(6A) -B(5A) -B(10A) 62.7(14)
 B(10A)-B(5A) -B(9A) 60.8(14)
 B(7A) -B(12A)-B(8A) 59.6(14)
 B(7A) -B(12A)-B(11A) 59.5(14)
 B(8A) -B(12A)-B(9A) 60.2(14)
 B(11A)-B(12A)-B(10A) 56.6(13)
 B(10A)-B(12A)-B(9A) 59.5(14)
 B(6A) -B(10A)-B(11A) 60.3(14)
 B(6A) -B(10A)-B(5A) 57.9(13)
 B(11A)-B(10A)-B(12A) 62.4(14)
 B(5A) -B(10A)-B(9A) 60.7(14)
 B(12A)-B(10A)-B(9A) 59.0(14)
 B(4A) -B(9A) -B(8A) 59.9(14)
 B(4A) -B(9A) -B(5A) 61.4(13)
 B(8A) -B(9A) -B(12A) 59.4(14)
 B(5A) -B(9A) -B(10A) 58.5(13)
 B(12A)-B(9A) -B(10A) 61.5(14)
 Rh(3A)-C(1A) -C(11A) 117.3(12)
 B(4A) -C(1A) -C(11A) 121.2(16)
 B(6A) -C(1A) -C(11A) 121.8(16)
 B(5A) -C(1A) -C(11A) 117.6(16)
 Rh(3A)-C(2A) -C(21A) 117.4(12)
 B(7A) -C(2A) -C(21A) 134.8(17)
 B(6A) -C(2A) -C(21A) 115.4(15)
 B(11A)-C(2A) -C(21A) 118.1(17)

B(6B) -C(1B) -B(5B) 66.6(14)
 Rh(3B)-C(2B) -B(7B) 69.5(10)
 B(7B) -C(2B) -B(11B) 68.9(13)
 B(6B) -C(2B) -B(11B) 66.4(13)
 Rh(3B)-B(4B) -C(1B) 64.5(10)
 Rh(3B)-B(4B) -B(8B) 62.3(11)
 C(1B) -B(4B) -B(5B) 53.5(12)
 B(8B) -B(4B) -B(9B) 58.2(13)
 B(5B) -B(4B) -B(9B) 59.4(13)
 Rh(3B)-B(7B) -C(2B) 65.9(10)
 Rh(3B)-B(7B) -B(8B) 65.0(11)
 C(2B) -B(7B) -B(11B) 55.8(12)
 B(8B) -B(7B) -B(12B) 59.2(13)
 B(11B)-B(7B) -B(12B) 59.3(12)
 Rh(3B)-B(8B) -B(4B) 66.4(11)
 Rh(3B)-B(8B) -B(7B) 67.4(11)
 B(4B) -B(8B) -B(9B) 58.3(13)
 B(7B) -B(8B) -B(12B) 63.3(13)
 B(12B)-B(8B) -B(9B) 57.5(13)
 C(1B) -B(6B) -C(2B) 93.3(14)
 C(1B) -B(6B) -B(5B) 54.5(12)
 C(2B) -B(6B) -B(11B) 54.7(12)
 B(11B)-B(6B) -B(10B) 55.6(12)
 B(5B) -B(6B) -B(10B) 54.8(12)
 C(2B) -B(11B)-B(7B) 55.3(12)
 C(2B) -B(11B)-B(6B) 58.9(12)
 B(7B) -B(11B)-B(12B) 60.2(12)
 B(6B) -B(11B)-B(10B) 63.6(13)
 B(12B)-B(11B)-B(10B) 59.5(12)
 C(1B) -B(5B) -B(4B) 56.8(13)
 C(1B) -B(5B) -B(6B) 58.8(13)
 B(4B) -B(5B) -B(9B) 58.4(13)
 B(6B) -B(5B) -B(10B) 65.3(14)
 B(10B)-B(5B) -B(9B) 61.2(14)
 B(7B) -B(12B)-B(8B) 57.5(13)
 B(7B) -B(12B)-B(11B) 60.5(12)
 B(8B) -B(12B)-B(9B) 61.8(14)
 B(11B)-B(12B)-B(10B) 57.7(12)
 B(10B)-B(12B)-B(9B) 61.8(13)
 B(6B) -B(10B)-B(11B) 60.8(13)
 B(6B) -B(10B)-B(5B) 60.0(13)
 B(11B)-B(10B)-B(12B) 62.8(13)
 B(5B) -B(10B)-B(9B) 62.6(14)
 B(12B)-B(10B)-B(9B) 57.5(13)
 B(4B) -B(9B) -B(8B) 63.4(14)
 B(4B) -B(9B) -B(5B) 62.1(14)
 B(8B) -B(9B) -B(12B) 60.7(14)
 B(5B) -B(9B) -B(10B) 56.2(13)
 B(12B)-B(9B) -B(10B) 60.7(13)
 Rh(3B)-C(1B) -C(11B) 121.4(11)
 B(4B) -C(1B) -C(11B) 120.4(14)
 B(6B) -C(1B) -C(11B) 119.1(14)
 B(5B) -C(1B) -C(11B) 112.8(14)
 Rh(3B)-C(2B) -C(21B) 117.5(11)
 B(7B) -C(2B) -C(21B) 121.7(14)
 B(6B) -C(2B) -C(21B) 122.8(14)
 B(11B)-C(2B) -C(21B) 117.3(14)

C(1A) -C(11A)-C(12A) 121.8(11)
C(1A) -C(11A)-C(16A) 118.2(11)
C(2A) -C(21A)-C(22A) 134.8(10)
C(2A) -C(21A)-C(26A) 105.1(10)
C(32A)-C(31A)-C(311) 127.3(10)
C(35A)-C(31A)-C(311) 124.0(10)
C(31A)-C(32A)-C(321) 128.5(10)
C(33A)-C(32A)-C(321) 122.3(10)
C(32A)-C(33A)-C(331) 122.9(10)
C(34A)-C(33A)-C(331) 128.7(10)
C(33A)-C(34A)-C(341) 123.2(10)
C(35A)-C(34A)-C(341) 128.7(10)
C(31A)-C(35A)-C(351) 126.6(10)
C(34A)-C(35A)-C(351) 125.4(10)

C(1B) -C(11B)-C(12B) 120.3(10)
C(1B) -C(11B)-C(16B) 119.6(10)
C(2B) -C(21B)-C(22B) 123.8(9)
C(2B) -C(21B)-C(26B) 116.1(9)
C(32B)-C(31B)-C(312) 131.9(9)
C(35B)-C(31B)-C(312) 119.6(9)
C(31B)-C(32B)-C(322) 123.0(9)
C(33B)-C(32B)-C(322) 128.8(9)
C(32B)-C(33B)-C(332) 125.6(9)
C(34B)-C(33B)-C(332) 126.3(9)
C(33B)-C(34B)-C(342) 121.0(9)
C(35B)-C(34B)-C(342) 130.7(9)
C(31B)-C(35B)-C(352) 132.0(9)
C(34B)-C(35B)-C(352) 119.5(9)

Table 2.11 Anisotropic Thermal Parameters (\AA^2) for

1,2-Ph₂-3-Cp*⁻-3,1,2-pseudo-closo-RhC₂B₉H₉ (13)

	U11	U22	U33	U23	U13	U12
Rh(3A)	0.0136(8)	0.0190(8)	0.0224(8)	0.0006(7)	0.0091(7)	-0.0007(7)
C(1A)	0.0171(52)	0.0431(58)	0.0373(55)	0.0034(54)	0.0058(49)	-0.0015(53)
B(4A)	0.0569(57)	0.0096(56)	0.0699(58)	-0.0004(54)	0.0496(51)	0.0076(55)
B(7A)	0.0771(61)	0.0291(58)	0.0142(55)	0.0135(53)	0.0082(55)	-0.0083(58)
B(8A)	0.0378(57)	0.0232(57)	0.0522(58)	-0.0090(55)	0.0245(53)	-0.0145(55)
B(11A)	0.0474(58)	0.0279(58)	0.0214(55)	0.0039(53)	0.0122(52)	0.0148(56)
B(5A)	0.0544(58)	0.0022(54)	0.0319(55)	0.0030(50)	0.0242(51)	0.0009(54)
B(12A)	0.0307(56)	0.0397(59)	0.0441(57)	-0.0059(57)	0.0191(51)	-0.0029(57)
B(10A)	0.0058(54)	0.0727(61)	0.0330(57)	-0.0284(57)	-0.0121(53)	0.0066(57)
B(9A)	0.0248(55)	0.0217(57)	0.0666(59)	0.0010(56)	0.0240(52)	-0.0041(54)
C(12A)	0.0368(54)	0.0270(56)	0.0896(58)	-0.0114(55)	0.0480(49)	-0.0006(52)
C(13A)	0.0227(54)	0.0457(58)	0.0511(57)	-0.0271(54)	0.0093(51)	-0.0003(54)
C(14A)	0.0337(55)	0.0481(59)	0.0737(58)	-0.0147(56)	0.0341(51)	-0.0048(55)
C(15A)	0.0885(59)	0.0878(62)	0.1105(61)	-0.0020(60)	0.0614(56)	0.0632(58)
C(16A)	0.0444(56)	0.0297(57)	0.1081(60)	0.0018(57)	0.0463(53)	0.0094(54)
C(11A)	0.0396(55)	0.0201(55)	0.0503(56)	-0.0164(52)	0.0187(51)	0.0093(53)
C(22A)	0.0400(55)	0.0697(61)	0.0851(59)	-0.0064(58)	0.0464(51)	-0.0027(56)
C(23A)	0.0849(60)	0.0738(61)	0.1263(62)	0.0083(60)	0.0583(57)	-0.0555(58)
C(24A)	0.0938(60)	0.0107(55)	0.1013(60)	-0.0106(56)	0.0569(56)	-0.0001(56)
C(25A)	0.0739(58)	0.0771(62)	0.1690(62)	0.0035(61)	0.0855(56)	0.0355(58)
C(26A)	0.0768(58)	0.1372(63)	0.0667(58)	-0.0513(59)	0.0552(52)	-0.0848(58)
C(31A)	0.0457(54)	0.0056(52)	0.0683(56)	0.0116(52)	0.0409(48)	0.0008(52)
C(32A)	0.0301(55)	0.0659(60)	0.0090(52)	-0.0053(52)	0.0040(48)	-0.0127(55)
C(34A)	0.0364(56)	0.1123(63)	0.0961(60)	0.0318(60)	0.0433(53)	0.0173(58)
C(35A)	0.0217(53)	0.0554(58)	0.0023(50)	0.0004(50)	-0.0022(47)	-0.0053(53)
Rh(3B)	0.0219(8)	0.0198(8)	0.0140(7)	0.0001(7)	0.0086(6)	-0.0015(7)
C(1B)	0.0094(49)	0.0516(58)	0.0170(50)	-0.0225(50)	0.0106(44)	-0.0193(50)
C(2B)	0.0159(50)	0.0201(54)	0.0357(53)	-0.0102(49)	0.0169(46)	-0.0018(49)
B(4B)	0.0440(58)	0.0147(57)	0.0472(58)	0.0053(54)	0.0199(53)	0.0017(55)
B(7B)	0.0123(52)	0.0317(57)	0.0348(56)	0.0138(53)	0.0138(49)	-0.0002(53)
B(8B)	0.0087(54)	0.1043(63)	0.0291(56)	-0.0309(58)	0.0027(51)	0.0054(58)
B(6B)	0.0306(55)	0.0388(59)	0.0338(56)	0.0032(56)	0.0146(50)	0.0025(57)
B(11B)	0.0244(54)	0.0368(58)	0.0277(56)	0.0035(53)	0.0157(50)	0.0062(54)
B(5B)	0.0261(55)	0.0626(61)	0.0287(56)	0.0161(56)	0.0166(50)	0.0115(57)
B(12B)	0.0236(54)	0.0331(57)	0.0159(52)	0.0004(54)	0.0060(48)	-0.0150(55)
B(10B)	0.0370(57)	0.0358(58)	0.0064(52)	0.0004(51)	0.0076(49)	0.0048(55)
B(9B)	0.0393(56)	0.0413(59)	0.0604(57)	0.0199(56)	0.0453(49)	0.0038(55)
C(12B)	0.0158(53)	0.0272(55)	0.0274(54)	0.0020(52)	-0.0126(50)	-0.0092(52)
C(13B)	0.0395(56)	0.0315(56)	0.0204(52)	0.0183(51)	0.0066(49)	0.0018(54)
C(14B)	0.0404(55)	0.0583(60)	0.0529(56)	-0.0015(55)	0.0339(49)	0.0071(56)
C(15B)	0.0456(56)	0.0384(58)	0.0960(60)	-0.0218(57)	0.0432(53)	-0.0044(55)
C(11B)	0.0459(56)	0.0362(57)	0.0399(54)	-0.0041(53)	0.0272(49)	0.0144(54)
C(22B)	0.0277(53)	0.0258(55)	0.0434(54)	0.0096(51)	0.0232(47)	-0.0037(51)
C(23B)	0.0318(57)	0.0770(61)	0.0529(58)	-0.0052(58)	0.0047(54)	-0.0178(57)
C(24B)	0.1137(62)	0.0215(57)	0.0886(60)	-0.0307(56)	0.0494(58)	-0.0205(58)
C(25B)	0.0558(57)	0.0629(61)	0.1163(60)	0.0208(59)	0.0666(52)	0.0096(57)
C(26B)	0.0780(58)	0.0188(57)	0.1468(61)	-0.0062(58)	0.0802(55)	0.0017(56)
C(21B)	0.0203(52)	0.0350(57)	0.0552(56)	-0.0008(53)	0.0279(47)	0.0093(52)
C(31B)	0.0402(54)	0.0671(60)	0.0296(53)	-0.0247(54)	0.0231(47)	-0.0278(56)
C(32B)	0.0380(54)	0.0252(55)	0.0351(54)	0.0088(50)	0.0248(48)	0.0074(52)
C(33B)	0.0360(54)	0.0991(62)	0.0355(54)	0.0108(56)	0.0324(47)	0.0170(57)
C(34B)	0.0672(59)	0.0676(60)	0.0134(52)	-0.0173(53)	0.0196(50)	-0.0030(58)
C(35B)	0.0506(58)	0.0481(59)	0.0510(58)	0.0316(55)	0.0079(55)	0.0030(57)

Despite the distorted cage geometry C(1A), C(2A), B(4A), B(7A) and B(8A) and C(1B), C(2B), B(4B), B(7B) and B(8B) are essentially co-planar, making angles of 4.2 and 1.7° with their respective lower four atom belt, and Rh(3A) and Rh(3B) are still quite definitely η^5 -bonded to the open (albeit distorted) pentagonal rings, with average Rh-B/C distances of 2.16 and 2.18 Å respectively. The Rh(3A)-B(6A) and Rh(3B)-B(6B) distances are 2.92(2) and 2.91(3) Å respectively, which are shorter than that usually observed in more regular icosahedra, but still too long to be considered bonding interactions.

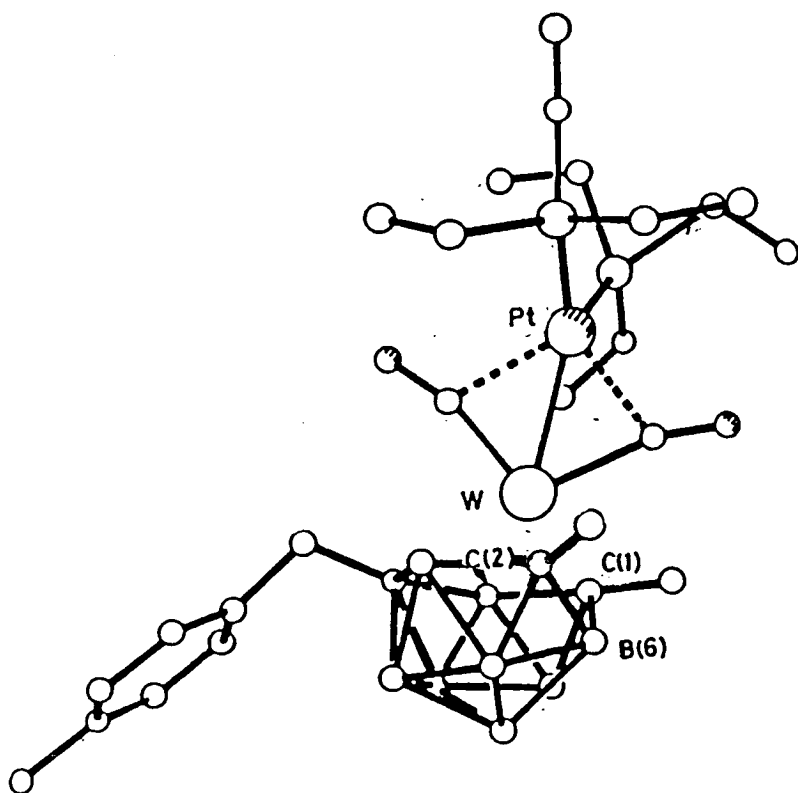
The very long cage carbon atom separation can be readily understood by considering the orientation of the phenyl cage substituents, which is best represented in Figure 4.12 and Figure 4.13. In molecule A the aromatic rings C(11A-16A) and C(21A-26A) are twisted by *ca.* 78 and 87° respectively away from the normal position (as defined for 10 and 11), presumably as a result of the presence of the bulky Cp* ligand. It therefore appears that the steric interaction between the two rings has forced the cage carbon atoms apart. In fact, even with the unusually long C(1A)-C(2A) distance, there is an extremely close H(12A)····H(22A) contact of 1.71 Å (significantly less than the sum of the van der Waals radii for two hydrogen atoms, 2.2 Å), suggesting some substantial steric strain in the molecule. Similarly in molecule B the phenyl rings C(11B-16B) and C(21B-26B) are twisted by 79 and 86° respectively, with a distance of only 1.85 Å between H(12B) and H(22B).

In both molecules the methyl carbon atoms do not lie in the plane of the C₅ pentagon, but are generally elevated above it, although EHMO studies have indicated that, in the absence of steric influences, the optimum conformation for a five-membered cyclic ligand is that in which ring substituents are coplanar with the pentagonal ring.⁸⁶ In molecule A C(311), C(321) and C(331) are at angles of 7.4, 10.0 and 5.5° to the C₅ plane, these carbon atoms being those nearest the phenyl cage substituents, with C(341) and C(351) marginally below this plane. In molecule B

C(312), C(322) and C(332) are also elevated above the C(31B-35B) plane, at angles of 5.8, 4.2 and 2.3° respectively, although in this case C(342) and C(352) also lie above the plane, at angles of 4.8 and 6.3° respectively. On the whole greater deviation from planarity occurs when the methyl carbon atoms are closer in space to the aromatic rings, and thus these observations may be attributed to steric crowding between the *exo*-polyhedral ligand and the cage substituents, even though the phenyl rings are substantially less elevated above the C₂B₃ face than is normally expected for cage substituents (*i.e.* C(11A) and C(21A) subtend elevation angles of 17.2 and 14.0° respectively, and C(11B) and C(21B) subtend angles of 14.7 and 20.5° respectively).

The distortion of this twelve-vertex carbametallaborane can be compared with that observed in the structure of the bimetallic system, PtW(CO)₂(PEt₃)₂{η⁶-C₂B₉H₈(CH₂C₆H₄Me)₂}⁸⁷ shown in Figure 4.14 below..

Figure 4.14 Structure of PtW(CO)₂(PEt₃)₂{η⁶-C₂B₉H₈(CH₂C₆H₄Me)₂}

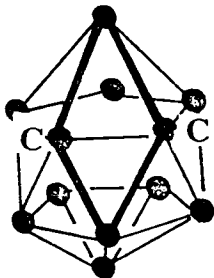


This species has been formally assigned an *iso-closo* cage geometry, in which the tungsten atom can be regarded as capping an open six-membered face of the carbaborane moiety. The cage carbon atom separation is 2.88Å and B(6) has been effectively drawn up towards the open face of the ligand, such that the W-B(6) distance is 2.51Å, and the metal atom is essentially ligated by all six atoms C(1), C(2), B(4), B(7), B(8), and B(6). However, there is some variation in bond lengths, with C(1)-W and C(2)-W being 2.02(2) and 2.04(2)Å compared with W-B(4) (2.40Å) and W-B(6). In addition the angle between B(5), B(9), B(11) and B(12) and B(5), B(11) and B(6) is 24.5° (slightly greater than that observed in 13A and 13B), resulting in long B(6)-B(5), B(11) and B(10) distances of 1.95(3), 1.95(3) and 1.93(3)Å respectively.

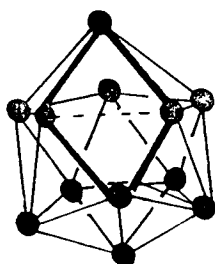
The extent of opening of the M, C(1), C(2), B(6) portion of the cages of 3-Cp*-3,1,2-*closo*-RhC₂B₉H₁₁, 13 and the bimetallic *iso-closo* species is illustrated in **Figure 4.15**. The structure of 13, which has molecular dimensions of intermediate value between *iso-closo* structure and the more regular *closo* species, may therefore be described as having a *pseudo-closo* cage geometry. Although similar distortion away from "true" *closo* geometry occurs in the latter two species, the reasons for this are quite different. Whilst in 13 the unusually long cage C-C distance results from the mutual repulsions of the adjacent phenyl substituents, the distortion in the carbawolfraborane is thought to be caused by the d⁴ metal atom preferring to be seven-coordinate.

Figure 4.15 Extent of Cage Opening in Twelve Vertex Polyhedra

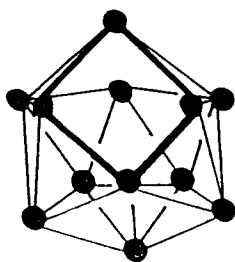
3-Cp*⁻-3,1,2-*closo*-RhC₂B₉H₁₁



1,2-Ph₂-3-Cp*⁻-3,1,2-*pseudo-closo*-C₂B₉H₉, (13)



PtW(CO)₂(PEt₃)₂{η⁶-C₂B₉H₈(CH₂C₆H₄Me)Me₂}

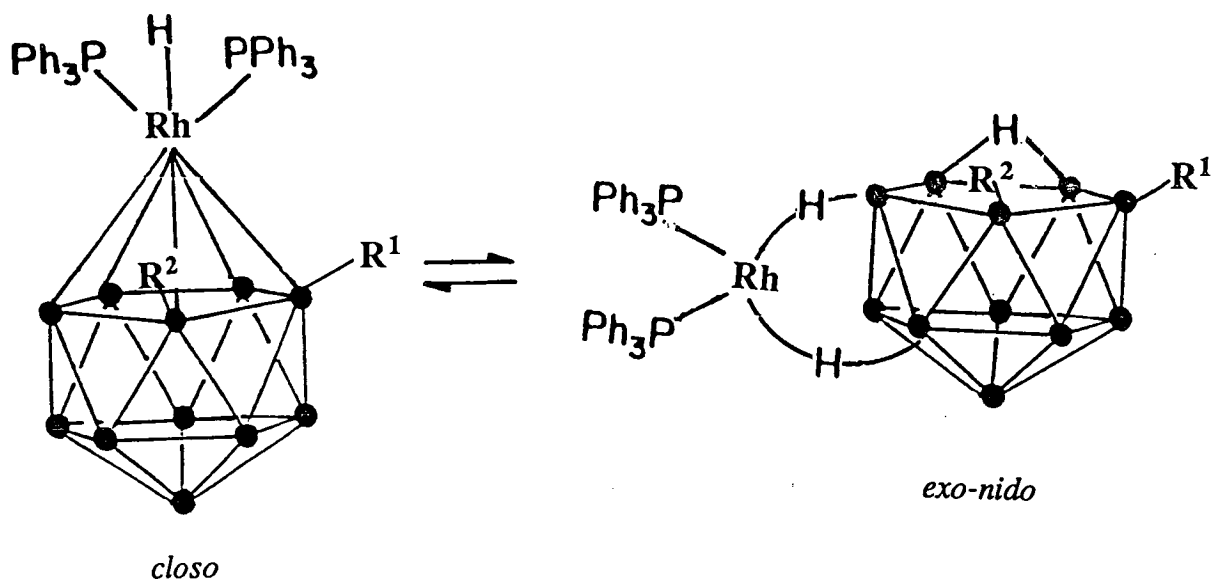


Interestingly, the ^{11}B n.m.r spectrum of the carbawolfraborane has a similar spread of chemical shift values as that observed in the spectrum of **13**, with one particularly high frequency signal at +28.9 p.p.m., attributed to B(8). Thus the quite substantial shift in the boron resonances of the latter, compared with the unsubstituted analogue (see Table 4.8), may to some extent be linked to the distortion of the polyhedron. This is not unduly surprising, as a change in the electronic distribution within the cage can indeed be expected to accompany a partial "opening" of the cage.

Suggestions for Further Work

In the light of this unprecedented structure, those of further carbametallaboranes in this series deserve future investigation. Obviously the structure of the (p-cymene)Ru analogue will now be of interest, especially given the similarities in the resonance patterns observed in the ^{11}B n.m.r. spectra of **12** and **13**. The synthesis of a hexamethylbenzene analogue of **12** should result in a complex having similar or possibly even greater steric overcrowding than the Cp^*Rh complex, and this may give rise to further distortion away from a "normal" *closo* cage geometry towards a twelve vertex *iso-closo* arrangement.

In addition, it would be of interest to attempt the synthesis of $1\text{-R}^1\text{-2-R}^2\text{-3,3-(Ph}_3\text{P)}_2\text{-3-H-3,1,2-closo-RhC}_2\text{B}_9\text{H}_9$ (where $\text{R}^1 = \text{R}^2 = \text{Ph}$) as species of this general type have been shown to be potential catalysts in, for example, alkene hydrogenation and isomerisation.⁶⁷ Successful catalysis requires the (reversible) formation in solution of a catalytically active *exo-nido* species, which is illustrated overleaf:



Catalytic activity of the system may be improved by increasing the steric bulk of the carbaborane cage substituents, which increases the concentration of the *exo-nido* species. A diphenyl derivative of this carboradaborane may well therefore exhibit some interesting catalytic properties.

Conclusions

The work contained in this Chapter has shown the somewhat surprising flexibility of twelve-vertex polyhedral systems incorporating two adjacent phenyl substituents. In the parent carbaborane, **10**, the cage carbon carbon distance is longer than that observed in unsubstituted *ortho*-carbaborane, which may be attributed to a certain degree of repulsion between the π -systems of the phenyl ring substituents. In the case of the carbamercuraborane, **11**, where a η^5 -bonded BH vertex has been "replaced" by a *pseudo* σ -bonded Ph_3PHg fragment, the cage carbon atoms are drawn closer together by electronic factors, and the phenyl rings twist synchronously by *ca.* 30° away from the normal position observed in **10A**, presumably to alleviate some substantial strain between the phenyl rings.

In the presence of an η^5 -bonded Cp^*Rh moiety above the open face, the twisting of the phenyl rings, by almost 90° , to accommodate the metal ligand fragment, has caused substantial distortion in the cage, with the carbon atoms forced apart, such that they are essentially non-bonding. This has necessitated the term *pseudo-closo* to describe this novel twelve-vertex carbarhodaborane.

Chapter 5

Experimental

As I went along I rehearsed what I meant to do, for I knew how easy it is, in the excitement of doing something for the first time, to forget the proper way to do it, the separate stages and which follows which. More than once I had known perfectly, in theory, how to do a chemistry experiment, but when confronted by the bunsen burner and the tube and all the rest of it, so different in reality from what they had been in thought, I had lost my head and made a mess of it.

L.P.Hartley, from *The Go-Between*

Introduction

This Chapter details the experimental procedures leading to the results described in Chapters 2 - 4. The Chapter comprises three sections:

Section A covers the synthetic methods employed in the preparation of the compounds discussed, including, where available, spectral and microanalytical data.

Section B describes the crystallographic techniques used in determination of the structures of compounds **2, 3, 4, 5, 6a, 10, 11** and **13**.

Section C describes the general methodology of extended Hückel molecular orbital calculations, and includes tables of atomic co-ordinates of the model compounds studied.

Section A: Synthetic Methods

General Techniques

All reactions were carried out under an atmosphere of dry, oxygen-free nitrogen using standard Schlenk techniques, with some subsequent manipulations in air.

Dichloromethane (CaH_2), tetrahydrofuran (Na wire, benzophenone) and n-hexane (Na wire) were dried and distilled immediately prior to use, diethyl ether was dried with Na wire, other solvents were used as received.

Infra-red spectra were recorded as KBr discs or solutions (referenced against the appropriate solvent) on a Perkin-Elmer 598 spectrophotometer.

N.m.r. spectra were recorded at ambient temperature (unless otherwise specified) on Varian VXR-600 (^{11}B , $^{11}\text{B}(\text{COSY})$, $^{11}\text{B}\{-^1\text{H}\}$, ^1H and $^1\text{H}\{-^{11}\text{B}\}$), Bruker WH-360 (^{11}B , $^{11}\text{B}\{-^1\text{H}\}$ and ^1H) and Bruker WP-200 (^{11}B , $^{11}\text{B}\{-^1\text{H}\}$, ^1H) spectrometers. Techniques for recording $^1\text{H}\{-^{11}\text{B}$ selective} and $^{11}\text{B}(\text{COSY})$ spectra have been published previously.⁸⁸⁻⁹⁰ Chemical shifts are reported relative to external SiMe_4 (^1H) and BF_3OEt_2 (^{11}B), with positive shifts to high frequency.

Starting Materials

The starting materials $\text{Ti}_2[7,8\text{-C}_2\text{B}_9\text{H}_{11}]^{24}$, $\text{Ti}_2[7\text{-Ph-}7,8\text{-C}_2\text{B}_9\text{H}_{10}]$,⁹¹ $\text{Ti}_2[7\text{-CH}_2\text{OCH}_3\text{-}7,8\text{-C}_2\text{B}_9\text{H}_{10}]$,⁹² $\text{Ti}_2[7,8\text{-(CH}_2\text{OCH}_3)_2\text{-}7,8\text{-C}_2\text{B}_9\text{H}_9]$,⁹² $[\text{PPh}_3\text{HgCl}_2]_2$,⁹³ $[(p\text{-cymene})\text{RuCl}_2]_2$ ⁹⁴ and $[\text{Cp}^*\text{RhCl}_2]_2$ ⁷⁵ were either prepared by published methods or by methods developed in the author's research group. All other materials used are commercially available and were used as supplied.

Synthesis of 1-Ph-3-(η^5 -C₉H₇)-3,1,2-closo-CoC₂B₉H₁₀, 2

Co(acac)₃ (0.52g, 1.46mmol) was dissolved in thf, and Tl₂[7-Ph-7,8-closo-C₂B₉H₁₀] (0.90g, 1.46mmol) was suspended in the resulting green solution. The mixture was stirred at room temperature and to it was added, dropwise, a freshly prepared solution of Li[C₉H₇] (1.46mmol) in thf (from equimolar amounts of BuLi and freshly distilled indene at 0°C). The resultant brown product was stirred overnight and filtered. Volatiles were removed from the filtrate *in vacuo*, and the resultant solid dissolved in CH₂Cl₂ (15ml) and filtered. The filtrate was concentrated and chromatographed on silica plates using a hexane/CH₂Cl₂ mixture (1:1) as eluant. Yellow (*R_f* 0.9, no B-H by i.r. spectroscopy) and orange (*R_f* 0.7, B-H containing) bands were collected, the latter obtained as a dark red solid from CH₂Cl₂ and subsequently identified as the target compound, 2. Yield 10%. Calculated (for C₁₇H₂₂B₉Co) : %C 53.4, %H 5.80; Found : %C 53.2, %H 5.72. I.r. ν_{\max} 2540cm⁻¹ (B-H).

N.m.r. Spectra (CD₂Cl₂)

¹¹B-¹H): δ 8.25(1B), 2.34(1B), -2.73[2B(coinident)], -3.62(1B), -6.32(1B), -11.00(1B), -16.74(1B) and -17.72(1B) p.p.m. The ¹H n.m.r. chemical shifts have been presented and discussed in Chapter 2.

Synthesis of 1-CH₂OCH₃-3-(η^5 -C₉H₇)-3,1,2-closo-CoC₂B₉H₁₀, 3

Similarly, Co(acac)₃, Tl₂[7-CH₂OCH₃-7,8-C₂B₉H₁₀] and Li[C₉H₇] (1.72mmol of each) were reacted together to afford, after work-up involving preparative tlc, the target compound, 3, as dark red microcrystals. Yield 5%. I.r. ν_{\max} 2530 cm⁻¹ (B-H).

N.m.r. Spectra (CD₂Cl₂)

¹¹B-¹H): δ 8.69(1B), 1.68(1B), -2.65(1B), -3.54(1B), -4.58(1B), -7.00(1B), -12.46(1B), -17.58(1B) and -19.94(1B) p.p.m.

¹H: δ 2.52 [s, 1H, H(2)], 3.53 (s, 3H, CH₃-O-), 3.61 and 3.72 (AB, ²J_{HH} 11Hz, 2H, -CH₂-O-), 5.66 [d of d (app. t), ³J_{HH} 3Hz, 3Hz, 1H, H(32)], 6.39 [d, ³J_{HH} 3Hz, 2H(coinicident), H(31,32)], and 7.44-7.61 [m, 4H, H(35-38)] p.p.m.

Synthesis of 1,2-(CH₂OCH₃)₂-3-(η⁵-C₉H₇)-3,1,2-closo-CoC₂B₉H₉, 4

Co(acac)₃, Tl₂[7,8-(CH₂OCH₃)₂-7,8-C₂B₉H₉] and Li[C₉H₇] (0.86mmol of each) were reacted together as described for the two previous reactions, except that this reaction was complete after 2.5 hours, and afforded the target compound, 4, after work-up involving preparative tlc. Yield 12%. I.r. ν_{max} 2540cm⁻¹ (B-H).

N.m.r. Spectra (CD₂Cl₂)

¹¹B-¹H): δ 8.93(1B), 1.86(1B), -1.65(2B), -5.12(2B), -14.19(2B) and -17.89(1B) p.p.m.

¹H: δ 3.17 and 3.39 (AB, ²J_{HH} 12Hz, 4H, -CH₂-O-), 3.34 (s, 6H, CH₃-O-), 5.70 [t, ³J_{HH} 3Hz, 1H, H(32)], 6.40 [d, ³J_{HH} 12Hz, 2H, H(31,32)] and 7.51-7.58 [m, 4H, H(35-38)] p.p.m.

Synthesis of 3-(η⁵-C₁₃H₉)-3,1,2-closo-CoC₂B₉H₁₁, 5

A thf solution of Li[C₁₃H₉] (1.079mmol) (made from equimolar amounts of ^tBuLi and C₁₃H₁₀ at -0°C) was added dropwise to a cooled (0°), stirred, suspension of Tl₂[7,8-C₂B₉H₁₁] (0.583g, 1.079mmol) and Co(acac)₃ (0.384g, 1.079mmol) in thf (20ml). After three hours the mixture was filtered and the filtrate evaporated *in vacuo*. CH₂Cl₂ was added to the resulting brown solid, the product filtered and the filtrate concentrated to a small volume. Tlc (CH₂Cl₂:hexane, 1:1) on silica plates afforded 5

as an amber band (R_f 0.45) in low yield (<5%). Dark red needles were grown by diffusion of hexane into a CH_2Cl_2 solution at -30°C , and an X-ray structure determination carried out, details of which are found in Section B of this chapter.

Synthesis of " $[(\text{C}_9\text{H}_7)\text{RhCl}_2]_2$ "

Typically, $\text{RhCl}_3 \cdot 3\text{H}_2\text{O}$ (2g, 7.6mmol) and freshly distilled indene (3.5ml, 30.1mmol) were refluxed in methanol (50ml) for 15 hours, during which time a brown solid was deposited. This was isolated by filtration, washed successively with methanol (2 x 10ml) and ether (2 x 10ml) and dried *in vacuo*. Further reflux (15hr) of the original filtrate afforded a second crop of material which was similarly recovered. Combined yield 0.95g, 43%. Calculated (for $\text{C}_{18}\text{H}_{14}\text{Cl}_4\text{Rh}_2$): %C 37.4, %H 2.42; Found: %C 36.7 %H 2.74. I.r. ν_{max} 3100(br), 3050(br, sh), 2960(m), 2930(w) (all C-H), 1515(w), 1450(m), 1385(m), 1335(s), 1260(w), 885(m), 835(m, br), 750(sh), 745(s), 735(sh), 570(m), 490(m), 340(sh), 335(sh), 330(w), 325(m), 240(w) and 230(w) cm^{-1} .

Reaction between " $[(\text{C}_9\text{H}_7)\text{RhCl}_2]_2$ " and $\text{Ti}_2[7,8\text{-C}_2\text{B}_9\text{H}_{11}]$

CH_2Cl_2 (10ml) was added to a solid mixture of " $[(\text{C}_9\text{H}_7)\text{RhCl}_2]_2$ " (0.101g, 0.175mmol) and $\text{Ti}_2[7,8\text{-C}_2\text{B}_9\text{H}_{11}]$ (0.203g, 0.35mmol) at -196°C . The mixture was allowed to warm to room temperature with stirring. After 2.5 hours the mixture was filtered under N_2 and the brown filtrate evaporated *in vacuo* to give a dark brown solid. Preparative tlc (CH_2Cl_2 :hexane, 3:1) afforded three main bands, yellow (R_f ca. 0.8), apricot (R_f ca. 0.6) and orange (R_f ca. 0.5), each of which was collected and recrystallised (CH_2Cl_2 :hexane, 1:3, -30°C) to afford microcrystals of the rhodium carbaborane compounds **6a**, **6b** and **6c** respectively.

3-((C₉H₆)Rh(C₉H₇))-8-((C₉H₆)Rh(C₉H₇))-3,1,2-closo-RhC₂B₉H₁₁, 6a

Yield 4%. Calculated (for C₂₂H₃₄B₁₈Rh₂): %C 37.81, %H 4.90; Found: %C 38.2, %H 5.09. I.r. ν_{\max} 2555cm⁻¹ (B-H).

N.m.r. Spectra (CD₂Cl₂)

¹H: δ 7.20 [m, 4H, H(25-28)], 6.50 [m, 4H, H(15-18)], 5.92 [d, 2H, H(21,23)], 5.84 [s, 2H, H(11,13)], 5.79 [t of d, ³J_{HH} 3Hz, ⁴J_{HH} 1Hz, 1H, H(22)], 3.80 [s, 2H, CH(1,2)], 3.71 [s, 2H, CH(1P,2P)]

¹¹B-¹H: Table 3.1 in Chapter 3 contains chemical shifts and assignments *via* ¹¹B-¹¹B COSY spectroscopy.

10-((C₉H₆)Rh(C₉H₇))-3,1,2-nido-C₂B₉H₁₁.0.5CH₂Cl₂, 6b

Yield 8%. Calculated (for C_{20.5}H₂₅B₉ClRh): %C 48.6, %H 4.97; Found: %C 49.3, %H 4.93. I.r. ν_{\max} 2525cm⁻¹ (B-H).

N.m.r. Spectra (CD₂Cl₂)

¹H: δ 7.23 (m, 2H) and 7.18 (m, 2H) [H(25-28)], 6.55 (m, 2H) and 6.58 (m, 2H) [H(15-18)], 6.01 [d, ³J_{HH} 3Hz, 2H, H(21,23)], 5.92 [t, ³J_{HH} 3Hz, 1H, H(22)], 5.91 [s, 2H, H(11,13)], 2.10 [s, 2H, H(7,8)], -1.54 [q, 1H, H(10_{endo})] p.p.m.

¹¹B-¹H: δ -9.60 [2B, B(9,11)], -13.77 [2B, B(5,6)], -17.81 [1B, B(3)], -20.79 [2B, B(2,4)], -26.39 [1B, B(10)], -37.08 [1B, B(1)] p.p.m.

¹H-¹¹B_{selective}: δ 2.21 [s, 2H, H(9,11)], 1.56 [s, 2H, H(5,6)], 1.85 [s, 1H, H(3)], 1.40 [s, 2H, H(2,4)], 0.68 [s, 1H, H(1)] p.p.m.

9-((C₉H₆)Rh(C₉H₇))-7,8-nido-C₂B₉H₁₁.0.5CH₂Cl₂, 6c

Yield 6%. Calculated (for C_{20.5}H₂₅B₉ClRh): %C 48.6, %H 4.97; Found: %C 48.6, %H 5.05. I.r. ν_{\max} 2520 cm⁻¹ (B-H).

N.m.r. Spectra (CD₂Cl₂)

¹H: δ 7.22 [m, 4H, H(25-28)], 6.65 [m, 4H, H(15-18)], 6.07 [s, 1H, H(11 or 13)], 6.01 [d, ³J_{HH} 3Hz, 2H, H(21 or 23)], 6.00 [d, ³J_{HH} 4Hz, 1H, H(23 or 21)], 5.97 [s, 1H, H(11 or 13)], 5.82 [d of d, ³J_{HH} 4Hz, 3Hz, 1H, H(22)], 2.45 [s, 1H, H(7 or 8)], 2.10 [s, 1H, H(8 or 7)], -2.60 [v br, 1H, H(10_{endo})] p.p.m.

¹¹B-({¹H}): δ -4.14 [1B, B(9)], -5.10 [1B, B(11)], -13.74 (1B), -16.16 (1B), -17.16 (1B), -20.82 (1B), -24.86 (1B), -29.45 [(1B, B(10))], -35.15 (1B) p.p.m.

¹H-({¹¹B_{selective}): δ 2.16 [s, 1H, H(11)], 1.90 (s, 1H), 1.75 (s, 1H), 1.86 (s, 1H), 1.16 (s, 1H), 0.90 (s, 1H), 0.90 (s, 1H), 0.59 [s, 1H, H(10_{exo})], 0.80 (s, 1H) p.p.m.

Reaction between "[C₉H₇)RhCl₂]₂" and Ti₂[7-(CH₂OCH₃)-7,8-C₂B₉H₁₀]

Similarly, "[C₉H₇)RhCl₂]₂" (0.100g, 0.173mmol) and Ti₂[7-(CH₂OCH₃)-7,8-C₂B₉H₁₀] (0.202g, 0.346mmol) were reacted in CH₂Cl₂ (15ml). After warming to room temperature and stirring for 40 mins filtration afforded a dark green solution. Preparative tlc (CH₂Cl₂:thf:hexane, 3:1:1) yielded an orange band (R_f 0.85), subsequently recovered to give microcrystals of 7-CH₂OCH₃-10-((C₉H₆)Rh(C₉H₇))-7,8-*nido*-C₂B₉H₁₀-CH₂Cl₂, 7. Yield 5%. Calculated (for C₂₃H₃₁B₉Cl₂ORh): %C 46.8, %H 5.18; Found: %C 46.9, %H 4.96. I.r. ν_{max} 2540cm⁻¹ (B-H).

N.m.r. Spectra

¹H (CD₂Cl₂): δ 7.23 (m, 2H) and 7.18 (m, 2H), [H(25-28)], 6.66 (m, 2H) and 6.58 (m, 2H) [H(15-18)], 6.01 (d, ³J_{HH} 3Hz, 1H) and 6.00 (d, ³J_{HH} 3Hz, 1H) [H(21,23)], 5.92 (s, 2H, H(11,13), coincident), 3.60 and 3.26 (AB, ²J_{HH} 10Hz, 2H, -CH₂-O-), 3.32 (s, 3H, -O-CH₃-O-), 2.14 [s, 1H, H(8)], -1.40 [br q, 1H, H(10)] p.p.m.

¹H ((CD₃)₂CO) (region between δ 6.4 and 5.8 p.p.m. only): δ 6.25 (d, ³J_{HH} 2Hz, 1H) and 6.24 (d, ³J_{HH} 3Hz, 1H) [H(21,23)], 5.95 (s, 2H, H(11,13) coincident), 5.93 [d

of d, $^3J_{\text{HH}}$ 3Hz, 2Hz, 1H, H(22)] p.p.m.

^{11}B - $\{^1\text{H}\}$ (CD_2Cl_2): δ -9.20 (1B), -10.02 (1B), -13.89 (1B), -14.85 (1B), -15.50 (1B), -17.64 (1B), -21.40 (1B), -26.36 (1B), -36.91 (1B) p.p.m.

Reaction between " $[(\text{C}_9\text{H}_7)\text{RhCl}_2]_2$ " and $\text{Ti}_2[7\text{-Ph-7,8-}\text{C}_2\text{B}_9\text{H}_{10}]$

Similarly, " $[(\text{C}_9\text{H}_7)\text{RhCl}_2]_2$ " (0.104g, 0.18mmol) and $\text{Ti}_2[7\text{-Ph-7,8-}\text{C}_2\text{B}_9\text{H}_{10}]$ (0.21g, 0.36mmol) were reacted in CH_2Cl_2 (15ml). After warming to room temperature and stirring for 15hrs filtration afforded an olive-green solution. Preparative tlc (CH_2Cl_2 :hexane, 4:1) gave rise to olive minor (R_f ca. 0.95) and orange major (R_f ca. 0.85) bands. The former was crystallised by slow evaporation of a CH_2Cl_2 solution to afford small crystals, subsequently shown by unit cell and space group determination to be 1-Ph-3-(C_9H_7)-3,1,2-*closo*- $\text{RhC}_2\text{B}_9\text{H}_{10}$, **8a**, by analogy with the previously characterised cobalt analogue, **2** (see Section B). The latter compound was recovered as a solid, and was characterised as 7-Ph-9/11- $\{(\text{C}_9\text{H}_6)\text{Rh}(\text{C}_9\text{H}_7)\}$ -7,8-*nido*- $\text{C}_2\text{B}_9\text{H}_{10}$, **8b**. Yield 2%. I.r. ν_{max} 2535 cm^{-1} (B-H).

N.m.r. Spectra (CD_2Cl_2) of **8b**

^1H : δ 7.33 [m, 2H, H(72,76)], 7.18 (m, 6H, H(73, 75, 25-28), coincident), 7.07 [m, 1H, H(74)], 6.65 [m, 4H, H(15-18)], 6.15 [s, 1H, H(11 or 13)], 5.99 [d, $^3J_{\text{HH}}$ 3Hz, 1H, H(21 or 23)], 5.96 [s, 1H, H(13 or 11)], 5.95 [d, $^3J_{\text{HH}}$ 3Hz, 1H, H(23 or 21)], 5.84 [d of d (app t), $^3J_{\text{HH}}$ 3Hz, 3Hz, 1H, H(22)], 2.79 [s, 1H, H(8)], -2.30 [v br, 1H, H(10_{endo})] p.p.m.

^{11}B - $\{^1\text{H}\}$: δ -4.29 (2B, coincident), -11.79 (1B), -12.50 (1B), -13.42 (1B), -20.74 (1B), -25.36 (1B), -28.39 (1B), -32.76 (1B) p.p.m.

Reaction between " $[(C_9H_7)RhCl_2]_2$ " and $Tl_2[7,8-(CH_2OCH_3)_2-7,8-C_2B_9H_9]$

Similarly, " $[(C_9H_7)RhCl_2]_2$ " (0.18g, 0.31mmol) and $Tl_2[7,8-(CH_2OCH_3)_2-7,8-C_2B_9H_9]$ (0.39g, 0.62mmol) were allowed to warm together with stirring in CH_2Cl_2 (20ml). After 15hrs the products were filtered, and the filtrate evaporated *in vacuo* to yield a purple solid. Preparative tlc (CH_2Cl_2) afforded 1,2- $(CH_2OCH_3)_2$ -3- (C_9H_7) -3,1,2-*closo*- $RhC_2B_9H_9$, 9, as a yellow solid. Yield 1% I.r. ν_{max} 2530 cm^{-1} (B-H).

N.m.r. Spectra ($CDCl_3$)

1H : δ 7.36 [app s, 4H, H(35-38)], 6.46 [d, $^3J_{HH}$ 3Hz, 2H, H(31,33)], 5.88 [t of d, $^3J_{HH}$ 3Hz, $^xJ_{HH}$ 1.5Hz, 1H, H(32)], 3.22 (s, 6H, -O- CH_3), 2.89 and 2.86 (AB, $^2J_{HH}$ 12Hz, 4H, - CH_2 -O) p.p.m.

^{11}B - $\{^1H\}$: δ 10.72 (1B), 5.06 (1B), -0.10 (2B), -6.56 (2B), -14.21 (2B), -19.85 (1B) p.p.m.

Reaction of " $[(C_9H_7)RhCl_2]_2$ " with $C_6H_{11}NC$

A solution of cyclohexyl-isocyanide, $C_6H_{11}NC$, (4.3mmol) in CH_2Cl_2 was added dropwise to a stirred suspension of " $[(C_9H_7)RhCl_2]_2$ " (0.1g, 0.174mmol) in CH_2Cl_2 (25ml). After two hours the dark brown filtrate was evaporated to yield an oily brown solid. Column chromatography [florisil (100-200 mesh) column, thf eluant] afforded a mobile amber band, which was collected and solvent removed *in vacuo* to give a brown solid. The 1H n.m.r. spectrum of this product could not be interpreted, and in any case did not contain resonances in the aromatic region, indicating the absence of an indenyl ligand. Thus it was concluded that the reaction did not proceed in an analogous manner to that of $[CpRhCl_2]_n$ with cyclohexyl isocyanide, (which gave an almost quantitative yield of $CpRhC_6H_{11}Cl_2$),⁷⁸ but rather gave a mixture of unidentified products which were not easily separated.

Reaction between 1,2,3-trimethylindene and $\text{RhCl}_3 \cdot 3\text{H}_2\text{O}$

A mixture of 1,2,3-trimethylindene, $\text{C}_{12}\text{H}_{13}$, (0.72g, 4.59mmol), prepared by a previously described method,⁸⁰ and $\text{RhCl}_3 \cdot 3\text{H}_2\text{O}$ (0.3g, 1.14mmol) was refluxed in methanol (15ml) for 60 hrs. The solution was filtered and the filtrate evaporated to yield a dry reddish-brown solid. Microanalysis figures indicated a very low hydrocarbon content, *i.e.* inconsistent with the formulation for the target compound, trimethylindenyl rhodium dichloride.

Synthesis of 1,2- Ph_2 -1,2-*closo*- $\text{C}_2\text{B}_{10}\text{H}_{10}$, 10

The following method is a modification of procedure published by M.M. Fein and co-workers.⁹⁵ Decaborane (3g, 24.6mmol) was dissolved in benzene (20ml), and $(\text{CH}_3)_2\text{S}$ (5ml) added, following which the mixture was refluxed for 6 hrs. After cooling, and addition of $\text{PhC}=\text{CPh}$ (4.51g, 25.3mmol) the mixture was stirred for 30 mins at room temperature, and then refluxed for a further 15 hrs. Solvent was removed *in vacuo*, resulting in a thick yellow oil. On addition of methanol (20ml), a bright yellow solid precipitated, and the suspension was filtered after 1 hour. The filtrate was stirred for another 4hrs, the volume of methanol then reduced to *ca.* 5ml, during which time a white precipitate of pure diphenylcarbaborane formed. This was filtered, washed with small amounts of methanol, and dried. Further diphenylcarbaborane was isolated from the yellow precipitate as follows: hot hexane was added to the latter, with vigorous stirring, and the mixture filtered while still warm. On evaporation of solvent from the filtrate, a pale yellow solid was obtained, which, after recrystallisation (acetone/water) afforded colourless crystals of pure 1,2- Ph_2 -1,2-*closo*- $\text{C}_2\text{B}_{10}\text{H}_{10}$. Overall yield 2.38g (33%). Calculated (for $\text{C}_{14}\text{H}_{20}\text{B}_{10}$): %C 56.76, %H 6.76; Found: %C 56.00, %H 6.89.

N.m.r. Spectrum (CDCl_3)

^{11}B - $\{^1\text{H}\}$: δ -1.73 (2B), -8.45 (4B), -9.72 (4B) p.p.m.

Synthesis of $\text{Ti}_2[7,8\text{-Ph}_2\text{-}7,8\text{-C}_2\text{B}_9\text{H}_9]$

1,2- Ph_2 -1,2-*closo*- $\text{C}_2\text{H}_{10}\text{H}_{10}$ (0.91g, 3.07mmol) and KOH (1.07g, 19.1mmol) were stirred in ethanol for 45 mins, and the mixture then refluxed for 6 hrs. After the solution cooled, solvent was removed *in vacuo*, and the resulting white solid dissolved in degassed water (15ml). The solution was filtered, and an aqueous solution of thallium acetate (3g, 12mmol) added to the filtrate, which caused immediate precipitation of a bright yellow solid. This was filtered, washed with water, ethanol and diethyl ether, and dried under vacuum. Yield 1.5g, 64% Calculated (for $\text{C}_{14}\text{H}_{19}\text{B}_9\text{Ti}_2$): %C 24.24, %H 2.80; Found: %C 24.9, %H 3.31.

Synthesis of 7,8- Ph_2 -10-*endo*- PPh_3Hg -7,8-*nido*- $\text{C}_2\text{B}_9\text{H}_9$, 11

Degassed methylene chloride (15ml) was added to a mixture of $\text{Ti}_2[7,8\text{-Ph}_2\text{-}7,8\text{-C}_2\text{B}_9\text{H}_9]$ (0.349g, 0.504mmol) and $[\text{PPh}_3\text{HgCl}_2]_2$ (0.269g, 0.252mmol) at -196°C . The mixture was warmed to room temperature with stirring (in a foil covered vessel), and after 20 mins was filtered to afford a pale yellow solution. Solvent was reduced to 2 ml, and a vast excess of hexane added. A creamy white flocculate precipitated, which was separated from a green oil, and dried *in vacuo*. This was dissolved in methylene chloride, and slow evaporation of this solution afforded very pale yellow crystals, which were identified as the target compound, 11. Yield 10%. I.r. ν_{max} 2540 cm^{-1} (B-H).

N.m.r. Spectrum (CD_2Cl_2)

^{11}B - $\{^1\text{H}\}$: δ -11.22 (5B, coincident), -13.67 (2B), -23.70 (1B), -28.87(1B).

Synthesis of 1,2- Ph_2 -3-(*p*-cymene)-3,1,2-*closo*- $\text{RuC}_2\text{B}_9\text{H}_9$, 12

Methylene chloride (20ml) was added to a mixture of $[\text{C}_{10}\text{H}_{14}\text{RuCl}_2]_2$ (0.2g, 0.33mmol) and $\text{Ti}_2[7,8\text{-Ph}_2\text{-}7,8\text{-C}_2\text{B}_9\text{H}_9]$ (0.453, 0.66mmol), and the products stirred at room temperature for 15 hrs. Filtration yielded a deep red solution, evaporation of

solvent from which resulted in a reddish-brown solid. Preparative tlc (methylene chloride:hexane, 1:1 eluant) afforded one major orange band (R_f 0.85), which was collected and identified as the target compound, **12**, by analysis of spectral data. Yield 15%. I.r. ν_{\max} 2580 cm^{-1} .

N.m.r. Spectra (CDCl_3)

^{11}B - $\{^1\text{H}\}$: δ 30.32 (1B), 15.58 (2B), 12.57 (1B), -0.45 (2B), -1.41 (2B), -20.13 (1B) p.p.m.

^1H : δ 7.59 [d, $^3J_{\text{HH}}$ 7Hz, 4H, H(12,16,22,26), (*ortho*)], 7.33 [d of d, app t, $^3J_{\text{HH}}$ 7Hz 7Hz, 4H, H(13,15,23,25), (*meta*)], 7.19 [t, $^3J_{\text{HH}}$ 7Hz, 2H, H(14,24), (*para*)], 5.38 and 5.13 [AB, $^3J_{\text{HH}}$ 3.5Hz, 4H, ($\text{H}_{\text{p-cymene}}$)], 2.05 [septet, $^3J_{\text{HH}}$ 7Hz, 1H, $\text{CH}(\text{CH}_3)$], 1.54 (s, 3H, CH_3), 1.02 [d, 6H, $\text{CH}(\text{CH}_3)_2$], p.p.m.

Synthesis of **1,2-Ph₂-3-Cp^{*}-3,1,2-pseudo-closo-RhC₂B₉H₉**

Methylene chloride (25ml) was added to a mixture of $[\text{Cp}^*\text{RhCl}_2]_2$ (0.4g, 0.65mmol) and $\text{Ti}_2[7,8\text{-Ph}_2\text{-7,8-C}_2\text{B}_9\text{H}_{11}]$ (0.90g, 1.30mmol), and the products stirred for 15 hrs. Filtration yielded a dark red solution, evaporation of which afforded a deep red solution. Preparative tlc (CH_2Cl_2 :hexane, 2:3) afforded one major dark orange band (R_f 0.8-0.9), which was collected and identified as **13**. Yield 8%. I.r. ν_{\max} 2570 cm^{-1} . Calculated (for $\text{C}_{24}\text{H}_{34}\text{B}_9\text{Rh}$): %C 55.15, %H 6.56; Found: %C 54.4, %H 6.47.

N.m.r. Spectra (CDCl_3)

^{11}B - $\{^1\text{H}\}$: δ 33.06 (1B), 12.93 (1B), 10.26 (2B), 4.04 (2B), -1.15 (2B) and -17.97 (1B) p.p.m.

^1H : δ 7.52 [d, $^3J_{\text{HH}}$ 4Hz, 4H, H(12,16,21,26) (*ortho*)] 7.30 [d of d, app t, $^3J_{\text{HH}}$ 4Hz, 4Hz, 4H, H(13,15,23,25) (*meta*)] 7.21 [t, $^3J_{\text{HH}}$ 4Hz, 2H, H(14,24) (*para*)], 1.29 [s, 15H, $(\text{CH}_3)_5\text{C}_5$]

Section B: Crystallographic Techniques

This section describes the experimental procedures involved in data collection and processing, and structure solution and refinement for each of the structures presented in Chapters 2 - 4. All data were collected on an Enraf-Nonius CAD4 diffractometer, fitted with a ULT-1 low-temperature device. Diffraction quality crystals of compounds 2-6a, 10, 11 and 13 were grown as described in the main body of the work.

Data were collected using graphite monochromated Mo- K_{α} X-radiation, $\lambda = 0.71069\text{\AA}$, by ω - 2θ scans in 96 steps, with ω scan width $0.8 + 0.34\tan\theta$. Data were corrected for Lorentz and polarisation effects, and (where necessary) for decay during data collection (*CADABS*⁹⁶). Heavy atoms were located by automatic direct methods (*SHELX86*⁹⁷) or by inspection of a Patterson map (*SHELX76*⁹⁸); see individual complexes. Subsequent atom location was by ΔF syntheses and iterative full-matrix least-squares refinement.⁹⁸ Where appropriate, cage C atoms were identified by a combination of refined (as B) isotropic thermal parameters and interatomic distances. Scattering factors for C,H,B,O,P and Cl were those inlaid in the programs. Those for Co, Rh, Hg, Cu and Ru were from *International Tables for X-ray Crystallography*.⁹⁹

After isotropic convergence, data were corrected empirically for absorption.¹⁰⁰ Thereafter, non-hydrogen atoms were generally allowed anisotropic thermal motion. Towards the end of the refinement process data were weighted according to $w^{-1} = [\sigma^2(F) + g(F^2)]$, where g is a variable. Each structure was then refined, usually by full-matrix least-squares, to convergence.

Geometrical calculations were performed using *CALC*¹⁰¹ and the molecular drawing facility used was *EASYORTEP*¹⁰², a modification of *ORTEP-II*.¹⁰³

The isotropic thermal parameter takes the form $\exp[-8\pi^2 U(\sin^2\Theta)/\lambda^2]$.

For anisotropic thermal parameters

$$U_{ij} = \exp[-2\pi^2(U_{11}a^2h^2 + U_{22}b^2k^2 + U_{33}c^2l^2 + 2U_{23}b^*c^*kl + 2U_{13}a^*c^*hl + 2U_{12}a^*b^*hk)]$$

The equivalent isotropic thermal parameter is defined as

$$U_{eq} = [\sum_i \sum_j U_{ij} a_i^* a_j^* a_i a_j] / 3$$

1-Ph-3-(η^5 -C₉H₇)-3,1,2-closo-CoC₂B₉H₁₀, 2

Crystal Data

C₁₇H₂₂B₉Co, $M = 382.59$, monoclinic, space group $C2/c$ $a = 17.732(11)$, $b = 13.186(3)$, $c = 17.739(7)\text{\AA}$, $\beta = 117.00(4)^\circ$, $V = 3695.0\text{\AA}^3$, from least-squares refinement of 25 centred reflections ($12 < \theta < 16^\circ$) at $185 \pm 1\text{K}$, $Z = 8$, $D_c = 1.375\text{ gcm}^{-3}$, $\mu(\text{Mo-K}\alpha) = 9.22\text{ cm}^{-1}$, $F(000) = 1568$.

Data Collection and Processing

Variable scan speeds between 0.79 - $2.35^\circ\text{min}^{-1}$. 2768 independent reflections measured ($1 < \theta < 25^\circ$, $+h +k \pm l$), of which 2741 had $F > 2.0\sigma(F)$. Data was corrected for slight crystal decay (8%) over the period of data collection (99 hrs).

Structure Solution and Refinement

Co position from Patterson synthesis; B, C and H_{cage} from full matrix least-squares refinement/ ΔF syntheses. Cage H atoms refined positionally, subject to a single X-H distance of $1.10(2)\text{\AA}$, indenyl and phenyl hydrogens set in fixed positions (C-H 1.08\AA). Empirical absorption correction applied after isotropic convergence; thereafter all non-H atoms allowed anisotropic thermal motion, H atoms refined with a common thermal parameter ($U_{\text{H}} = 0.0434(23)\text{\AA}^2$) at convergence. $g = 0.000303$. $R = 0.0434(23)$, $R_w = 0.0525$, $S = 1.293$. Max. and min. residues in final ΔF map 0.20 and $-0.20\text{e}\text{\AA}^{-3}$.

1-CH₂OCH₃-3-(η^5 -C₉H₇)-3,1,2-closo-CoC₂B₉H₁₀, 3

Crystal Data

C₁₃H₂₂B₉CoO, M = 350.54, monoclinic, space group $P2_1/c$, $a = 12.382(3)$, $b = 8.914(5)$, $c = 15.523(9)$, $\beta = 103.60(4)^\circ$, $V = 1665\text{\AA}^3$, from least-squares refinement of 25 centred reflections ($14 < \theta < 16^\circ$) at $185 \pm 1\text{K}$, $Z = 4$, $D_c = 1.398\text{ gcm}^{-3}$, $\mu(\text{Mo-K}\alpha) = 10.21\text{ cm}^{-1}$, $F(000) = 720$.

Data Collection and Processing

Variable scan speeds between 0.79 and $2.35^\circ\text{min}^{-1}$. 2654 independent reflections measured ($1 < \theta < 25^\circ$, $+h +k \pm l$), yielding 2651 with $F > 2.0\sigma(F)$. No crystal movement or decay noted.

Structure Solution and Refinement

Co position from Patterson synthesis; B, C, O, and H atoms from full matrix least-squares refinement/ ΔF syntheses. All hydrogen atoms fully refined. Empirical absorption correction applied after isotropic convergence; thereafter all non-H atoms allowed anisotropic thermal motion, H atoms having isotropic thermal parameters in the range $U_H = 0.021(5)\text{--}0.102(13)\text{\AA}^2$ at convergence. $g = 0.002296$. $R = 0.0269$, $R_w = 0.0428$, $S = 0.832$. Max. and min. residues in final ΔF map 0.24 and $-0.47\text{e}\text{\AA}^{-3}$.

1,2-CH₂OCH₃-3-(η^5 -C₉H₇)-3,1,2-closo-CoC₂B₉H₉, 4

Crystal Data

C₁₅H₂₆B₉CoO₂, $M = 394.58$, monoclinic, space group $P2_1/n$, $a = 10.927(4)$, $b = 14.743(4)$, $c = 11.789(6)$, $\beta = 90.61(4)^\circ$, $V = 1899.0\text{\AA}^3$, from least-squares refinement of 25 centred reflections ($14 < \theta < 16$) at $185 \pm 1\text{K}$, $Z = 4$, $D_c = 1.380\text{ gcm}^{-3}$, $\mu(\text{Mo-K}\alpha) = 9.06\text{ cm}^{-1}$, $F(000) = 816$.

Data Collection and Processing

Variable scan speeds between $0.82\text{-}2.06^\circ\text{min}^{-1}$. 3094 independent reflections measured ($1 < \theta < 25$, $+h$, $+k$, $\pm l$), yielding 3087 with $F = 2.0\sigma(F)$. No crystal movement or decay noted.

Structure Solution and Refinement

Co position from direct methods; B, C, O, H atoms from iterative full-matrix least-squares refinement/ ΔF synthesis. Empirical absorption correction applied after isotropic convergence. All non-H atoms allowed anisotropic thermal motion. All H atoms fully refined with thermal parameters in the range $U_H = 0.014(5)\text{-}0.078(11)\text{\AA}^2$ at convergence. $g = 0.001416$. $R = 0.0290$, $R_w = 0.0488$, $S = 1.169$. Max. and min. residues in final ΔF map 0.29 and $-1.29\text{e}\text{\AA}^{-3}$.

3-(η^5 -C₁₃H₉)-3,1,2-closo-CoC₂B₉H₁₁, 5

Crystal Data

C₁₅H₂₀B₉Co, $M = 356.55$, orthorhombic, space group $P2_12_12_1$, $a = 8.759(3)$, $b = 13.037(3)$, $c = 15.366(4)\text{\AA}$, $V = 1754.7(8)\text{\AA}^3$, from least-squares refinement of 25 centered reflections ($5 < \theta < 12$) at $291 \pm 1\text{K}$, $Z = 4$, $D_c = 1.349\text{ g cm}^{-3}$, $\mu(\text{Mo-K}\alpha) = 9.66\text{ cm}^{-1}$, $F(000) = 728$.

Data Collection and Processing

Variable scan speeds between 0.824 - $1.83^\circ\text{min}^{-1}$. 3050 independent reflections measured ($1 < \theta < 25^\circ$, $+h$, $+k$, $\pm l$), of which 2182 had $F > 2.0\sigma(F)$. No crystal movement or decay noted.

Structure Solution and Refinement

Co position from direct methods; C, B, H_{cage} atoms from iterative full-matrix least squares refinement/ ΔF syntheses. Empirical absorption correction applied after isotropic convergence. Equivalent reflections ($h0l$ and $h0\bar{l}$; $0kl$ and $0k\bar{l}$; and $00l$ and $00\bar{l}$) merged ($R_{\text{merge}} = 0.032$) to afford a final set of 1930 reflections. All non-H atoms refined with anisotropic thermal parameters. Cage H atoms allowed positional refinement subject to a single X-H distance of $1.05(1)\text{\AA}$, fluorenyl H atoms set in idealized positions with C-H 1.08\AA . Cage and fluorenyl H atoms refined with separate group thermal parameters, $0.039(8)$ and $0.103(12)\text{\AA}^2$ respectively at convergence. $g = 0.000473$. $R = 0.0793$, $R_w = 0.0605$, $S = 1.16$. Max. and min. residues in final ΔF map 0.86 and $-1.36\text{e}\text{\AA}^{-3}$.

3-(C₂B₉H₁₁)-8-((C₉H₆)Rh(C₉H₇))-3,1,2-closo-RhC₂B₉H₁₁, 6a

Crystal Data

C₂₂H₃₄B₁₈Rh₂, $M = 698.91$, orthorhombic, space group *Pbca*, $a = 12.296(8)$, $b = 19.69(4)$, $c = 29.030(18)\text{\AA}$, $V = 7028.8\text{\AA}^3$, from least-squares refinement of 25 centred reflections ($2 < \theta < 11^\circ$) at $185 \pm 1\text{K}$, $Z = 8$, $D_c = 1.321\text{ gcm}^{-3}$, $\mu(\text{Mo-K}\alpha) = 9.38\text{ cm}^{-1}$, $F(000) = 2768$. (D_c , μ and $F(000)$ assume no solvate.)

Data Collection and Processing

Variable scan speeds between $0.79\text{--}2.35^\circ\text{min}^{-1}$. 4140 independent reflections measured ($1 < \theta < 15^\circ$, $\pm h \pm k \pm l$), of which 1759 had $F > 2.0\sigma$. No crystal movement or decay was noted.

Structure Solution and Refinement

Rh positions from direct methods; B and C from full matrix least-squares refinement/ ΔF syntheses. Cage C atoms, C(1) and C(2), were identified by combination of refined (as B) isotropic thermal parameters and interatomic distances, and agree with the conclusions from the n.m.r. studies that this cage is substituted at B(8). C(1') was identified by its refined (as B) isotropic thermal parameter, but definitive location of the other cage carbon atom was not possible, and sites (2') and (4') were assigned occupancies of 5.5e ((B + C)/2). Indenyl H atoms were set in calculated positions, riding on their respective C atoms, and given an invariant U value of 0.07\AA^2 . Cage H atoms were not located. Following isotropic convergence, an empirical absorption correction was applied, and data were then merged to afford 985 unique reflections, $R_{\text{merge}} = 0.038$. Rhodium atoms were allowed with anisotropic thermal motion, and in the final stages data were weighted with $g = 0.00168$. 6a crystallises with badly disordered solvate molecules, the best model of which involved 8 carbon atoms with fixed U of 0.04\AA^2 and a (common) refined population parameter of 0.614(24). Even this model does not represent a chemically recognisable

fragment of either CH_2Cl_2 or hexane. $R = 0.1072$, $R_w = 0.1210$, $S = 1.319$. Max. and min. residues in final ΔF map 1.10 and $-0.81\text{e}\text{\AA}^{-3}$.

1-Ph-3-(C₉H₇)-3,1,2-closo-RhC₂B₉H₁₀, 8a

Crystal Data

$\text{C}_{17}\text{H}_{22}\text{B}_9\text{Rh}$, $M = 426.56$, monoclinic, space group $C2/c$, $a = 17.710(16)$, $b = 13.214(8)$, $c = 18.81(3)\text{\AA}$, $\beta = 119.86(10)^\circ$, $V = 3817.5\text{\AA}^3$, from least-squares refinement of 25 centred reflections ($3 < \theta < 8^\circ$) at $291 \pm 1\text{K}$, $Z = 8$, $D_c = 1.484\text{ gcm}^{-3}$, $\mu(\text{Mo-K}\alpha) = 8.78\text{ cm}^{-1}$, $F(000) = 1712$.

This compound is isomorphous with previously characterised cobalt analogue, 2, and this fact, coupled with its weak diffraction, did not justify data collection.

1,2-Ph₂-1,2-closo-C₂B₁₀H₁₀, 10

Crystal Data

C₁₄H₂₀B₁₀, $M = 296.41$, monoclinic, space group $P2_1/c$ $a = 10.832(4)$, $b = 24.890(13)$, $c = 13.924(2)\text{\AA}$, $\beta = 111.88(2)^\circ$, $V = 3483.0\text{\AA}^3$, from least-squares refinement of 25 centred reflections ($6 < \theta < 12^\circ$) at $291 \pm 1\text{K}$, $Z = 8$, $D_c = 1.13\text{ gcm}^{-3}$, $\mu(\text{Mo-K}\alpha) = 0.51\text{ cm}^{-1}$, $F(000) = 1232$.

Data Collection and processing

Variable scan speeds between $1.10 - 3.30^\circ\text{min}^{-1}$. 6121 independent reflections measured ($1 < \theta < 25^\circ$, $+h +k \pm l$), of which 3779 had $F > 2.0\sigma$. No measurable crystal decay or movement.

Structure Solution and Refinement

C, and B atom positions from direct methods, and H_{cage} from full matrix least-squares refinement/ ΔF syntheses. Phenyl hydrogens set in fixed positions (C-H 1.08\AA). Empirical absorption correction applied after isotropic convergence; thereafter all non-H atoms allowed anisotropic thermal motion. Independent molecules refined in alternate cycles (248 variables in each cycle). Phenyl and cage H atoms refined with a common thermal parameter ($U_{\text{H}} = 0.077(2)\text{\AA}^2$) at convergence. $g = 0.000200$. $R = 0.0703$, $R_w = 0.0992$, $S = 0.928$. Max. and min. residues in final ΔF map 0.18 and $-0.29\text{e}\text{\AA}^{-3}$.

7,8-Ph₂-10-endo-(PPh₃Hg)-7,8-nido-C₂B₉H₉.CH₂Cl₂, 11

Crystal Data

C₃₂H₂₄Pb₁₃CH₂Cl₂, $M = 822.33$, monoclinic, space group $P2_1$ $a = 10.953(2)$, $b = 13.274(3)$, $c = 11.528\text{\AA}$, $\beta = 90.074(12)$, $V = 1676.1\text{\AA}^3$, from least-squares refinement of 25 centred reflections ($12 < \theta < 13^\circ$) at $291 \pm 1\text{K}$, $Z = 2$, $D_c = 1.629\text{ gcm}^{-3}$, $\mu(\text{Mo-K}\alpha) = 48.22\text{ cm}^{-1}$, $F(000) = 796$.

Data Collection and processing

Variable scan speeds between $0.87 - 2.35^\circ\text{min}^{-1}$. 2677 independent reflections measured ($1 < \theta < 25^\circ$, $+h +k \pm l$), of which 2656 had $F > 2.0\sigma$. No measurable crystal decay or movement.

Structure Solution and Refinement

Hg position from Patterson synthesis, P, C, B, Cl and and H_{cage} from full matrix least-squares refinement/ ΔF syntheses. Cage H atoms allowed positional refinement subject to a single B-H distance of $1.06(1)\text{\AA}$. Phenyl hydrogens set in fixed positions (C-H 1.08\AA). Empirical absorption correction applied after isotropic convergence; thereafter all non-H atoms allowed anisotropic thermal motion. Model refined by least-squares on F in two blocks (mercury triphenylphosphine and carbaborane cage, 182 and 264 variables respectively) to convergence. Phenyl and cage H atoms refined with a common thermal parameter ($U_H = 0.037(5)\text{\AA}^2$) at convergence. Data weighted according to $w^{-1} = [\sigma^2(F) + 0.000200F^2]$. $R = 0.0214$, $R_w = 0.0241$, $S = 1.078$. Max. and min. residues in final ΔF map 0.20 and $-0.18\text{e}\text{\AA}^{-3}$.

1,2-Ph₂-3-Cp*⁻-3,1,2-pseudo-closo-Rh₂B₉H₉, 13

Crystal Data

C₂₄H₃₄B₉Rh, $M = 522.74$, monoclinic, space group $P2_1/a$ $a = 17.622(10)$, $b = 18.266(3)$, $c = 18.039(6)\text{\AA}$, $\beta = 118.410(35)^\circ$, $V = 5107.2\text{\AA}^3$, from least-squares refinement of 25 centred reflections ($10 < \theta < 12^\circ$) at $185 \pm 1\text{K}$, $Z = 8$, $D_c = 1.359\text{ gcm}^{-3}$, $\mu(\text{Mo-K}\alpha) = 6.69\text{ cm}^{-1}$, $F(000) = 2144$.

Data Collection and Processing

Variable scan speeds between $1.20\text{-}2.75^\circ\text{min}^{-1}$. 4852 independent reflections measured ($1 < \theta < 22^\circ$, $+h +k \pm l$), of which 4823 had $F > 2.0\sigma(F)$.

Structure Solution and Refinement

Rh(3A) and Rh(3B) positions found from Patterson synthesis; C, B and two ghost rhodium atoms, Rh(3X) and Rh(3Y), were located by full matrix least-squares refinement/ ΔF syntheses. The latter were assigned as such by their chemically non-sensible positions, and the fact that their co-ordinates are *pseudo* symmetry related to Rh(3A) and Rh(3B) ($x, 0.5-y, z$). After free refinement Rh(3X) had a part occupancy of 10% and Rh(3Y) part occupancy of 5%. This implies that there is 10% and 5% disorder in molecules A and B respectively. After initial location carbon atoms in five- and six-membered rings were refined in fixed planar rings. Phenyl hydrogen atoms were fixed subject to a C-H distance of 1.08\AA , and methyl hydrogens fixed subject to a similar distance from the methyl carbon atom, and at a common distance [$2.1(0.02)\text{\AA}$] to the relevant ring carbon atom. Cage H atoms, in calculated positions, subject to a single X-H distance of $1.10(2)\text{\AA}$, were not refined. Empirical absorption correction applied after isotropic convergence; thereafter atoms were refined with a mixture of isotropic and anisotropic thermal parameters. Independent molecules refined in alternate cycles, of 261 variables. All non-cage H atoms refined with a common thermal parameter ($U_H = 0.129(6)\text{\AA}^2$) at convergence. $g = 0.001621$.

$R = 0.1236$, $R_w = 0.1499$, $S = 1.394$. Max. and min. residues in final ΔF map 0.78 and -0.86\AA^{-3} .

Section C: Extended Hückel Molecular Orbital Calculations

Introduction

Extended Hückel molecular orbital (EHMO) calculations^{104,105} have been widely used for probing general structural problems in organometallic chemistry. Although the molecular orbital energies obtained are often inaccurate, the results do reflect maximum overlap criteria and broad electronegativity trends. In consequence, the preferred conformation and rotational barriers are often accurately predicted by the extended Hückel method.

General Methodology^{106,107}

In order to run an EHMO calculation, a model of the molecule is required, with co-ordinates in orthogonal Angstrom space, together with a basis set of atomic orbital (AO) parameters, for all the elements in the molecule.

Molecular orbitals (MO's) are derived by the linear combination of atomic orbital (LCAO) approach. Ψ , the mathematical function for an MO, is derived from corresponding AO's, Ψ_i and Ψ_j , according to the following equation:

$$\Psi = c_i\Psi_i + c_j\Psi_j$$

where c_i and c_j are the AO coefficients.

The AO wavefunctions are represented by normalised Slater-type orbitals (STO's) which have the form:

$$\Psi_{lmn} = r^{n-1} \exp^{-\zeta r} Y_{ml}(\theta, \phi)$$

where n is related to the principal quantum number, and $Y_{ml}(\theta, \phi)$ are spherical

harmonics.

The orbital exponent, ζ , defines the diffuseness of STO's in physical terms, and is related to the effective nuclear charge, i.e.

$$\zeta = (Z - \sigma)/n$$

where Z is the nuclear charge, and σ a screening constant

In order to calculate orbital energies, a secular determinant is set up from equations of the type shown below, using evaluated Hamiltonian operators (H_{ii} and H_{ij}) and overlap integrals (S_{ij}).

$$\sum c_{ij}(H_{ij} - S_{ij}E) = 0$$

where $H_{ii} = \int \Psi_i H \Psi_i$, $H_{ij} = \int \Psi_i H \Psi_j = \int \Psi_j H \Psi_i$ and $S_{ij} = \int \Psi_i \Psi_j$.

The H_{ii} 's used are the valence shell ionisation energies (VSIE's), which may be optimised by charge iteration procedures. H_{ij} 's are calculated using the modified Wolfsberg-Helmholtz formula:

$$H_{ij} = K' S_{ij} (H_{ii} + H_{jj}) / 2$$

where $K' = K + \Delta + \Delta^2 + \Delta^4 (1 - K)$

and $\Delta = (H_{ii} - H_{jj}) / (H_{ii} + H_{jj})$

Optimisation of H_{ii} 's by Charge Iteration

For models of compounds 1 -> 5, H_{ii} 's for cobalt were initially optimised by charge iteration. This involves implementing a complex function, of the form:

$$H_{ii} = -VSIE(Q)$$

$$\text{where } VSIE(Q) = AQ^2 + BQ + C$$

where the parameters A, B, and C are defined from multiconfigurational spectral data on the atoms and their charged ions.¹⁰⁸ The cycles are repeated until self-consistent charges result (*i.e.* $< 10^{-4}e$ change in any atomic charge between cycles).

Atomic orbital parameters used for the calculations discussed in this work are the following:

AO	H_{ii} (eV)	ζ_1^a	ζ_2^a	c_1^b	c_2^b
H1s	-13.60	1.30			
B2s	-15.20	1.30			
B2p	-8.50	1.30			
C2s	-21.40	1.625			
C2p	-11.40	1.625			
Co3d	-12.075	5.55	2.10	0.56786	0.60586
Co4s	-9.128	2.00			
Co4p	-5.515	2.00			

^aexponents, ^bco-efficients in double-zeta expansion

Bond Overlap Populations

The bond overlap population between two atoms, r and s, is defined by:

$$P_{rs} = \sum \sum (N C_{in} c_{jn} S_{ij})$$

where there are n MO's, c_{in} is the coefficient of Ψ in the n^{th} MO, N is the number of electrons in the orbital.

P_{rs} is a measure of the bond strength and thus calculated overlap populations may be compared with structurally observed bond distances between certain atoms.

Calculations Performed on Models of 1 to 5

A series of molecular orbital calculations were performed on models of 1 to 5, to generate the sum of one-electron energies for different conformations of the models. The models implemented were made up of two molecular fragments; an idealized model of an icosahedron, representing the $\{\text{CoC}_2\text{B}_9\text{H}_9\text{R}^1\text{R}^2\}$ fragment, and an idealized model of $[\text{C}_9\text{H}_7]^-$ (or $[\text{C}_{13}\text{H}_9]^-$). The bond distances and angles used were the following: $\text{B-B} = \text{B-C} = \text{C-C}_{\text{cage}} = 1.75\text{\AA}$, $\text{B-H} = \text{C-H}_{\text{cage}} = 1.20\text{\AA}$, $\text{Co-B} = \text{Co-C} = 2.05\text{\AA}$, $\text{C-C}_{\text{hydrocarbon}} = 1.40\text{\AA}$, $\text{C-H}_{\text{hydrocarbon}} = 1.08\text{\AA}$, $\text{C-C}_{\text{methyl}} = 1.54\text{\AA}$, $\text{Co-C-C-H}_{\text{methyl}} = 0^\circ$, $\text{Co-C-C-H}_{\text{phenyl}} = 90^\circ$.

Co-ordinates for the idealized icosahedral fragment, {CoC₂B₉H₁₁}

H1	0.00000	0.00002	-2.86439
H2	0.00000	-2.56198	-1.28100
H3	-2.43660	-0.79169	-1.28100
H4	-1.50590	2.07270	-1.28100
H5	1.50590	2.07270	-1.28100
H6	2.43660	-0.79169	-1.28100
H7	-1.50590	-2.07270	1.28100
H8	-2.43660	0.79169	1.28100
H9	0.00000	2.56198	1.28100
H10	2.43660	0.79169	1.28100
H11	1.50590	-2.07270	1.28100
B1	0.00000	0.00000	-1.66437
B2	0.00000	-1.48864	-0.74432
B3	-1.41580	-0.46001	-0.74432
B4	-0.87500	1.20436	-0.74432
B5	0.87500	1.20436	-0.74432
B6	1.41580	-0.46001	-0.74432
C7	-0.87500	-1.20436	0.74432
B8	-1.41580	0.46001	0.74432
B9	0.00000	1.48864	0.74432
B10	1.41580	0.46001	0.74432
C11	0.87500	-1.20436	0.74432
CO	0.0000	0.0000	2.1538

Co-ordinates for phenyl substituent, replacing H11, in the model of 2

C111	1.6795	-2.3118	1.4287
C112	3.0284	-2.1058	1.7417
C116	1.0665	-3.5309	1.7418
C113	3.7644	-3.1189	2.3678
C114	3.1514	-4.3380	2.6809
C115	1.8025	-4.5440	2.3679
H112	3.5538	-1.0608	1.4733
H113	4.9206	-2.9423	2.6360
H114	3.7823	-5.2064	3.2175
H115	1.2771	-5.5890	2.6362
H116	-0.0897	-3.7075	1.4735

Cage substituent coordinates for $(C_9H_7)CoC_2B_9H_{10}CH_3$, model of 3

C111	1.6795	-2.3118	1.4287
H111	2.1364	-2.9407	0.6789
H112	1.0216	-2.9064	2.0450
H113	2.4484	-1.8698	2.0450

(Note that for this calculation the ether function, CH_2OCH_3 , is modelled by a methyl group, which has replaced H11).

Co-ordinates for the cage substituents in the idealized model of 4

C71	-1.6795	-1.2044	0.74432
H71	-2.1364	-2.9407	0.6789
H72	-1.0216	-2.9065	2.0450
H73	-2.4484	-1.8698	2.0450
C111	1.6795	-2.3118	1.4287
H111	2.1364	-2.9407	0.6789
H112	1.0216	-2.9064	2.0450
H113	2.4484	-1.8698	2.0450

(Note that in this calculation both ether functions are modelled by methyl groups, replacing H7 and H11).

Co-ordinates for the indenyl (or fluorenyl) ligands were varied according to rotation of the fused-aromatic ligand about the Co·····B(10) (called B1 in the model) axis, in steps of 18°. By plotting the sum of energies calculated for each different conformation of the models representing 1 to 5 against the angle of rotation, θ , the minimum energy conformation for each model could be deduced (See Chapter 2).

Atom co-ordinates for the idealized model of $[C_9H_7]^-$

C95	1.40000	-2.17590	3.82240
C92	0.00000	1.19090	3.82240
C94	0.70000	-0.96350	3.82240
C99	-0.70000	-0.96350	3.82240
C98	-1.40000	-2.17590	3.82240
C96	0.70000	-3.38830	3.82240
C97	-0.70000	-3.38830	3.82240
C91	-1.13260	0.36800	3.82240
C93	1.13260	0.36800	3.82240
H92	0.00000	2.27090	3.82240
H93	2.15970	0.70170	3.82240
H91	-2.15970	0.70170	3.82240
H98	-2.48000	-2.17590	3.82240
H97	-1.24000	-4.32360	3.82240
H96	1.24000	-4.32360	3.82240
H95	2.48000	-2.17590	3.82240

where the angle of rotation, θ , is 0°, corresponding to a *cis*-eclipsed conformation, in which the ring-junction carbon atoms, C94 and C99, lie directly above the cage carbon atoms, C(1) and C(2) (or C7 and C11, as labelled in the model).

Atomic co-ordinates for the idealized model of $[C_{13}H_9]^-$

C95	-2.50203	-0.65909	3.82240
C92	1.13261	-0.36801	3.82240
C94	-1.13266	-0.36800	3.82240
C99	-0.70003	0.96348	3.82240
C98	-1.63678	2.00387	3.82240
C96	-3.43878	0.38130	3.82240
C97	-3.00615	1.71278	3.82240
C91	0.69998	0.96345	3.82240
C93	0.00000	-1.19088	3.82240
H93	-0.00003	-2.27083	3.82240
H98	-1.30304	3.03101	3.82240
H97	-3.72881	2.51538	3.82240
H96	-4.49517	0.15675	3.82240
H95	-2.83577	-1.68623	3.82240
C913	2.50203	-0.65909	3.82240
C910	1.63678	2.00387	3.82240
C912	3.43878	0.38130	3.82240
C911	3.00615	1.71278	3.82240
H910	1.30304	3.03101	3.82240
H911	3.72881	2.51538	3.82240
H912	4.49517	0.15675	3.82240
H913	2.83577	-1.68623	3.82240

Where the angle of rotation, θ , is 0° , corresponding to the conformation in which C94 and C99 lie directly above the cage carbon atoms, C(1) and C(2).

Calculations performed on Model of 10

The sum of one-electron energies was calculated for varying conformations of a model of 10, in which two phenyl substituents were synchronously rotated about the C(1)-C(11) and C(2)-C(21) bonds (C9-C91 and C12-C121 in the model), in steps of 10°. The sum of energies for conformations at each angle, θ , of twist away from a 90° torsion about C9-C91 and C12-C121 (*i.e.* where C9-C12-C121-C122/C126 = C12-C9-C91-C92/C96 = 90°), giving the energy curve shown in Figure 4.3, Chapter 4. The model was constructed using the bond distances and angles previously described in this Section for models of compounds 1-5.

Calculations were also carried out on models of 1-Ph-1,2-*closo*-C₂B₁₀H₁₁ and 1,2-*closo*-C₂B₁₀H₁₂, where one or both phenyl groups in the model of 10 were replaced by H(1) and H(2) respectively.

Atomic Co-ordinates for the Model of 10

ATOM	H1	0.0000	1.5059	-2.4366
ATOM	H2	0.0000	-1.5059	-2.4366
ATOM	H3	-2.4366	0.0000	-1.5059
ATOM	H4	-1.5059	2.4366	0.0000
ATOM	H5	1.5059	2.4366	0.0000
ATOM	H6	2.4366	0.0000	-1.5059
ATOM	H7	-1.5059	-2.4366	0.0000
ATOM	H8	-2.4366	0.0000	1.5059
ATOM	H10	2.4366	0.0000	1.5059
ATOM	H11	1.5059	-2.4366	0.0000
ATOM	B1	0.0000	0.8750	-1.4158
ATOM	B2	0.0000	-0.8750	-1.4158
ATOM	B3	-1.4158	0.0000	-0.8750
ATOM	B4	-0.8750	1.4158	0.0000
ATOM	B5	0.8750	1.4158	0.0000
ATOM	B6	1.4158	0.0000	-0.8750
ATOM	B7	-0.8750	-1.4158	0.0000
ATOM	B8	-1.4158	0.0000	0.8750
ATOM	C9	0.0000	0.8750	1.4158
ATOM	B10	1.4158	0.0000	0.8750
ATOM	B11	0.8750	-1.4158	0.0000
ATOM	C12	0.0000	-0.8750	1.4158
ATOM	H92	2.14340	2.94590	4.7666
ATOM	H93	2.14340	4.24710	6.8719
ATOM	H94	0.00000	4.89770	7.9246
ATOM	H95	-2.14340	4.24710	6.8719
ATOM	H96	-2.14340	2.94590	4.7666
ATOM	H122	-2.14340	-2.94590	4.7666
ATOM	H123	-2.14340	-4.24710	6.8719
ATOM	H124	0.00000	-4.89770	7.9246
ATOM	H125	2.14340	-4.24710	6.8719
ATOM	H126	2.14340	-2.94590	4.7666
ATOM	C91	0.00000	2.86310	4.6326
ATOM	C92	1.20810	3.22980	5.2259
ATOM	C93	1.20810	3.96320	6.4126
ATOM	C94	0.00000	4.32990	7.0059
ATOM	C95	-1.20810	3.96320	6.4126
ATOM	C96	-1.20810	3.22980	5.2259
ATOM	C121	0.00000	-2.86310	4.6326
ATOM	C122	-1.20810	-3.22980	5.2259
ATOM	C123	-1.20810	-3.96320	6.4126
ATOM	C124	0.00000	-4.32990	7.0059
ATOM	C125	1.20810	-3.96320	6.4126
ATOM	C126	1.20810	-3.22980	5.2259

where $\theta = 0^\circ$

References

1. M.F.Hawthorne, D.C.Young and P.A.Wegner, *J.Am.Chem.Soc.*, 1965, **87**, 1818.
2. W.L.Jorgenson and L.Salem, "*The Organic Chemist's Book of Orbitals*" , Academic Press, New York, 1973.
3. D.M.P.Mingos, *J.Chem.Soc.,Dalton Trans.*, 1977,602
4. M.F.Hawthorne, D.C.Young, T.D.Andrews, D.V.Howe, R.L.Pilling, A.D.Pitts, M.Reintjes, L.F.Warren and P.A.Wegner, *J.Am.Chem.Soc.*,1968, **90**, 879.
5. R.M.Wing, *J.Am.Chem.Soc.*,1968,**90**,4828.
6. L.F.Warren,Jr. and M.F.Hawthorne, *J.Am.Chem.Soc.*,1968,**90**,4823.
7. D.M.P.Mingos, M.I.Forsyth and A.J.Welch, *J.Chem.Soc.,Dalton Trans.*, 1978, 1363.
8. H.M.Colquhoun, T.J.Greenhough and M.G.H.Wallbridge, *J.Chem.Soc.,Dalton Trans.*, 1985, 761.
9. J.W.Faller, R.H.Crabtree and A.Habib, *Organometallics*, 1985, **4**, 929.
10. S.A.Westcott, A.A.Kakkar, G.Stringer, N.J.Taylor and T.B.Marder, *J.Organomet.Chem.*, 1990, **394**, 777.
11. J.L.Atwood, R.Shakir, J.T.Malito, M.Herberhold, W.Kremnitz, W.P.E.Bernhagen and H.G.Alt, *J.Organomet.Chem.*, 1979, **165**, 65.
12. C.Kowala and J.A.Wunderlich, *Acta.Cryst.*, 1976, **B32**, 820.

13. M.Crocker, M.Green, J.A.K.Howard, N.C.Norman and D.M.Thomas, *J.Chem.Soc.,Dalton Trans.*, 1990, 2299.
14. D.E.Smith and A.J.Welch, *Organometallics*, 1986, 5, 760.
15. H.Beall, *Boron Hydride Chemistry*, ed. E.L.Muetterties, Academic Press, New York, 1975.
16. W.E.Hill, F.A.Johnson and R.W. Novak, *Inorg.Chem.*, 1975, 14, 216.
17. R.N.Grimes, *Carboranes*, Academic Press, New York, 1970.
18. R.K.Bohn and M.D.Bohn, *Inorg.Chem.*, 1971, 10, 350.
19. D.Voet and W.N.Lipscomb, *Inorg.Chem.*, 1964, 3, 1679.
20. V.N.Kalinin, N.I.Kobel'Kova, A.V.Astakhin, A.I.Gusev and L.I.Zakharkin, *J.Organomet.Chem.*, 1978, 149, 9.
21. F.Tebbe, P.M.Garrett and M.F.Hawthorne, *J.Am.Chem.Soc.*, 1964, 86, 5016.
22. M.F.Hawthorne and P.A.Wegner, *ibid.*, 1968, 90, 4392.
23. J.L.Spencer, M.Green and F.G.A.Stone, *J.Chem.Soc.,Chem.Comm.*, 1972, 1178.
24. M.P.Garcia, M.Green, F.G.A.Stone, R.G.Somerville, A.J.Welch, C.E.Briant, D.N.Cox and D.M.P.Mingos, *J.Chem.Soc.,Dalton Trans.*, 1985, 2343.
25. E.J.M.Hamilton and A.J.Welch, *Polyhedron*, 1990, 9, 2407.
26. e.g. N.N.Greenwood and A.Earnshaw, in *"The Chemistry of the Elements"*, Pergamon, Oxford, 1982.
27. S.A.Miller, J.A.Tebboth and J.F.Tremaine, *J.Chem.Soc.*, 1952, 632.

28. T.J.Kealy and P.L.Pauson, *Nature*, 1951, **168**, 1039.
29. J.Wunderlich and W.N.Lipscomb, *J.Am.Chem.Soc.*, 1960, **82**, 4427.
30. W.N.Lipscomb, *Boron Hydrides*, Benjamin Press, New York, 1963.
31. K.Wade, *Chem.Comm.*, 1971, 792.
32. W.H.Eberhardt, B.Crawford,Jr. and W.N.Lipscomb, *J.Chem.Phys.*, 1954, **22**, 989.
33. J.Buchanan, E.J.H.Hamilton, D.Reed and A.J.Welch, *J.Chem.Soc.,Dalton Trans.*, 1990, 677.
34. H.M.Colquohoun, T.J.Greenhough and M.G.H.Wallbridge, *J.Chem.Soc.,Chem.Comm.*, 1976, 1019.
35. H.M.Colquohoun, T.J.Greenhough and M.G.H.Wallbridge, *Acta Cryst.*, 1977, **B33**, 3604.
36. D.M.P.Mingos and M.I.Forsyth, *J.Organomet.Chem.*, 1978, **146**, C37.
37. H.M.Colquohoun, T.J.Greenhough and M.G.H.Wallbridge, *J.Chem.Soc.,Chem.Comm.*, 1977, 737.
38. Evans and Mingos, *J.Organometal.Chem.*, 1982, **232**, 171.
39. Y.Do, H.C.Kang, C.B.Knobler and M.F.Hawthorne, *Inorg.Chem.*, 1987, **26**, 2348.
40. T.B.Marder, D.C.Roe and D.Milstein, *Organometallics*, 1988, **7**, 1451.
41. P.Caddy, M.Green, L.E.Smart, and N.White, *J.Chem.Soc.,Chem.Comm.*, 1978, 839.

42. H.Bonneman, *Angew.Chem.,Int.Ed.Engl.*, 1985, **30**, 181.
43. C.White and R.J.Mawby, *Inorg.Chim.Acta.*, 1970, **4**, 261.
44. P.Caddy, M.Green, E.O'Brien, L.E.Smart and P.Woodward, *J.Chem.Soc.,Dalton Trans.*, 1980, 962.
45. T.B.Marder and I.D.Williams, *J.Chem.Soc.,Chem.Comm.*, 1987, 1478.
46. J.L.Atwood and R.Shakir, *Acta.Cryst.*, 1981, **B37**, 1656.
47. J.H.Burns, P.G.Laubereau, *Inorg.Chem.*, 1971, **10**, 2789.
48. J.L.Atwood, W.E.Hunter, D.C.Hrncir, E.Samuel, H.Alt, and M.D.Rausch, *Inorg.Chem.*, 1975, **14**, 1757.
49. A.K.Kakkar, S.F.Jones, N.J.Taylor, S.Collins and T.B.Marder, *J.Chem.Soc.,Chem.Comm.*, 1989, 1454.
50. A.N.Nesmeyanov, N.A.Ustynyuk, L.G.Makarova, V.G.Andnanov, Yu Struchkov, S.Andrae, Y.A.Ustynyuk and S.G.Malyugina, *J. Organomet.Chem.*, 1978, **159**, 189.
51. J.S.Merola, R.T.Macmarac, D.Van Engen, *J.Am.Chem.Soc.*, 1986, **108**, 329.
52. R.M.Kowaleski, A.L.Rheingold, W.C.Trogler and F.Baslo, *ibid*, 1986, **108**, 2460.
53. H.Bönnemann, B.Bogdanovic and G.Wilke, *Angew.Chem.,Int.Ed.Engl.*, 1967, **6**, 804.
54. P.Seiler and J.D.Dunitz, *Acta.Cryst.*, 1979, **B35**, 2020.
55. A.Almennigen, E.Gard, A.Haaland and J.Brunvoll, *J.Organomet.Chem.*, 1976,

107, 273.

56. L.Hedberg and K.J.Hedberg, *Chem.Phys.*, 1970, **53**, 1228; P.Seiler and J.D.Dunitz, *Acta.Cryst.*, 1980, B36, 2255.

57. D.St.Clair, A.Zalkin and D.H.Templeton, *J.Am.Chem.Soc.*, 1970, **92**, 1173.

58. F.V.Hansen, R.G.Hazell, C.Hyatt and G.D.Stucky, *Acta Chem.Scand.*, 1973, **27**, 1210.

59. R.M.Wing, *J.Am.Chem.Soc.*, 1970, **92**, 1187.

60. J.W.Johnson and P.M.Treichel, *ibid*, 1977, **99**, 1427.

61. J.W.Treichel and J.W.Johnson, *J.Organomet.Chem.*, 1975, **88**, 207,215,227.

62. V.Kunz and W.Nowachi, *Helv.Chim.Acta*, 1967, **50**, 1052.

63. M.Kaftory, *Acta Crystallogr.*, 1980, **36**, 2971.

64. R.G.Swisher, K.Sinn, and R.N.Grimes, *Organometallics*, 1985, **4**, 896.

65. J.W.Hull and W.L.Gladfelter, *ibid*, 1984,**3**, 605.

66. R.N.Grimes, *Comprehensive Organometallic Chemistry*; G.Wilkinson, F.G.A.Stone and E.W.Abel, Eds.; Pergamon Press: Oxford, 1981; Vol.1, pp 459-542.

67. P.E.Behnken, J.A.Belmont, D.C.Busby, M.S.Delaney, R.E.King III, C.W.Kreiendahl, T.B.Marder, J.J.Wilczynski, M.F.Hawthorne, *J.Am.Chem.Soc.*, 1984, **106**, 3011; J.D.Hewes, M.Thompson and M.F.Hawthorne, *Organometallics*, 1985, **4**, 13.

68. A.Fessenbecker, M.Stephen, R.N. Grimes, H.Pritzkow, U.Zenneck and W.Siebert, *J.Amer.Chem.Soc.*, 1991, **113**, 3061.

69. V.R.Miller, R.Weiss and R.N.Grimes, *J.Am.Chem.Soc.*, 1977, **99**, 5646.
70. T.L.Venable and R.N.Grimes, *Inorg.Chem.*, 1982, **21**, 887.
71. T.P.Hanusa and L.J.Todd, *Polyhedron*, 1985, **4**, 2063.
72. X.L.R.Fontaine, H.Fowkes, N.N.Greenwood, J.D.Kennedy and M.Thornton-Pett, *J.Chem.Soc.,Dalton Trans.*, 1986, 547.
73. X.L.R.Fontaine, N.N.Greenwood, J.D.Kennedy, K.Nestor, M.Thornton-Pett, S.Hermanek, T.Jelinek and B.Stibr, *ibid*, 1990, 681.
74. R.J.Angelici and E.D.Fisher, *J.Am.Chem.Soc.*, 1963, **85**, 3733.
75. J.Powell and B.L.Shaw, *J.Chem.Soc,A*, 1968, 583.
76. J.W.Kang, K.Mosely and P.M.Maitlis, *J.Am.Chem.Soc.*, 1969, **91**, 5970.
77. M.R.Churchill, S.A.Julis and F.J.Rotella, *Inorg.Chem.*, 1977, **16**, 1137.
78. B.L.Booth, R.N.Haszeldine and M.Mill, *J.Chem.Soc.,Dalton Trans.*, 1978, 617.
79. F.Farone, V.Marsala and G.Tresoldi, *J.Organomet.Chem.*, 1978, **152**, 337.
- 80.R.J.McKinney, *J.Chem.Soc.,Chem.Commun.*, 1980, 603.
81. C.U.Pittman,Jr. and W.G. Miller, *J.Am.Chem.Soc.*, 1973, **95**, 2947.
82. N.I.Kirillova, T.V. Klimova, Yu.T.Struchkov and V.I.Stanko, *Izv.Akad.Nauk.SSSR, Ser.Khim.* (English Translation), 1979, 2296.
83. S.V.Lindeman, I.A.Khotina, M.M.Teplyakov, Y.T.Struchkov, V.V.Korshak, *Makromol.Chem.*, 1988, **189**, 471.

84. M.Brown, J.Plesec, K.Base, B.Stibr, X.L.R.Fontaine, N.N.Greenwood and J.D.Kennedy, *Magnetic Resonance in Chemistry*, 1989, **27**, 947.
85. J.A.Potenza, W.M.Lipscomb, G.D.Vickers and H.Schroeder, *J.Am.Chem.Soc.*, 1966, **88**, 628.
86. M.Elian, M.L.Chen, D.M.P.Mingos and R.Hoffmann, *Inorg.Chem.*, 1976, **15**, 1148.
87. M.J.Attfield, J.A.K.Howard, A.N.de M.Jelfs, C.M.Nunn and F.G.A.Stone, *J.Chem.Soc.,Dalton Trans.*, 1987, 2219.
88. J.D.Kennedy and B.Wrackmeyer, *J.Magn.Reson.*, 1980, **38**, 529. 89. A.Bax and R.Freeman, *ibid*, 1981, **42**, 164; 1981, **44**, 542.
90. T.L.Venable, W.C.Hutton and R.N.Grimes, *J.Am.Chem.Soc.*, 1982, **104**, 4716.
91. B.D.Reid and A.J.Welch, unpublished results.
92. K.F.Shaw and A.J.Welch, *Polyhedron*, in press.
93. R.C.Evans, F.G.Mann, H.S.Peiser and D.Purdie, *J.Chem.Soc.*, 1940, 1209.
94. M.A.Bennett, T.-N.Huang, T.W.Matheson and A.K.Smith, *Inorg. Synth.*, 1982, **21**, 75.
95. M.M.Fein, J.Bobinski, N.Mayes, N.Schwarz and M.S.Cohen, *Inorg.Chem.*, 1963, **6**, 1111.
96. R.O.Gould and D.E.Smith, University of Edinburgh, 1986.
97. G.M.Sheldrick, University of Gottingen, Germany, 1986.
98. G.M.Sheldrick, University of Cambridge, 1976.

99. "International Tables for X-ray Crystallography", Kynoch Press, Birmingham, 1974, 4, 99.
100. N.G.Walker and D.Stuart, *Acta Crystallogr.*, 1983, A39, 158.
101. R.O.Gould and P.Taylor, University of Edinburgh, 1986.
102. P.R.Mallinson, University of Glasgow, 1982.
103. C.K.Johnson, Report *ORNL-5138*, Oak Ridge National Laboratory, Tennessee, U.S.A., 1976.
104. R.Hoffmann and W.N.Lipscomb, *J.Chem.Phys.*, 1962, 36, 2179.
105. R.Hoffmann, *J.Chem.Phys.*, 1963, 36, 2179.
106. J.Howell, A.Rossi, D.Wallace, K.Haraki and R.Hoffmann, *ICON*, Quantum Chemistry Program Exchange, Univ. Indiana, 1977, no. 344.
107. J.H.Ammeter, H.-B.Burgi, J.C.Thibeault and R.Hoffmann, *J.Am.Chem.Soc.*, 1982, 100, 3686.
108. C.J.Ballhausen and H.B.Gray, *Molecular Orbital Theory*, Benjamin, New York, 1965.

Appendices

Appendix 1: Additional Atom Co-ordinates

Hydrogen Atom Co-ordinates for 2

	x	y	z
H(2)	0.2756	0.4710	0.2346
H(4)	0.2770	0.1383	0.2852
H(5)	0.2402	0.2526	0.4036
H(6)	0.2387	0.4647	0.3646
H(7)	0.4373	0.4246	0.2668
H(8)	0.4551	0.1942	0.3131
H(9)	0.4193	0.1767	0.4607
H(10)	0.4002	0.3812	0.5119
H(11)	0.4076	0.5252	0.3887
H(12)	0.5204	0.3412	0.4471
H(12)	0.1465	0.4899	0.2224
H(13)	-0.0081	0.4954	0.1437
H(14)	-0.0909	0.3370	0.1076
H(15)	-0.0173	0.1727	0.1514
H(16)	0.1389	0.1666	0.2334
H(33)	0.1843	0.1506	0.1100
H(32)	0.3478	0.1087	0.1595
H(31)	0.4258	0.2795	0.1504
H(38)	0.3602	0.4850	0.0839
H(37)	0.2287	0.5849	0.0247
H(36)	0.0941	0.5119	0.0048
H(35)	0.0815	0.3342	0.0365

Hydrogen Atom Co-ordinates for 5

	x	y	z
H(5)	0.1971	0.1582	1.3420
H(6)	0.4441	0.0034	1.3540
H(7)	0.6184	0.1073	1.0863
H(10)	0.5263	0.2031	1.3760
H(11)	0.7034	0.0731	1.2610
H(9)	0.3020	0.3257	1.2525
H(4)	0.1227	0.1863	1.1840
H(1)	0.2092	0.0004	1.2359
H(12)	0.6399	0.2844	1.2144
H(8)	0.4101	0.2850	1.0902
H(2)	0.4731	-0.0369	1.1595
H(33)	0.1643	0.1957	0.9869
H(38)	0.2448	-0.2098	1.0920
H(35)	-0.0997	0.0993	1.0733
H(36)	-0.1762	-0.0544	1.1506
H(37)	-0.0098	-0.2042	1.1633
H(310)	0.5179	-0.1603	1.0126
H(313)	0.4531	0.1938	0.8847
H(312)	0.6750	0.0953	0.8590
H(311)	0.7207	-0.0749	0.9258

Disordered Solvent Atom Co-ordinates for 6a

	x	y	z
Cx (1)	0.628	0.290	0.282
Cx (2)	0.476	0.273	0.309
Cx (3)	0.577	0.237	0.281
Cx (4)	0.522	0.314	0.294
Cx (5)	0.670	0.226	0.286
Cx (6)	0.583	0.174	0.284
Cx (7)	0.384	0.243	0.292
Cx (8)	0.463	0.179	0.296

Hydrogen Atom Co-ordinates for 6a

	x	y	z
H (13)	0.8446	0.1289	0.6250
H (11)	0.7115	-0.0359	0.5572
H (18)	0.9196	-0.1003	0.5234
H (15)	1.0864	0.1017	0.6020
H (16)	1.1964	0.0145	0.5666
H (17)	1.1230	-0.0842	0.5340
H (23)	0.8218	0.0559	0.7242
H (22)	0.6795	-0.0429	0.6989
H (21)	0.7814	-0.1465	0.6562
H (25)	1.0713	0.0328	0.7270
H (26)	1.2047	-0.0063	0.6751
H (27)	1.1848	-0.1239	0.6541
H (28)	1.0072	-0.1737	0.6397

Hydrogen Atom Co-ordinates for 10

	x	y	z
H (3A)	0.9442	0.0425	0.3835
H (4A)	0.8550	0.1467	0.2910
H (5A)	0.6656	0.1254	0.0886
H (6A)	0.6554	0.0118	0.0559
H (7A)	0.7287	-0.0183	0.4076
H (8A)	0.7521	0.0995	0.4409
H (9A)	0.5658	0.1544	0.2508
H (10A)	0.4412	0.0696	0.0966
H (11A)	0.5418	-0.0379	0.1965
H (12A)	0.4885	0.0475	0.3180
H (12A)	1.0693	0.0759	0.3158
H (13A)	1.2505	0.0836	0.2498
H (14A)	1.2037	0.0775	0.0644
H (15A)	0.9758	0.0632	-0.0564
H (16A)	0.7950	0.0514	0.0071
H (22A)	0.9828	-0.0408	0.3939
H (23A)	1.0963	-0.1260	0.3899
H (24A)	1.0182	-0.1823	0.2383
H (25A)	0.8239	-0.1567	0.0881
H (26A)	0.7026	-0.0716	0.0896
H (3B)	0.4770	0.2345	0.7043
H (4B)	0.3718	0.3152	0.5572
H (5B)	0.3247	0.2689	0.3577
H (6B)	0.3949	0.1579	0.3982
H (7B)	0.2878	0.1513	0.6852
H (8B)	0.1930	0.2669	0.6488
H (9B)	0.0882	0.2855	0.4286
H (10B)	0.1073	0.1806	0.3208
H (11B)	0.2334	0.1033	0.4923
H (12B)	0.0340	0.1801	0.5034
H (12B)	0.6111	0.2921	0.6678
H (13B)	0.8397	0.3134	0.6869
H (14B)	0.9360	0.2756	0.5704
H (15B)	0.7997	0.2185	0.4261
H (16B)	0.5714	0.1949	0.4071
H (22B)	0.5835	0.1698	0.7692
H (23B)	0.7632	0.1056	0.8522
H (24B)	0.8039	0.0308	0.7526
H (25B)	0.6602	0.0194	0.5715
H (26B)	0.4761	0.0819	0.4871

Hydrogen Atom Co-ordinates for 11

	x	y	z
H(12)	0.5763	0.5801	0.3550
H(13)	0.7819	0.5040	0.3438
H(14)	0.8268	0.3766	0.1905
H(15)	0.6784	0.3427	0.0391
H(16)	0.4811	0.4308	0.0360
H(22)	0.5814	0.7116	0.1821
H(23)	0.5934	0.8983	0.1990
H(24)	0.4078	0.9939	0.2411
H(25)	0.2133	0.9107	0.2787
H(26)	0.2009	0.7232	0.2669
H(32)	0.4294	0.6765	-0.0123
H(33)	0.3536	0.6671	-0.2124
H(34)	0.1819	0.5551	-0.2601
H(35)	0.0971	0.4441	-0.1118
H(36)	0.1716	0.4512	0.0920
H(10)	0.0520	0.5362	0.4620
H(6)	0.0583	0.4118	0.6822
H(2)	0.2149	0.2484	0.6705
H(3)	0.1425	0.1222	0.4701
H(4)	-0.0585	0.2060	0.3645
H(5)	-0.1230	0.3998	0.4581
H(11)	0.2988	0.4330	0.5836
H(9)	0.0233	0.3845	0.2568
H(1)	-0.0492	0.2322	0.6175
H(72)	0.3272	0.0977	0.4247
H(73)	0.5388	0.0371	0.4132
H(74)	0.7115	0.1556	0.4424
H(75)	0.6686	0.3357	0.4668
H(76)	0.4569	0.3976	0.4767
H(82)	0.0773	0.0991	0.2623
H(83)	0.1460	0.0238	0.0790
H(84)	0.3066	0.1049	-0.0386
H(85)	0.4036	0.2614	0.0358
H(86)	0.3369	0.3365	0.2176

Hydrogen Atom Co-ordinates for 13

	x	y	z
H (4A)	0.0051	0.0585	0.4830
H (7A)	-0.0876	0.3108	0.4504
H (8A)	-0.1107	0.1519	0.5075
H (6A)	-0.0301	0.2025	0.2524
H (11A)	-0.1544	0.3007	0.2627
H (5A)	-0.0644	0.0511	0.2942
H (12A)	-0.2373	0.2274	0.3516
H (10A)	-0.2136	0.1487	0.2181
H (9A)	-0.1787	0.0614	0.3664
H (12A)	0.1401	0.2010	0.3494
H (13A)	0.2695	0.1418	0.3561
H (14A)	0.3012	0.0119	0.3988
H (15A)	0.2035	-0.0588	0.4349
H (16A)	0.0741	0.0004	0.4283
H (22A)	0.1214	0.2922	0.3381
H (23A)	0.1708	0.4155	0.3231
H (24A)	0.0921	0.5255	0.3295
H (25A)	-0.0359	0.5123	0.3510
H (26A)	-0.0852	0.3890	0.3660
H (31A)	0.1607	0.4035	0.6280
H (31B)	0.0517	0.3988	0.5498
H (31C)	0.1343	0.3923	0.5213
H (32A)	0.2375	0.3163	0.5230
H (32B)	0.2354	0.2236	0.4949
H (32C)	0.3037	0.2520	0.5993
H (33A)	0.1951	0.0644	0.6262
H (33B)	0.2818	0.1223	0.6429
H (33C)	0.2053	0.0974	0.5395
H (34A)	0.0249	0.1411	0.6810
H (34B)	0.1248	0.0967	0.7141
H (34C)	0.0390	0.0812	0.6119
H (35A)	0.0016	0.3484	0.6250
H (35B)	0.0323	0.2836	0.7066
H (35C)	-0.0515	0.2632	0.6048
H (4B)	0.4574	0.4504	0.9582
H (7B)	0.5391	0.1925	0.9528
H (8B)	0.5731	0.3385	0.9967
H (6B)	0.2762	0.2891	0.7490
H (11B)	0.4246	0.1897	0.7645
H (5B)	0.3448	0.4422	0.7737
H (12B)	0.5833	0.2774	0.8409
H (10B)	0.4229	0.3381	0.7039
H (9B)	0.5326	0.4401	0.8477
H (12B)	0.1992	0.2975	0.8360
H (13B)	0.0733	0.3554	0.8381
H (14B)	0.0777	0.4869	0.8734
H (15B)	0.2080	0.5603	0.9066
H (16B)	0.3339	0.5024	0.9045
H (22B)	0.2406	0.2030	0.8682
H (23B)	0.1769	0.0808	0.8618
H (24B)	0.2569	-0.0309	0.8632
H (25B)	0.4006	-0.0206	0.8708
H (26B)	0.4642	0.1015	0.8772
H (31X)	0.4396	0.1130	1.1325
H (31Y)	0.5069	0.1142	1.0850
H (31Z)	0.3938	0.1140	1.0217
H (32X)	0.2526	0.2953	1.0391
H (32Y)	0.2910	0.2125	1.0948
H (32Z)	0.2616	0.2169	0.9868

H(33X)	0.4185	0.4557	1.1042
H(33Y)	0.3480	0.4073	1.1304
H(33Z)	0.3210	0.4202	1.0238
H(34X)	0.6346	0.3785	1.1615
H(34Y)	0.5703	0.4177	1.2018
H(34Z)	0.5494	0.4381	1.0982
H(35X)	0.6186	0.1708	1.1337
H(35Y)	0.6550	0.2425	1.2082
H(35Z)	0.6464	0.2561	1.1077

Appendix 2: Lectures and Courses Attended

Recent Advances in Inorganic Chemistry

Drs. A.J.Welch, L.J.Yellowlees, S.K.Chapman and M.Schroeder

Inorganic Medicinal Chemistry

Dr. S.K.Chapman

Structural Methods in Inorganic Chemistry

Professors D.H.W.Rankin and E.A.V.Ebsworth

Departmental Research Seminars and Colloquia

Inorganic Section Meetings

European Collaboration on BNCT, Plenary Meeting, Munich, 1989

Workshop on the Chemistry of BNCT, Ross Priory,
University of Strathclyde, 1990

Intraboron IX, X and XI, Annual Meetings of British Boron Chemists

Imeboron VII, International Meeting on Boron Chemistry, Torun, Poland, 1990

B.C.A. Residential Crystallography School, Aston, Birmingham, April 1991